KFA

KERNFORSCHUNGSANLAGE JÜLICH GmbH

Projektleitung Energieforschung
International Energy Agency IEA

Implementing Agreement for Co-Operation in the Development of Large Scale Wind Energy Conversion Systems

12th Meeting of Experts - Aerodynamic Calculational Methods for WECS

Organised by:
Project Management for Energy Research (PLE) of the
Nuclear Research Establishment Jülich (KFA) on behalf of the
Federal Minister of Research and Technology,
the Fluid Mechanics Department
of the Technical University of Denmark

Jül - Spez - 304
March 1985
ISSN 0343-7639

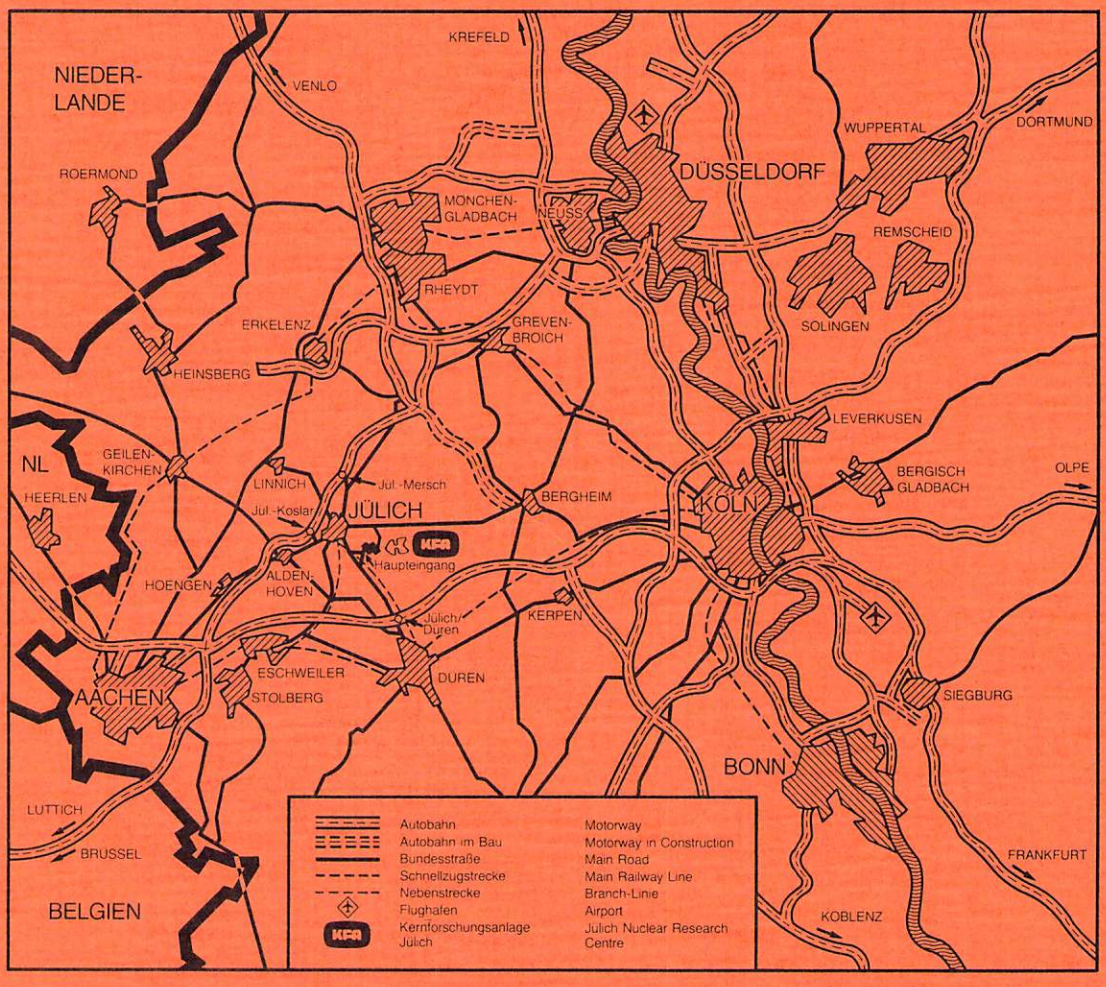

Als Manuskript gedruckt

Spezielle Berichte der Kernforschungsanlage Jülich – Nr. 304

Projektleitung Energieforschung Jül - Spez - 304

Zu beziehen durch: ZENTRALBIBLIOTHEK der Kernforschungsanlage Jülich GmbH

Postfach 1913 · D-5170 Jülich (Bundesrepublik Deutschland)

Telefon: 02461/610 · Telex: 833556-0 kf d

Implementing Agreement for Co-Operation in the Development of Large Scale Wind Energy Conversion Systems

12th Meeting of Experts - Aerodynamic Calculational Methods for WECS

Copenhagen, October 29-30, 1984

Organised by:
Project Management for Energy Research (PLE) of the
Nuclear Research Establishment Jülich (KFA) on behalf of the
Federal Minister of Research and Technology,
the Fluid Mechanics Department
of the Technical University of Denmark

Scientific Coordination:
M. Petersen (Techn. Univ. of Denmark)
R. Windheim (PLE-KFA Jülich)

CONTENTS

AERODYNAMIC CALCULATIONAL METHODS FOR WECS

Recent Developments in Theoretical Modelling, and Experimental Verification of Theoretical Results.

Introductory Note
prepared by

B.Maribo Pedersen
Technical University of Denmark

Introduction.

Aerodynamic calculations on wind-turbine rotors to determine performance and structural loading now have been carried out for a number of years, and for different WECS configurations.

Also experimental results now are avaiable from a number of installations so that verification of theoretical predictions can be made to some extent.

This has made it appropriate to arrange an expert meeting under the LS-WECS agreement where the state of the art and the needs for further development is discussed, and where also the impact of experiments on theoretical modelling can be illustrated.

It is felt that the main emphasis of this meeting should be on the aerodynamics pertaining to horizontal axis machines insofar that the main thrust in most countries has been on the development of this type of WECS. However the challenge in a proper modelling of the flow through a vertical axis rotor should be adressed as well.

Below is listed some questions which should be adressed at this expert meeting. The list should not be considered as exhaustive, as it is the result of one persons views. In particular the contemporary problems in VA-rotor calculations are not too well known to the author, so please add on any relevant headings to the list.

Questions to be adressed.

- How do we deal with rotors operating in the near stall and post-stall regime ?
  Can this three-dimensional problem be reduced to a pseudo two-dimensional one, at least for engineering purposes ?
- The simplified theory breaks down in the high tip-speed range of operation.
  How do we deal with that ?
- How far have we come in developing vortex models for wake and induced velocity calculations ?
- How fast does the wake and hence the induced velocities respond to changes in inflow conditions(turbulence)or to pitch changes during power regulation ?
- Many rotors operate with partial span control. Does this pose special problems for the aerodynamic calculations ?
- Rotors operating in shear flow or in yaw develop yawing and tilting moments. Does our calculational methods treat this regime in an adequate way ?
- Do we have adequate data on airfoil sections ?
- Is there a need for developing special airfoil sections for wind turbine rotors ?
- Can our methods for calculation of the aerodynamically generated noise be considered good enough ?

As far as possible the above issues should be elucidated also with reference to measured data.

POLARENMESSUNGEN AN DEN PROFILEN

FX 84-W-097

FX 84-W-127

FX 84-W-140

FX 84-W-175

FX 84-W-218

D.Althaus

Die Windkanalmodelle mit einer Profiltiefe t = 0,5 m wurden im Laminarwindkanal mit den üblichen Meßverfahren vermessen. Der Profilwiderstand wurde durch Integration längs der Spannweite bestimmt.

Die glatten Profile wurden bei Re = 0,7 / 1,0 und 1,5 Millionen untersucht. Bei Re = 1,0 Millionen wurde die Lage der Umschlagspunkte mit dem Stethoskop bestimmt. Zusätzlich wurden bei dieser Reynoldszahl Messungen mit einem Stolperdraht vom Durchmesser d = 2 mm (d/t = 0.004) direkt auf der Profilnase (x = 0, y = 0) durchgeführt.

In den Tabellen 1 bis 5 sind die Koordinaten der Profile enthalten, die Konturen sind in den Diagrammen 1 bis 5 dargestellt. Die potentialtheoretischen Geschwindigkeitsverteilungen für 4 verschiedene Anstellwinkel sind in den Diagrammen 6 bis 10 enthalten. Die Diagramme 11 bis 15 zeigen die c_a-c_w-Polaren und Umschlagslagen, die Diagramme 16 bis 20 die Momentenbeiwerte um den t/4-Punkt.

Stuttgart, Februar 1984

FX 84-W-97

NR	X/T	YO/T	YU/T
1	1.00000	0.00000	0.00000
2	0.99893	0.00006	0.00003
3	0.99572	0.00028	0.00012
4	0.99039	0.00069	0.00021
5	0.98296	0.00137	0.00029
6	0.97347	0.00230	0.00025
7	0.96194	0.00363	0.00014
8	0.94844	0.00527	-0.00009
9	0.93301	0.00730	-0.00048
10	0.91573	0.00975	-0.00099
11	0.89668	0.01255	-0.00168
12	0.87592	0.01581	-0.00250
13	0.85355	0.01939	-0.00343
14	0.82967	0.02331	-0.00448
15	0.80438	0.02753	-0.00560
16	0.77779	0.03198	-0.00679
17	0.75000	0.03660	-0.00801
18	0.72114	0.04131	-0.00924
19	0.69134	0.04609	-0.01047
20	0.66072	0.05071	-0.01164
21	0.62941	0.05525	-0.01279
22	0.59755	0.05957	-0.01389
23	0.56526	0.06348	-0.01490
24	0.53270	0.06715	-0.01587
25	0.50000	0.07022	-0.01677
26	0.46730	0.07278	-0.01759
27	0.43474	0.07496	-0.01837
28	0.40245	0.07619	-0.01909
29	0.37059	0.07695	-0.01974
30	0.33928	0.07715	-0.02036
31	0.30866	0.07640	-0.02089
32	0.27886	0.07521	-0.02137
33	0.25000	0.07333	-0.02178
34	0.22221	0.07071	-0.02208
35	0.19562	0.06774	-0.02232
36	0.17033	0.06405	-0.02240
37	0.14645	0.06012	-0.02232
38	0.12408	0.05564	-0.02206
39	0.10332	0.05082	-0.02158
40	0.08427	0.04575	-0.02087
41	0.06699	0.04050	-0.01987
42	0.05156	0.03516	-0.01857
43	0.03806	0.02978	-0.01694
44	0.02653	0.02444	-0.01495
45	0.01704	0.01922	-0.01260
46	0.00961	0.01418	-0.00987
47	0.00428	0.00936	-0.00673
48	0.00107	0.00480	-0.00323
49	-0.00000	0.00083	0.00083

DICKE/T...= 0.098 RUECKLAGE/T= 0.339
WOELBUNG/T= 0.029 RUECKLAGE/T= 0.371
PROFILTIEFE...= T

Tabelle 1

FX 84-W-127

NR	X/T	YO/T	YU/T
1	1.00000	0.00000	0.00000
2	0.99893	0.00011	0.00008
3	0.99572	0.00050	0.00028
4	0.99039	0.00121	0.00053
5	0.98296	0.00233	0.00081
6	0.97347	0.00385	0.00096
7	0.96194	0.00594	0.00106
8	0.94844	0.00847	0.00095
9	0.93301	0.01159	0.00065
10	0.91573	0.01525	0.00019
11	0.89668	0.01939	-0.00058
12	0.87592	0.02410	-0.00153
13	0.85355	0.02923	-0.00269
14	0.82967	0.03477	-0.00407
15	0.80438	0.04063	-0.00559
16	0.77779	0.04675	-0.00725
17	0.75000	0.05297	-0.00899
18	0.72114	0.05923	-0.01077
19	0.69134	0.06550	-0.01258
20	0.66072	0.07143	-0.01434
21	0.62941	0.07719	-0.01605
22	0.59755	0.08254	-0.01770
23	0.56526	0.08726	-0.01920
24	0.53270	0.09159	-0.02062
25	0.50000	0.09509	-0.02191
26	0.46730	0.09785	-0.02305
27	0.43474	0.10007	-0.02411
28	0.40245	0.10111	-0.02503
29	0.37059	0.10146	-0.02582
30	0.33928	0.10117	-0.02653
31	0.30866	0.09962	-0.02711
32	0.27886	0.09753	-0.02758
33	0.25000	0.09468	-0.02797
34	0.22221	0.09086	-0.02816
35	0.19562	0.08665	-0.02829
36	0.17033	0.08165	-0.02822
37	0.14645	0.07635	-0.02795
38	0.12408	0.07043	-0.02747
39	0.10332	0.06416	-0.02674
40	0.08427	0.05762	-0.02571
41	0.06699	0.05091	-0.02437
42	0.05156	0.04413	-0.02268
43	0.03806	0.03735	-0.02059
44	0.02653	0.03067	-0.01810
45	0.01704	0.02416	-0.01516
46	0.00961	0.01791	-0.01176
47	0.00428	0.01193	-0.00791
48	0.00107	0.00632	-0.00356
49	-0.00000	0.00097	0.00097

DICKE/T...= 0.128 RUECKLAGE/T= 0.339
WOELBUNG/T= 0.038 RUECKLAGE/T= 0.402
PROFILTIEFE...= T

Tabelle 2

FX 84-W-140

NR	X/T	YO/T	YU/T
1	1.00000	0.00000	0.00000
2	0.99893	0.00014	0.00010
3	0.99572	0.00061	0.00035
4	0.99039	0.00147	0.00072
5	0.98296	0.00281	0.00106
6	0.97347	0.00462	0.00135
7	0.96194	0.00708	0.00157
8	0.94844	0.01006	0.00152
9	0.93301	0.01371	0.00133
10	0.91573	0.01795	0.00085
11	0.89668	0.02276	0.00010
12	0.87592	0.02817	-0.00084
13	0.85355	0.03405	-0.00212
14	0.82967	0.04037	-0.00361
15	0.80438	0.04700	-0.00528
16	0.77779	0.05392	-0.00714
17	0.75000	0.06088	-0.00909
18	0.72114	0.06787	-0.01112
19	0.69134	0.07483	-0.01315
20	0.66072	0.08134	-0.01516
21	0.62941	0.08764	-0.01713
22	0.59755	0.09344	-0.01895
23	0.56526	0.09851	-0.02067
24	0.53270	0.10311	-0.02227
25	0.50000	0.10678	-0.02368
26	0.46730	0.10959	-0.02494
27	0.43474	0.11179	-0.02610
28	0.40245	0.11271	-0.02705
29	0.37059	0.11284	-0.02789
30	0.33928	0.11230	-0.02863
31	0.30866	0.11035	-0.02919
32	0.27886	0.10782	-0.02965
33	0.25000	0.10450	-0.03000
34	0.22221	0.10011	-0.03017
35	0.19562	0.09531	-0.03026
36	0.17033	0.08969	-0.03014
37	0.14645	0.08375	-0.02982
38	0.12408	0.07716	-0.02928
39	0.10332	0.07021	-0.02847
40	0.08427	0.06299	-0.02737
41	0.06699	0.05561	-0.02592
42	0.05156	0.04817	-0.02410
43	0.03806	0.04076	-0.02187
44	0.02653	0.03346	-0.01920
45	0.01704	0.02639	-0.01606
46	0.00961	0.01958	-0.01242
47	0.00428	0.01312	-0.00830
48	0.00107	0.00708	-0.00363
49	-0.00000	0.00102	0.00102

DICKE/T...= 0.141 RUECKLAGE/T= 0.339
WOELBUNG/T= 0.043 RUECKLAGE/T= 0.435
PROFILTIEFE...= T

Tabelle 3

FX 84-W-175

NR	X/T	YO/T	YU/T
1	1.00000	0.00000	0.00000
2	0.99893	0.00016	0.00011
3	0.99572	0.00069	0.00038
4	0.99039	0.00170	0.00077
5	0.98296	0.00326	0.00107
6	0.97347	0.00539	0.00134
7	0.96194	0.00828	0.00136
8	0.94844	0.01179	0.00115
9	0.93301	0.01612	0.00069
10	0.91573	0.02114	-0.00023
11	0.89668	0.02685	-0.00143
12	0.87592	0.03328	-0.00303
13	0.85355	0.04025	-0.00503
14	0.82967	0.04776	-0.00729
15	0.80438	0.05562	-0.00989
16	0.77779	0.06383	-0.01270
17	0.75000	0.07204	-0.01568
18	0.72114	0.08029	-0.01875
19	0.69134	0.08848	-0.02183
20	0.66072	0.09612	-0.02488
21	0.62941	0.10347	-0.02783
22	0.59755	0.11027	-0.03057
23	0.56526	0.11614	-0.03316
24	0.53270	0.12145	-0.03553
25	0.50000	0.12575	-0.03756
26	0.46730	0.12896	-0.03939
27	0.43474	0.13146	-0.04099
28	0.40245	0.13260	-0.04222
29	0.37059	0.13272	-0.04327
30	0.33928	0.13213	-0.04408
31	0.30866	0.12995	-0.04457
32	0.27886	0.12703	-0.04489
33	0.25000	0.12333	-0.04495
34	0.22221	0.11831	-0.04472
35	0.19562	0.11283	-0.04437
36	0.17033	0.10648	-0.04366
37	0.14645	0.09968	-0.04266
38	0.12408	0.09214	-0.04133
39	0.10332	0.08417	-0.03966
40	0.08427	0.07585	-0.03761
41	0.06699	0.06730	-0.03515
42	0.05156	0.05865	-0.03223
43	0.03806	0.04995	-0.02884
44	0.02653	0.04135	-0.02495
45	0.01704	0.03293	-0.02053
46	0.00961	0.02473	-0.01560
47	0.00428	0.01689	-0.01010
48	0.00107	0.00942	-0.00412
49	-0.00000	0.00309	0.00309

DICKE/T...= 0.176 RUECKLAGE/T= 0.339
WOELBUNG/T= 0.045 RUECKLAGE/T= 0.435
PROFILTIEFE...= T

Tabelle 4

FX 84-W-218

NR	X/T	YO/T	YU/T
1	1.00000	0.00000	0.00000
2	0.99893	0.00012	0.00006
3	0.99572	0.00053	0.00017
4	0.99039	0.00135	0.00028
5	0.98296	0.00268	0.00016
6	0.97347	0.00454	-0.00011
7	0.96194	0.00718	-0.00078
8	0.94844	0.01043	-0.00184
9	0.93301	0.01456	-0.00327
10	0.91573	0.01942	-0.00533
11	0.89668	0.02504	-0.00780
12	0.87592	0.03149	-0.01076
13	0.85355	0.03855	-0.01425
14	0.82967	0.04628	-0.01811
15	0.80438	0.05448	-0.02235
16	0.77779	0.06309	-0.02687
17	0.75000	0.07189	-0.03158
18	0.72114	0.08078	-0.03643
19	0.69134	0.08973	-0.04124
20	0.66072	0.09819	-0.04600
21	0.62941	0.10639	-0.05067
22	0.59755	0.11421	-0.05498
23	0.56526	0.12102	-0.05906
24	0.53270	0.12726	-0.06289
25	0.50000	0.13270	-0.06614
26	0.46730	0.13683	-0.06906
27	0.43474	0.14022	-0.07165
28	0.40245	0.14247	-0.07356
29	0.37059	0.14339	-0.07511
30	0.33928	0.14356	-0.07628
31	0.30866	0.14231	-0.07673
32	0.27886	0.13999	-0.07685
33	0.25000	0.13702	-0.07647
34	0.22221	0.13241	-0.07543
35	0.19562	0.12722	-0.07416
36	0.17033	0.12124	-0.07219
37	0.14645	0.11449	-0.06968
38	0.12408	0.10686	-0.06661
39	0.10332	0.09863	-0.06299
40	0.08427	0.08988	-0.05881
41	0.06699	0.08069	-0.05405
42	0.05156	0.07118	-0.04874
43	0.03806	0.06145	-0.04283
44	0.02653	0.05158	-0.03639
45	0.01704	0.04169	-0.02938
46	0.00961	0.03182	-0.02188
47	0.00428	0.02212	-0.01385
48	0.00107	0.01257	-0.00537
49	-0.00000	0.00396	0.00396

DICKE/T...= 0.220 RUECKLAGE/T= 0.339
WOELBUNG/T= 0.034 RUECKLAGE/T= 0.402
PROFILTIEFE...= T

Tabelle 5

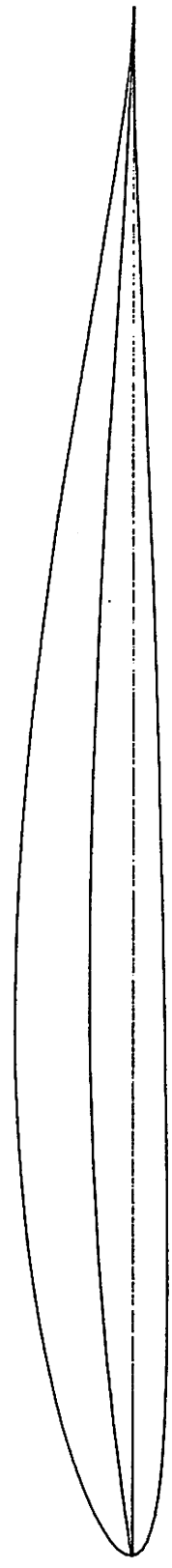

FX 84-W-97

Diagramm 1

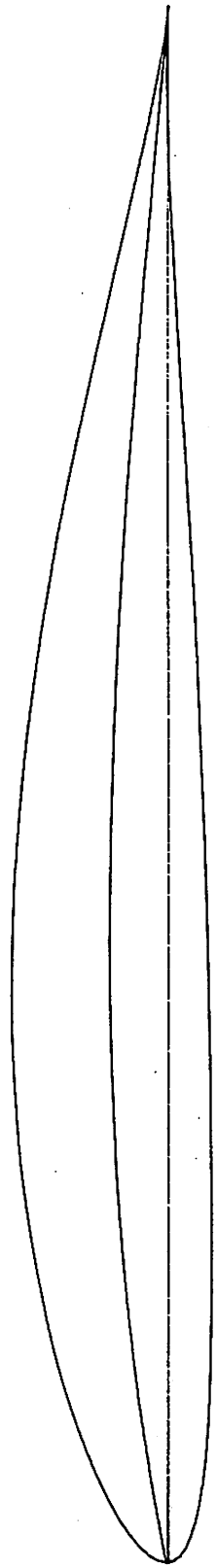

FX 84-W-127

Diagramm 2

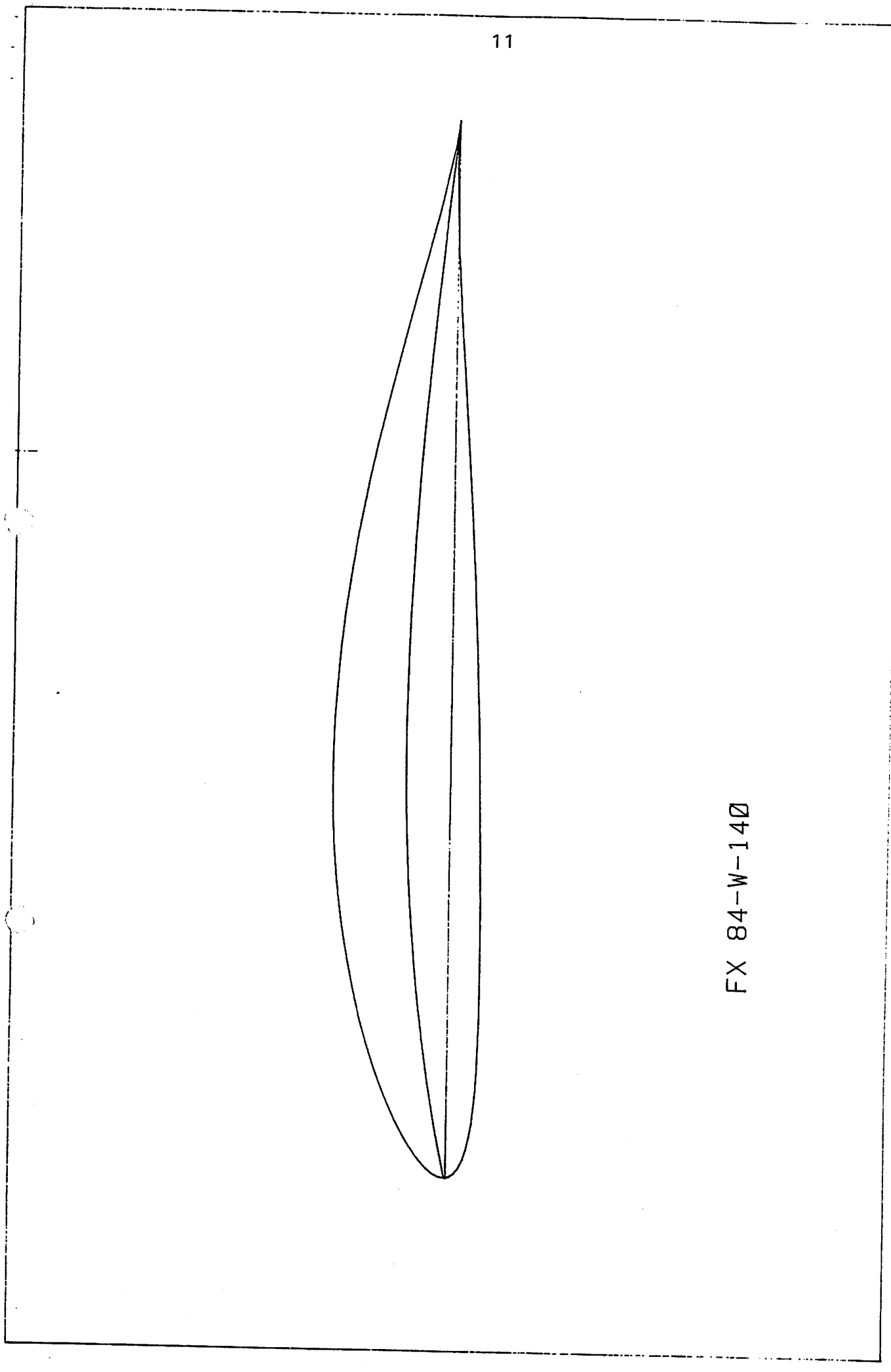

Diagramm 3

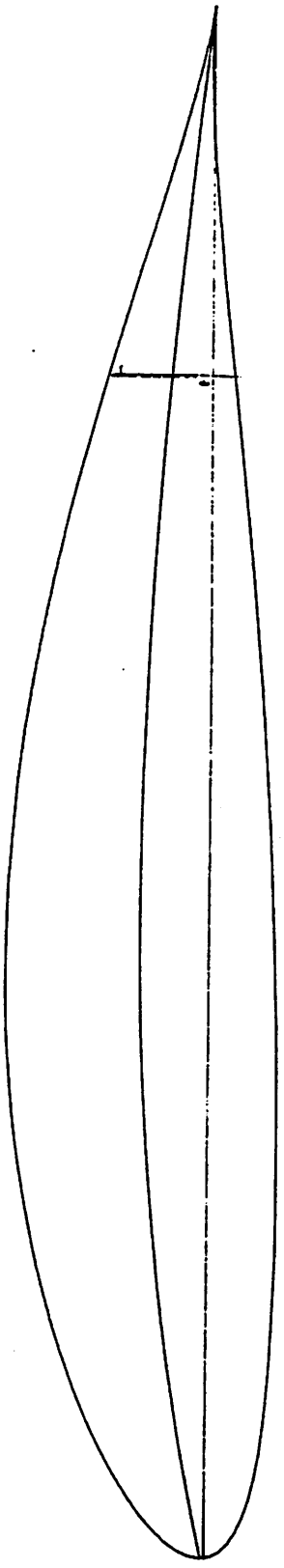

FX 84-W-175

Diagramm 4

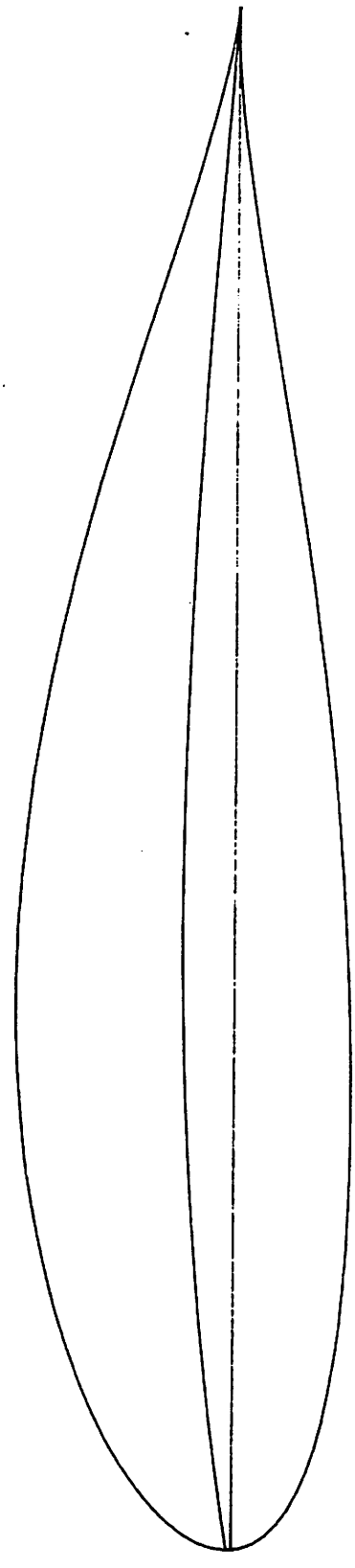

FX 84-W-218

Diagramm 5

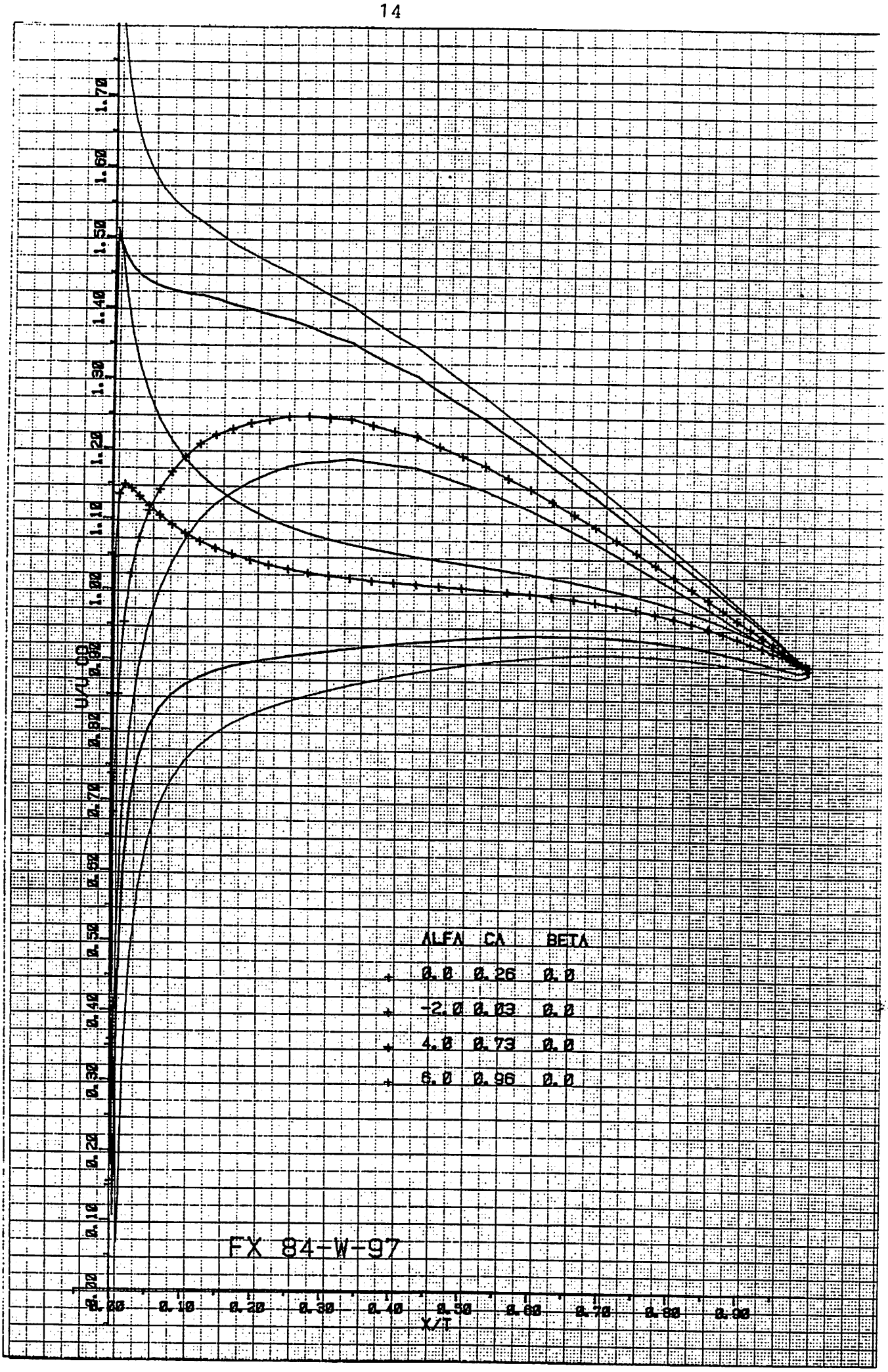
ALFA CA BETA
+ 0.0 0.26 0.0
+ -2.0 0.03 0.0
+ 4.0 0.73 0.0
+ 6.0 0.96 0.0
FX 84-W-97
U/U0
X/T
0.00
0.10
0.20
0.30
0.40
0.50
0.60
0.70
0.80
0.90
1.70
1.60
1.50
1.40
1.30
1.20
1.10
1.00
0.90
0.80
0.70
0.60
0.50
0.40
0.30
0.20
0.10

Diagramm 6

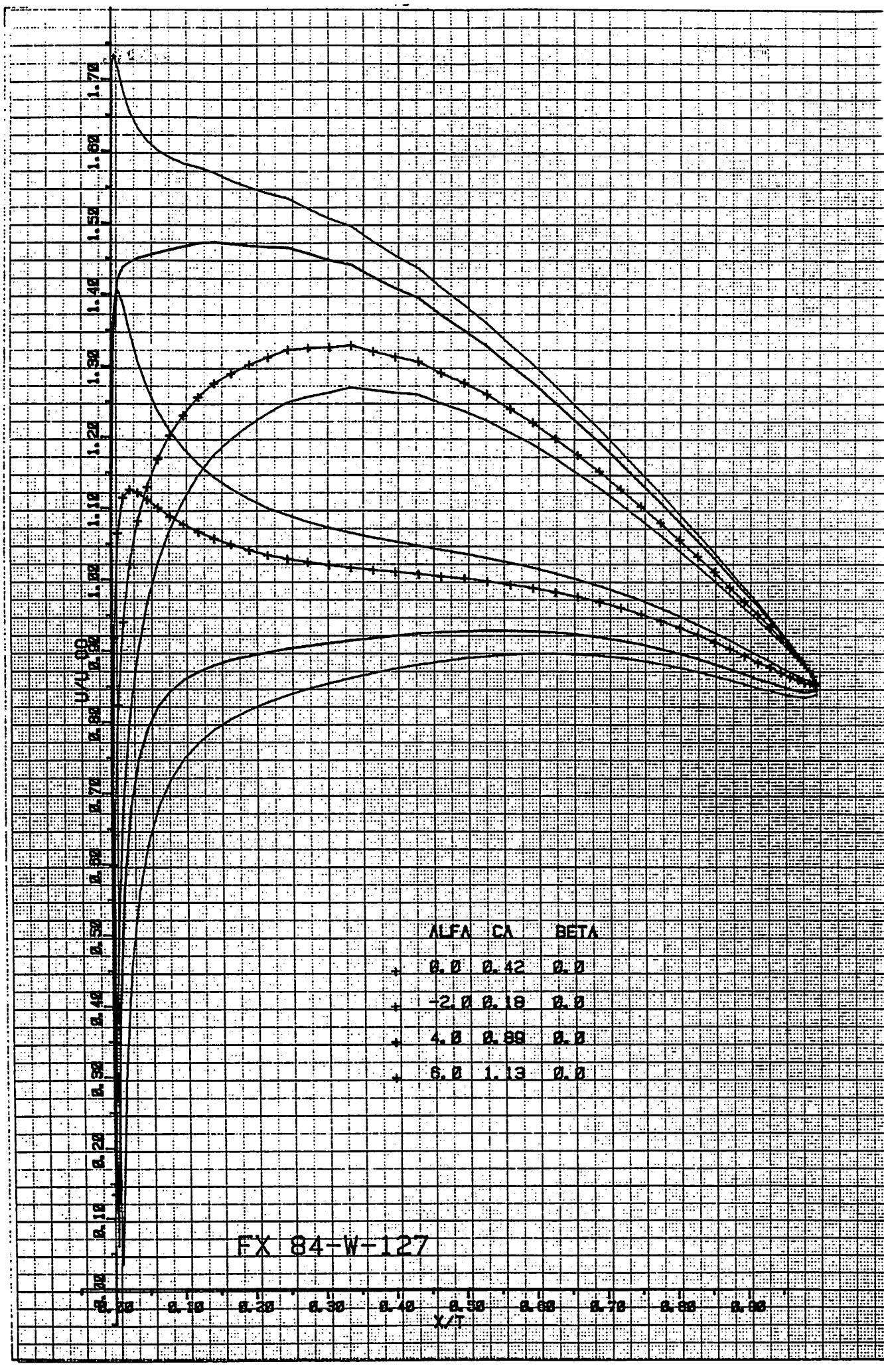
U/U∞
X/T
ALFA CA BETA
+ 0.0 0.42 0.0
+ -2.0 0.18 0.0
+ 4.0 0.89 0.0
+ 6.0 1.13 0.0
FX 84-W-127

Diagramm 7

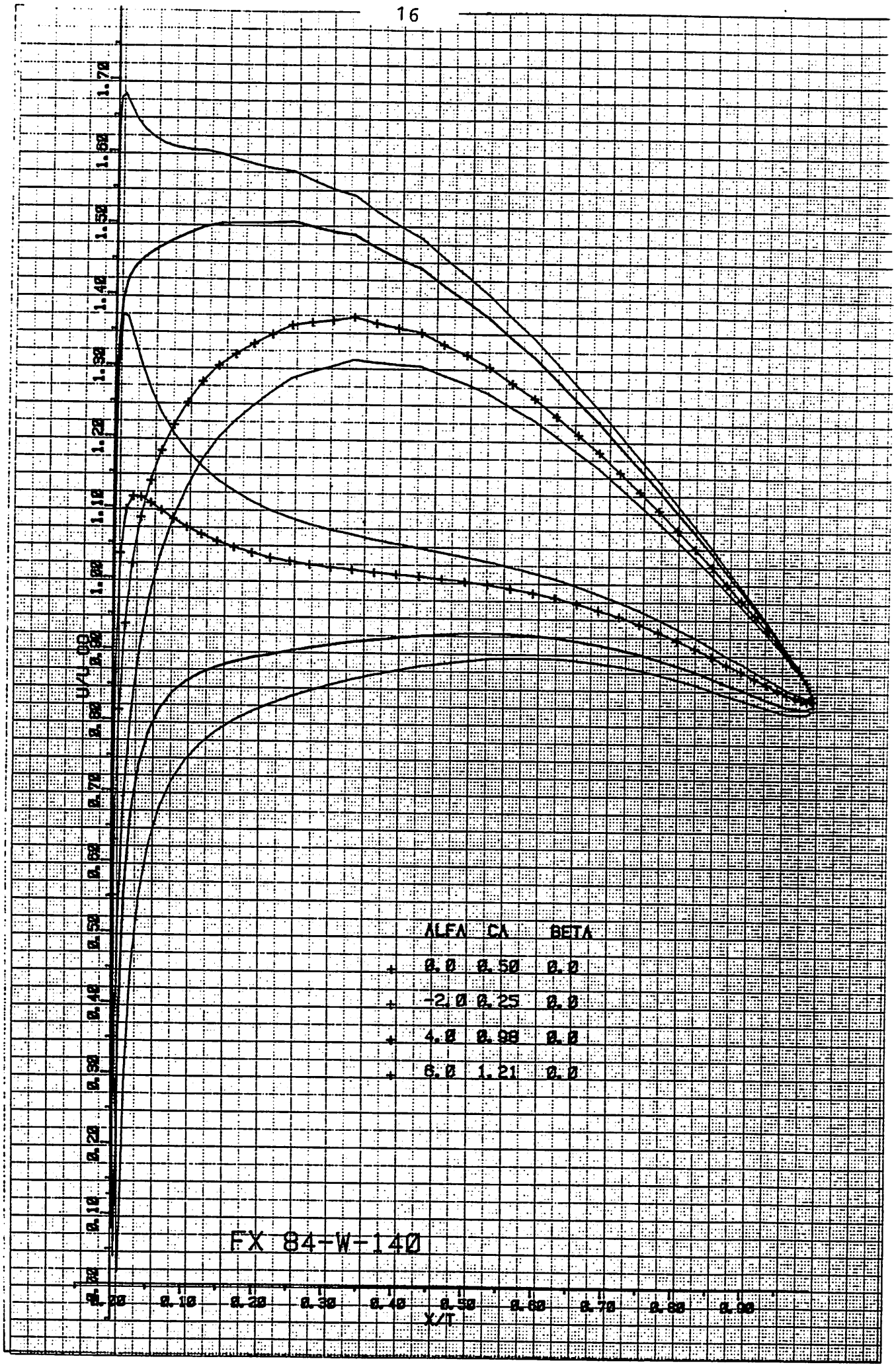
ALFA CA BETA
+ 0.0 0.50 0.0
+ -2.0 0.25 0.0
+ 4.0 0.98 0.0
+ 6.0 1.21 0.0
FX 84-W-140
U/Uo
X/T

Diagramm 8

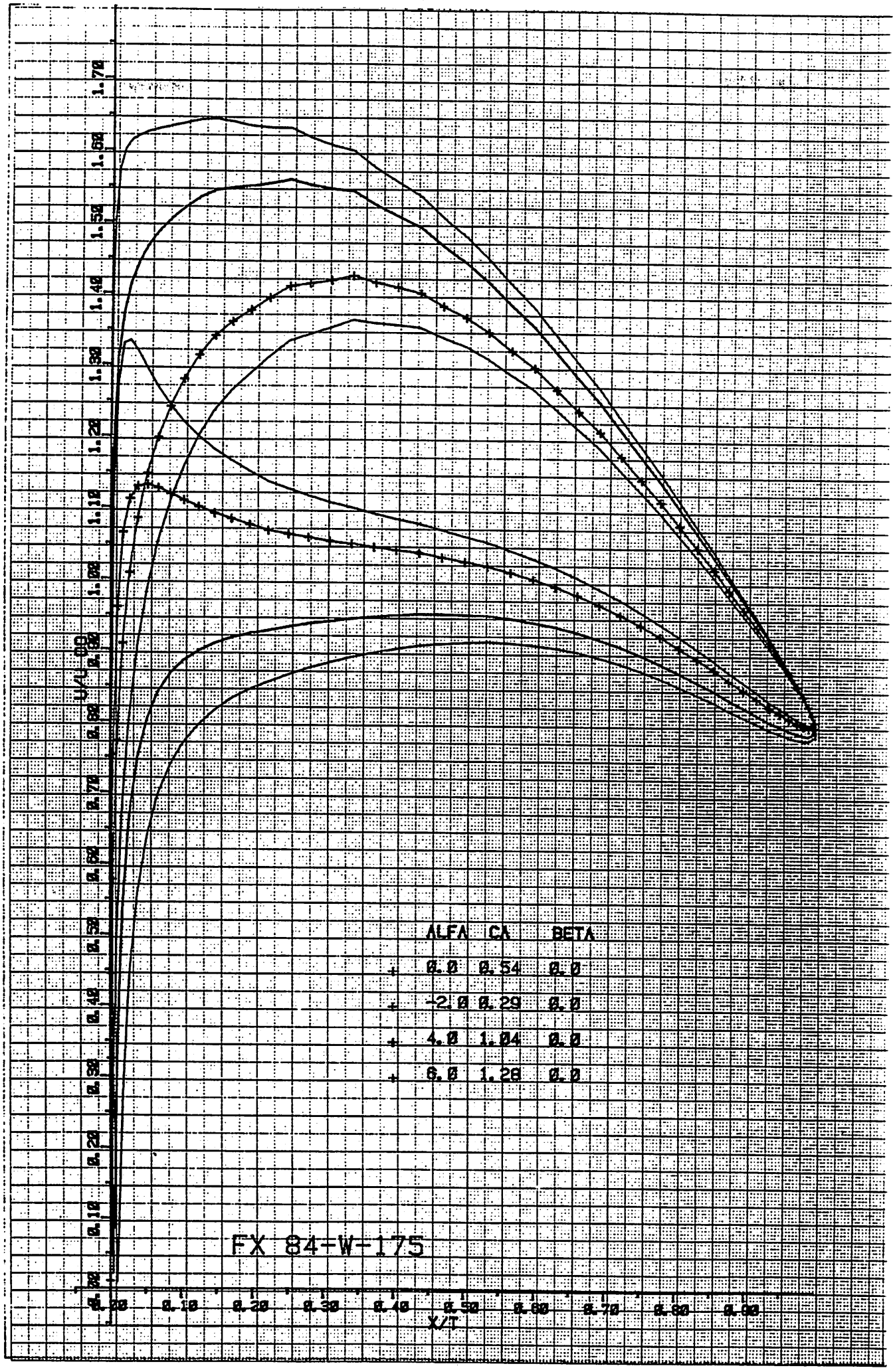
ALFA CA BETA
+ 0.0 0.54 0.0
+ -2.0 0.29 0.0
+ 4.0 1.04 0.0
+ 6.0 1.28 0.0
FX 84-W-175
U/U0
X/T
0.00
0.10
0.20
0.30
0.40
0.50
0.60
0.70
0.80
0.90
1.00

Diagramm 9

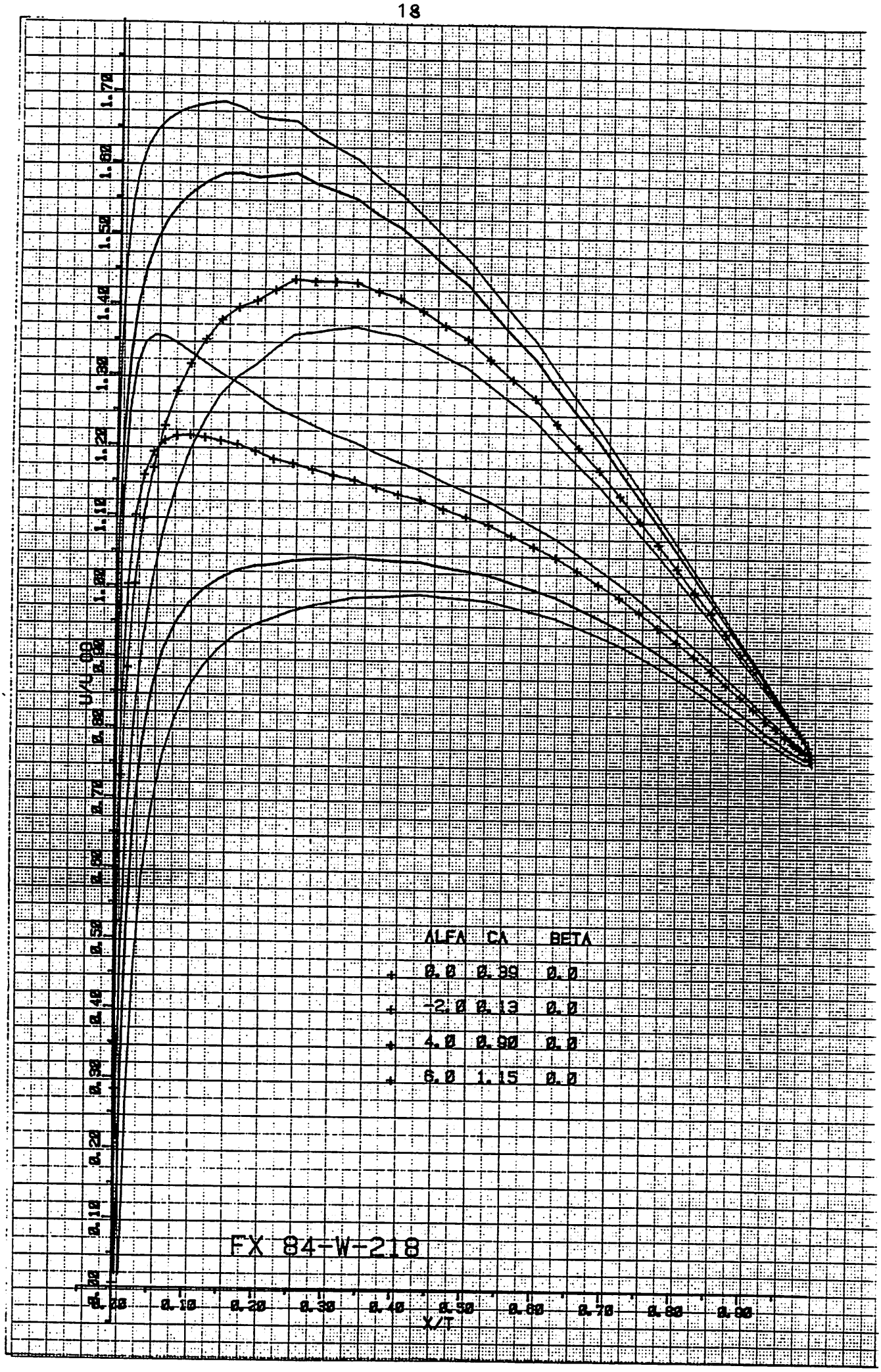

Diagramm 10

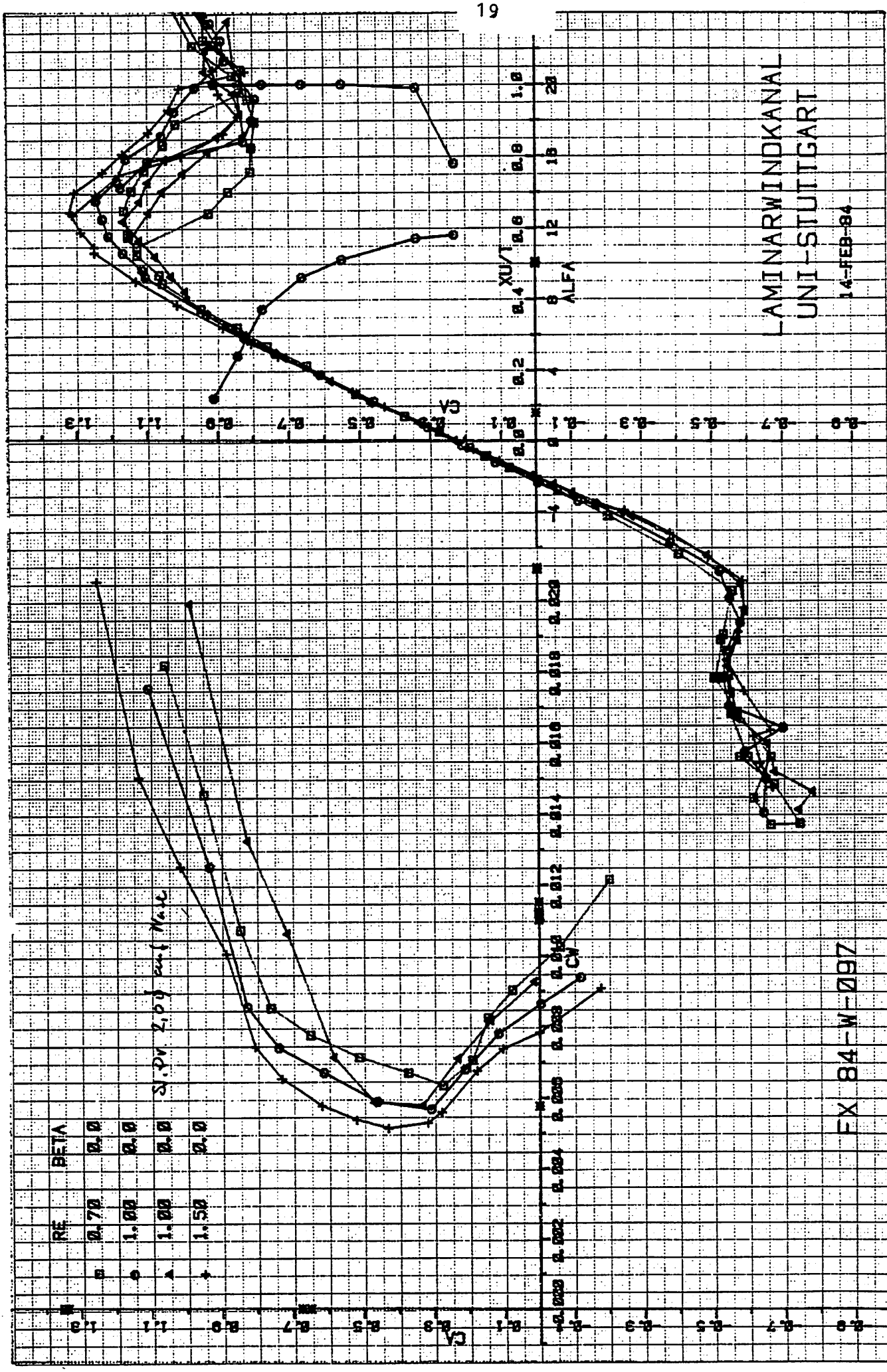
LAMINARWINDKANAL
UNI-STUTTGART
14-FEB-84
FX 84-W-097
RE BETA
0.70 0.0
1.00 0.0
1.00 0.0
1.50 2.0
CA
CW
XU/T
ALFA

Diagramm 11

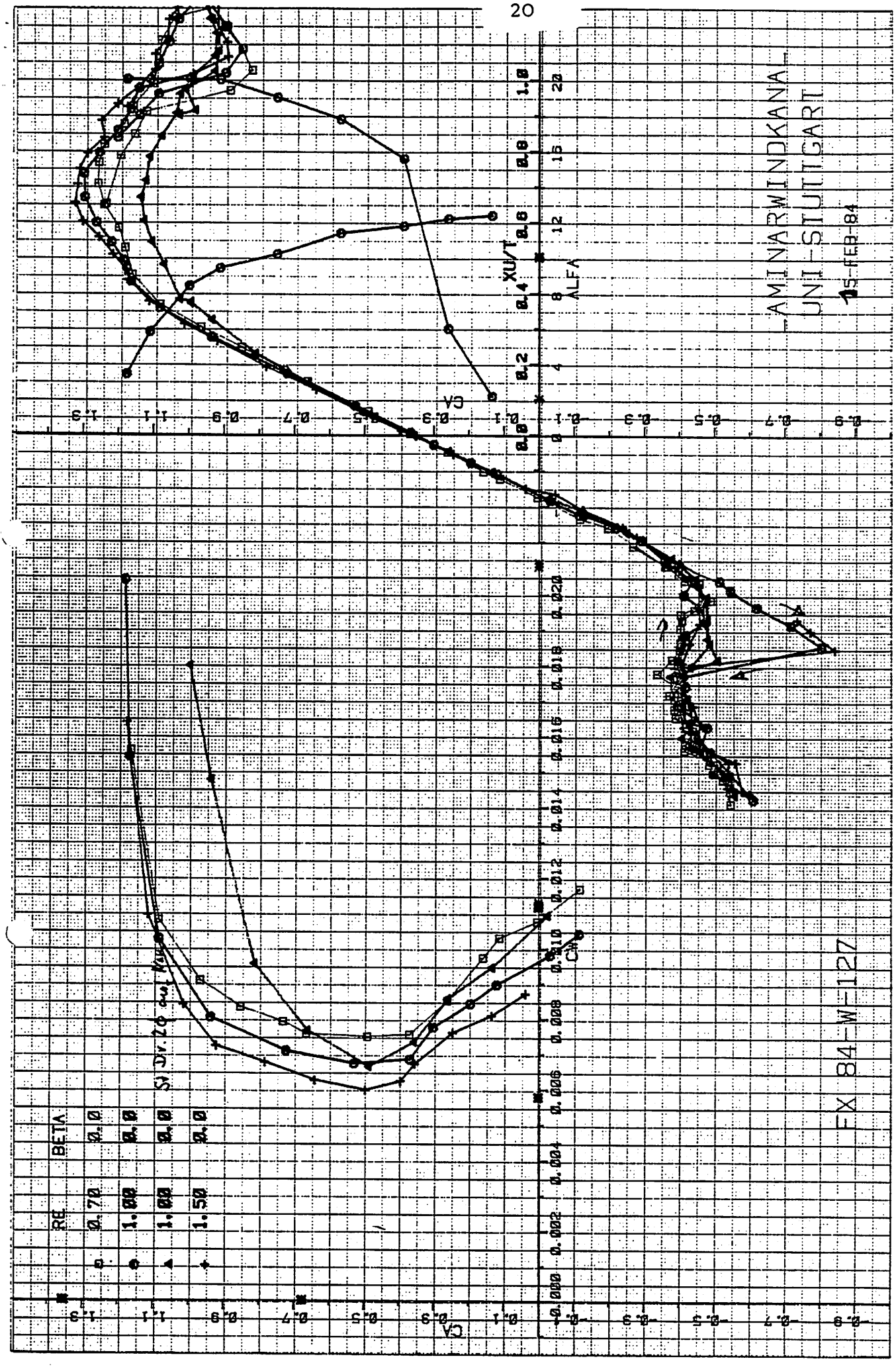
AMINARWINDKANA
UNI-STUTTGART
15-FEB-84
FX 84-W-127
POL 301
RE BETA
0.70 0.0
1.00 0.0
1.00 0.0
1.50 0.0
CA
ALFA
XU/T
CM

Diagramm 12

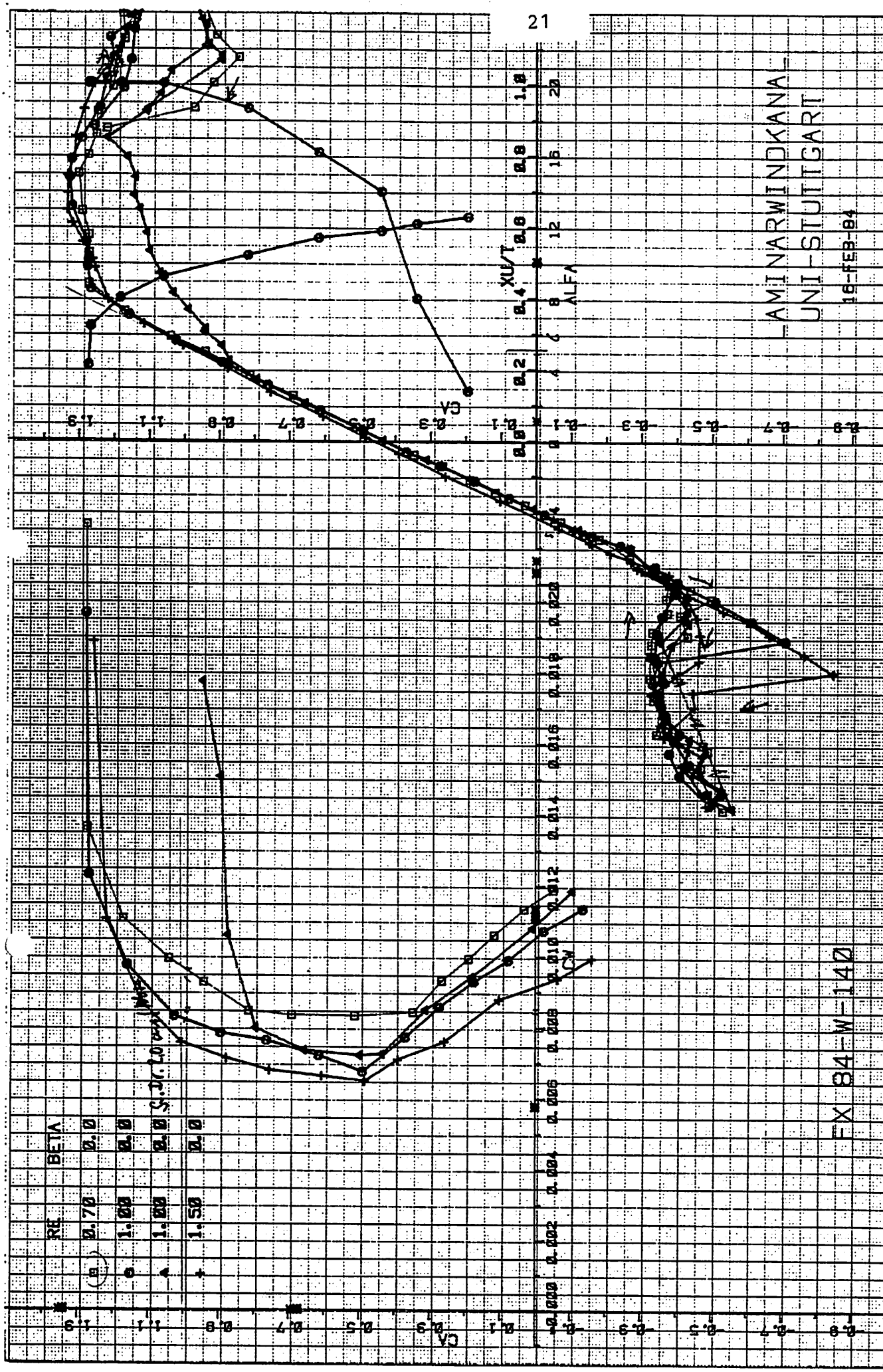

Pr 392

Diagramm 13

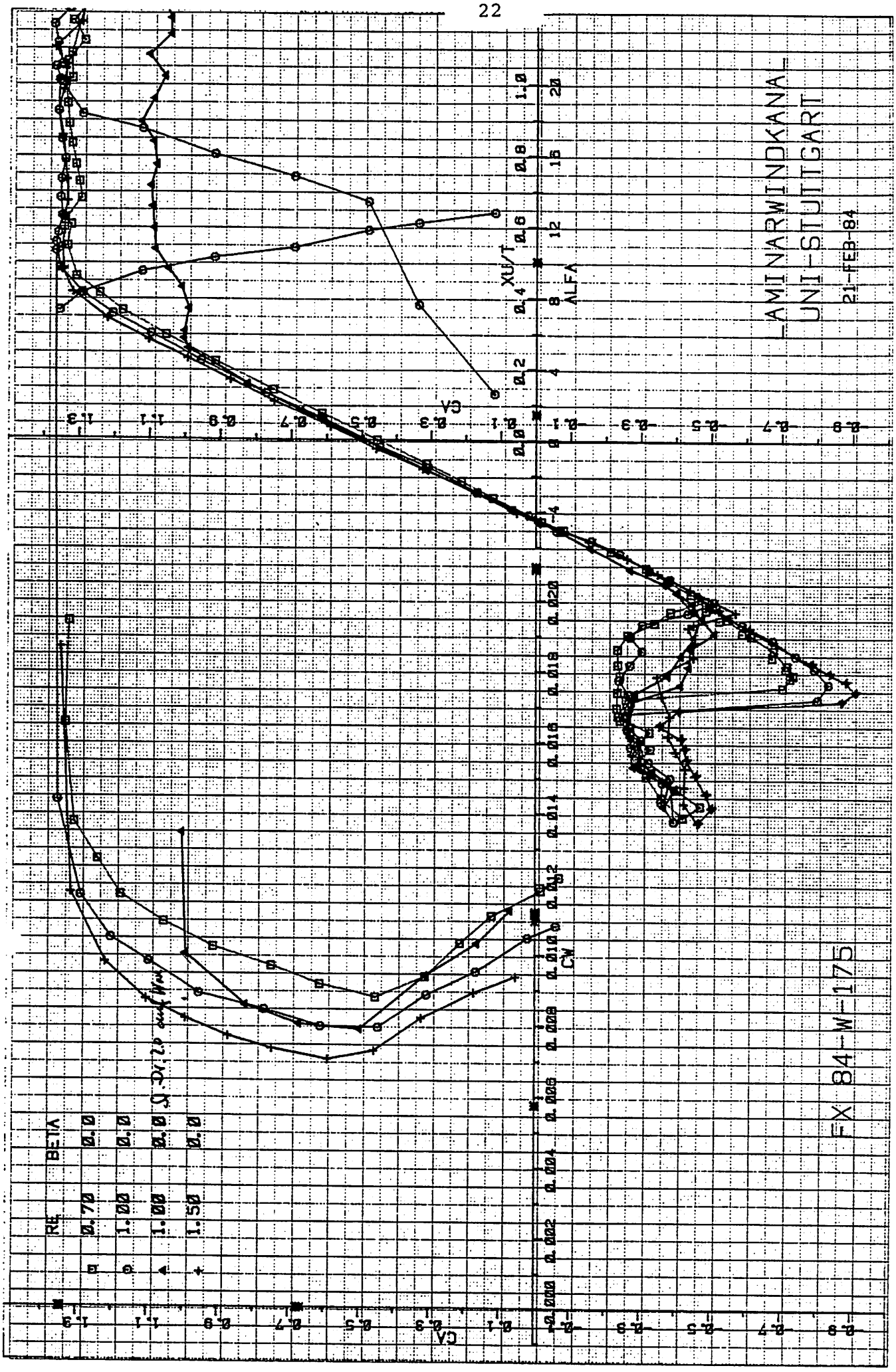
LAMINARWINDKANAL
UNI-STUTTGART
21-FEB-84
FX 84-W-175
RE BETA
2.700 0.0
1.000 0.0
1.000 0.0
1.500 0.0
CA
CW
ALFA
XU/T
POL 342

Diagramm 14

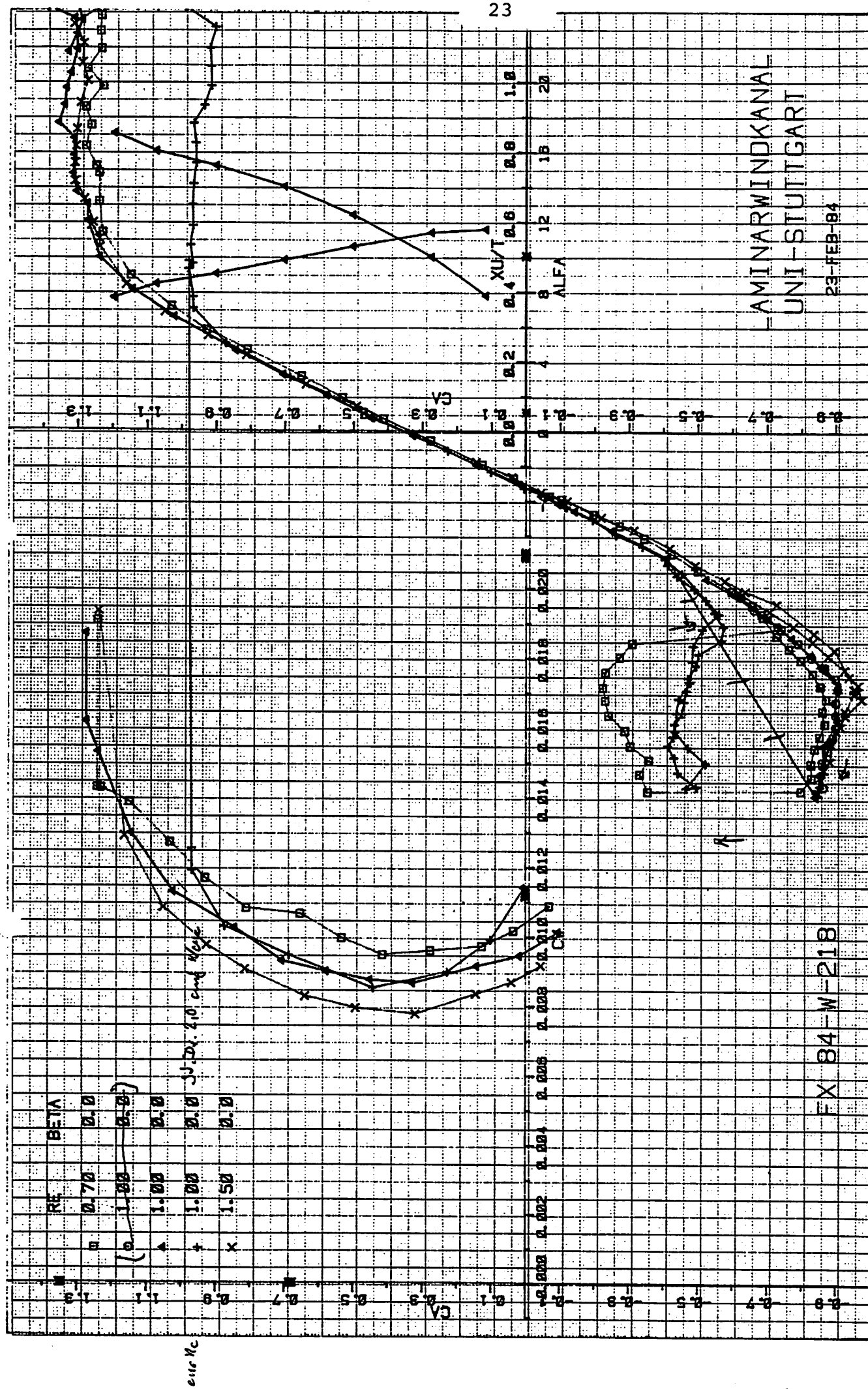
LAMINARWINDKANAL
UNI-STUTTGART
23-FEB-84
EX 84-W-21B
RE
BETA
ALFA
XU/T
CA
CW
Rl 394

Diagramm 15

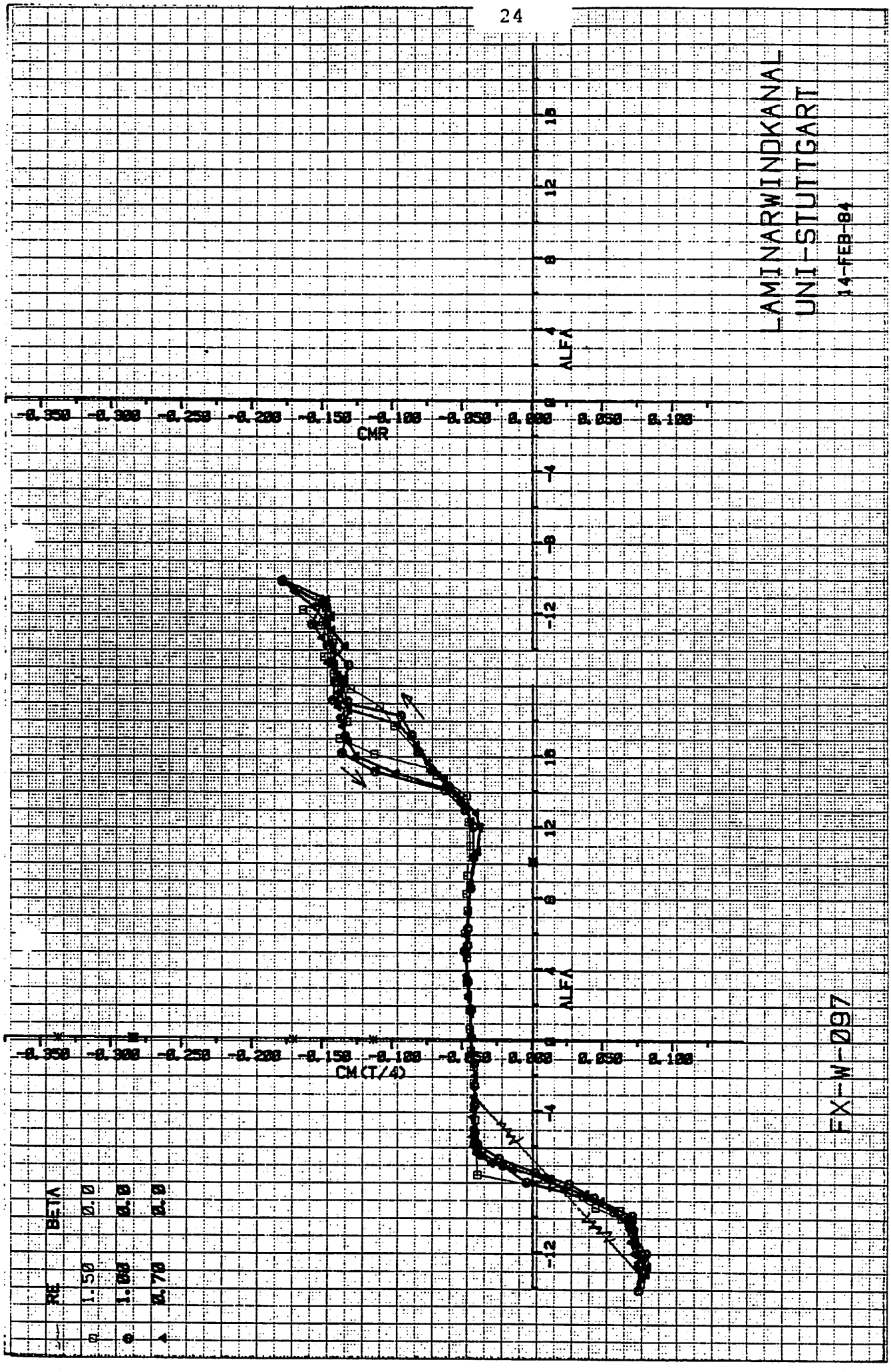

CM 300

Diagramm 16

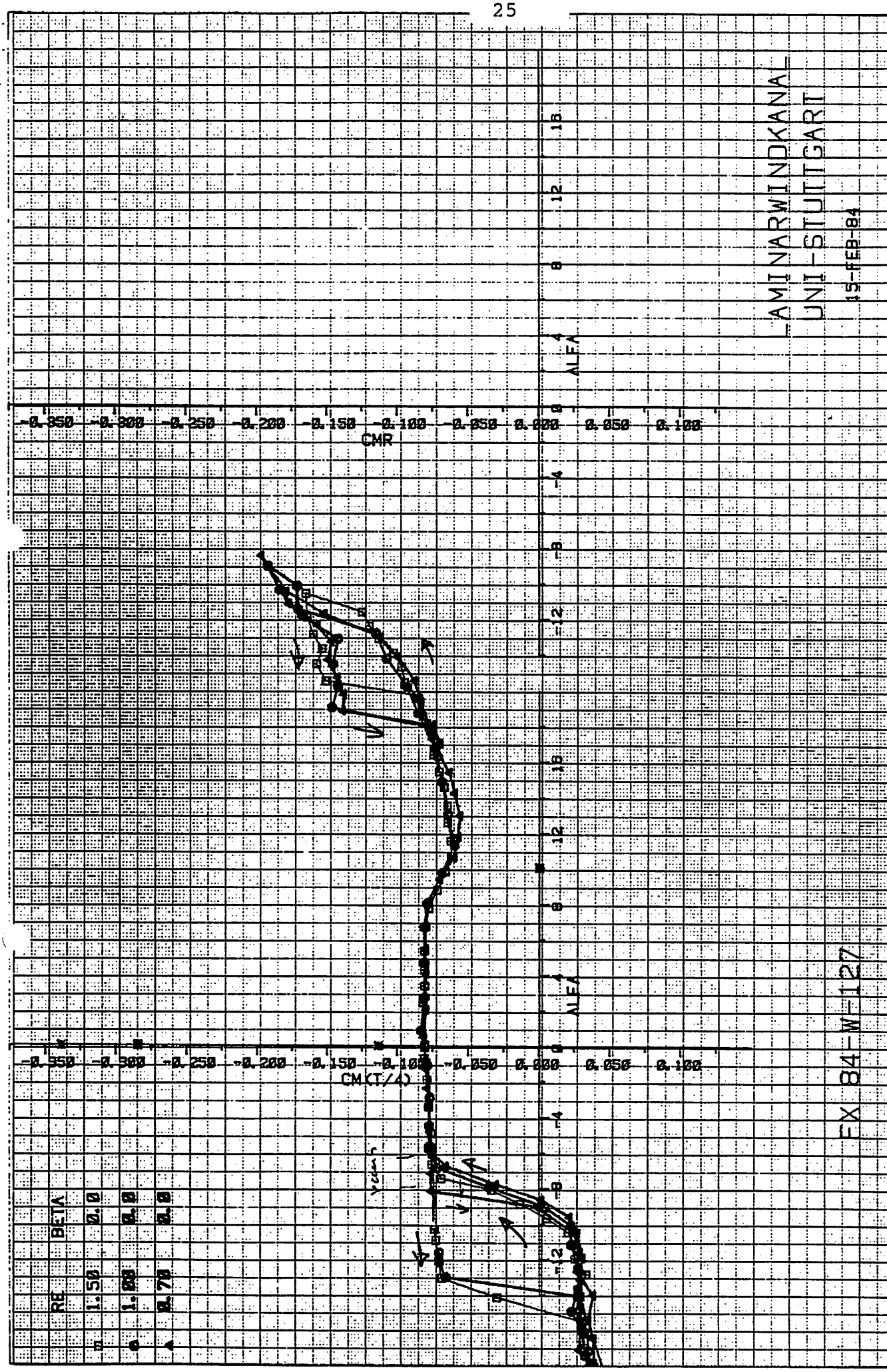
-AMINARWINDKANA-
UNI-STUTTGART
15-FEB-84
CM 391
EX 84-W-127
CMR
CM(T/4)
ALFA
RE
BETA
1.50 2.0
1.00 0.0
0.70 0.0

Diagramm 17

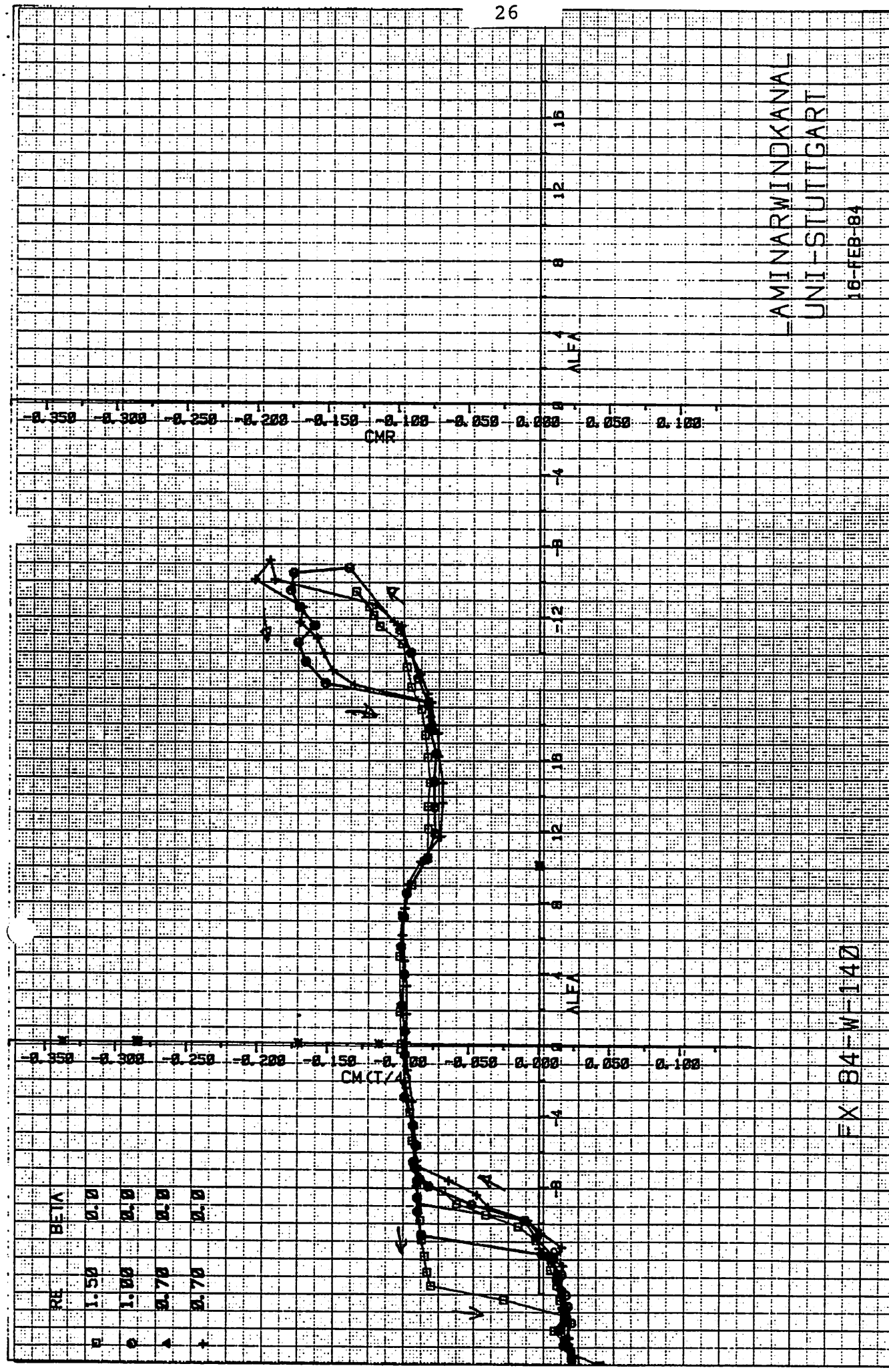
LAMINARWINDKANAL
UNI-STUTTGART
16-FEB-84
FX 84-W-140
CM 342
ALFA
CMR
CM(T/4)
BETA
RE
1.50
1.00
2.70
2.70
2.0
2.0
2.0
2.0

Diagramm 18

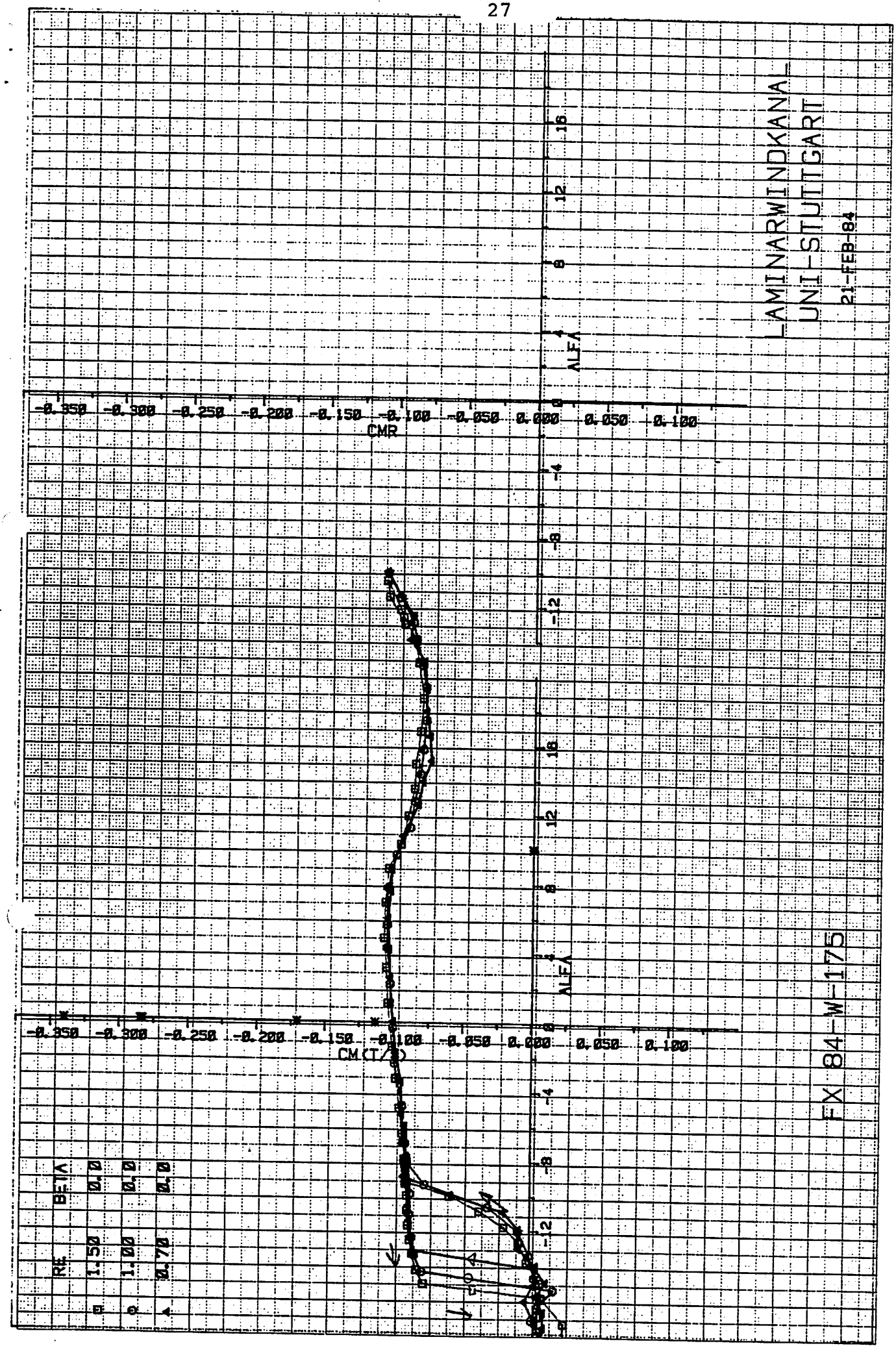
LAMINARWINDKANAL
UNI-STUTTGART
21-FEB-84
FX 84-W-175
CM 393
CMR
CM(T/S)
ALFA
BETA
RE
1.50
1.00
0.70
0.0
0.0
0.0

Diagramm 19

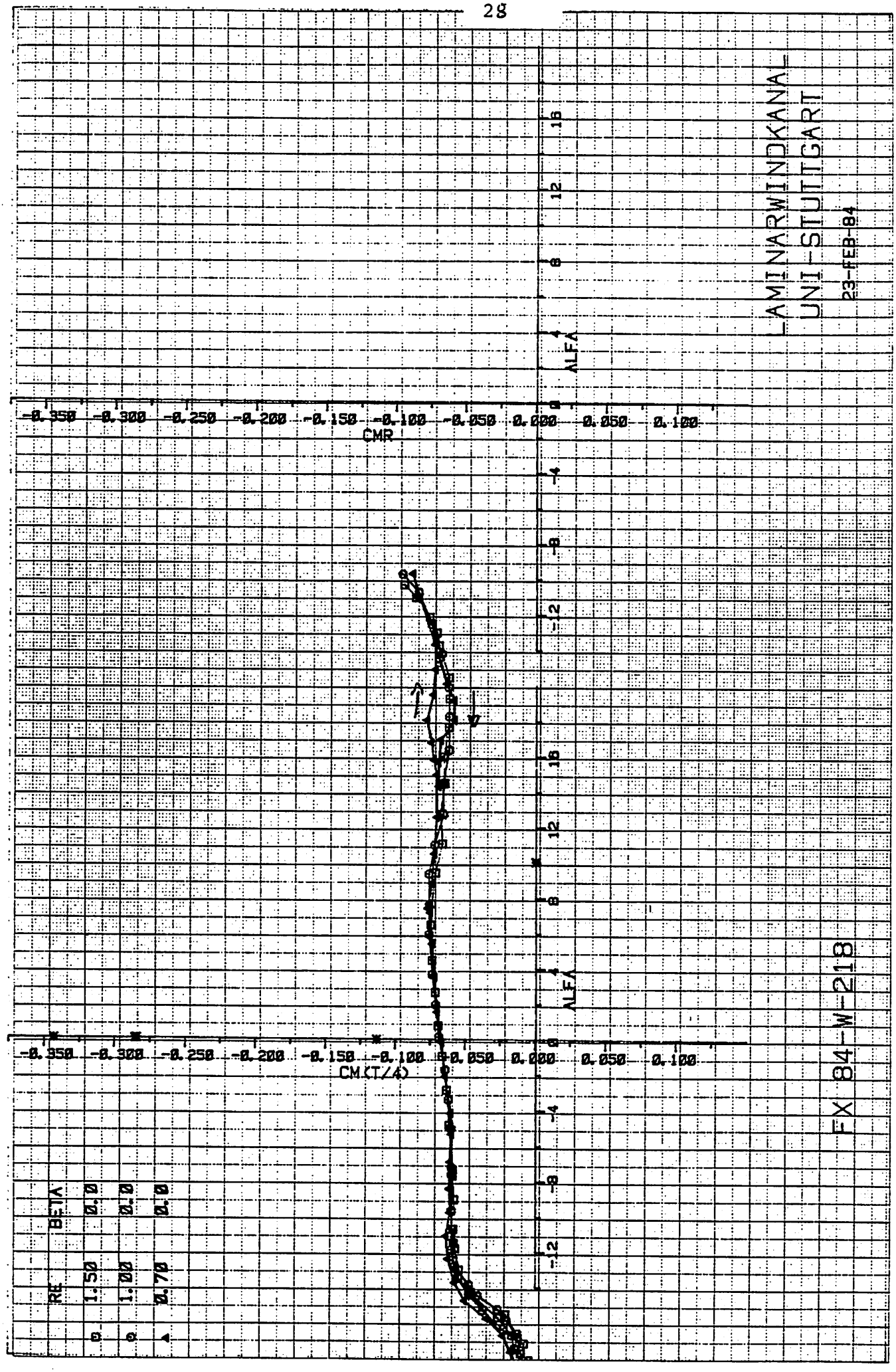

Diagramm 20

CM 394

'DEVELOPMENT IN AERODYNAMIC CALCULATION METHODS'

M.B. ANDERSON

UNSTEADY AERODYNAMICS

The model includes :-

a) for the attached flow region the loads are calculated via a generalised indicial lift function based on the Wagner function;

b) the angle of attack is defined at the 3/4 chord location and thus pitching velocity and virtual mass terms are included;

c) leading edge stall is incorporated by means of a simple time delay based on distance travelled in semi-chord;

d) trailing edge stall is incorporated via Kirchoffs law and two first order lags.

LEADING EDGE STALL

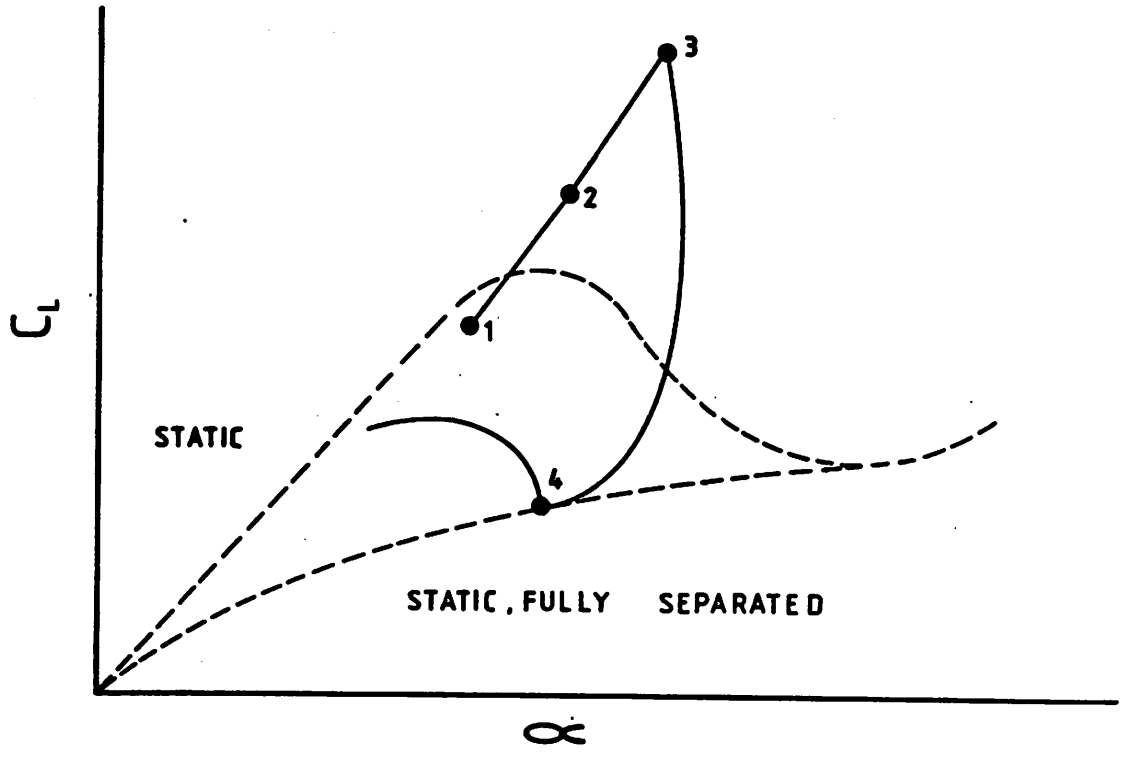

Fig. 1

.1 Delimits the region of attached flow determined by the break in pitching moment;

1-2 Generation of leading edge vortex;

.2 Pitching moment divergence;

2-3 Leading vortex traverses chord;

.3 Leading vortex shed from trailing edge;

3-4 Lift decays to fully separated conditions;

.4 Re-attachment

TRAILING EDGE STALL

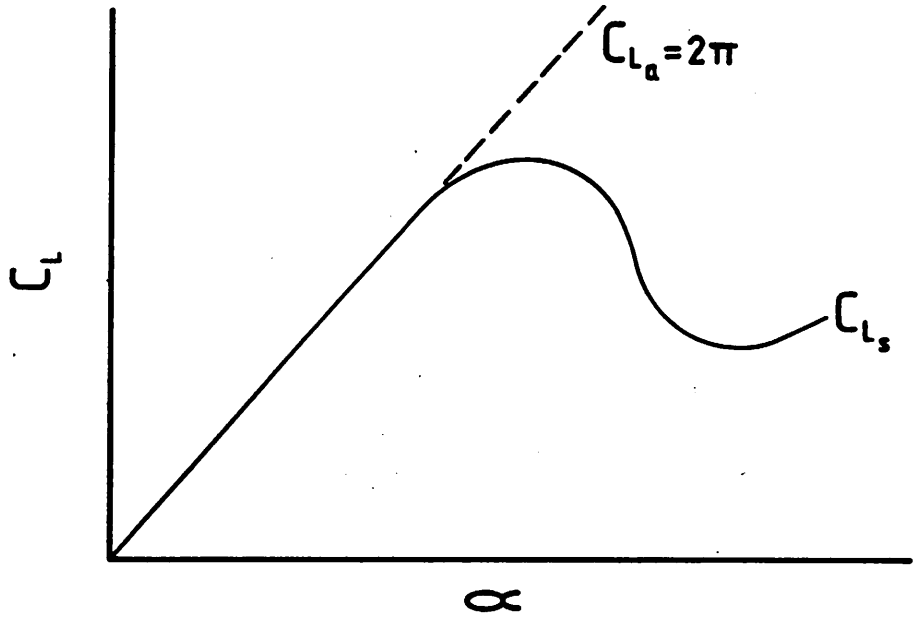

Fig. 2

Kirchoff Flow Approximation

$$\frac{C_{L_s}}{C_{L_a}} = \frac{1}{4}\left(1 + f^{1/2}\right)^2$$

(f = flow reversal point)

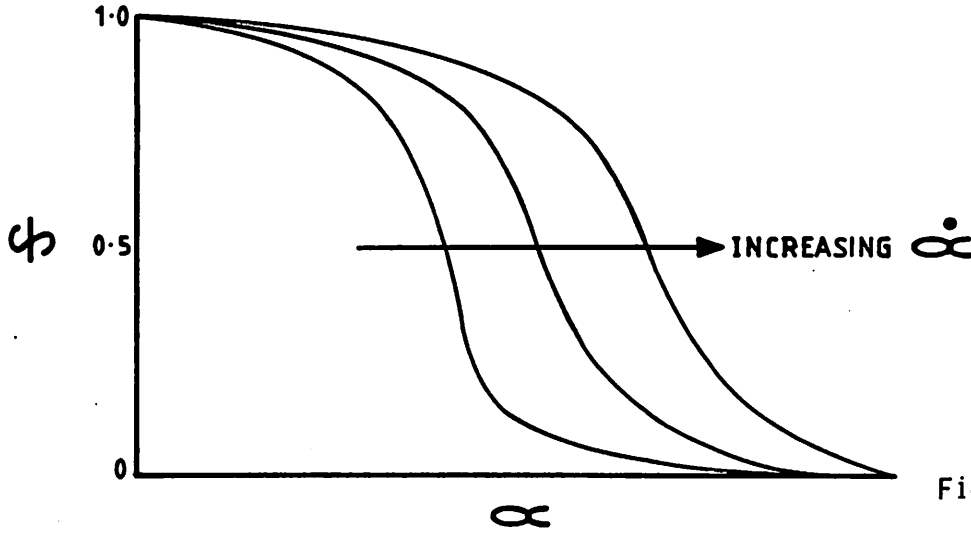

Fig. 3

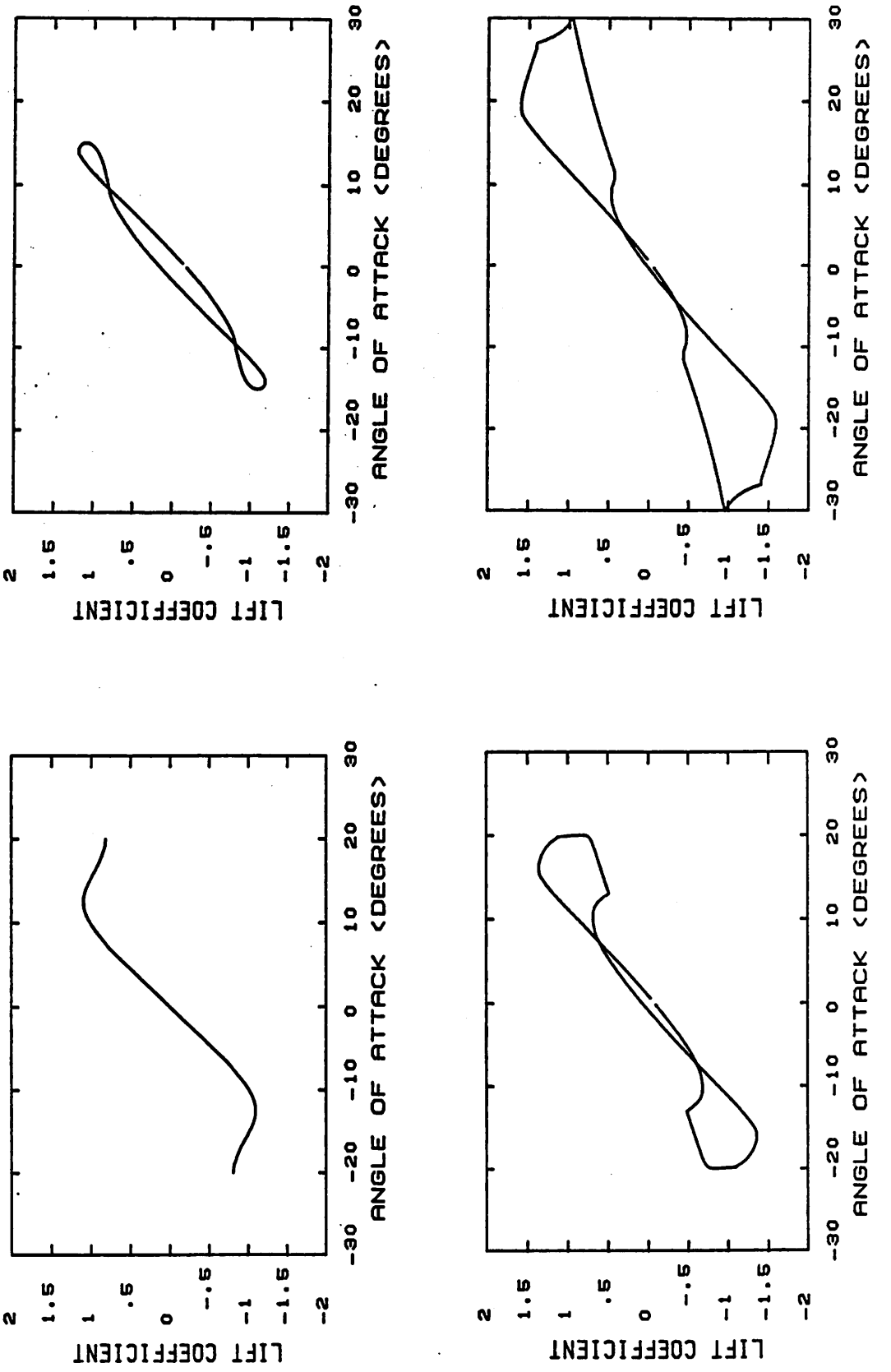

Fig. 4 NACA 0015, chord 1.25m oscillating about it 1/4 point at a reduced frequency of 0.05.

TURBULENCE : TIME DOMAIN SIMULATION

A set of N homogenous Gaussian processes (f; (y) (j = 1,2, ...N), with zero mean can be generated from the following series;

$$f_j(y) = \sum_{m=1}^{N} \sum_{L=1}^{L} |H_{jm}(\omega_L)| (2\Delta\omega)^{1/2} \cos(y\omega_L + \theta_{jm}(\omega_L) + \phi_{mL}) \quad (1)$$

where the matrix H(w) satisfies the equation

$$S(\omega) = \bar{H}(\omega) H(\omega)^T$$

where S(w) is the target cross-spectral density matrix and is Hermitian. L is the number of discrete frequencies w_L and θ_{jm} represents the phase of H_{jm}. ϕ_{mL} are a set of random numbers taken from a uniform distribution between 0 and 2π. Equation (1) can be thought of representing a set of N(N+1)/2 interconnected filters through which n indpendent white noise sources are passed, see Fig. 5. An efficient way to evaluate the double summation is to use FFT techniques.

A comparison of the real (from Battelle experiment, see Fig. 6) and simulated theoretical estimates of the single point power spectra of the velocity fluctuations are shown in Fig. 7. Fig. 8 presents a comparison between the coherence function estimates of the real and simulated data. Presented in Fig. 9 is an isovent map of a horizontal slice of the 3-dimensional simulated wind field; contours are at 0.5 m/s intervals.

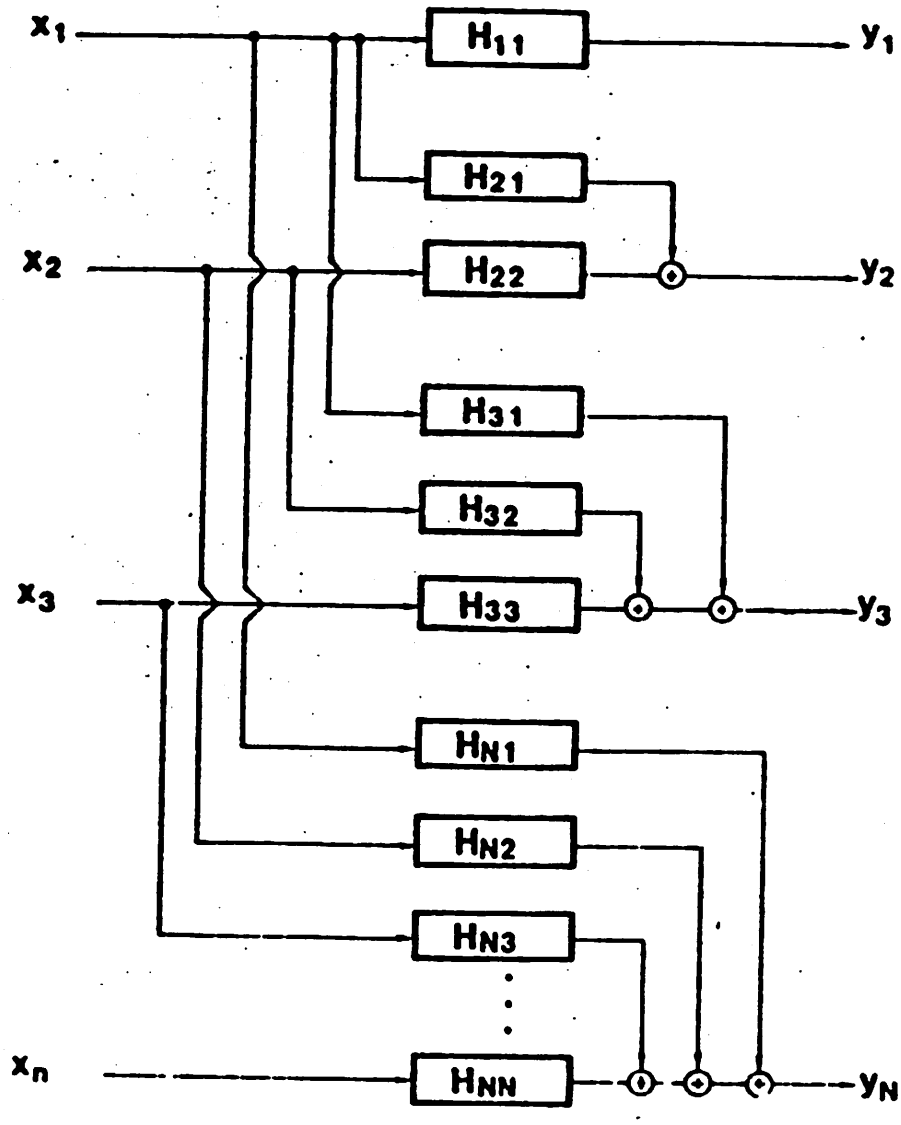

Fig. 5 Schematic representation of equation 1.

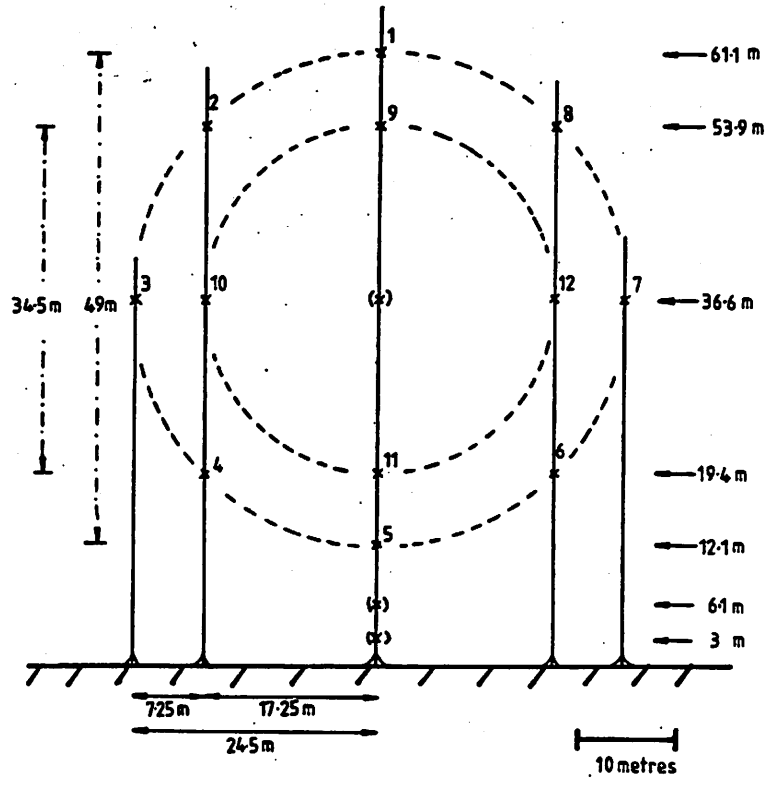

Fig. 6 Geometry of Battelle vertical plane array.

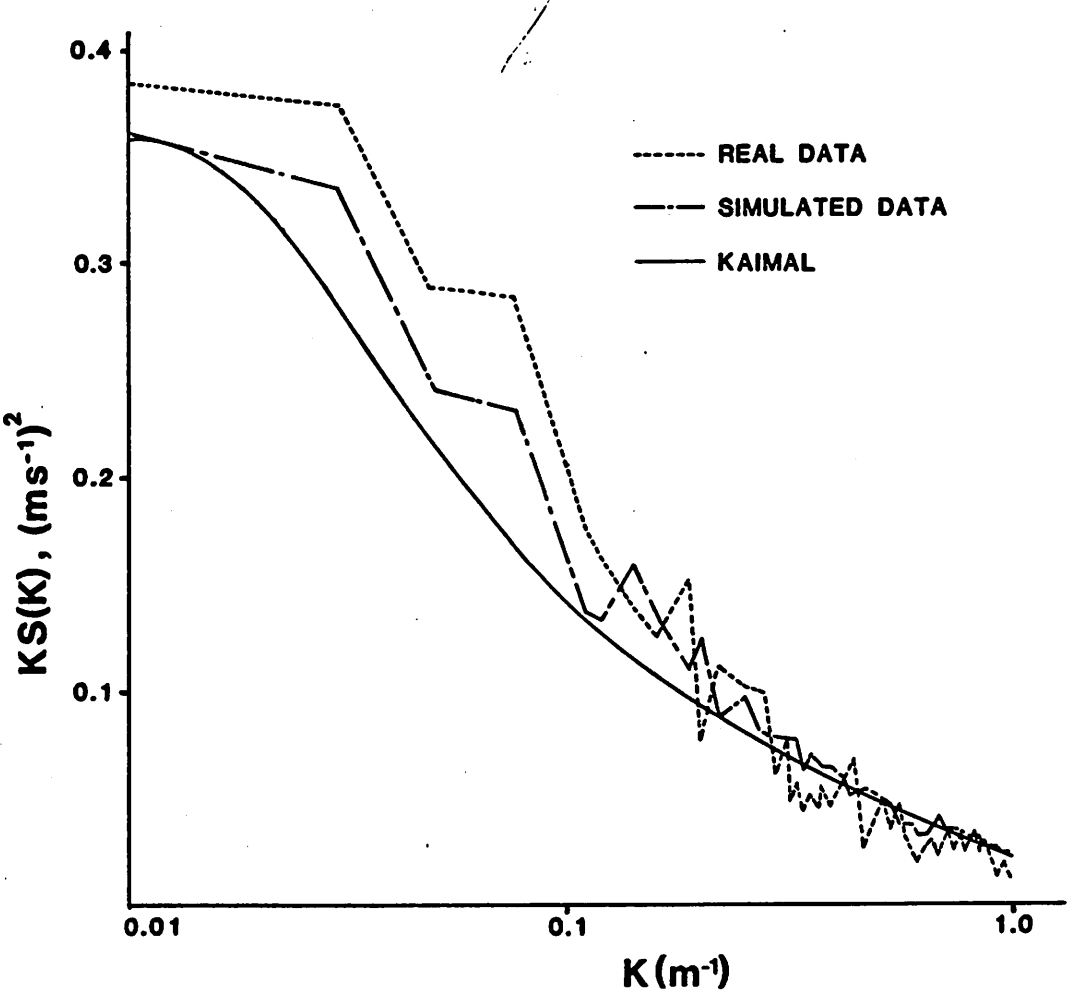

Fig. 7 A comparison of the real, simulated and theoretical estimates of the single point power spectra of the wind velocity fluctuations for anemometer position 1.

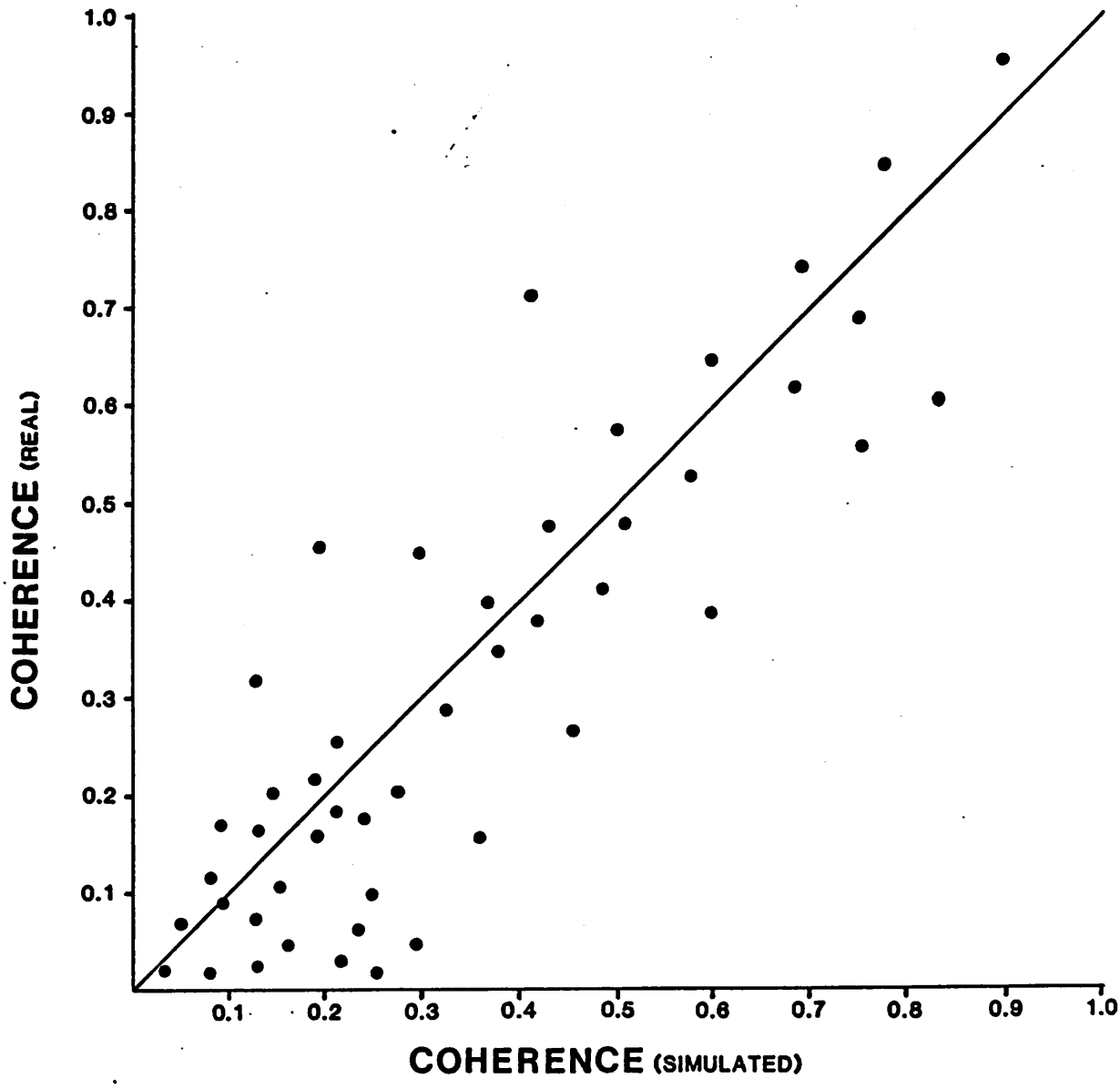

Fig. 8 A comparison of the coherence function estimtes of the real and simulated wind fields.

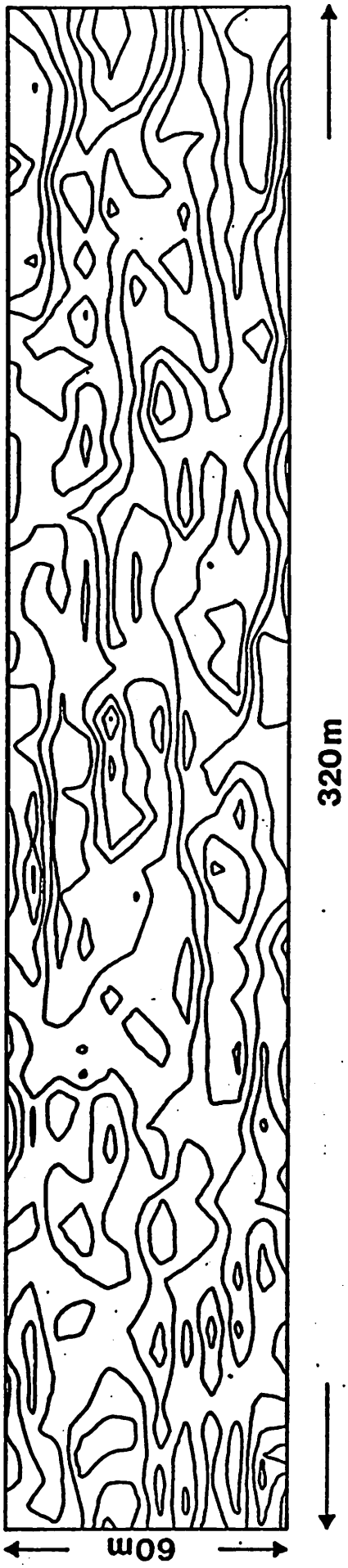

Fig. 9 Isovent map of a horizontal 2-dimensional slice of a 3-dimensional simulated wind field. Contour interval is 0.5 m/s.

AN ANALYTICAL THEORY FOR ROTOR-TIPVANE PERFORMANCE AND COMPARISON WITH EXPERIMENTAL RESULTS

Th. van Holten

Summary
A theoretical method for the performance estimation of tipvane wind turbines is outlined in the paper, and compared with some full-scale experimental results recently obtained. The performance estimates are based on a flowmodel where an infinite number of turbine blades is assumed. Agreement between theory and experiments is shown to be satisfactory.

1. Introduction

At the Delft University of Technology research is done on tipvane windturbines. Tipvanes are relatively small auxiliary wings mounted on the tips of turbine-blades (fig. 1). The vane lift is in the direction of the rotorcentre so that by reaction the oncoming flow is deflected radially outwards. The resulting diffuser effect causes an increase of massflow through the turbine (fig. 2). Compared with conventional turbines, higher powercoefficients are possible, even surpassing the socalled Betz-limit for windturbines.
The laboratory research has covered windtunnel- and towing tank model experiments (ref. 1). Full-scale performance testing has started recently on a 8,5 m diameter rotor. In view of the lack of experience with rotors of such an unconventional configuration, careful theoretical and experimental aero-elastic investigations on the full-scale rotor have preceded the aerodynamic experiments (ref. 2 and 3). The aerodynamic investigations were likewise accompanied by the development of theory:

a) computer programs were developed for the detailed analysis of loaddistributions (ref. 4),
b) a flowmodel based on the assumption of an infinite number of blades was developed for the purpose of performance estimates.

It is the latter analysis which will be briefly outlined in the present paper, and the results of which will be compared with some preliminary full-scale test-results now available.

2. Analytical model of the flow

The model described below was developed with the purpose to analyze the overall forces, total power, and average velocities. It assumes an infinite number of turbineblades and tipvanes. Such a model of the flow is equivalent to a time-averaged analysis. The model is based on the assumption of small disturbances, which means that free vorticity convects along trajectories parallel to the undisturbed velocity.

2.1 Tipvane-model

The functioning of the tipvanes is represented by a circular band of vorticity as sketched in fig. 3. The way to arrive at such a simplified flow model will be explained with the help of fig. 4, which shows socalled "undersynchronous operation", i.e. a flowcondition where no direct vortex interaction occurs.
We assume for a moment that the lift on the tipvanes is constant along the span, so that the trailing vorticity is concentrated in two discrete tipvortices. In linearized theory these vortices lie on a straight cylindrical surface with radius R and trace out helical paths. The flow associated with this vortex configuration is unsteady in an inertial frame of reference. The time averaged flow

field is obtained by taking the limit of an infinite number of tipvanes, taking care that the same radial force per unit length along the turbine circumference is generated by the infinite array of tipvanes as by the finite number of tipvanes. The helical vortices in this limit form a continuous, semi-infinite vortex-cylinder. Now it should be remembered that the tipvorticity emanating from the upstream vane-tips has equal strength but opposite direction compared with the trailing vorticity from the downstream vane-tips. The two vortex-cylinders associated with the upstream and downstream vane-tips cancel each other, except for a band of vorticity with a width equal to the span of the tipvanes. We have thus arrived at the model of fig. 3. When the vane-lift points towards the centre-line of the turbine, an overall circulation is established with such a direction that the vortex band induces a Venturi-type of flow like in fig. 2. A more careful analysis given in ref. 5 shows that the same is true for the case of general spanwise liftdistributions along the tipvanes.

The average velocity increment in the disc plane due to the functioning of the tipvanes will be denoted by $\overline{\delta V}$, and may be expressed like:

$$\overline{\delta V} = \alpha \cdot \frac{\Gamma}{R} \tag{1}$$

where Γ stands for the total circulation of the circumferential band of vorticity. The proportionality constant α is a function of the spanwise lift distribution along the tipvanes. According to an asymptotic analysis given in ref. 6, in the case of an elliptic distribution it is given by:

$$\alpha = \frac{1}{\pi} \{\ln \left(\frac{4}{b_e/R}\right) + \tfrac{1}{2}\} \tag{2}$$

where b_e is the effective span, i.e. the part of the span where due to vortex interactions (explained below) most of the lift is concentrated.
The radial distribution of the velocity $\delta V(x)$, (where $x = r/R$), induced by the vortex band may be approximated by:

$$\delta V(x) \cdot \frac{2\pi R}{\Gamma} = \pi - \{\pi - \delta V(1) \frac{2\pi R}{\Gamma}\} e^{-A(1-x)} \tag{3}$$

where

$$\delta V(1) \cdot \frac{2\pi R}{\Gamma} = \frac{4}{b_e/R} \left(1 - \frac{b_e/R}{16}\right) - \tfrac{1}{2} \ln \left(\frac{b_e/R}{32}\right) \tag{4}$$

$$A = \frac{1}{2C} + \frac{1}{2C}\sqrt{1 - 4C} \tag{5}$$

with

$$C = \frac{\pi/2 - \alpha \cdot \pi}{\pi - \delta V(1) \frac{2\pi R}{\Gamma}} \tag{6}$$

The band of vorticity associated with the tipvanes induces in its own plane an axial velocity δw of an average magnitude

$$\delta w = \beta \cdot \frac{\Gamma}{R} \tag{7}$$

This selfinduction velocity δw corresponds to the convectionvelocity of a free vortex ring in still air. The proportionality constant β is, again according to the analysis of ref. 6, given by:

$$\beta = \frac{1}{4\pi} \cdot \{\ln \left(\frac{32}{b_e/R}\right) - \frac{5}{6}\} \tag{8}$$

The above given theory remains valid in the limiting case of "synchronous" operation, i.e. the flow condition where the vortex from the upstream vane-edge

just touches the downstream edge of the next vane.

We now proceed to the case of socalled "over-synchronous" operation, i.e. a condition where strong vortex-interaction occurs. In fig. 5 the array of tip-vanes is drawn in a flat plane as if one were looking down on a formation flight of birds. Looking from the rear of the formation there is a certain amount of overlap of the wingspans so that a part of each vane is immersed in the downwash of the preceding one. Fig. 6 shows the resulting liftdistribution along a vane, as calculated by the methods described in ref. 4. It is seen that the part of the span which is immersed in a downwash region loses its lift. As a consequence the tipvortex originating in this region of the vane is shifted inboard, towards the edge of the more effective part of the vane. This trailing vortex is thus shifted towards the point where the vane is "hit" by the tipvortex of the preceding vane (fig. 5). The result is, that the newly formed tipvortex and the vortex from the preceding vane almost entirely annihilate each other. What has been left is a "saw-tooth" vortex running from vane to vane, roughly forming a vortex ring around the turbine (fig. 7). Numerous flow visualisations have confirmed the actual occurrence of the saw tooth vortex. The saw tooth vortex of the real flow is in fact the same as the vortex band of the linearized flowmodel of fig. 3, be it in a rolled-up form. The model of fig. 3 and the results (1) through (8) are applicable to both under- and over-synchronous operation, since the strong vortex interactions in fact result in synchronous operation at an effectively reduced span b_e (socalled "auto-synchronization").
The total circulation Γ may now be related to the lift of the vane by considering the bound part of the saw-tooth:

$$\Gamma = \tfrac{1}{2}\, \hat{C}_\ell \quad c \quad \Omega R \tag{9}$$

where $\hat{C}_\ell$ is the maximum liftcoefficient occurring somewhere along the vane-span. In the saw tooth model the liftcoefficient would equal $\hat{C}_\ell$ for all the sections along a part of the span equal to b_v where b_v (the socalled "vortex span") is the lateral distance between the free branches of the saw tooth vortex. In the real flow, C_ℓ varies more smoothly along the vane-span of course (see fig. 6). We may write:

$$\hat{C}_\ell = C_L \cdot \frac{b}{b_v} \tag{10}$$

and by combining eqs. (9) and (1) it is thus found:

$$\frac{\overline{\delta V}}{U} = \frac{\alpha}{2} \cdot C_L \frac{c}{R} \frac{b}{b_v} \cdot \lambda \tag{11}$$

where λ = tipspeed - ratio $\Omega R/U$

Finally, in fig. 8 an even more general flow-state has been sketched such as often occurs during "off-design" conditions. The trailing vortex sheet rolls up into a tipvortex at A, which drifts along with the local flow after the passing of the vane. The average convection velocity of the vortex is denoted vectorially by $\underline{W}$ (lower part of fig. 8). In general $\underline{W}$ is not parallel to the free stream velocity $\underline{U}$ due to the functioning of the powerturbine which induces a radial flow component. Upon arrival of the next vane, the vortex has drifted from A to B at which position by the previously explained flowmechanisms it causes the release of a new, counterrotating vortex at C. It is seen that in this case too the eqs (1) to (10) may be used. The "vortex-span ratio" is from fig. 8:

$$\frac{b_v}{b} = \frac{2\pi}{N} \cdot \frac{R}{b} \frac{1}{\lambda} \cdot \frac{W}{U} \tag{12}$$

where N = number of tipvanes.

The tipspeed ratio where the vane-span becomes too short to "intercept" the free vortex at B depends, apart from the span, on the "rolling-up offset-distance" kb_e (see fig. 8) which for a rectangular vane planform typically has a value of the order $0,1 \cdot b_e$.

2.2 Turbinemodel

For the functioning of the powerturbine the well-known model of a semi-infinite vortex tube is used. The axial velocity induced by the vortex cylinder in the disc plane is v_i and far downstream $2v_i$ (fig. 3). Velocities in the surface of the vortex-cylinder itself have half this value. Thus, the powerturbine induces exactly at its entrance-lip an axial velocity $\frac{1}{2}v_i$ which must be taken into account when the local flow environment experienced by the tipvanes is analyzed.

2.3 Model for wake mixing

Turbulent mixing of the wake flow with the surrounding flow is for propeller- or windturbineperformance usually considered unimportant. In contrast, in the case of a tipvane turbine wake mixing effects are found to have an important influence. The Venturi-type of flow through a tipvane-turbine leads to a much larger wake expansion and consequently also to a much longer and wider wake region with sub-ambient pressures compared with the conventional turbine.
Since the wake flow is not shielded from the external flow by a material wall, some amount of mixing always occurs in this region of reduced pressure.
The resulting situation is shown schematically in fig. 9 which should be compared with fig. 2.
In the flows without mixing (fig. 2), a certain minimum value of the final wake velocity is needed in order to ensure a positive mass flow through the system and to prevent the flow from collapsing into the turbulent wake state. In fig. 9, however, the turbine can extract more energy per unit of mass flow before encountering the turbulent wake state, since the minimum value of the velocity now occurs at the "entrance" of the "low pressure reservoir". At this point not only kinetic energy has been given up by the fluid, but also some potential energy. Due to mixing in the low pressure reservoir with a stream of secondary air, there is momentum added to the turbine flow before it is finally exhausted into the ambient atmosphere. The effect is usually called "ejector effect", since there is some resemblance with an ejector pump placed behind the turbine. The effect of wake mixing may, alternatively, be compared with the effect of a favourable pressure gradient in the ambient air. A favourable gradient would in the wame way postpone the occurrence of the turbulent wake state by relaxing the condition that the final wake pressure must come back to the undisturbed pressure.
The turbulent mixing process itself can at present not yet be brought into a simple analytical model. The ultimate effect of the turbulent mixing can be modelled simply, by introducing an element into the analytical model which simulates a reduced "back pressure" experienced by the turbine. The additional analytical element must preferably be a solution of the potential equation so that one is certain that the fundamental conservation laws of the flow are not violated.
The simplest simulation of the ejector-effect by an element consistent with potential theory is a vortex ring having large dimensions compared with the wake, and placed sufficiently far downstream so that it does not induce in any direct way additional velocities in the turbine plane.
Denoting the additional velocity induced by the vortex ring at "infinity" by δV_e, application of Bernoulli's theory to the flow outside the wake yields the pressure p_e in the far wake:

$$\frac{p_e - p_o}{\frac{1}{2}\rho U^2} = -\frac{\overline{\delta V_e}}{U}\left(2 + \frac{\overline{\delta V_e}}{U}\right) \qquad (13)$$

3. Momentum-analysis of the tipvane turbine

A control-volume will be considered as shown in fig. 3. Within this volume three kinds of external forces may be discerned:

a. An axial force D_{ax} exerted on the air by the power turbine. It is written in non-dimensional form as

$$C_{D_{ax_1}} = \frac{D_{ax}}{\frac{1}{2}\rho U^2 \pi R^2} \tag{14}$$

b. An axial force of the magnitude $N.L_{vanes} \sin(\gamma_{id})$. As was shown in fig. 8 the span of the vanes must be inclined somewhat, so that the freely convecting vane-vortices are exactly intercepted by the next vane. When the local flow-direction is γ_{id} (= ideal tiltangle of the vane-span) the vane lift gives rise to the above given axial force, or in non-dimensional form: $C_{D_{ax_2}} = C_L \cdot \sigma_v \cdot \lambda^2 \gamma_{id}$ where $\sigma_v = \frac{N.S_{vane}}{\pi R^2}$ is the vane-solidity.

c. It is also shown in fig. 8 that for an arbitrary tiltangle $\gamma \neq \gamma_{id}$ the vane-vortex system is not exactly closed, and will locally accelerate or decelerate a part of the fluid. The non-dimensional force associated with this addition to the turbine-function is $C_{D_{ax_3}} = C_L \sigma_v \cdot \lambda^2(\gamma-\gamma_{id})$.

The volume of air Q entering the control-volume through the sides is per unit time:

$$Q = A \cdot \overline{\delta v}_e - 2v_i \pi r_e^2 \tag{15}$$

with A = frontal area of the control surface, and r_e = radius of final wake. It is found that this volume of air must be assumed to have an average axial velocity $U + \frac{1}{2} \cdot \delta v_e$, in order to make the final results independent from A, as they should be. The momentum conservation law applied to the whole of the control volume then yields:

$$C_{D_{ax_1}} + C_{D_{ax_2}} + C_{D_{ax_3}} = 4 \cdot \frac{\overline{v}_i}{U}\left(1 - \frac{\overline{v}_i}{U} + \frac{\delta\overline{v}}{U}\right) + 2 \cdot \frac{\overline{v}_i}{U}\frac{\delta\overline{v}_e}{U} \cdot \frac{1 - \frac{\overline{v}_i}{U} + \frac{\delta\overline{v}}{U}}{1 - 2\frac{\overline{v}_i}{U} + \frac{\delta\overline{v}_e}{U}} \tag{16}$$

Both the forces $C_{D_{ax_1}}$ and $C_{D_{ax_3}}$ change the total pressure of the flow, in contrast to the force $C_{D_{ax_2}}$. Application of Bernoulli's law along a streamline from far upstream to a point immediately upstream of the discplane, as well as applying it along a streamline running from immediately downstream of the discplane to far downstream, yields:

$$C_{D_{ax_1}} + C_{D_{ax_3}} = 4 \cdot \frac{\overline{v}_i}{U}\left(1 - \frac{\overline{v}_i}{U} + \frac{\delta\overline{v}_e}{U}\right) \tag{17}$$

Subtracting (17) from (16):

$$C_{D_{ax_2}} = 4 \cdot \frac{\overline{v_i}}{U}\left(\frac{\overline{\delta v}}{U} - \frac{\overline{\delta v_e}}{U}\right) + 2 \cdot \frac{\overline{v_i}}{U} \cdot \frac{\overline{\delta v_e}}{U} \cdot \frac{1 - \frac{\overline{v_i}}{U} + \frac{\overline{\delta v}}{U}}{1 - 2\frac{\overline{v_i}}{U} + \frac{\overline{\delta v_e}}{U}} \qquad (18)$$

The quantities $\overline{v_i}$ and $\overline{\delta v_e}$ occurring in (17) denote average velocities. We can by analogy with the usual propeller-analysis, also apply (17) to individual annuli of the flow. When doing so, it should be remembered that the term $C_{D_{ax_3}}$ indicates the axial force in an outer shell of the wake surrounding the wake of the power turbine itself. The induced velocity in the inner annuli is thus found from the expression:

$$\frac{v_i}{U}(x) = \tfrac{1}{2}\{1 + \delta v_e/U(x)\} - \tfrac{1}{2}\cdot\sqrt{\{1 + \delta v_e/U(x)\}^2 - C_{d_{ax}}(x)} \qquad (19)$$

It should be emphasized, that eq. (19) would <u>not</u> follow from a straightforward application of momentum theory to the individual flow annuli, the reason being that the pressure forces on the annuli-surfaces do not cancel out. The axial force $C_{D_{ax_2}}$ due to the tipvanes is "transmitted" via such pressure forces to the individual annuli with the result that the correct momentum balance is restored per annulus.
According to the velocity diagram of fig. 10:

$$C_{d_{ax}}(x) = C_{\ell}(x) \cdot \sigma(x) \cdot \lambda^2 x^2 = \left\{\frac{1 - \frac{v_i}{U}(x) + \frac{\delta v}{U}(x)}{\lambda x} - \theta(x)\right\} \cdot \sigma(x)\ \lambda^2 x^2 \qquad (20)$$

with $x = r/R$ and $\sigma = \frac{Nc}{2\pi r}$.

It is seen from (19) that the value of $C_{d_{ax}}$ where the flow in the annulus breaks down into a turbulent wake state is given by

$$(C_{d_{ax}})_{max} = \{1 + \delta v_e/U(x)\}^2 \qquad (21)$$

By means of (21) the strength of the ejector-effect may be estimated empirically from experiments.
When the value of the vane lift coefficient C_L is known the system of equations so far derived is sufficient to determine quantitatively the performance of the power turbine in the presence of tipvanes.
The performance of the vanes themselves (C_L and C_D) cannot be predicted by the theory derived above. The momentum considerations do, however, provide us with the flow-angles experienced by the tipvanes, since γ_{id} is known from (18) and the local velocity w of fig. 8 is given by

$$w = U \cdot \{1 - \tfrac{1}{2}\frac{\overline{v_i}}{U} + \frac{\beta}{\alpha} \cdot \frac{\overline{\delta v}}{U}\} \qquad (22)$$

4. Tipvane performance

Simple geometry gives the mean angle of attack α of the effective part of the vane:

$$\alpha = \theta - \sin\gamma \sin\Lambda - \frac{W}{U} \cdot \frac{1}{\lambda} (\gamma - \gamma_{id}) - \frac{v_{i_{vane}}}{\Omega R} \qquad (23)$$

The first term θ is the geometrical incidence of the vanes (nose-in positive, so that the positive liftdirection is towards the rotorcentre). The second term is associated with the rotational velocity ΩR, which has a component perpendicular to the vane-surface when both the tiltangle γ and the yaw-angle Λ are non-zero.
The third term gives the effect of a non-ideal tilt-angle, i.e. such a tilt-angle that the span is not parallel to the local velocity $\underline{W}$. Finally the fourth term represents, what in classical wing theory is called the induced angle of attack. For a brief outline of the determination of the induced angle of attack we again consider the array of tipvanes as a formation of wings. The Trefftz plane is drawn in fig. 11. W . r. to the first wing an elliptical coordinate system (η,φ) is fixed, defined by:

$$\begin{aligned} x &= \tfrac{1}{2} b_e \cosh\eta \cdot \cos\varphi \\ y &= \tfrac{1}{2} b_e \sinh\eta \cdot \sin\varphi \end{aligned} \qquad (24)$$

The two-dimensional velocity potential in the Trefftz plane due to an elliptical liftdistribution along the effective span b_e is given by:

$$\phi = b_e \cdot \Omega R \cdot \frac{C_{L_e}}{\pi A_e} e^{-\eta} \sin\varphi \qquad (25)$$

where the quantities C_{L_e} and the aspect ratio A_e are both referred to the effective span b_e (see for the value of b_e fig. 8). The induced velocity caused by the entire formation of wings and wakes is then found to be:

$$v_{i_{vane}} = \Omega R \cdot \frac{C_{L_e}}{\pi A_e} (1 - \cos\varphi_o \cdot e^{-\eta_o}) \qquad (26)$$

where the point (η_o,φ_o) indicates the position of the edge of the first "returning" vortex sheet closest to the vane under consideration (point B in fig. 8).
It is seen that in the case of perfect vortex-synchronization (i.e. when B and C in fig. 8 coincide) there is no induced velocity $v_{i_{vane}}$ since $\varphi_o = 0$ and $\eta_o = 0$. On the other hand, when there is a large gap between B and C ($\eta_o \to \infty$), the classical result of a single wing is obtained. Since the position of B is to a certain extent determined by the roll-up offset distance kb_e, a small overlap of the geometrical projections of the wings on the Trefftz plane is needed before perfect vortex-synchronization occurs.
Now multiplying eq. (23) by the two-dimensional lift-curveslope C_{ℓ_α} and substituting (26) into it, we find:

$$C_{L_e} = \frac{C_{\ell_\alpha}}{1 + \frac{C_{\ell_\alpha}}{\pi A_e} (1 - \cos\varphi_o \cdot e^{-\eta_o})} \cdot \{\theta - \sin\gamma \sin\Lambda - \frac{W}{U} \frac{1}{\lambda} (\gamma - \gamma_{id})\} \qquad (27)$$

whereas the vane-dragcoefficient is by a similar analysis found to be:

$$C_{D_i} = \frac{C_{L_e}^2}{\pi A_e}\left(1 - \cos\varphi_o\, e^{-\eta_o}\right) - C_{L_e} \cdot \frac{W}{U} \cdot \frac{1}{\lambda}\left(\gamma - \gamma_{id}\right) \qquad (28)$$

The latter result shows that in the case of perfect vortex-synchronization the induced drag coefficient of a tipvane is zero.

5. Experimental verification

For the purpose of verification of the outlined theory, numerous experiments have been done in windtunnels and in a towing-tank, whereas also full-scale tests on a 8,5 meter diameter tipvane rotor have recently started and have already yielded some preliminary results.
Ref. 1 describes in slightly more detail the windtunnel and towing-tank experiments. A few results will be given below.
Fig. 12 shows measured and calculated characteristics of a windtunnelmodel in which the turbine was simulated by gauzes around which tipvanes were rotating. Pitot-static tube traverses behind the gauzes were made to determine velocities and total pressures. In the diffuser diagram of fig. 12 these are shown in integrated form, with turbine blockage C_D on the horizontal axis and the total velocity through the simulated turbine $^{ax}_{1}$ along the vertical axis. The large centrifugal forces acting on the tipvanes prevented liftmeasurements to be made on the tipvanes, so that the latter measurements had to be done on a geometrically similar model in a towing tank. Although the experiments in water were only partially succesfull, the general level of vane liftcoefficients predicted by the theory was confirmed.
Fig. 13 shows a typical distribution of velocity and total pressure, measured and calculated for the same test set-up as above.
Fig. 14 shows measurements of tipvane-drag. As indicated by equation (28), correct vortex synchronization will lead to a flowstate where the tipvanes do not experience induced drag. This is confirmed by fig. 14.
Fig. 1 shows the 8.5 m diameter rotor used for full-scale tests and fig. 15 gives some preliminary results of measured and predicted performance. It should be stressed that the configuration is not yet optimized (the vane lift can be increased further, whereas powerblades will later be mounted having slightly more twist).

6. Conclusions

Relatively simple theory based on the assumption of an infinite number of blades can be derived for tipvane-windturbines. A satisfactory agreement between theory and experiments is found.

7. References

1. Th. van Holten, Concentrator systems for wind energy, with emphasis on tipvanes, Wind Engineering Vol. 5 No. 1, 1981.
2. P.C. Hensing and J.J.W. Opdam, The influence of a tipvane on the aeroelastic stability of a rotorblade. Part I: Mechanical influences, Report LR-274, Delft University of Technology, Department of Aerospace Engineering.
3. G.J.W. van Bussel, P.C. Hensing and G.A.M. van Kuik, Aerodynamic and Aeroelastic Research on Tipvane Turbines, Report LR-302, Delft University of Technology, Department of Aerospace Engineering.
4. G.J.W. van Bussel, Th. van Holten, G.A.M. van Kuik, Aerodynamic Research on Tipvane Windturbines, AGARD Conference Preprint No. 334, Prediction of Aerodynamic Loads on Rotorcraft, April 1982.

5. Th. van Holten, Performance analysis of a windmill with increased power-output due to tipvane induced diffusion of the airstream, Memorandum M-224, Delft University of Technology, Department of Aerospace Engineering.
6. Th. van Holten, Higher-order asymptotic expressions for the velocity field of a propeller duct or an array of tipvanes in axisymmetric flow, Memorandum M-280, Delft University of Technology, Department of Aerospace Engineering.

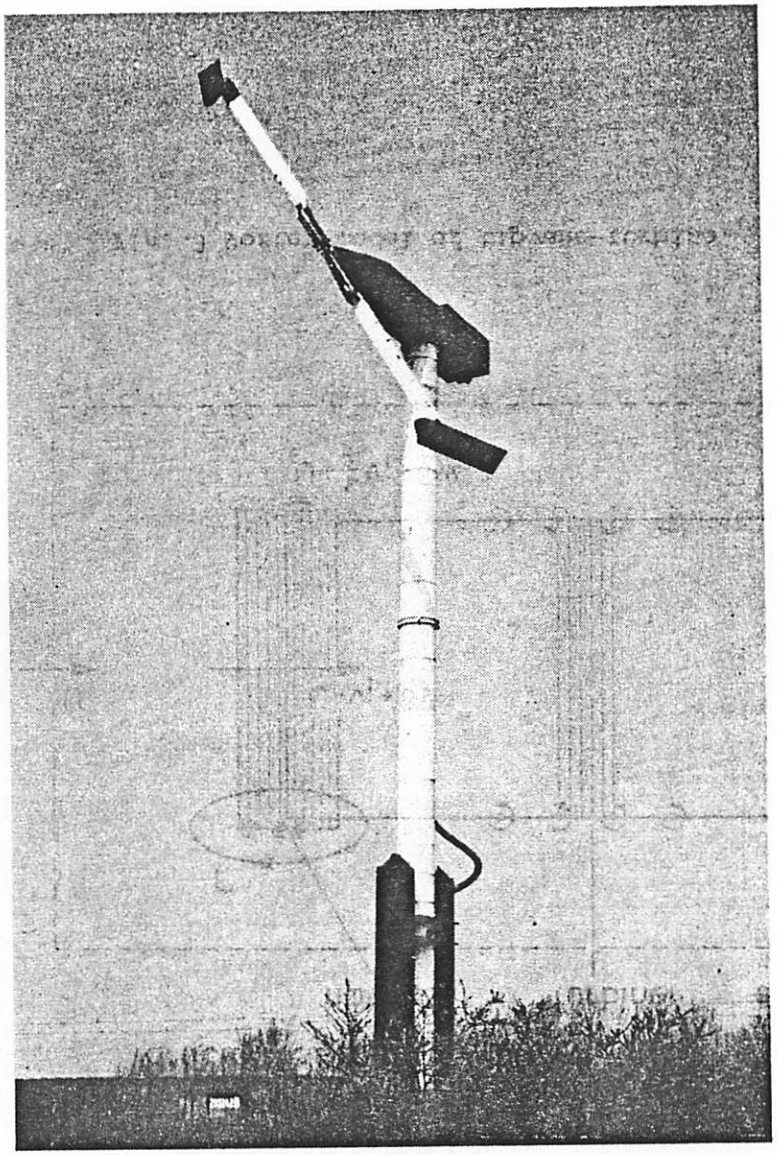

Fig. 1 Full-scale tipvane testrotor,
8.5 meter diameter.

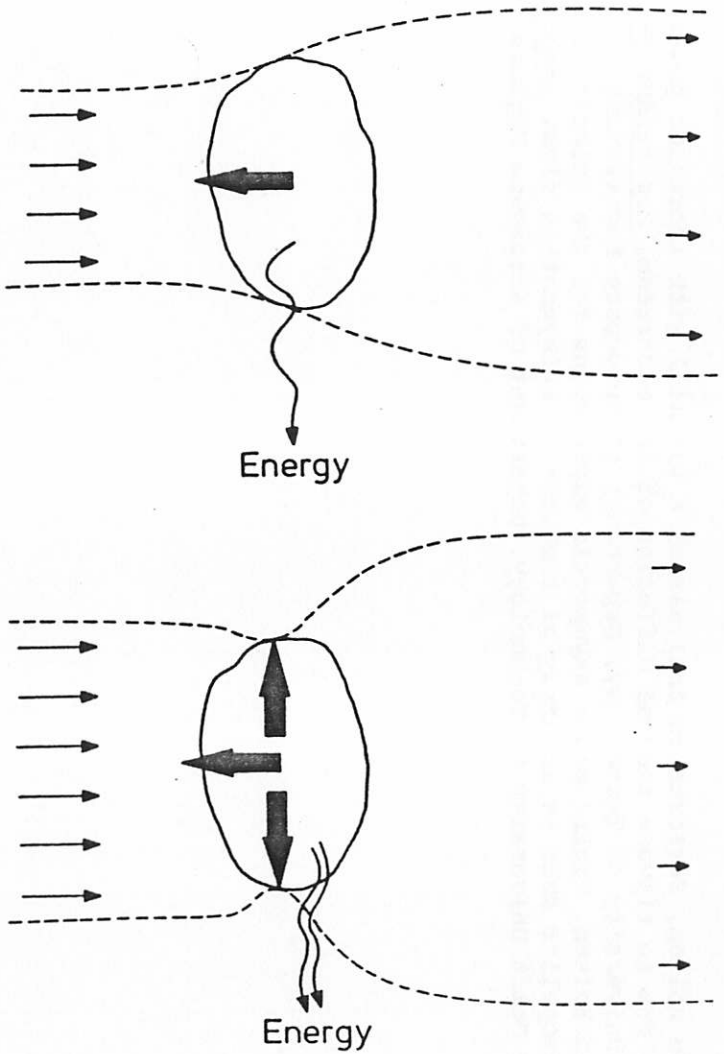

Fig. 2 Flow type for conventional turbine and turbine with cross-wind forces.

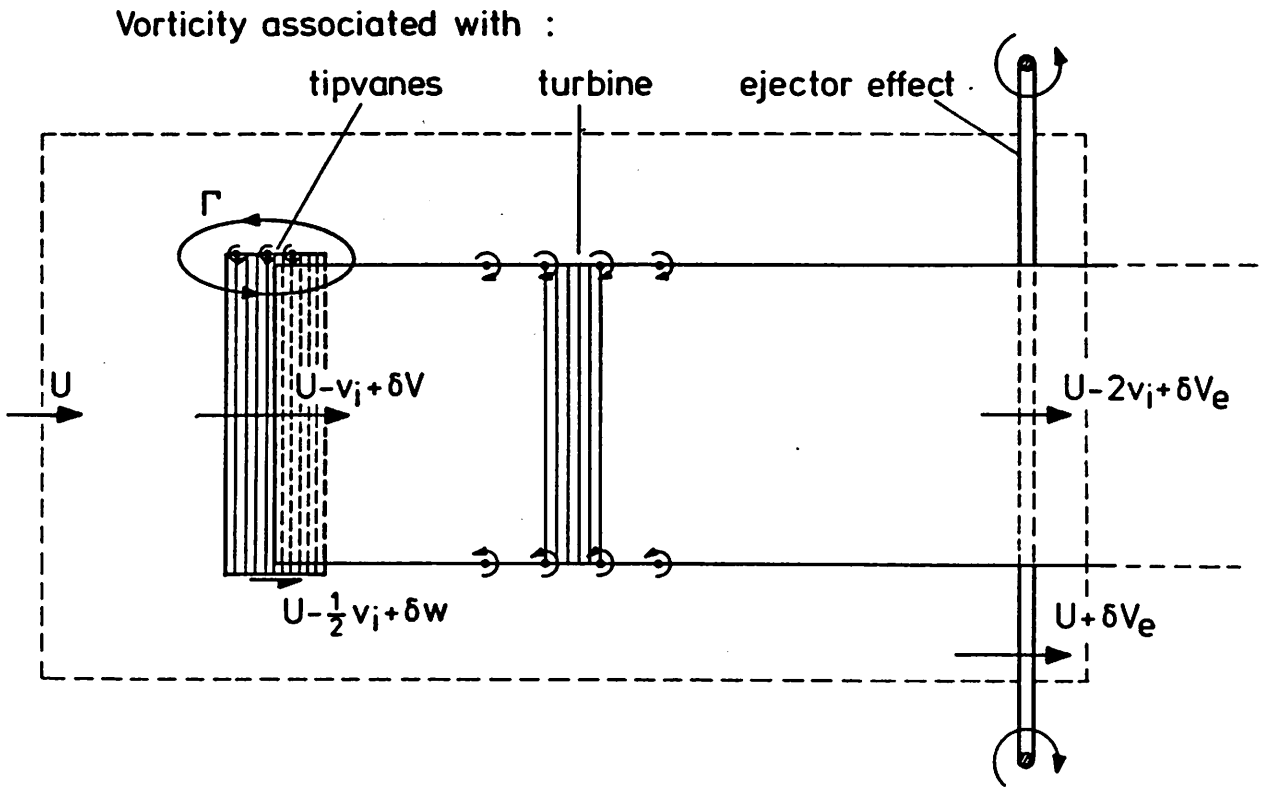

Fig. 3 Vortex model of tipvane-turbine.

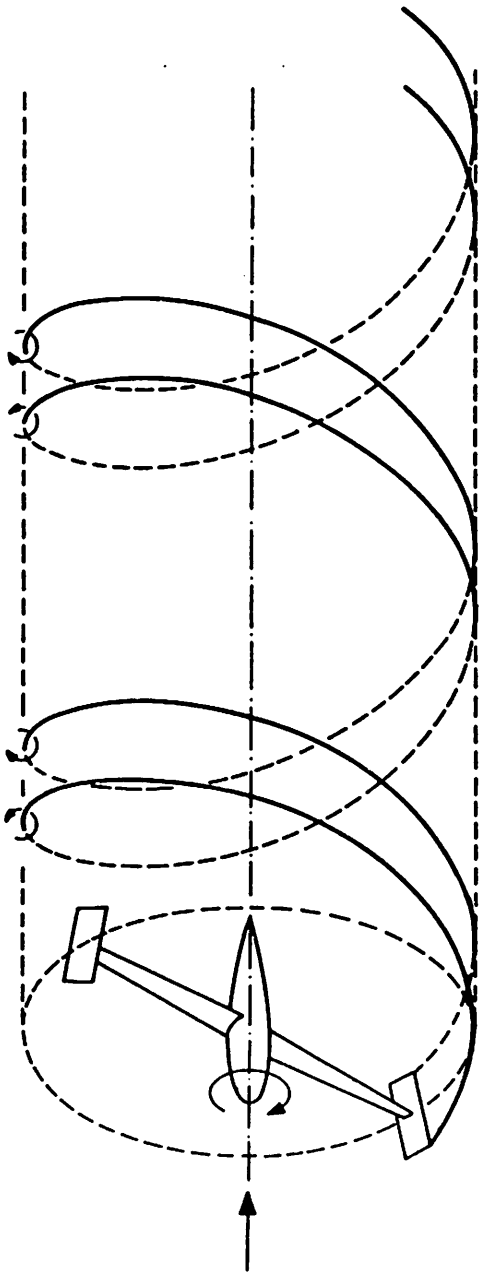

Fig. 4 Undersynchronous operation of tipvane turbine.

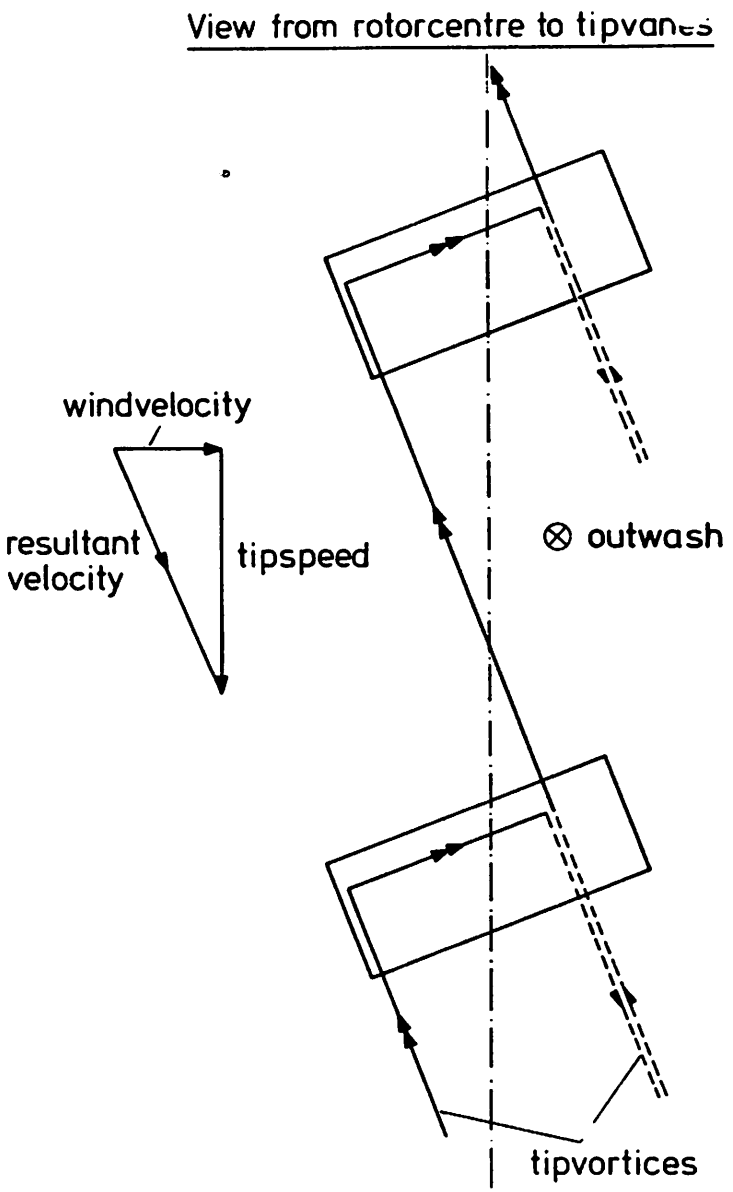

Fig. 5 Oversynchronous operation.

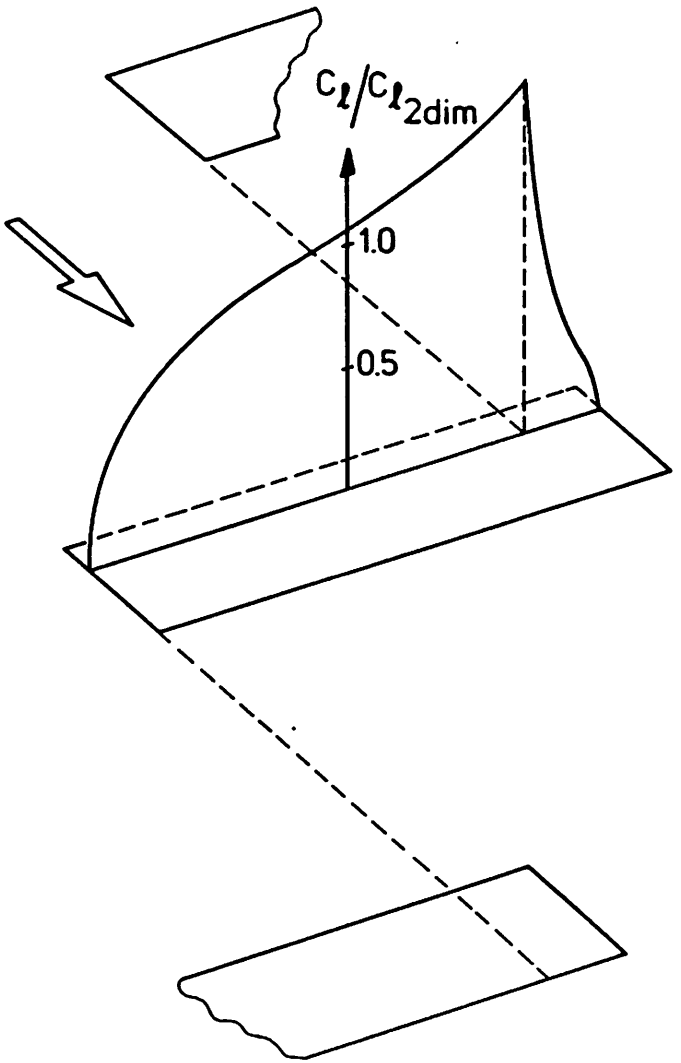

Fig. 6 Liftdistribution on vane during oversynchronous operation.

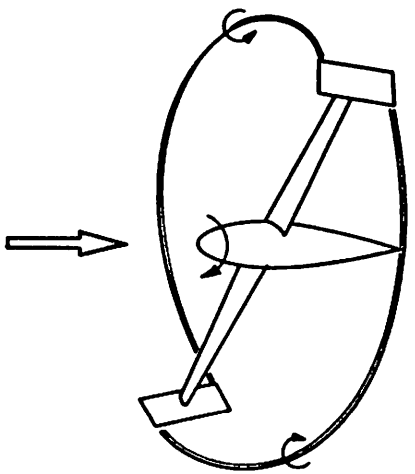

Fig. 7 Saw-tooth vortex during over-synchronous operation

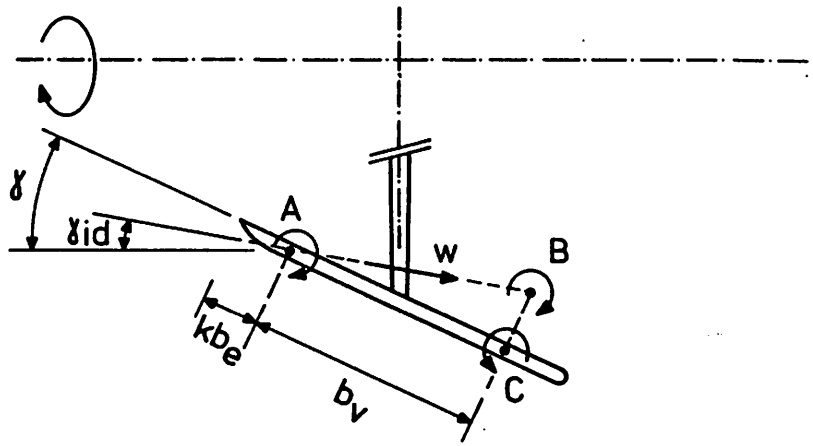

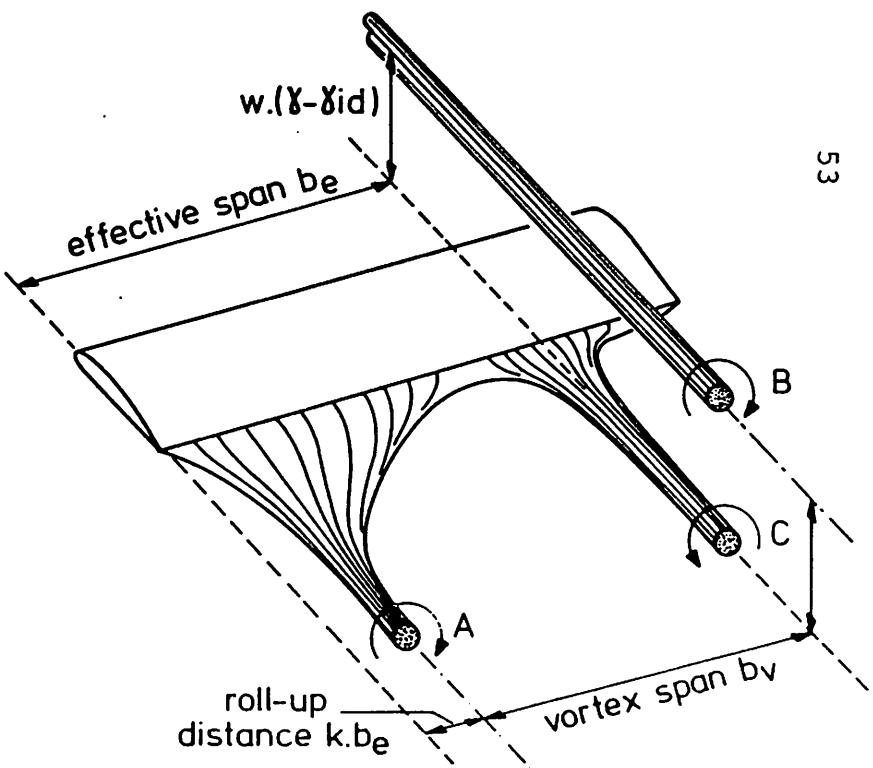

Fig. 8 Off-design condition with vane tilt-angle too large.

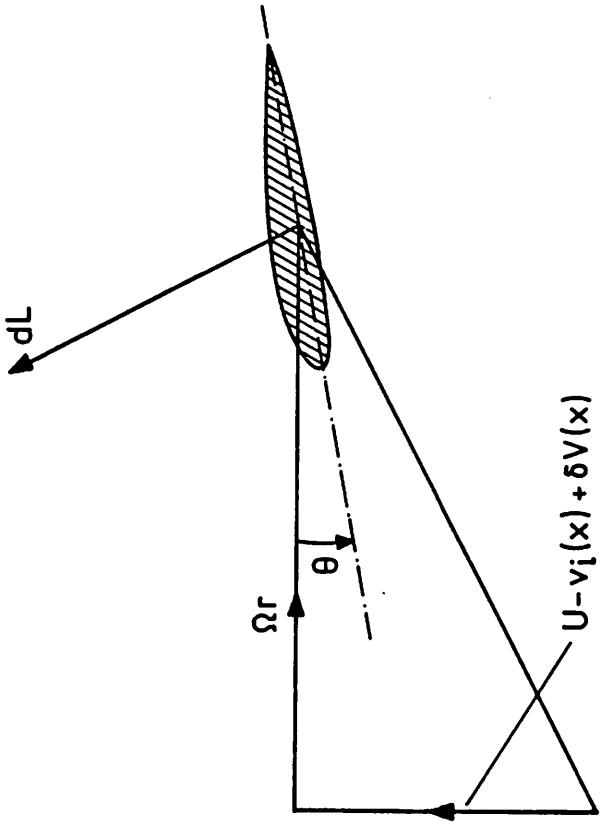

Fig. 10 Velocity diagram for element of powerblade.

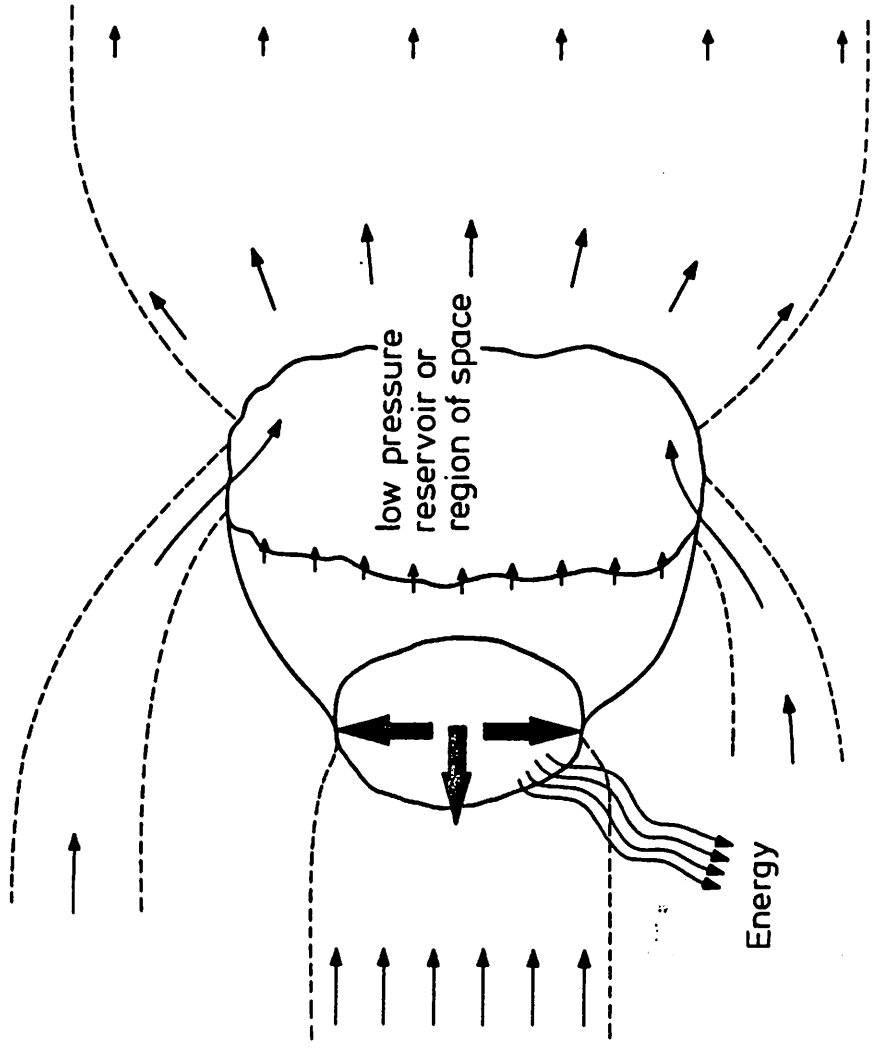

Fig. 9 Physical model explaining ejector-effect

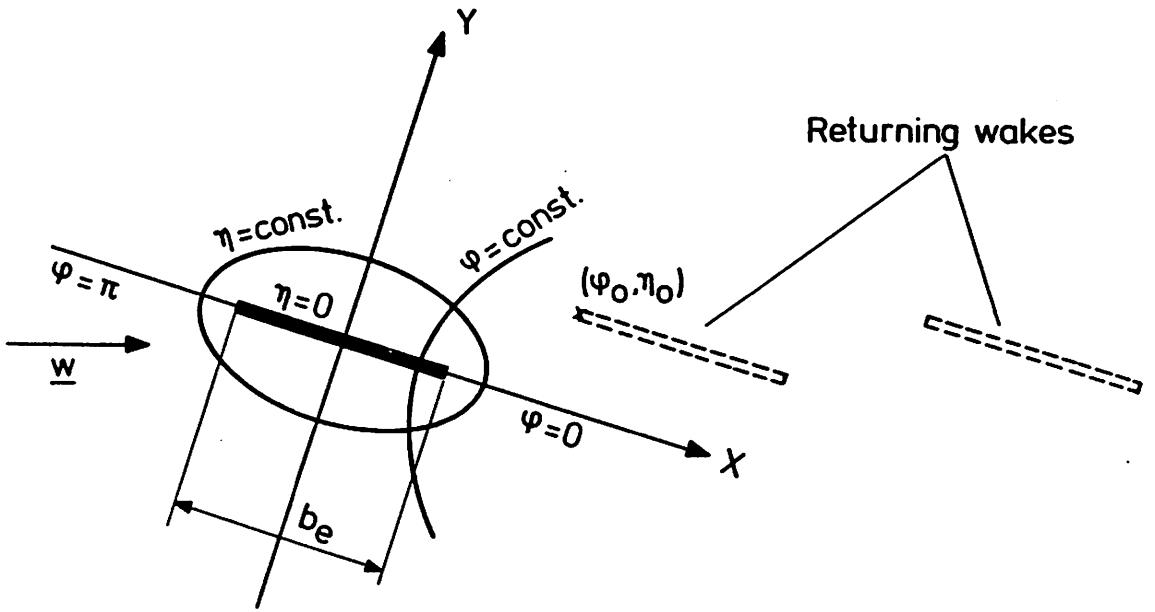

Fig. 11 Analysis of induced velocity in Trefftz-plane.

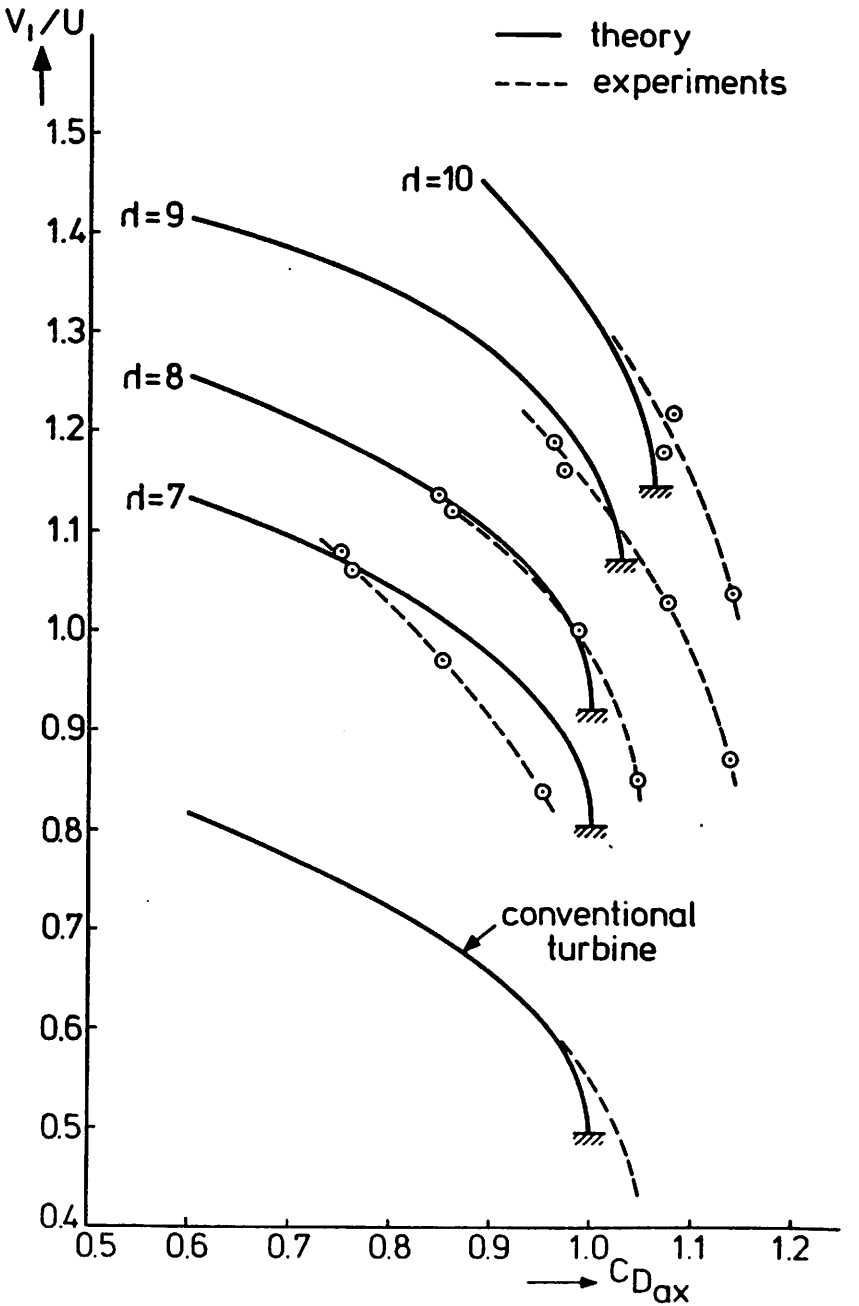

Fig. 12. Calculated and measured diffuser-characteristics of windtunnelmodel with gauze-simulation of power turbine.

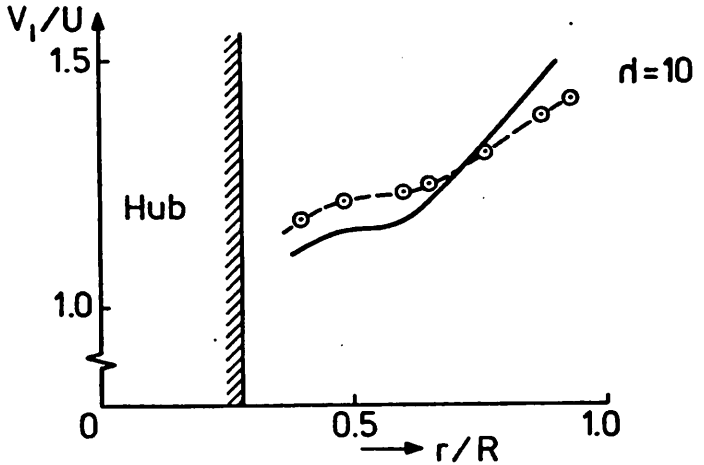

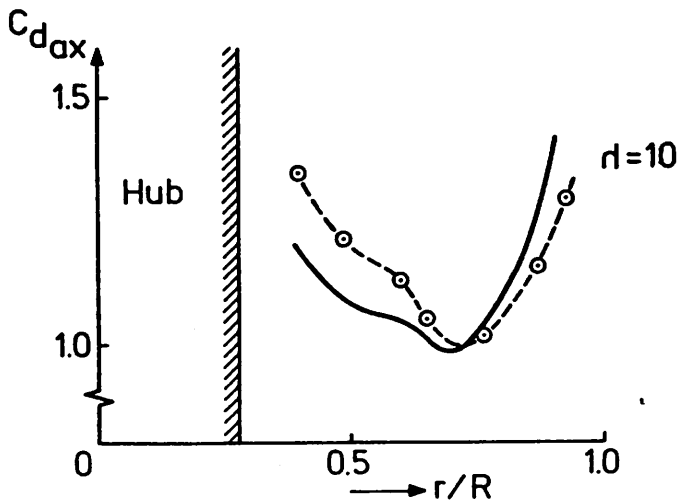

Fig. 13 Calculated and measured distribution of velocity and total pressure-loss in turbine plane

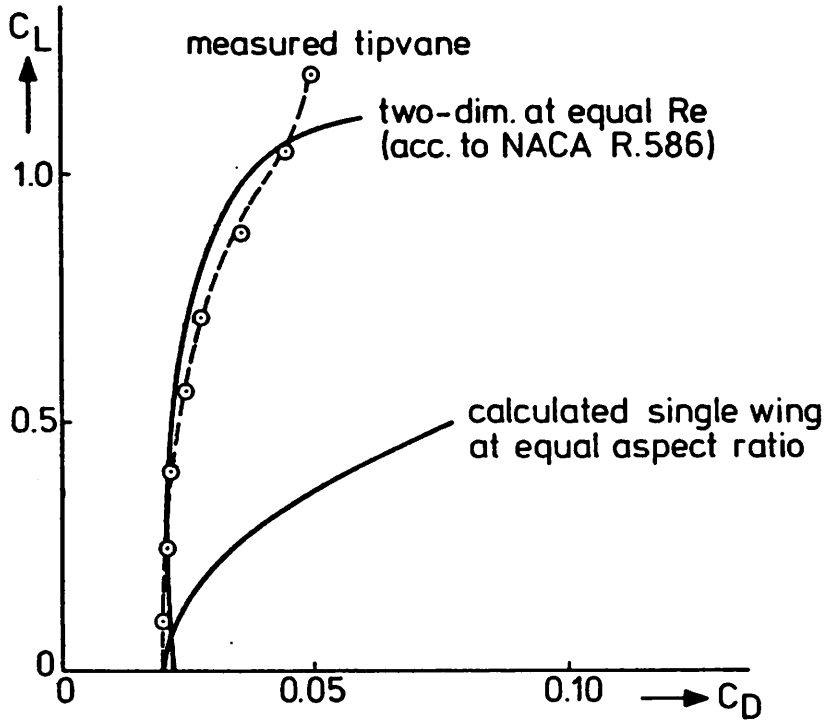

Fig. 14 Measured tipvane dragpolar.

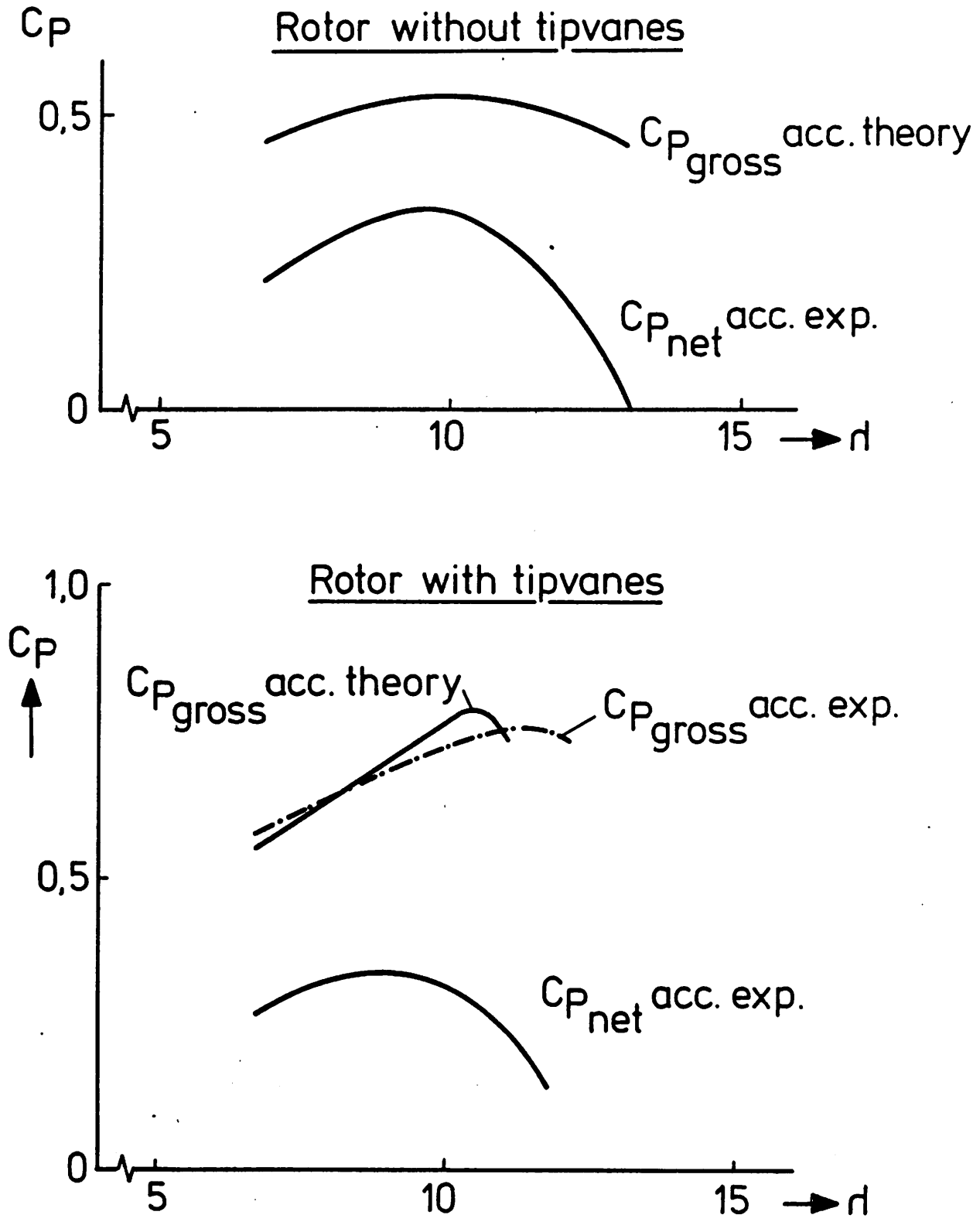

Fig.15: Break-even tests at small vane-lift $C_{L_{vane}}$ =0.4 (vanes just drive themselves). $C_{P_{gross}}$ with tipvanes obtained by adding to experimental $C_{P_{net}}$ the losses as measured on rotor without vanes, as well as adding losses corresponding to separately measured vane-profiledrag.

AEROFOIL CHARACTERISTICS OF ROTATING BLADES

by

D.J. Milborrow and J.N. Ross

SUMMARY

Changes in aerofoil characteristics, due to radial outflows on the blades of axial flow fans, were first reported some 40 years ago. The studies yielded high lift coefficients, up to a maximum of 3, near the blade roots. More recently radial migration of the boundary layer on the suction surface of a blade was photographed during fan tests at CERL.

This paper discusses the findings of detailed measurements made at a number of radial stations on a rotating model wind turbine blade. These also yielded lift coefficients higher than two dimensional values in the post-stall region, comparable with estimates from a recent American study, but less than the early fan test results. The present study also yielded drag coefficients which were higher than 2-D values but this may be a function of the small scale of the experiment. Further avenues of analysis are discussed which may lead to clarifiction of the discrepancies.

1. INTRODUCTION

Although estimates of the performance of low solidity fan and wind turbine rotors are usually made using standard two-dimensional aerofoil data, there is evidence that this approach may not always be adequate. Himmleskamp (1945) argued that three dimensional effects substantially altered aerofoil characteristics, particularly at angles of attack above the stalling incidence measured in two dimensional flow. These conclusions were derived from tests on axial flow fan blades and it was found that the maximum lift coefficient increased towards the blade root, values as high as 3 being derived.

It is possible that these phenomena are due to centrifuging of the boundary layer on the aerofoil towards the blade tips, so that separation is suppressed. Radial pressure gradients also cause marked streamline displacements and these have been measured during fan tests at CERL. Flow visualisation, using synchronised flash photography was also used to examine the flow on the blades. A typical flow pattern, observed on the suction side of an axial flow fan blade, is shown in Figure 1.

The possibility of similar phenomena occurring on wind turbine blades was discussed by De Vries (1979) and by Tangler (1982). Both concluded that post-stall lift was higher than expected. Viterna and Janetzke (1982) inferred aerofoil characteristics from performance measurements on full scale rotors. They also concluded that post-stall lift coefficients were increased and derived, in addition, estimates of drag coefficient which were markedly lower than conventional values in the post-stall region. They were not able, however, to deduce any radial variations of aerofoil characteristics.

The present measurements were made as part of a study of the capabilities and limitations of using wind turbine models of modest size for studies of aerodynamic performance and wakes. It was reasoned that such rotors could be used for fundamental studies provided their performance could be properly quantified. It was therefore necessary to check the rotor performance against predictions, which in turn raised the question of the accuracy of the appropriate aerofoil data. A study was initiated to measure, as directly as possible from rotating blades, angles of attack and the corresponding lift coefficients, using, respectively, the non-intrusive properties of laser anemometery and small total pressure probes with a wide angle of acceptance.

2. OBJECTIVES

The objectives of the study were:-

(i) To establish a procedure for measuring aerofoil characteristics on rotating blades and

(ii) to derive aerofoil data for a blade of known section, for comparison with standard, two dimensional data.

3. EXPERIMENTAL EQUIPMENT AND PROCEDURE

The tests were carried out in the working section of the CERL low speed wind tunnel, which is 4.5 m wide and 1.5 m high.

The model rotor was 0.66 m diameter, with two blades of 4415 aerofoil section and 0.032 m chord. The power absorption and control systems have been described by Metherell et al (1982); this paper also described the laser

Doppler system, used to measure the radial distribution of axial velocity, one chord downsteam of the rotor blades. Measurements of total pressure were made at the same plane, which was selected so as to be close enough to enable "rotor plane" values to be measured, but sufficiently distant to minimise errors due to periodicity or bound vorticity on the rotor blades. This point is discussed later. The pressure probes were of the standard venturi type, with a wide range of acceptance angle, and were linked by tubing to a micromanometer. The reference pressure was taken from a total pressure tube in the undisturbed flow, upstream of the rotor.

Measurements of velocity and pressure were recorded at radii between 30% and 97% of the rotor radius, over a range of tip speed/wind speed ratios between 4 and 11. Measurements of the electrical power generated were recorded and corrections made for mechanical and electrical losses up to the measuring point. Direct measurements of rotor thrust were also made, using strain gauges mounted at the base of the support tower.

4. RESULTS AND ANALYSIS

4.1 Rotor Power and Thrust

Since chord-based Reynolds Numbers for the rotor blades were in the range 2×10^4 to 1.2×10^5, performance data for the rotor were critically dependent on rotor speed. Reynolds Number variations have been taken into account in preparing the comparisons between theoretical and experimental values of power and thrust shown in Figure 2 and 3. The agreement between the thrust curves is reasonable, which indicates that lift values are in fair agreement with predictions. The agreement between the power curves is less good, the discrepancy at low tip speed ratios probably being due to the aerofoil drag being higher than predicted.

More detailed comparisons of velocity ratio, as a function of radius are made in Figure 4. These comparisons show reasonable agreement, especially in the mid-span region, but there are discrepancies, near the blade root, where the measured velocity ratio was consistently lower than predicted. This indicated that the lift was higher than predicted.

4.2 Derivation of Aerofoil Data

4.2.1 Angle of Attack

The laser was used to measure mean axial velocity as close to the rotor as possible, as described above. This yielded a mean value, f, say. Since tip loss correction factors express the ratio of the mean reduced velocity to the reduced velocity sensed at the blade (Wilson and Lissaman, 1974) we have:-

$$K(F - g) = (F - f) \qquad \ldots\ldots\ldots (1)$$

where K is the tip loss correction, g the velocity "seen" by the blade section, and F the free stream velocity. Given K, F and f, it was possible to determine g. At radius r, with rotational speed Ω, it was then possible to determine the relative flow angle, $\phi (= \tan^{-1} g/\Omega r)$ and the angle of attack ($\alpha = \phi - \beta$, where β is the blade angle). The tip loss correction factor is, in fact, a function of ϕ and hence of g rather than f and it was therefore necessary to iterate to find the solution to equation (1).

4.2.2 Lift Coefficients

The lift coefficient was also derived from the velocity measurements. The measured velocity ratios were used to derive thrust coefficients, using the standard momentum relationship:-

$$C_T = 4a(1 - a), \text{ where } a = 1 - f/F$$

Lift coefficients were then derived from the thrust coefficients using the standard relationship:

$$C_T = \sigma C_L / \sin^2 \beta$$

where σ is the local solidity and β the flow inlet angle, ($= \tan^{-1} F/\Omega r$). Lift coefficients are plotted against angle of attack in Fig. 5.

4.2.3 Drag Coefficients

The total pressure drop recorded by the probe was due partly to the momentum loss associated with the lift and partly to aerofoil drag. It may easily be shown that the pressure drop due to drag is given by:-

$$\Delta p_D / \tfrac{1}{2} \rho F^2 = \sigma C_D / \sin^2$$

This quantity could not be measured directly but could be inferred by subtracting the pressure drop due to lift:-

$$\Delta p_L / \tfrac{1}{2} \rho F^2 = \sigma C_L / \sin^2$$

from the overall pressure drop

Below stall the contribution due to drag was quite small and so the pressure measurements provided a check on the lift values derived from the momentum equation. The agreement was very good. Above stall there were insufficient data points to establish the drag curve with certainty but the indications are that higher values prevail than measured in two dimensional flow (Fig. 6). This may however be due to the scale of the experiment. It is interesting to note that the values of (lift + drag), also plotted in Fig. 6, reach levels comparable with the lift coefficients quoted by Himmelskamp (1945).

4.3 Blade setting angle

Although the blade angle was set at 3° there was a little uncertainty over the exact value, partly due to the accuracy of the jig, partly to the need to determine the angle between the true chord line and the undersurface (used for setting purposes). When the aerofoil data were originally evaluated the lift-incidence curve was displaced by 1° from the anticipated position in the linear region and it was reasonable to assume that this was due to an error in establishing the blade setting angle. The setting angle was therefore taken as 2° for further analysis and theoretical estimates.

An alternative method of estimating the drag coefficient was devised by examining the proposition that drag appears as increased turbulence. If this assumption is made it may readily be shown that the drag coefficient is given by:-

$$\sigma C_D = (v'/F)^2 \sin^2 \phi$$

However, this procedure cannot be regarded as highly accurate, partly due to the difficulties associated with measuring the turbulence, partly due to the conversion of the drag loss into energy forms other than turbulence. The values calculated were, in fact, quite low, which supports this latter hypothesis. On the other hand, the fact that low values of drag coefficient were derived indicates that the turbulence measurements were not affected by bound vorticity on the rotor blades. It may then be inferred that the pressure measurements, made at the same time, were also unaffected and represent true mean values.

5. DISCUSSION OF RESULTS

When the lift curve inferred from the measured velocity ratios was compared with the 2-dimensional dataset for the aerofoil section, extremely close agreement was found below stalling incidence. Above stalling incidence (around 12°) the experimental values of lift coefficient were consistently higher than the 2-D values. The maximum discrepancy was around 0.4, falling again as the angle of attack increased towards 30°. The generally good agreement between measured and predicted values of overall thrust coefficient confirmed that modifications to lift were not large. The measured trends are in line with the findings of Viterna and Janetzke (1982) and, in practice, the values of lift coefficient derived in this study were quite close to their values. This agreement is encouraging, since aerofoil data tend to be independent of Reynolds Number and section profile beyond the stall.

It is more difficult to infer whether the drag coefficients are also subject to modification but the discrepancy between the predicted and measured values of performance coefficient at low tip speed ratios implies that drag coefficients may be higher than measured in the 2-dimensional case. The detailed measurements supported this deduction, with quite high values of drag coefficient being derived, rising to 2 at an angle of attack around 30°. Viterna and Janetzke (1982) found lower drag below stall, but above stall they predicted lower drag coefficients than in the 2-D case.

It is interesting to note that the values of (lift + drag) measured by the pressure probe, i.e. up to 3, are in line with the values of lift coefficient derived by Himmelskamp (1945). However, a study of his analytical procedure indicates that he was able to discriminate between lift and drag, but the point requires further study.

Finally it may be noted that the good agreement between measured and predicted velocity ratios at 39 Hz rotational speed (covering a range of angles of attack below stall) points to the accuracy of the measuring techniques and the aerodynamic theory and indicates that small rotors can be used for basic aerodynamic studies, despite the low blade Reynolds Numbers.

6. CONCLUSIONS

The flow pattern shown in Fig. 1, showing radial migration of the boundary layer, would seem to indicate that some modifications to aerofoil data may be expected on rotating blades. This has been confirmed by the present tests and by a number of other studies.

By making detailed measurements at several radii and over a range of operating conditions it has been possible to obtain estimates of the lift coefficient of a rotating blade over a range of angles of attack up to 30°. At angles of attack below stall, these estimates were very close to values obtained from 2-dimensional tests. Approaching and beyond stall the derived values were higher than the 2-D values and the maximum discrepancy was around 0.4.

This study has therefore supported the conclusions of Viterna and Janetzke (1982) but not reproduced the findings of Himmelskamp (1945), who derived very high lift values. However, the present tests did yield values of (lift + drag) similar to those of Himmelskamp. A study of his experimental and analytical techniques indicates that they were able to discriminate between lift and drag and hence his measurements must continue to carry weight.

The question of drag is therefore unresolved although there is evidence from the present tests that drag may increase both above and below stall.

7. FURTHER WORK

The fan tests of which the flow visualisation study was a part (Gardner and Milborrow, 1979) tended to yield low drag values below stall and there were indications that stall was delayed. These data will be re-examined. An additional cross-check on the derived lift coefficients is available in the form of a measurement of the swirl angle.

Two further datasets are available from model wind turbine tests at CERL. Wilmshurst et al. (1984) used blades of arbitrary section for experiments in the high thrust region and the 2-D characteristics of the blades have recently been measured. More recently an extensive series of tests on a model of the Howden HWP-300 series wind turbine has been carried out; this model had a larger blade root chord and hence a higher Reynolds Number; tests in yaw were also carried out. If the cause of the phenomenon is radial outflow of the boundary layer this would be enhanced in yaw at one horizontal azimuthal position of the blade and inhibited at the other; variations in the derived lift coefficients may therefore be expected.

8. ACKNOWLEDGEMENTS

The assistance of Messrs K.A. Richardson and M.W. Weston in setting up the model, running the tests and analysing the data is gratefully acknowledged. The work was carried out at Central Electricity Research Laboratories and this paper is published by permission of the Central Electricity Generating Board.

9. REFERENCES

Gardner, B.R. and Milborrow, D.J., 1978. A technique for testing large cooling tower fans. Proc. Conf. on testing of fans and systems, London, I.Mech.E.

Himmelskamp, H., 1945. Profile investigations on a rotating airscrew. Ph.D dissertation Gottingen.

Metherell, A.J.F., Sawyer, A., Wilson, D.M.A., Milborrow, D.J. and Ross, J.N., 1982. Wind tunnel studies of interacting wind turbines. Proc. 4th Brit. Wind Energy Assoc. Conf., Cranfield. BHRA.

Tangler, J.L., 1981. Comparison of wind turbine performance prediction and measurement. Proc. Small Wind Turbine Systems Conference, Boulder Colorado. SERI/CP-635-1212.

Viterna, L.A. and Janetzke, D.C., 1982. Theoretical and experimental power from large horizontal-axis wind turbines. DOE/NASA/20320-41.

De Vries, D., 1979. Wind tunnel tests on a model of a two-bladed horizontal axis wind turbine. NLR TR 79071 L.

Wilmshurst, S., Metherell, A.J.F., Wilson, D.M.A., Milborrow, D.J. and Ross, J.N., 1984. Wind turbine rotor performance in the high thrust region. Proc 6th Brit. Wind Energy Assoc. Conf., Reading. C.U.P.

Wilson, R.E. and Lissaman, P.B.S., 1974. Applied aerodynamics of wind power machines. Report WSF-RA-N-74-113. NTIS, Springfield, Virginia.

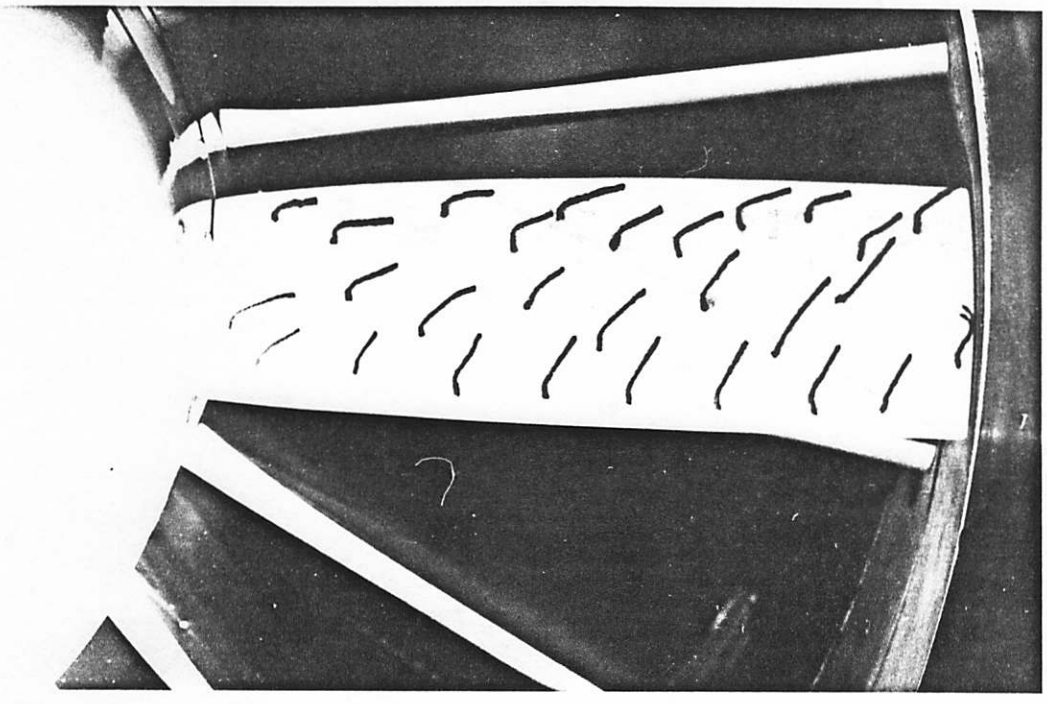

Leading edge at bottom of picture and blade tip on right

Fig. 1 Flow visualisation on a rotating fan blade

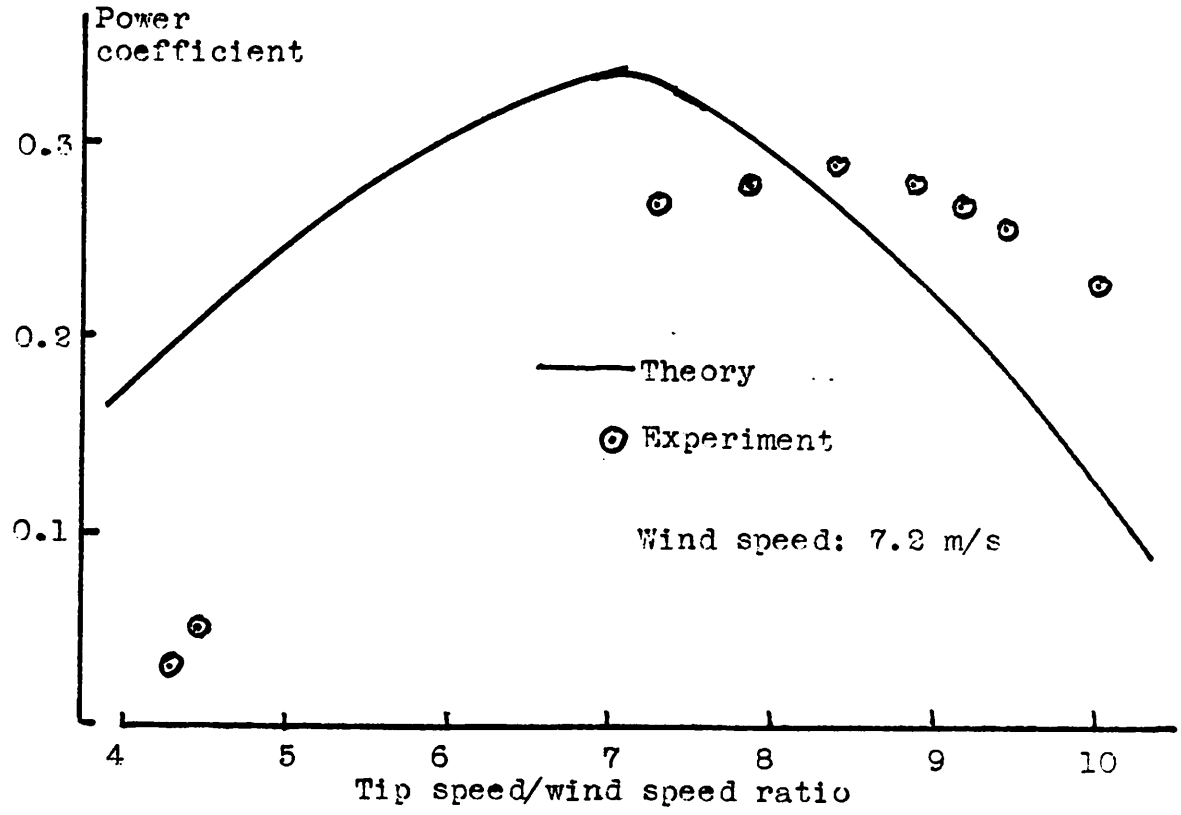

Fig. 2 Power coefficient of model rotor

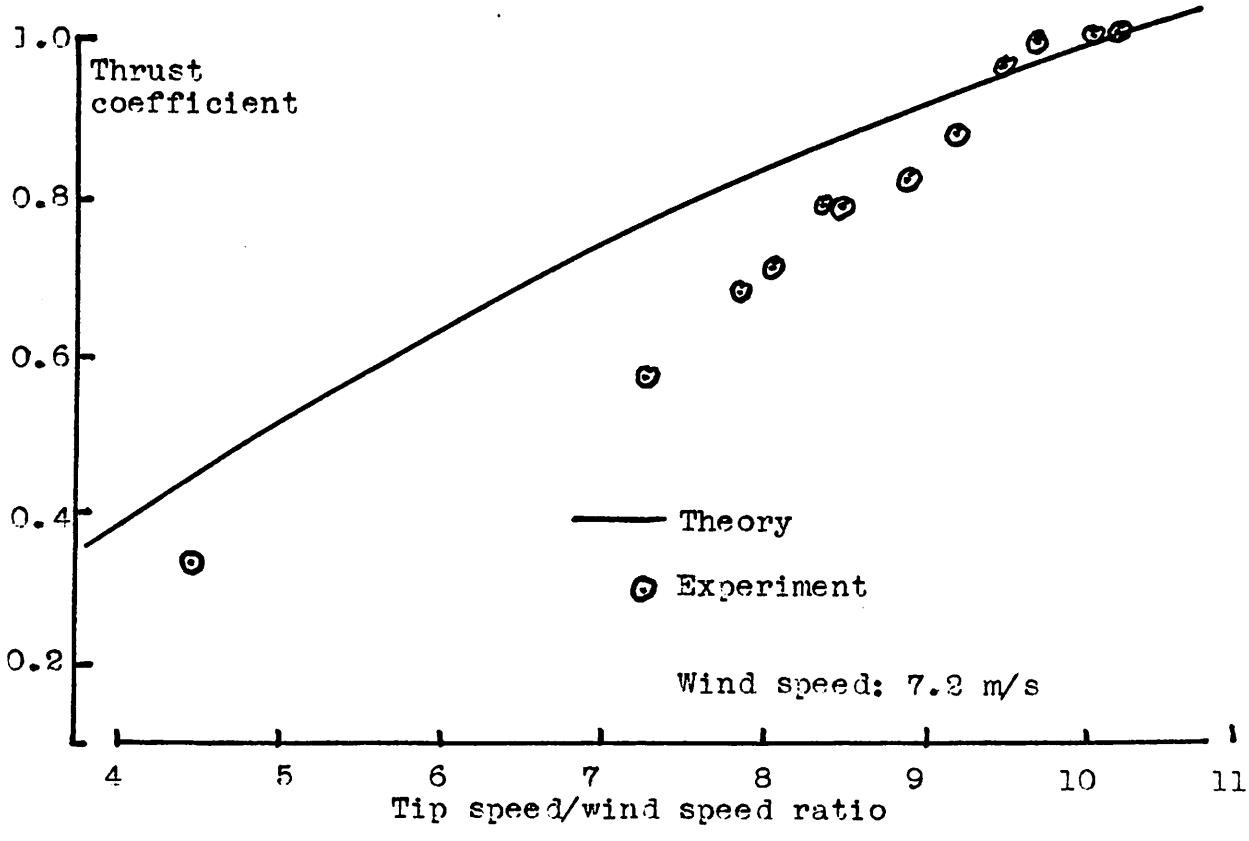

Fig. 3 Thrust coefficient of model rotor

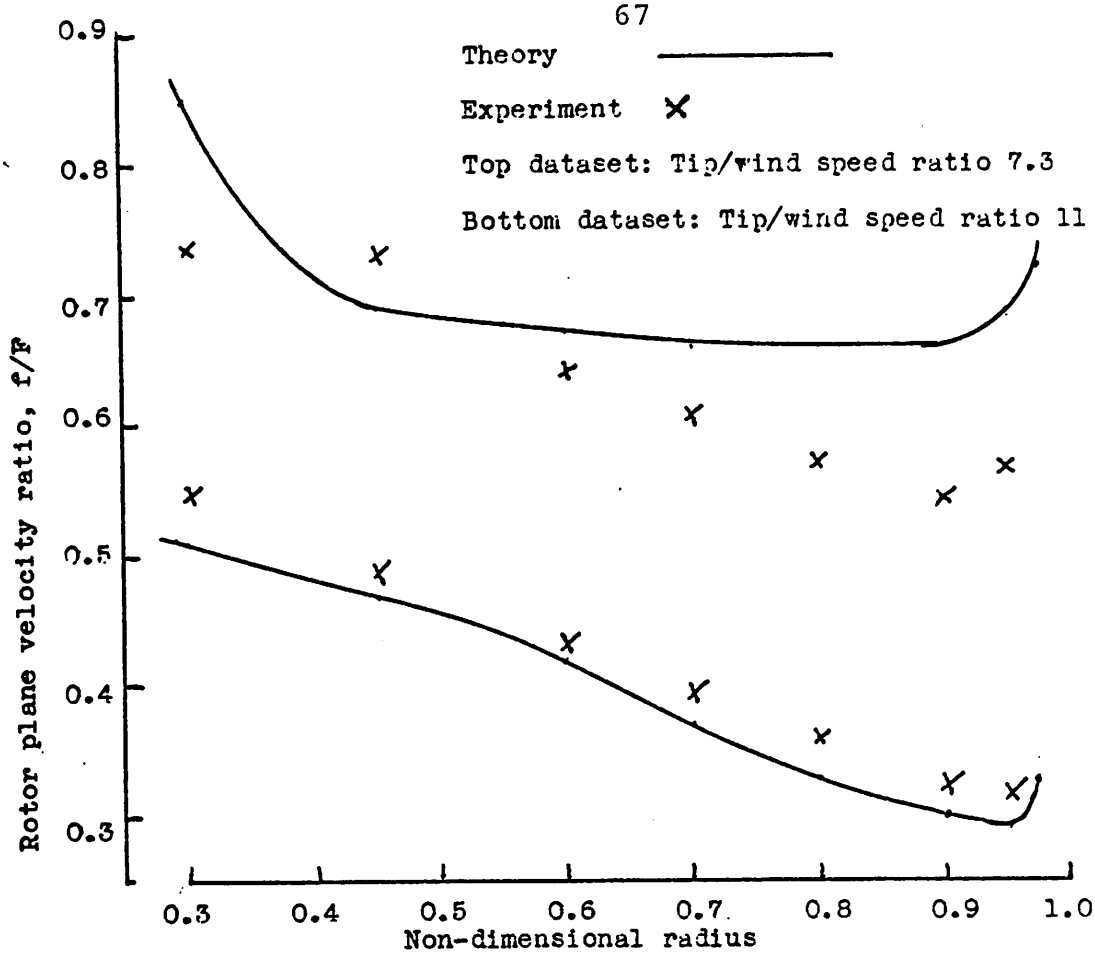

Fig. 4 Velocity ratios measured at rotor plane

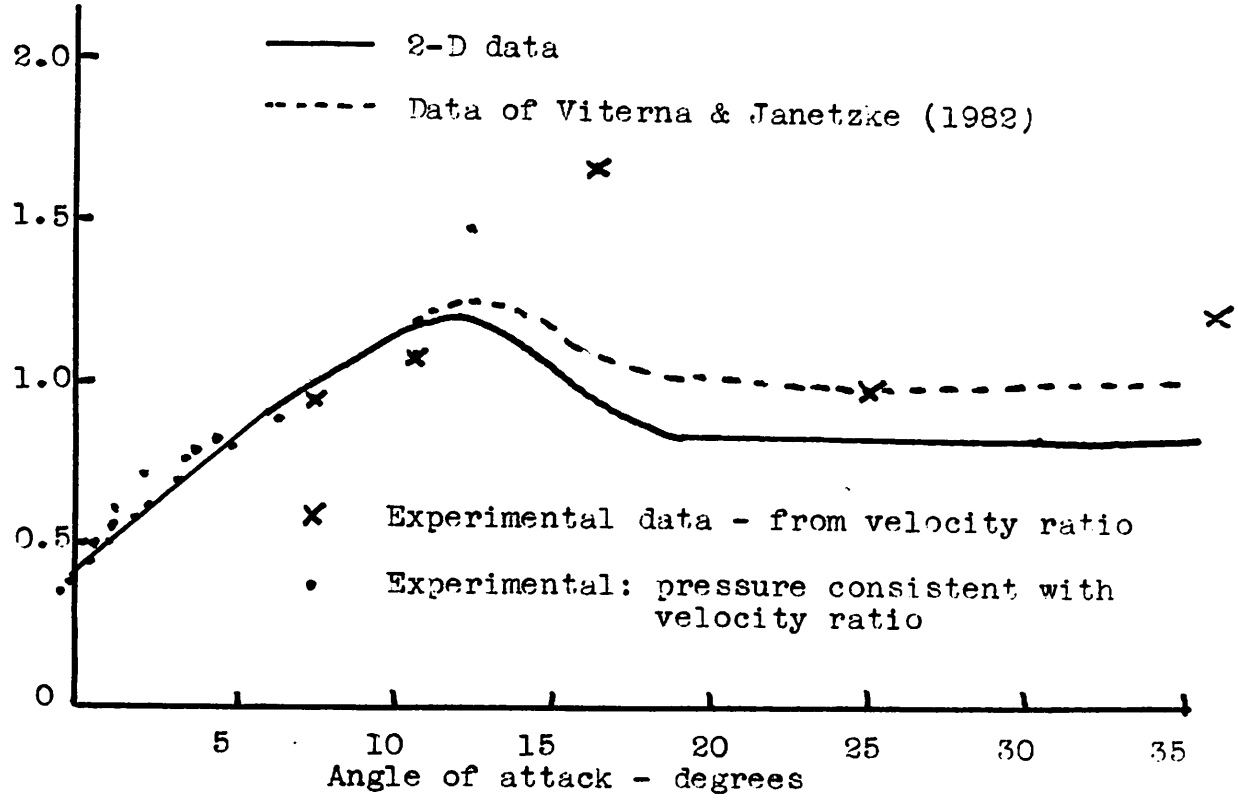

Fig. 5 Lift coefficients inferred from the tests

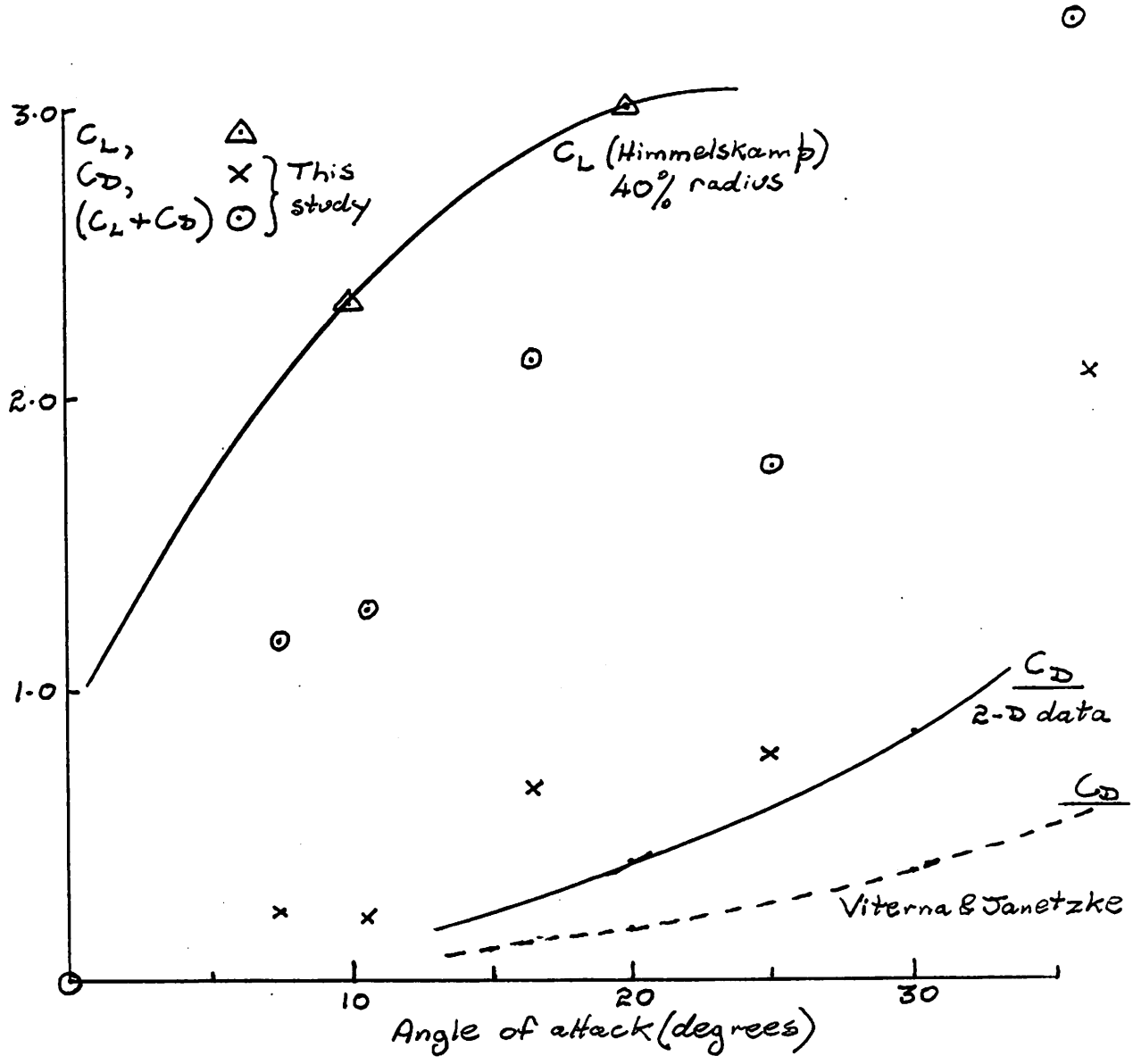

Fig. 6 Comparison of aerofoil characteristics

Björn Montgomerie

UNSTEADY AERODYNAMICS APPLIED TO THE HORIZONTAL AXIS WIND TURBINE DISK

****

1. INTRODUCTION

At FFA, the wind power group,among other things, has the responsibility to develop methods and knowledge aiming at the capacity to model and calculate the dynamic behavior of complete wind turbines. The dynamics of the tower, nacelle and rotor are caused by the response of the elastic structure to external forces i.e. aerodynamic and gravitational forces. The method derived and presented here is concerned with the aerodynamic forces only. The method is the result of the following requirements:

a. To yield external forces to the equations of motion for a complete elastic structure horizontal axis wind turbine elastic model.

b. To include relevant unsteady effects for improved time history (simulation) and force calculation.

c. To hold the volume of the unsteady method down in order not to make the computer runs unduly lengthy.

Aerodynamic methods frequently seen in most programs of this nature, are implemented as a part of the complete method here as well. As an addition the unsteady effects are applied to the aerodynamic induction factor, normally denoted a. The advantage of this approach is to allow easy addition and inclusion of the unsteady effects to an already existing method for aerodynamic force calculation.

2. STEADY AERODYNAMICS

Aerodynamic forces emanate from the air acting on the blades as they rotate. The blade tips thus circumscribe a circle whose plane is referred to as the disk plane. Aerodynamic forces on the tower and nacelle are ignored in this context. The basic requirement of the force calculation is to predict the forces acting on a number of blade elements as defined by the analyst. Ten to twenty elements are typically chosen. By properly equating the force resulting from blade element/2-D-aero theory to the momentum lost in the wake flow, in the annular part of the wake corresponding to the element, the assumed value of the induction can be found. Usually iteration will have to be applied for this purpose. In order to respect item 1.c above the moment of momentum, corresponding to the rotation of the wake flow, was neglected. The rotation of the wake flow is therefore not included. Furthermore, when calculating a, viscous effects are ignored when matching the loss of axial momentum to the thrust caused by the lift on the blade elements. For the final force calculation they are included, however.

The neglect of wake rotation is a genuine simplification of normally

applied theory, whereas the exclusion of viscous effects can be supported by theoretical considerations. By comparing results from another program at FFA (including both wake rotation and profile drag effects, the latter for calculation of the induction) it was found that the two methods produced nearly identical results even far from the design point.

As pointed out above, a method for the calculation of steady aerodynamics is required. It was presented here very briefly since such methods are well described elsewhere in the literature. The emphasis of this text is therefore on the extention of the steady to the unsteady aerodynamic theory.

3) SOME BASIC CONCEPTS OF POTENTIAL FLOW THEORY

Those elements of potential flow theory that are relevant to the problem are first presented in this paragraph. The ideas utilizing the potential flow theory are laid out in 4.

A central part of the development of the induction theory is the concept of the vortex filament. The filament is assigned the capacity to be able to produce induced velocity in the ambient air. The direction and the size of the induced velocity is governed by the Biot-Sawartz' law originally developed for the magnetizing field around an electric conductor. In this context, however, the law relates the vorticity strength of the vortex filament to the induced velocity. The induced velocity is

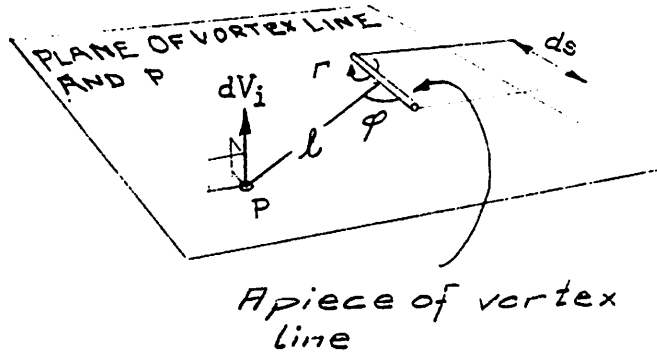

Fig. 1

$$dV_i = (\Gamma \sin\varphi\, ds)/(4\pi l^2) \qquad (1)$$

All quantities included are defined in Fig.1. For a vortex that is annular, see Fig. 2, Eq. (1) can be integrated around the circle to yield an induction on the center line. Considering the center line component only

$$a = V_c/V = (\Gamma/(2*R*V))*(1+(X/R)^2)^{-\frac{3}{2}} \qquad (2)$$

Potential flow theory allows the influence from several vortex lines to be added at any point in space. (Vector addition.) The influence from several rings, as in Fig. 3, is simply the sum of contributions from all rings present. Whence, from several rings

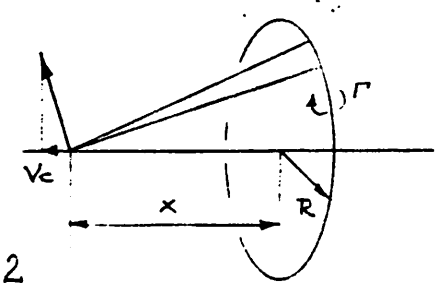

Fig. 2

$$a = \sum_i (\Gamma/(2RV)*(1+(X_i/R)^2)^{-\frac{3}{2}} \qquad (3)$$

Eq. (3) immediately lends itself to computer implementation including any amount of rings.

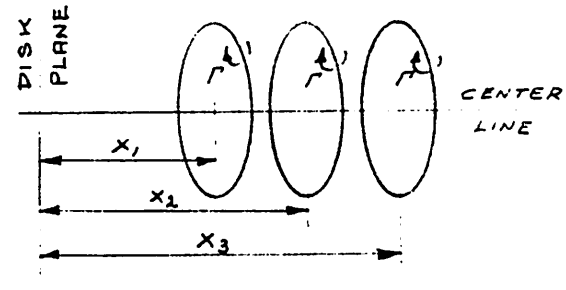

Fig. 3

Another basic fact considered below is that according to Helmholtz' rule a vortex filament,in a non-viscous continous fluid, must form a closed loop.

4. UNSTEADY INDUCTION AT THE DISK

Unsteady aerodynamic theory for rotors includes at least two major parts of influence.

Firstly, on a short time scale, a step change of circumstances at the profile causes delayed lift effects that has a duration which is in the order of magnitude of a few time equivalent chords. Translated to terms of rotation the effects referred to have vanished after say 20 degrees of azimuthal displacement. This is equivalent to a fraction of a second for most rotors of interest. Although it is important this effect is not dealt with in this context.

Secondly there are unsteady effects that, responding to a step change, linger on for a number of seconds. For a megawatt wind turbine the delay can be in an order of magnitude of half a minute. These are the long time scale unsteady effects. They constitute the substance of this text.

A horizontal axis wind turbine, or a propeller, generates an aerodynamic force associated with the strength of the part of the vortex that is located along the blade. According to Helmholtz' rule the vorticity can not end on the blade but must have some continuation. Although vorticity is shead, with varying strength, along the full length of the blade the concentration of shed vorticity takes place from near the blade tip and from somewhere near the root. A thought that immediately comes to mind is therefore to approximate the shed vorticity as being concentrated to the very tip and the center line. The two must be united downstream in order to form a closed loop.
The vortex system thus consists of four parts. The part on the blade itself C (the bound vortex) generates the blade forces together with the rotational speed and the wind speed. The part that is shed from the tip will form a helix pattern. Since the induction velocity is perpendicular to the vortex line the induced velocity will have a major component along the center line direction. A lesser component is directed so as to cause a rotation of the wake flow around the center line. Also a radial flow component exists. The center part of the vortex has mainly the function to rotate the wake flow because of its extent in a near straight line along the center line. The remainder of the closed loop vortex filament is the radial part that joins the tip helix with the central vortex line. Since it will effect the induction on the blade only initially its influence will be ignored altogether.

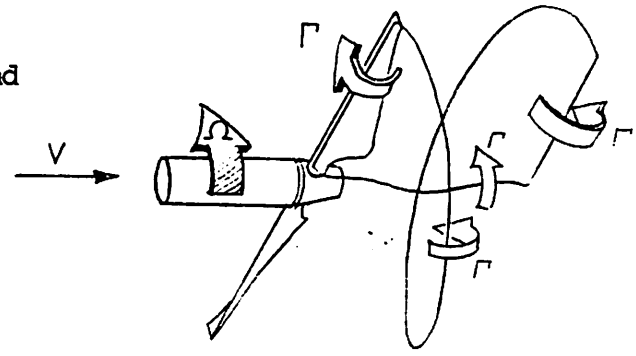

Fig. 4

Because of expediency it is desirable to further simplify the vortex model. This is carried out by approximating the helix pattern with a sequence of vortex rings in accordance with Fig. 3. The center vortex is ignored since , from experience it is known that the rotation of the flow normally is insignificant. The vortex model, for wake induction calculation, therefore is reduced to a number of vortex rings. The next step in the development of this method is to find the adequate vorticity strength, radii, number of rings, spacing between consecutive rings et c. The take off point for the founding ideas is the step change in circumstances at the disk.

Any new situation, that must be assigned the requirement that it is small and that it occurs in a step, can serve as a model for the development of the following ideas. As an example a sudden pitch change, of a small fraction of a degree, may be used for this purpose. To make the mathematical treatment easy a number of rules for the development of the wake vorticity will be constructed. No mathematical stringency burdens this presentation. At the moment the progression of thoughts will be presented in a heuristic fashion. Its merits and shortcomings will be discussed later.

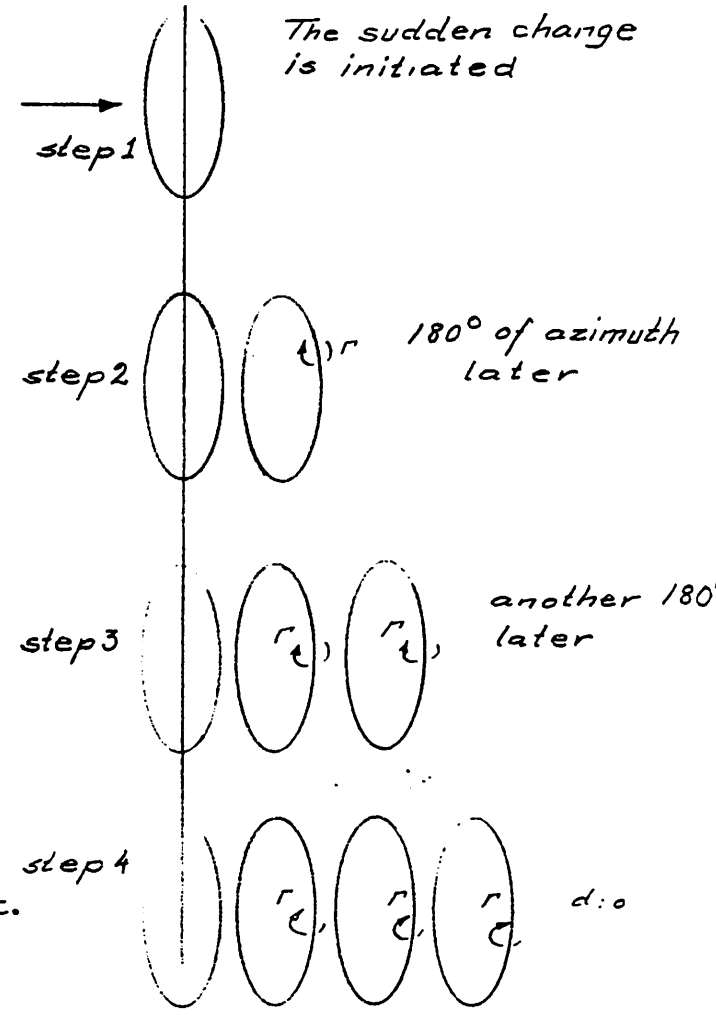

Fig. 5

In the adjacent figure, at step number 1., the sudden change in pitch takes place. This immediately produces a closed loop votex filament whose strength is obtained from the difference in lift coefficient caused by the step change. For an very small change the strength of the incremental vorticity that is shed will be defined by the circumstances that prevailed before the step change took place. The incremental vorticity in the wake will affect the disk but only to an ignorable extent. Therefore the actual strength of the vortex rings is immaterial. It can be set to a value=1. The accumulated induction on the disk from several rings will then approach an unpredictable but assymptotic level. The example from one computer run seen in Fig. 6 reaches a value of 5.3. It is not even used since the 'time' constant only is of interest.

One difficulty that must be overcome is the complication that the velocity, with which the rings drift downstream, varies along the down stream coordinate. This variation could be calculated but would require a complicated mathematical representation in computerized form. Alongsi-

de with this particular problem is the associated expansion of the wake expansion which undoubtedly would cause a widening of the ring diameters. Also a densification of the rings down stream would occur. It seems that a densification would tend to increase the induction whereas the accompaning widening would reduce it. The effects are counteractive. Although no attempt was made to veryfy the relative size of their influence they were left outside this analysis. For future improvements of this theory they should be included.

A simple replacement for the variation of the downstream drift of the rings is therefore some sort of weighted average constant velocity. In general the notion that the induction far down stream is twice that at the disk can serve this need. Therefore the average velocity in the wake was assumed to be .5*(V(1-a)+V(1-2a))=.5*V*(1-1.5a). This is the velocity that was used to produce the time constant curves, see explanations below. The distance between the rings is this velocity multiplied by the time it takes to complete an azimuthal sweep of 180 degrees in the case of a two-bladed rotor. If the distance is measured in rotor radii rather than meters or feet the expression for the distance becomes

$$\text{Rel. Dist.} = \pi(1-1.5*a)/\lambda \qquad (4)$$

The distances in Fig. 3 are obtained by summation of the relative distances according to (4). This together with Eq. (3) explains why the 'time' constant C becomes a function of both a and λ.

Of all part results calculated the induction at the disk is the more interesting. Although only calculated at the center of the disk, the value obtained was used to represent the whole disk.

The induction at the disk, using the center line value across the disk, will, if plotted, appear as a dotted function, each dot representing the result of compound induction from all rings at every time step that corresponds to the birth of a new ring. These dots were united with a curve faired through the dots in an induction vs time diagram. Several such diagrams were produced for different combinations of initial induction and tip speed to wind speed ratios. All of these curves look like simple time lag functions responding to a step. One example is included here in Fig. 6. By fitting an exponential function to each one of these curves it was possible to plot the corresponding 'time' constant as a function of initial induction and speed ratio. This function, called C, has been plotted as a carpet in Fig. 7. More exactly the response function has been suitably normalized in order to allow different curves from different size turbines to collapse on the single carpet plot. Thus the "time" lag curves have number of chords downstream on the X axis rather than genuine time. The vorticity strength on the Y axis is not important as explained above.

5. USING THE RESULTS OF THE ANALYSIS

In order to use Fig. 7 the parameter a must first be calculated. Since a is the very parameter to be calculated a time integration method can either use the value of a at the beginning of the time step or use more accurate time integration schemes such as Runge-Kutta in order to improve the numerics of the calculation. The induction at the disk can be obtained using

$$a(t)=a_{OLD}+(1-e^{-\frac{x}{C}})(a_{\substack{NEW\\steady}}-a_{OLD}) \quad (5)$$

(5) shows how the induction at the disk responds to a step change. For each time step, however, a new value for C must be obtained from interpolation in Fig. 6. The induction calculated with some method for steady performance must be provided for the complete calculation. Eq. (5) indicates the interesting possibility to fully utilize steady methods in addition to the unsteady effects thus making full use of an abundance of already developed steady methods without modification.

The more general and therefore more useful calculation, however, is the induction responding to arbitrary changes in circumstances. The step change results described above can be utilized for this extended purpose in one of two ways. Either the response to arbitrary changes in circumstances are handled using a Duhamel type of integration. The author explored these possibilities implemented in FORTRAN code. Before numerical results were even calculated it was realized that the other appeaent approach would be more attractive from a computational stand point. The Duhamel type of approach was therefore discarded in favor of direct time integration of the differential equation whose solution is the exponential function. The main advantage seemed to be the ease of handling because of much reduced code and its administration.

The differential equation, whose solution is the exponential function, is

$$Y+\dot{Y}*Ctime=f(t) \quad (6)$$

Y is the response function and f(t) is the 'driving' function whose value will be approached with delay by Y. In this particular application f(t) is the steady induction calculated as if circumstances at the disk had prevailed for a long time at each time step. Ctime is the genuine time constant obtained from C as follows.

$$Ctime=C*\lambda/(\Omega*(1-\eta*2*a)) \quad (7)$$

C is seen plotted in Fig. 6. By rewriting Eq (6)

$$\dot{Y}=\frac{1}{Ctime}*(f(t)-Y) \quad (8)$$

the technique of direct time integration becomes immediately obvious. The part of the program, used by the author, that implements the long time scale aerodynamic effects essentially only includes Eqs. (7) and (8) and a tabulation of the carpet plot represented by Fig. 6. An extra nterpolation routine was also necessary in this case. It should be mentioned that the program so far only has the capacity to handle a uniform inflow to the disk. I.e. no ground wind shear layer has yet been included. The inclusion of non-uniformity over the disk complicates the theory considerably as discussed below.

6. SOME PRELIMINARY RESULTS

The most basic numerical experiment that could be devised consists of a straight forward performance calculation. The performance program (as opposed to the program that calculated C, once for all) was run using the unsteady option. The computer run starts with the program having no knowledge of what the induction was at the very outset. Therefore the

initial induction is=0. Physically this corresponds to the hypothetical situation that the wind and the air were turned on suddenly while the rotor was rotating at nominal speed. This artificial step change includes a distinct difference from the step change depicted in Fig. 6. When the unsteady method is used in the performance program the time integration procedure fetches different values of the parameter C. Therefore the step change, in this case, is the compound effect of a simple step response and a time constant that changes with time.

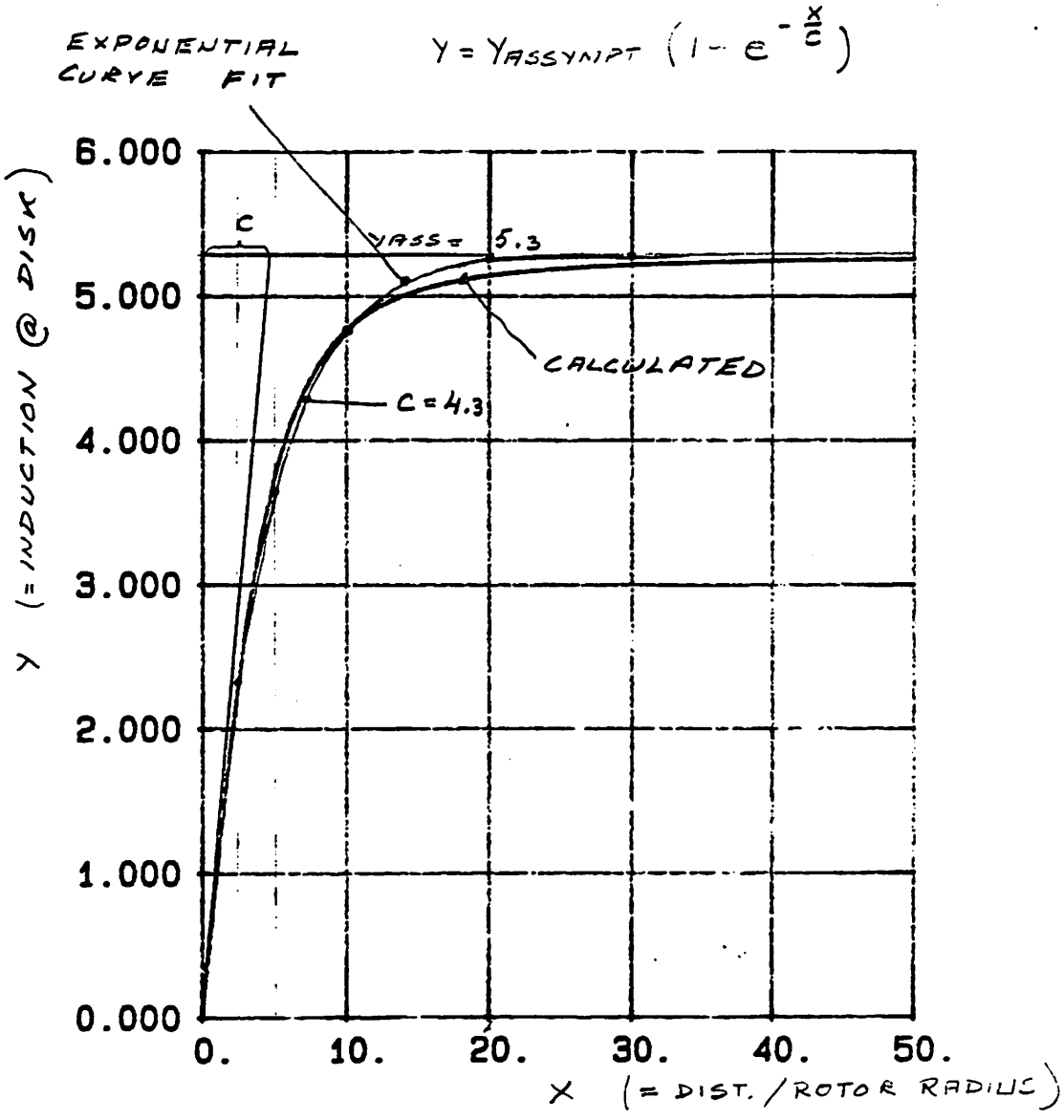

Fig. 6 , Time lag curve.

CONDENSED ANALYSIS OF INDUCTION CURVES

C IS THE TIME CONSTANT TO BE USED FOR "FUNCTION MATURATION" IN:

$$\frac{F}{\text{ASYMPTOTIC VALUE OF } F} = 1 - e^{-\frac{x}{C}}$$

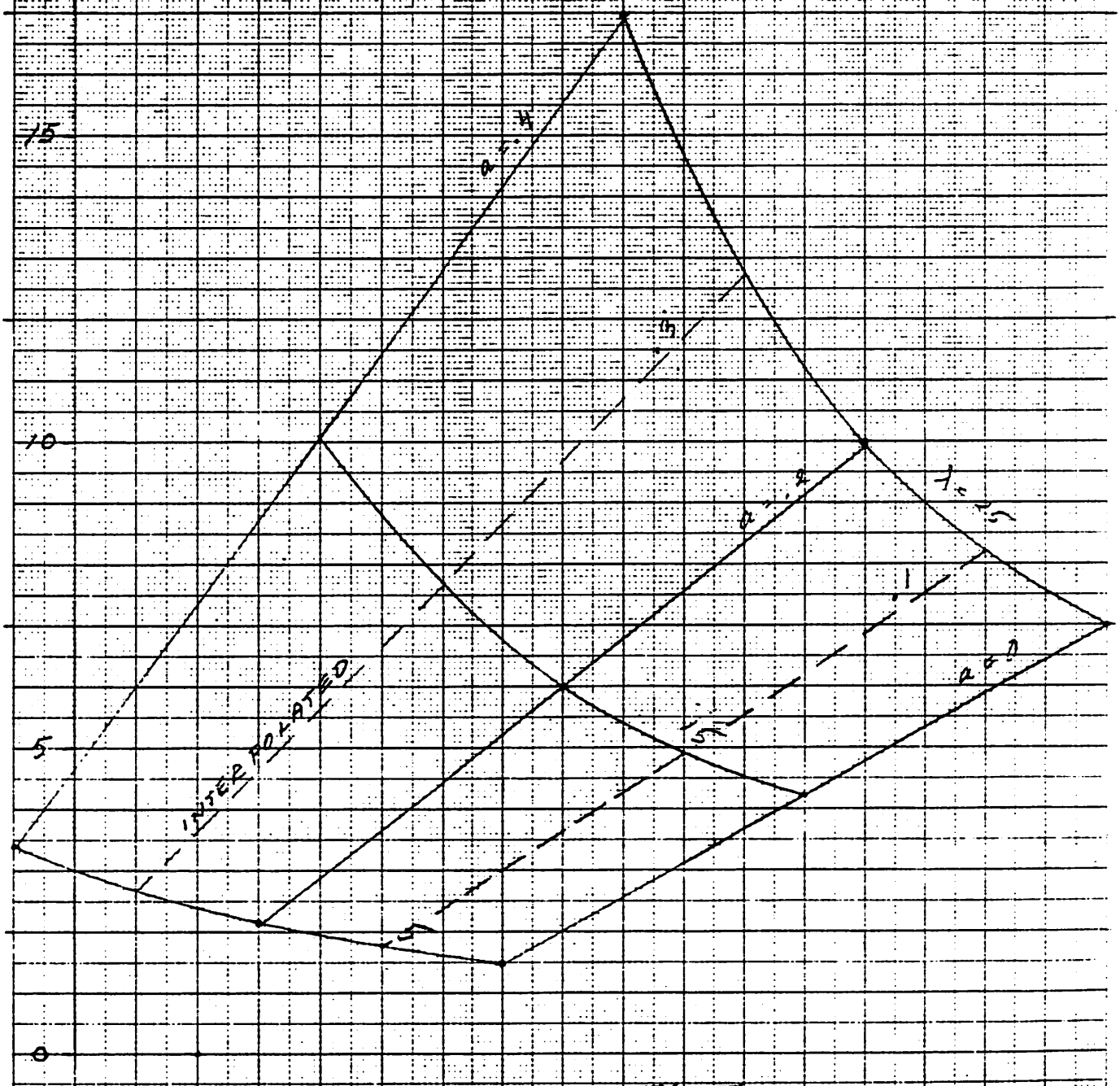

Fig. 7

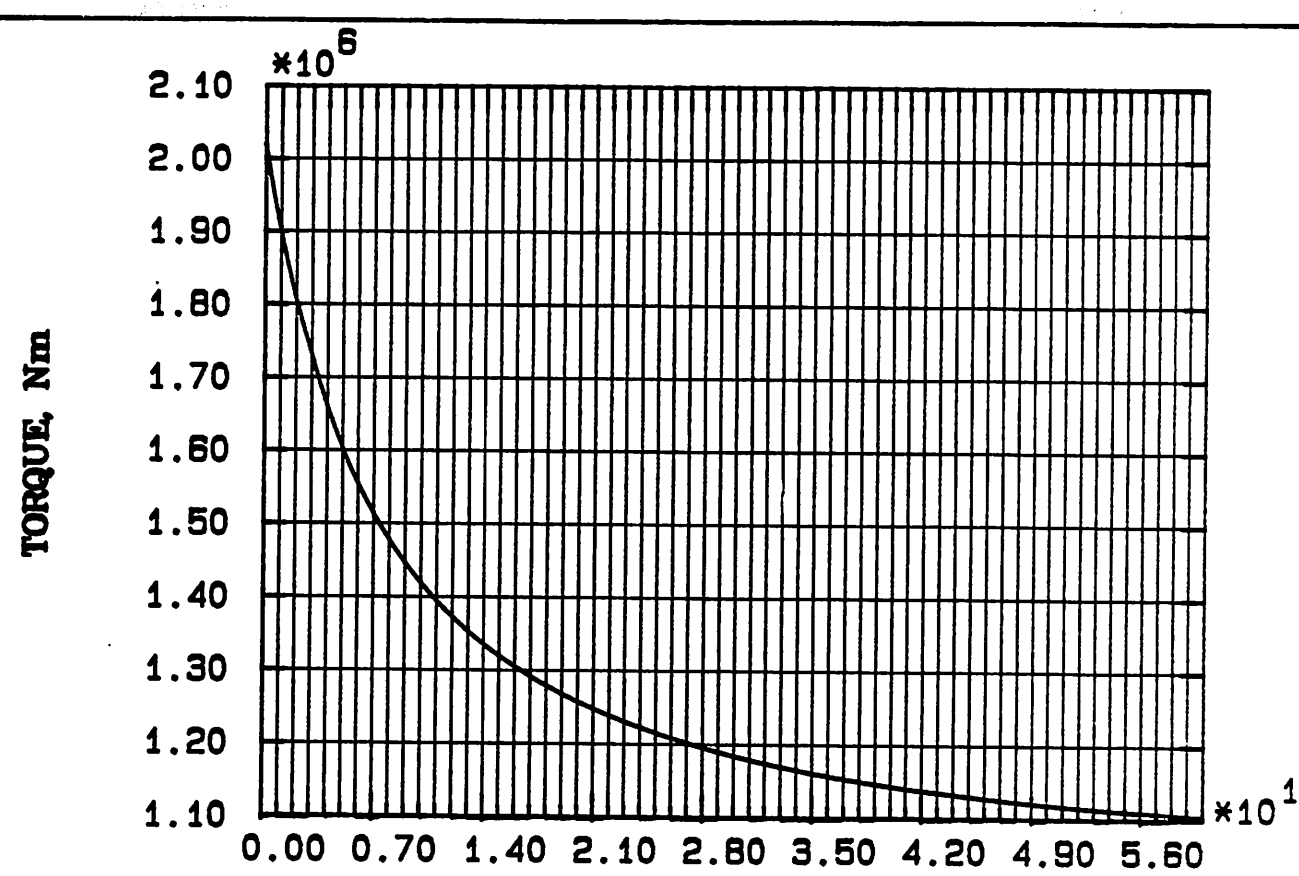

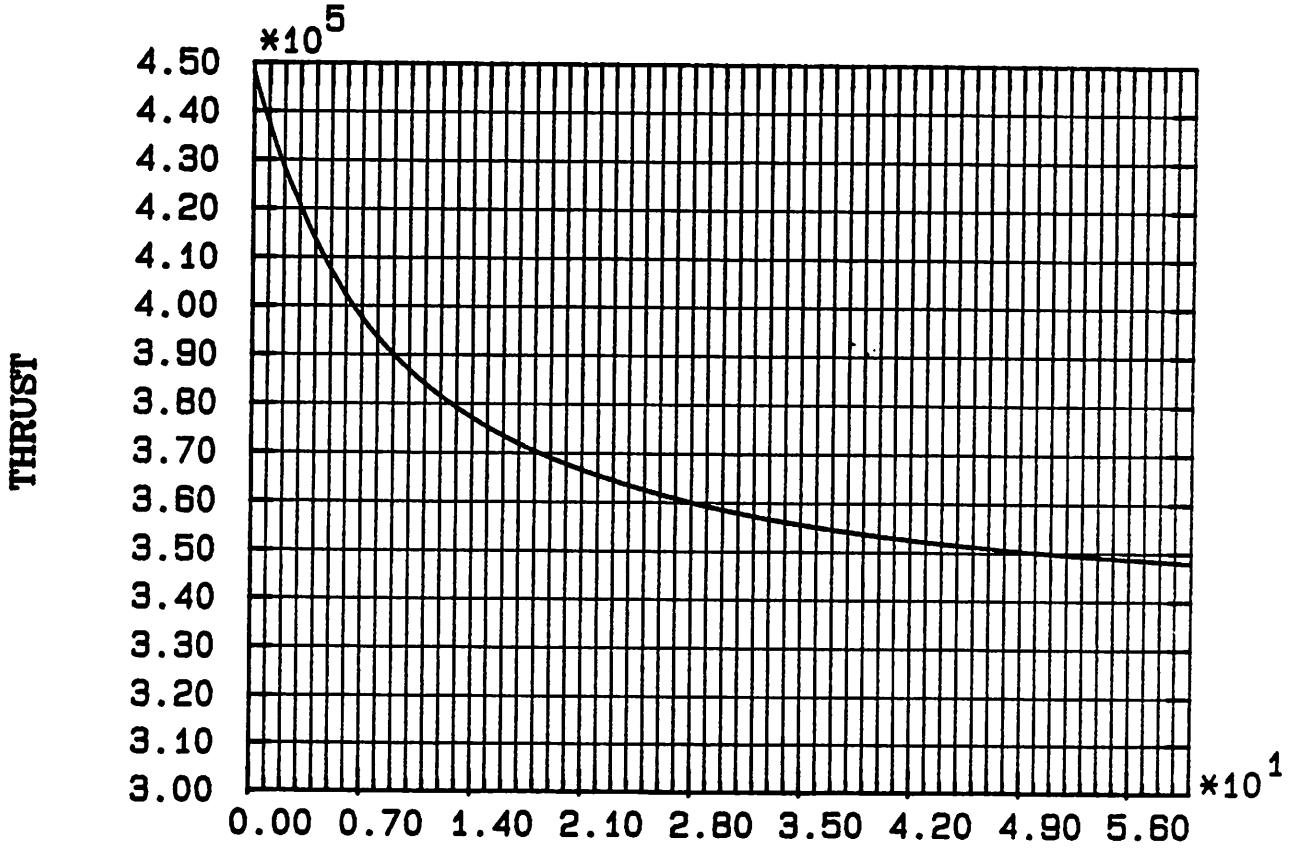

WTS-3 Response, unsteady aero. Fixed pitch & tower.

Fig. 8

Fig. 8 does not show the induction directly. Since the induction increses from zero to some assymptotic value the wind velocity at the disk consequencially decreases. The decrease in wind speed is equivalent with a decrease in angle of attack at the blade elements causing the blade element forces and therefore the integrated forces on the rotor to decrease. As can be seen in Fig. 8 the thrust should be nearly proportional to the angle of attack since the main force vector direction is in the general axial direction. Therefore the decrease is from 4.5E5 to 3.45E5. This is equivalent to a 23% decrease from a non-induction situation. The particular parameter combination chosen for the computer run is at design point. Therefore a Betz type optimization of the induction indicates a value of .333. The reason that the torque does not decrease as much as the velocity decrease through the disk (=.333*V) is that the blade geometry, for the no induction part of the time history, is poorly matched. The induction increase, decreasing the velocity through the disk, causes the appropriate matching of blade geometry to the aerodynamic environment. Thus the right hand part of the diagram is relatively better in terms of performance.

The torque curve displays a drastic change from 2.1E6 to 1.1E6. This 50% decrease is the compound effect of partly the force vector decrease partly the change of direction of same force vectors. Although the test case is an extreme idealization it nevertheless gives an insight into the reason for the gross underestimation of force changes that results from, say a pitch change, using methods that only include steady induction calculation. A real life case that has several similarities with the assumptions behind Fig. 8 is the start of the wind turbine from no rotation. If the pitch schedule is precalculated using steady aerodynamic theory only the observer present at the test site should be amazed at the acceleration of the rotor which by far would exceed the calculated value. For the same reason the aerodynamic braking deceleration of the rotor at shut-down would be much higher than expected.

The consequencies of comparing steady vs unsteady methods can be seen in various numerical exercises. One such variation is seen in Fig. 9. Here the preconditions that were set up were considerably more complicated than those just described. The performance program was run with the tower motion option at work. This includes a simple mass/spring system representing the tower data first bending mode. A simple control system representation is also part of this program. The control algorithm is

$$\text{Pitch rate} = KQ*(\text{Torq}-\text{Torqref})+KZ*(\text{Tower acceleration}) \qquad (9)$$

This represents an extreme simplification of the Karlkronavarvet/Hamilton Standard WTS-3 (3MW) machine control system at above rated speed. The first term corresponds to the primary regulating function. The second term is a compensation for tower motion. If it were not present the control system would not be able to tell the difference between genuine wind change response and apparent relative wind change caused by the tower rocking motion. The capacity to tell the two apart can be of vital importance in cases where the control system cut-off frequency is higher than the tower natural frequency.

In the context of fatigue evaluation it is of interest to know what the damping of the tower motion might be. Using the program both with and without the unsteady option several runs were made using different values of the tower acceleration feedback parameter KZ (nominal=3). Again the more complete method using unsteady aerodynamics turns out more severe (less desirable) data. At least for the wind chosen the

unsteady curve (the upper of the two) means that the damping is not as good as expected if steady methods were used only. In this respect the difference is not as spectacular as in the first case studied, however.

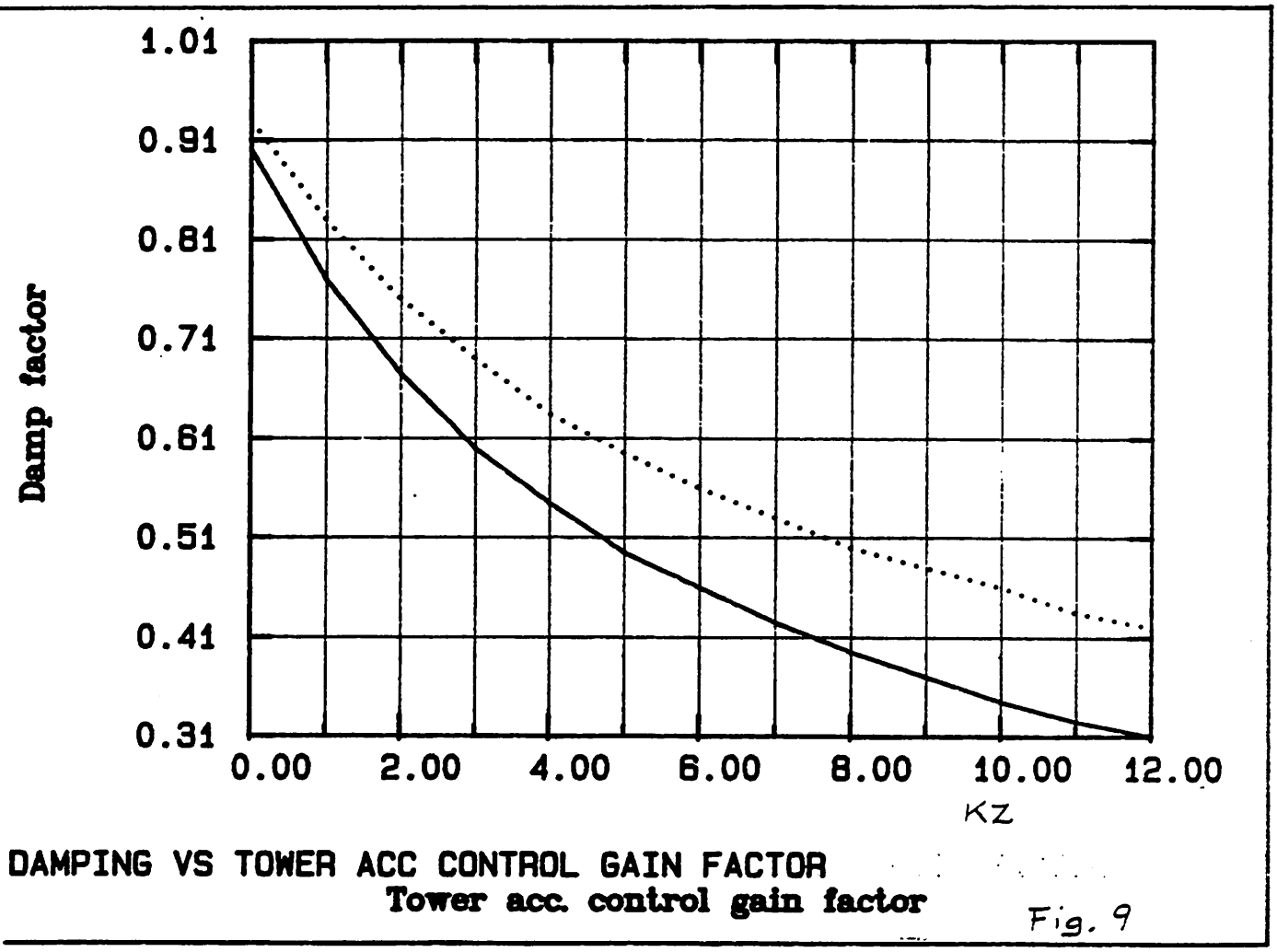

Fig. 9

The third study carried out with the performance program was designed to pruduce results that are more easily checkable against measured data. The pitch angle is artificially let to oscillate sinusoidally. The program options including unlocked tower and nominal wind speed = 8 m/s were used. Since the tower first mode frequency = .36 Hz it must be avoided. Also the first blade mode frequencies of about 1.3 Hz must be avoided. .8 is inbetween the two. Therefore it was chosen. Furthermore the maximum pitch rate, because of hydraulic flow limits, is at 4 deg/s. Half this amount was chosen. A maximum pitch deviation must also be honored in order not to give excessive forces on a real machine. All of these considerations give the following pitch change rule.

Pitch rate (deg/sec) = 2*sin(5.03*t)

In retrospect, having obtained the numerical results, the pitch rate should have been reduced considerably since the force responses were considerable and therefore unfit as a recommendation for testing. The results do, however, contain useful information. It was therefore decided that they be part of this paper rather than rerunning the program and subsequent plotting procedures.

The performance program was run for two cases using steady and unsteady performance calculation methods. The response in forces and motion were recorded and plotted. One example of all plots that were analyzed is seen below.

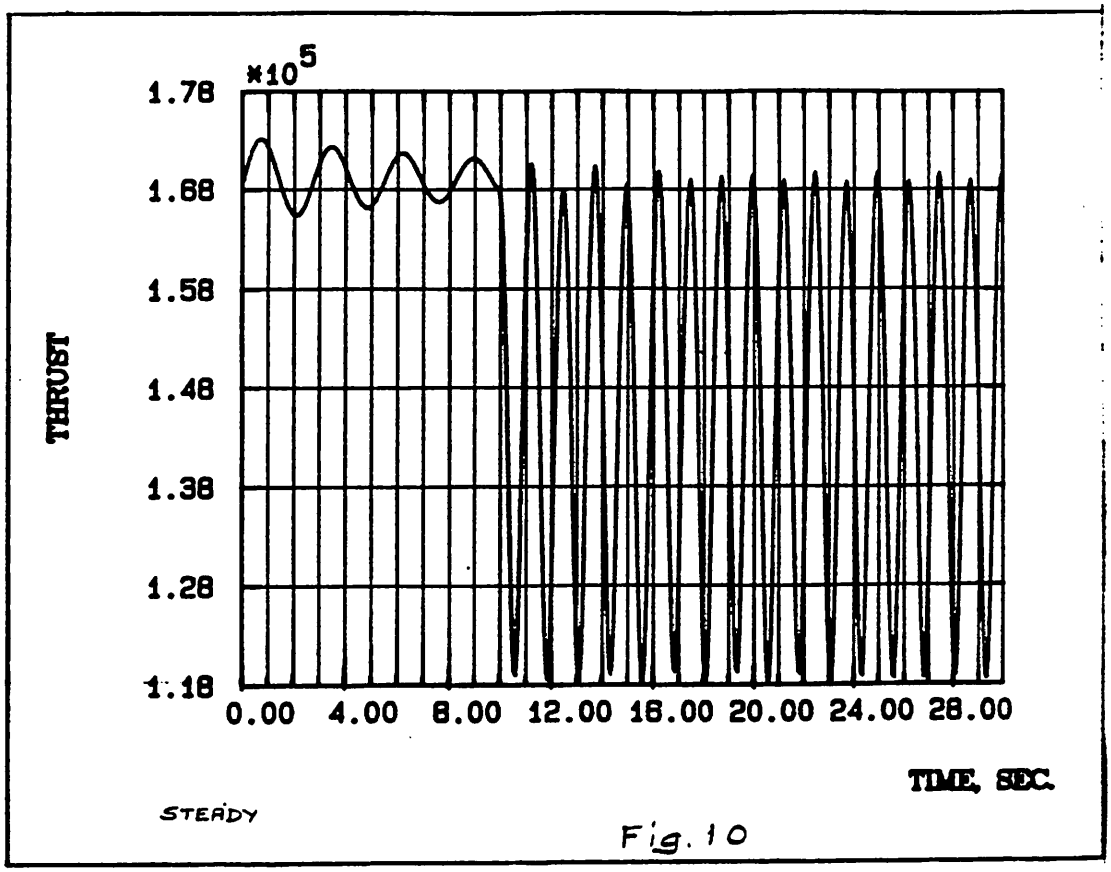

Fig. 10

Before the onset of the pitch oscillation the thrust is seen to oscillate as a response to the tower rocking motion. This rocking is the result of the tower responding to the sudden thrust at time zero when the calculation starts integrating the motion. A slight damping of the tower amplitude can be discerned. After ten seconds the pitch oscillation causes the thrust to respond. The average amplitude of this oscillation is found in the table below. All basic values in it were obtained in this way from the corresponding diagrams. The ratios, at the lower line in the table, is the essence of this particular study. For anyone who is concerned with say fatigue the figures should serve as an alarm clock against relying on steady performance methods. In the case of torque, and associated blade forces, the miscalculation can apparently be as large as a factor 4 to 5. The wind was intentionally chosen low such that the differences would appear distinctly. In the higher wind regimes the difference is less. The present performance model, with time history calculation for tower motion and induction over the disk, does not have flexible blades. The real machine would therefore experience slightly lower values of response because the blades would yield to both thrust and torque. If, therefore, measured data were to be used in place of the unsteady results this may affect the ratios in the table slightly but not much.

TABLE FOR RESPONSE AMPLITUDES

Method	Tower displmt	Torque	Thrust	Tower acc.	Tower vel.
Unsteady	.07m	1.8e5	1.2e5	.9 m/s2	.2 m/s
Steady	.022	.4 e5	.5e5	.4	.09
$\frac{\text{Unsteady}}{\text{Steady}}$	3.2	4.5	2.4	2.25	2.2

It should be emphasized that the table values are changes in parameters not absolute values. The values were obtained as the amplitudes of oscillation for each quantity listed in the table.

7. EXPLANATION OF THE DIFFERENCE BETWEEN STEADY AND UNSTEADY METHODS

The torque is more sensitive to changes in circumstances than the thrust. The reason is that a change of blade element lift force size is accompanied by a tilt of same vector the effects going in different directions if the steady method is used. When the unsteady method is used it essentially means that the induction is independent of the pitch angle during a relatively short period of time. This causes the change of the local angles of attack to be equal to the pitch change initially. Therefore the unsteady method would produce a thrust change and a torque change that are both crudely speaking proportional to the pitch change. The steady induction method can be thought of as counteracting every pitch change, although it does not fully eliminate its influence. There is no such elimination immediately following a pitch change in reality or in the unsteady method. Therefore changes in pitch or wind pay, so to speak, full dividend initially. This is experienced as larger forces. It is hoped that the figure below will lend further support to the understanding of the differences.

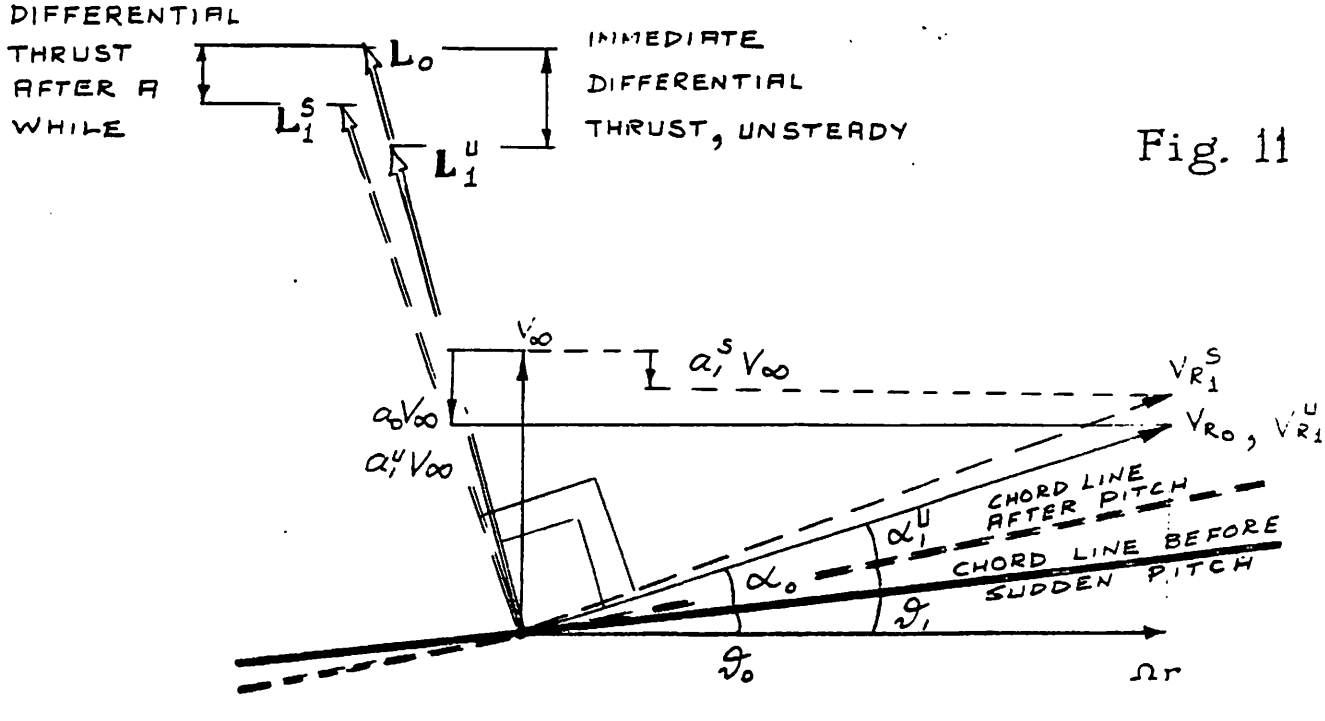

Fig. 11

Fig. 11 depicts the hypothetical, but instructive, case where a blade element on the rotor is subjected to a sudden pitch change. This change will eventually cause the vorticity that is shed in the wake to increase in power and it will therefore excert an ever increasing but assymptotic influence on the rotor itself.

In Fig. 11 the following notations are used.

V = Wind velocity.
α = Angle of attack.
ϑ = Local pitch angle.
a = Relative induction.
L = Lift force on the blade element.
Ω = The rotor rotational velocity.
r = The radial location of the (mid-point of) blade element.
∞ = Subscript, circumstances for ambient conditions.
o = ---------- " ---------- at rest before sudden pitch change.
1 = ---------- " ---------- after --------- " --------
R = --- " ---- to indicate resulting velocity.
s = Superscript indicating steady circumstances that will prevail after a long time in reality. It also indicates circumstances that will be calculated (erroneously) with steady methods even immediately after the sudden pitch change. The unsteady method, in contrast, will gradually sneak up toward this value after a while.
u = Superscript to indicate unsteady circumstances immediately after the sudden change.

8. EPILOG

It is hoped that the material presented in this write-up will serve as a useful base for discussions on this seemingly important topic. In no way is it mathematically stringent. Nor is there any measured data available ,at the time of writing, in quantitative support of the conclusions inherent in the three numerical exercises presented. As more experience is accumulated in the future the usefulness of the suggested method will be put to the test. For this reason a more complete report on this topic is foreseen.

Aerodynamic Theory in the Calculation of the GROWIAN Rotor Compared with some Experimental Data

BY

R. Pernpeintner, G. Huss, E. Hau

1. Introduction

For the prediction of rotor performance of wind turbines many theories have been published, most of which have derived from theoretical propeller models. Betz, Glauert, Prandtl, Goldstein, Hütter should be mentioned as the best-known authors. They used more or less idealized models of the rotor aerodynamics. A rather useful method is the so-called "strip theory" or "blade element theory" which was adapted for wind turbines by Lissaman and Wilson.

The blade element theory can also be used for the calculations of the aerodynamic loads on rotor blades. But the physical modeling and the equations used for this theory let expect uncertainties in some operational modes. These items are in particular: operation at very low tip speed ratios, vortex state, instationary and unsymetrical inflow conditions, fast blade pitch changes and partial span pitching.

This paper indents to give a survey of the comparison of calculations done by the strip theory with different theories. Furthermore the theoretical values shall be compared to experimental data from wind tunnel tests and data measured at the large German wind energy converter GROWIAN.

2. Aerodynamic Modelling of Performance and Load Calculations in Steady Flow Conditions

2.1 Aerodynamic Modelling

The blade element theory which is described in detail by Lissaman and Wilson (1) for wind turbines with horizontal axis was used for GROWIAN performance calculations (2, 3). In contrary to Betz and Glauert it considers a wind rotor with a finite number of blades. The flow is assumed to be incompressible, viscous and rotating. Tip losses due to trailed vorticity are considered by correction factors according to Prandtl or Goldstein (fig. 1).

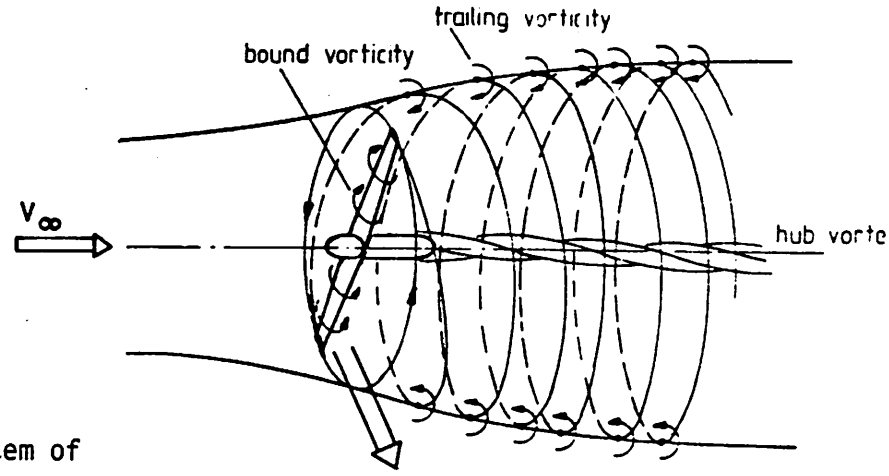

Fig. 1: Idealized vortex system of a horizontal-axis wind turbine

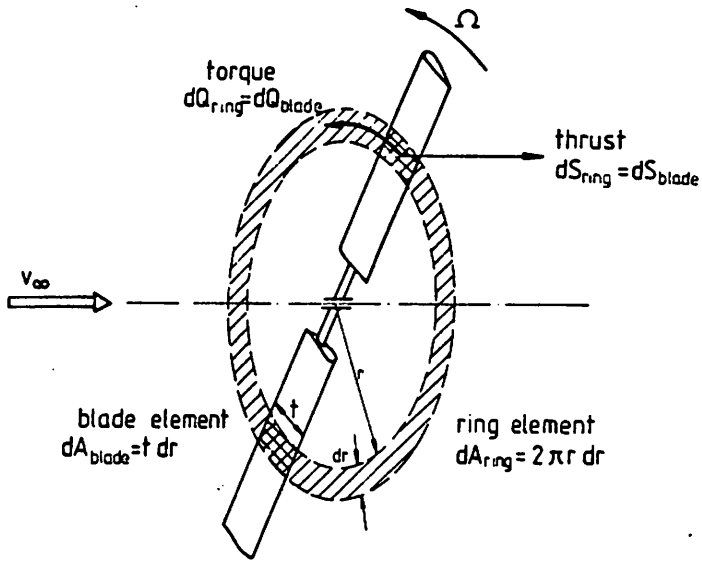

Fig. 2: Physical modelling of the blade element theory

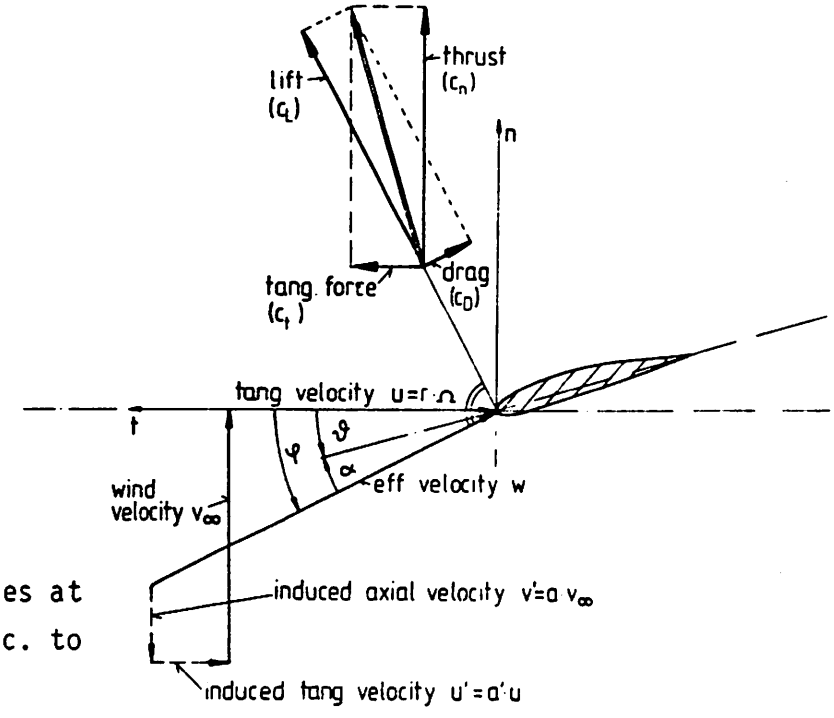

Fig. 3: Flow conditions and forces at a local blade element acc. to blade element theory

The flow model is based on the equations of linear and angular momentum at a streamed ring element in the rotor plane and combines them with the aerodynamic airfoil characteristics of the corresponding blade element (fig 2,3).

These equations make it possible to calculate the velocities at the rotor plane, which are induced by the blades and the wake. The flow state can be defined with these velocities.

By means of the strip theory the rotor performance and the loads acting on the blades can be predicted for a given rotor configuration in a defined operational state.

The rotor configuration is described as:

- rotor diameter D
- number of blades B
- blade geometry (chord t, twist Θ, thickness d)
- airfoil characteristics (lift-drag relation $C_L = f(C_D)$)

The operational state is to be defined by:

- tip speed ratio λ
- wind speed V
- blade pitch angle $\varphi_{.7}$ at 70% radius

The aerodynamic loads at the blades and the rotor performance parameters which result are:

- lift L and drag D
- thrust S and tangential force T
- rotor power P_R
- rotor power coefficient C_p

The power coefficient C_p is the efficiency of extracting power from the wind.

$$C_p = \frac{P_{Rotor}}{P_{Wind}} = \frac{P_{Rotor}}{\rho/2 \cdot V^3 \cdot A_{Rotor}}$$

2.2 Comparison with Wind Tunnel Tests

In order to verify the performance calculation with the blade element theory a 1:25 scale model of the GROWIAN rotor was submitted to wind tunnel tests. The rotor (4 m in diameter) was tested in the 7x7 pre-chamber of the DFVLR wind tunnel in Göttingen and was located upwind of the supporting structure in order to eliminate shading effects (fig.4). For the carbon fibre rotor blades Clark Y airfoil sections with 11% to 25% relative thickness were used, because only for these sections aerodynamic data at low Reynolds-numbers, necessary due to model scaling, were available for calculation.
It should be pointed out that the comparison between the theoretical and experimental data - shown below - is carried out for the 4 m model rotor.

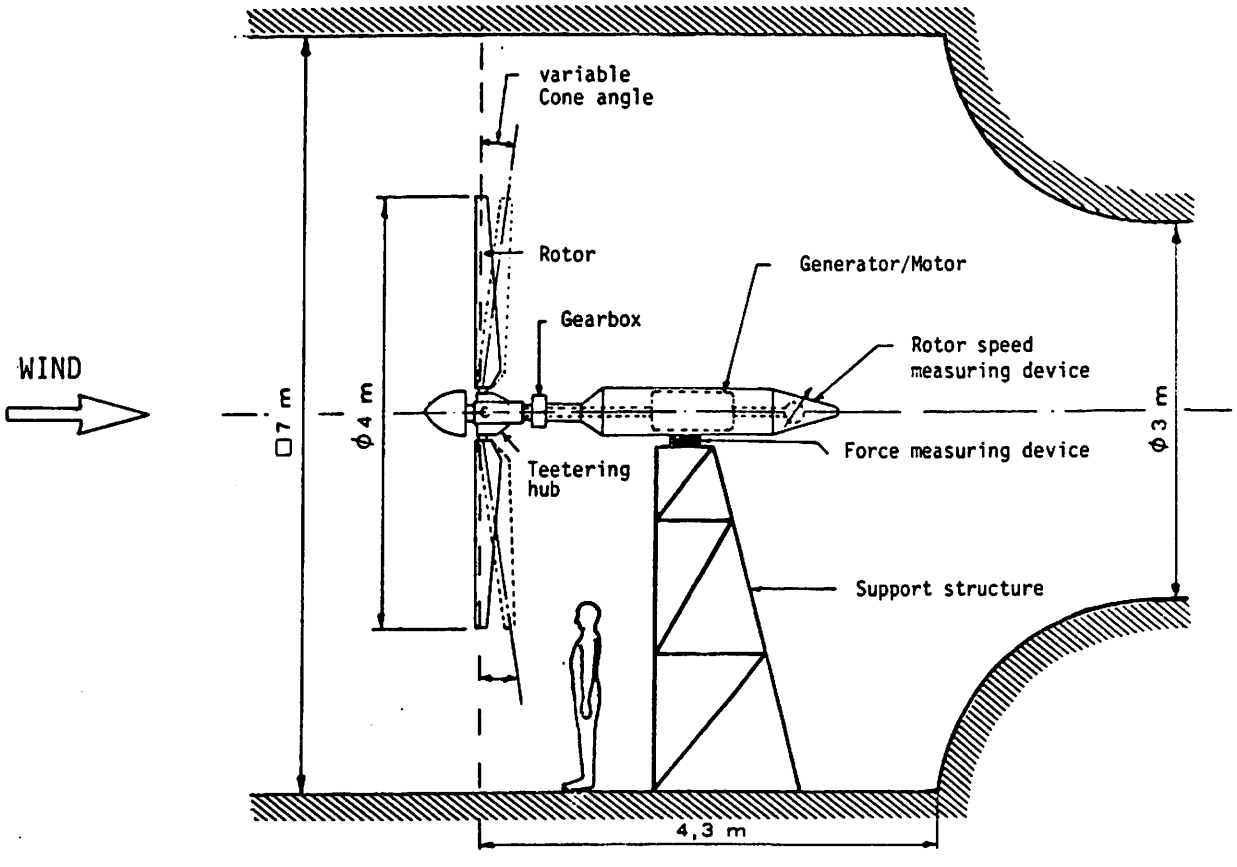

Fig. 4: GROWIAN rotor model in the pre-chamber of the wind tunnel at DFVLR Göttingen

Up to the point where recirculation (vortex state) is predicted to occur, the experimental data presented here for several blade pitch angles and rotational speeds (fig. 5a - d) show a fairly good agreement with the calculated C_p- λ -curves (4). The experimental data vary slightly with the adjusted rotor speed, due to the different behaviour of the airfoil characteristics at different Reynolds-numbers.
Beyond the "vortex state", which is predicted by the theory for small blade pitch angles at high tip speed ratios, the theory is no longer valid. The wind tunnel tests show, that the power coefficient decreases slowly similar to the C_p- λ- curves for other pitch angles.

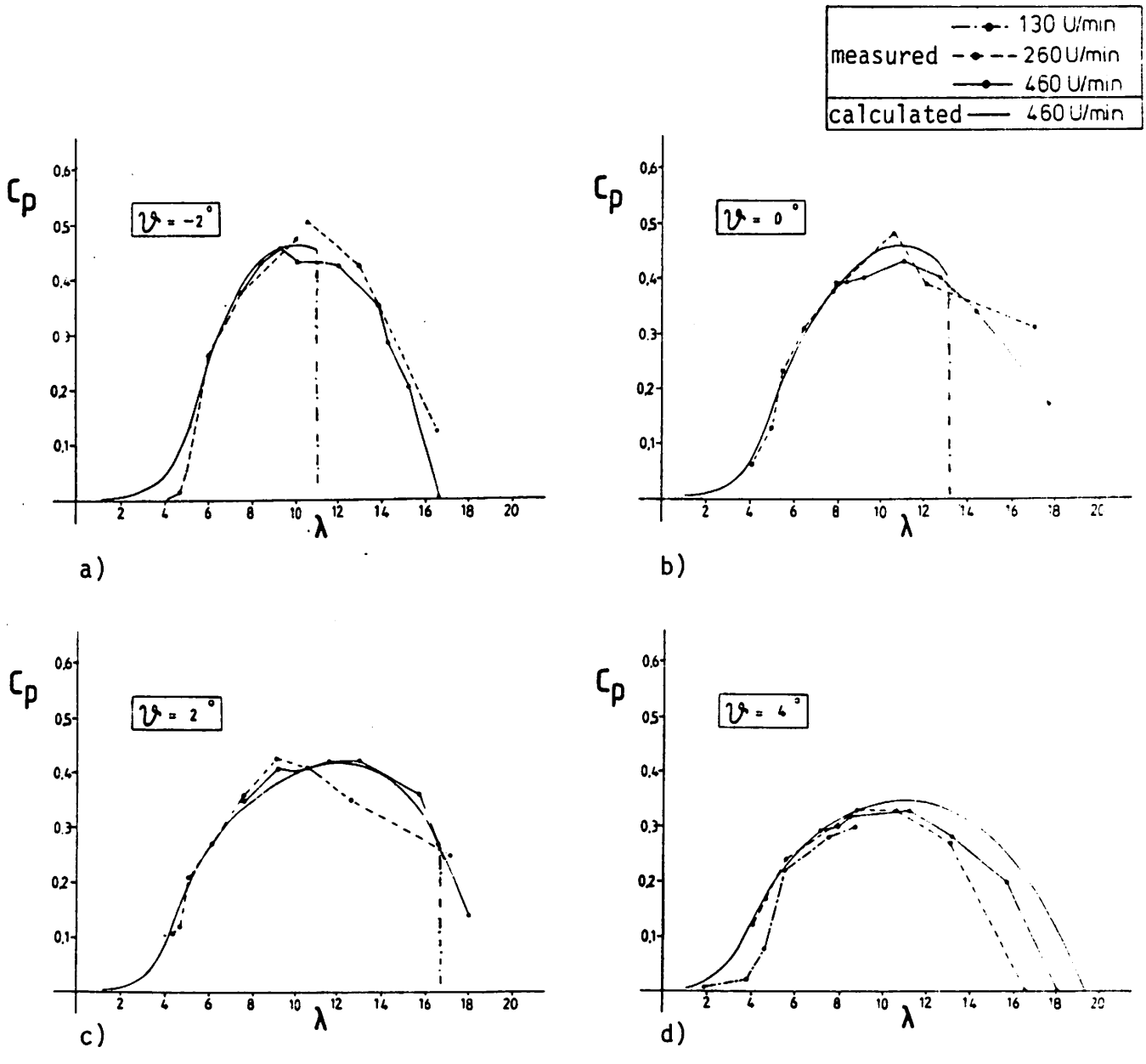

Fig. 5: Measured and calculated power coefficient of the GROWIAN-model

Regarding the overall shape, the design tip speed ratio and the maximum power coefficient, the calculated performance characteristics of the model rotor and of GROWIAN are very similar (fig. 6a, b). Due to this fact, it seems that the experience gained by the wind tunnel test can be transferred to the full scale GROWIAN.

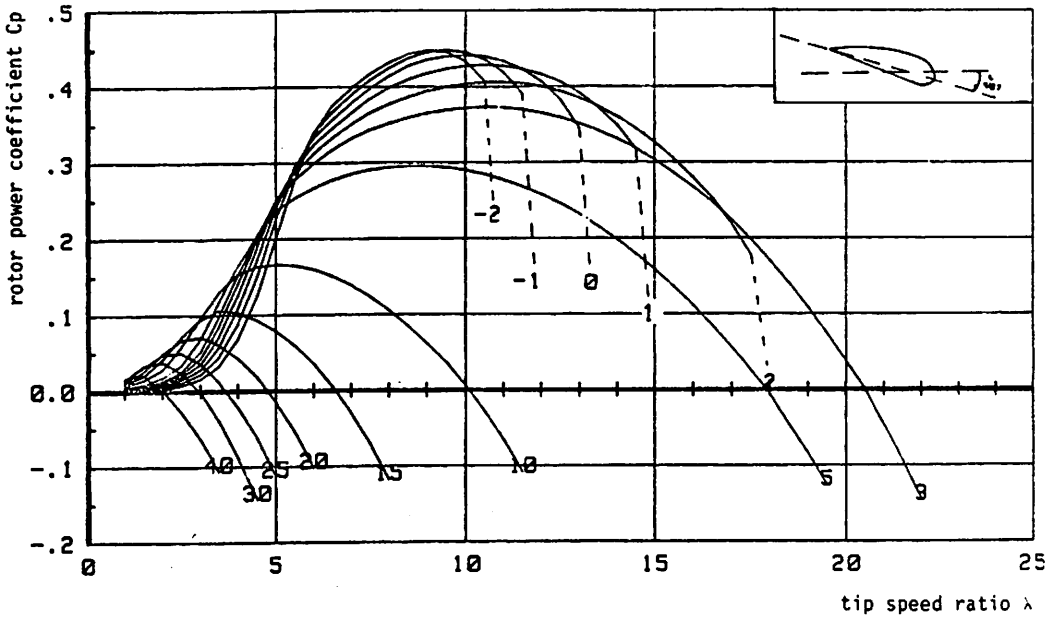

Fig. 5a: Calculated rotor performance characteristic of GROWIAN

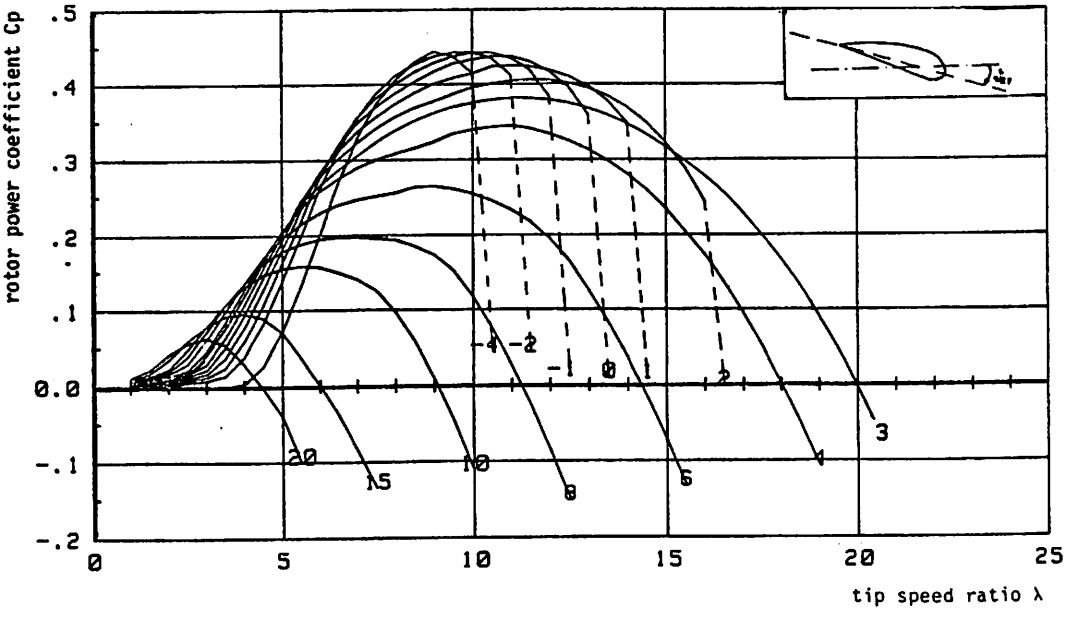

Fig. 5b: Calculated rotor performance characteristic of the 4 m-model-rotor

2.3 Correlation with Measured Data from GROWIAN

Regarding the rotor power characteristic (C_p-λ), a comparison between experimental data of the full scale GROWIAN with the theoretical ones is not available up to now. Fig. 7 therefore shows the calculated power curve compared to the power data of GROWIAN measured in several operational campaigns. The wind speed, measured at hub height at the spur of GROWIAN approx. 25 m upstream of the rotor, is corrected with data obtained by two wind measurement towers 70 m upstream of GROWIAN (5).

As expected for quasistationary operation in homogenous wind condition, the calculated power curve fits the measured data in a sufficient way.

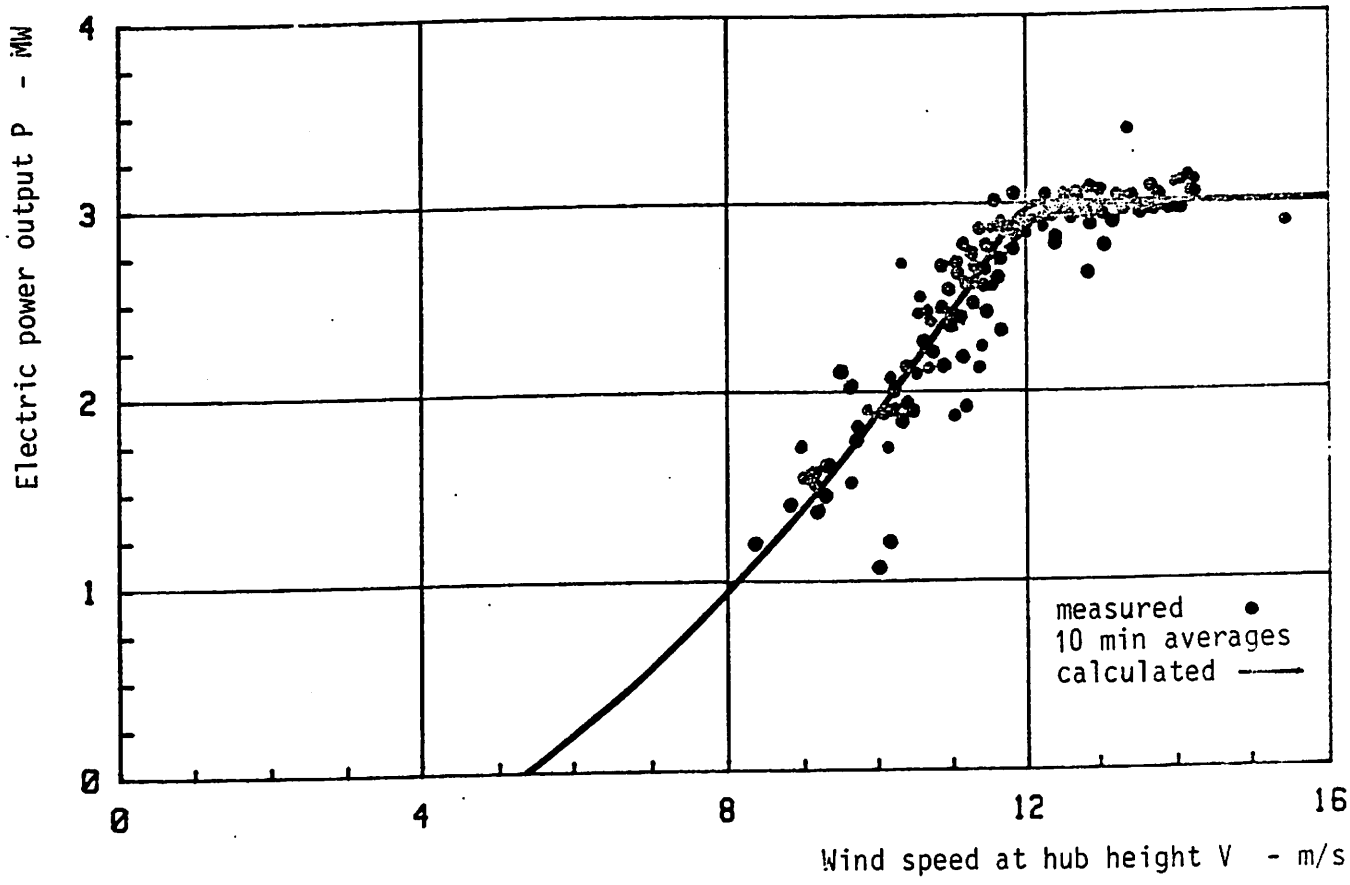

Fig. 7: Correlation of measured and calculated power output of GROWIAN

3. Rotor Behaviour at Low Tip Speeds and in Instationary operation modes

3.1 Operation at Low Tip Speed Ratios

As the validity of the strip theory was presumed to fail at the parked turbines and at very low tip speed ratios ($\lambda < 1$), a simple aerodynamic modelling of the rotor was developed (6). It calculates the aerodynamic forces at the blade on the basis of the classical lifting line theory according to Prandtl, but is solved by means of the numerical method of Multhopp (7).

This model considers only the spanwise induction of the flow due to the trailing vortices. The axial and tangential velocities in the rotor plane induced by the wake are neglected. This assumption seems to be allowed for turbines with few rotor blades, high blade setting angles and low rotation speed. For the GROWIAN-rotor the torque coefficient calculated with the simple model is plotted in fig. 8 and compared to the values resulting from the Lissaman-Wilson theory. The plots show a fairly good agreement of both computational models. The simplified model provides somewhat higher values.

The values provided by the GROWIAN measurement however reflect a 10 to 20% lower level than the theoretical ones.

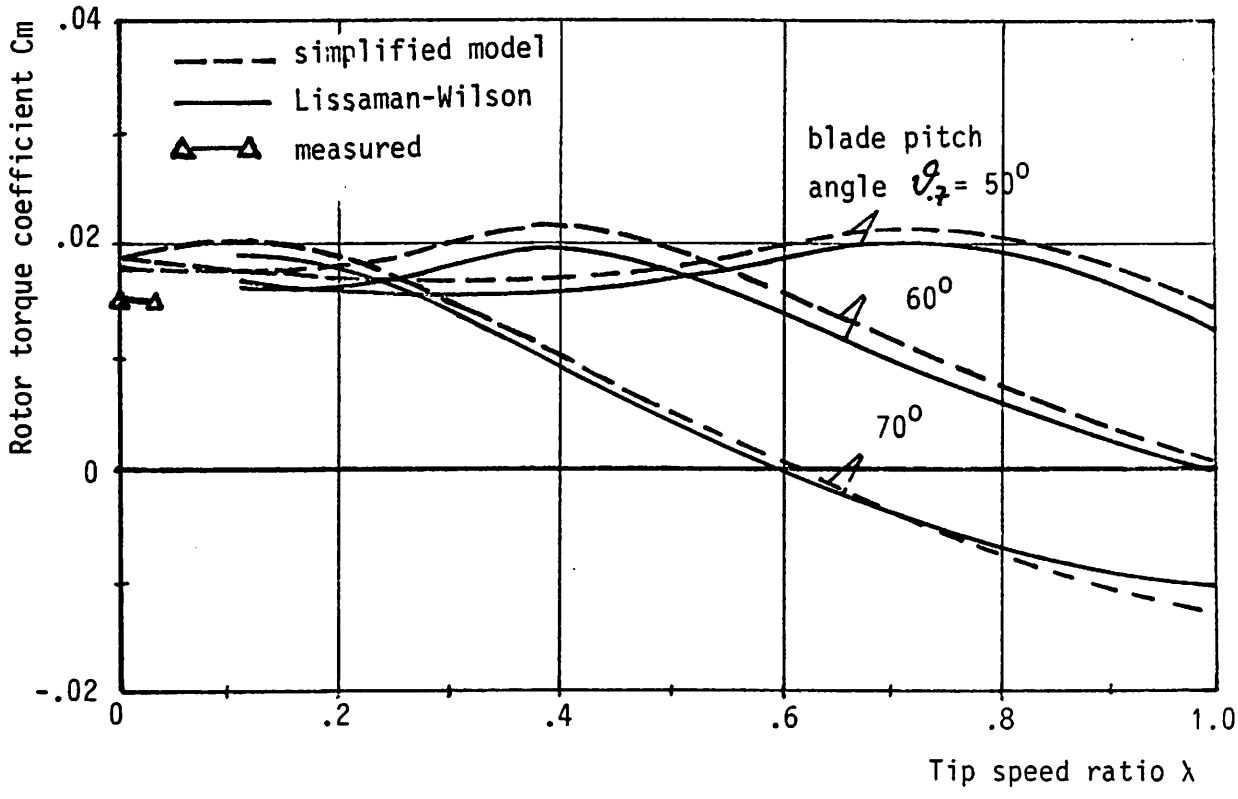

Fig. 8: Rotor torque coefficient for low tip speed ratios for the GROWIAN rotor

3.2 Application of the Calculation Methods in Rotor Start-up and Shut-down Procedures

Some essential problems are involved in the application of aerodynamic modelling to the start-up and shut-down procedures.

The first one concerns the aerodynamic data of airfoil sections. For most airfoils data are only available for angles of attack ranging from small negative values up to the stall region at positive lift coefficients. But above all for start-up and shut-down procedures, lift and drag coefficients are required for angles of attack ranging from -90^{o} to $+90^{o}$. Assumptions, based on characteristics from different but similar airfoils, were made for GROWIAN's design. Fig. 10 reflects measured and assumed values for the airfoil FX 79-W-151 A, which was supplemented in the post stall region by the characteristic of NACA 0012.

A second problem is also combined with the aerodynamic behaviour of airfoils. The pitching of the blades is an instationary operation procedure. Therefore the question arises, at what pitching rate instationary aerodynamics have to be taken into account.

Another problem arises, especially in connection with the blade element theory. The theoretical model is based on a stationary, homogenous wake model. However, with respect to the variation of the axial and circular induction during the blade pitching procedure, there are doubts whether the stationary model is still adequate. Furthermore, it should be generally clarified whether the blade element theory according to (1) has to be expanded to a three-dimensional model.

As an example where all these problems may be involved, an emergency shut-down of GROWIAN, which occurred during commissioning, was recalculated. Fig.11a and b show the time history of wind speed (at hub height) and blade pitch angle during an emergency shut-down. The blade pitching is a fixed procedure which is - once actuated - not controlled by the operation control system. Fig.11c reflects the time history of the rotational speed at the high speed shaft.

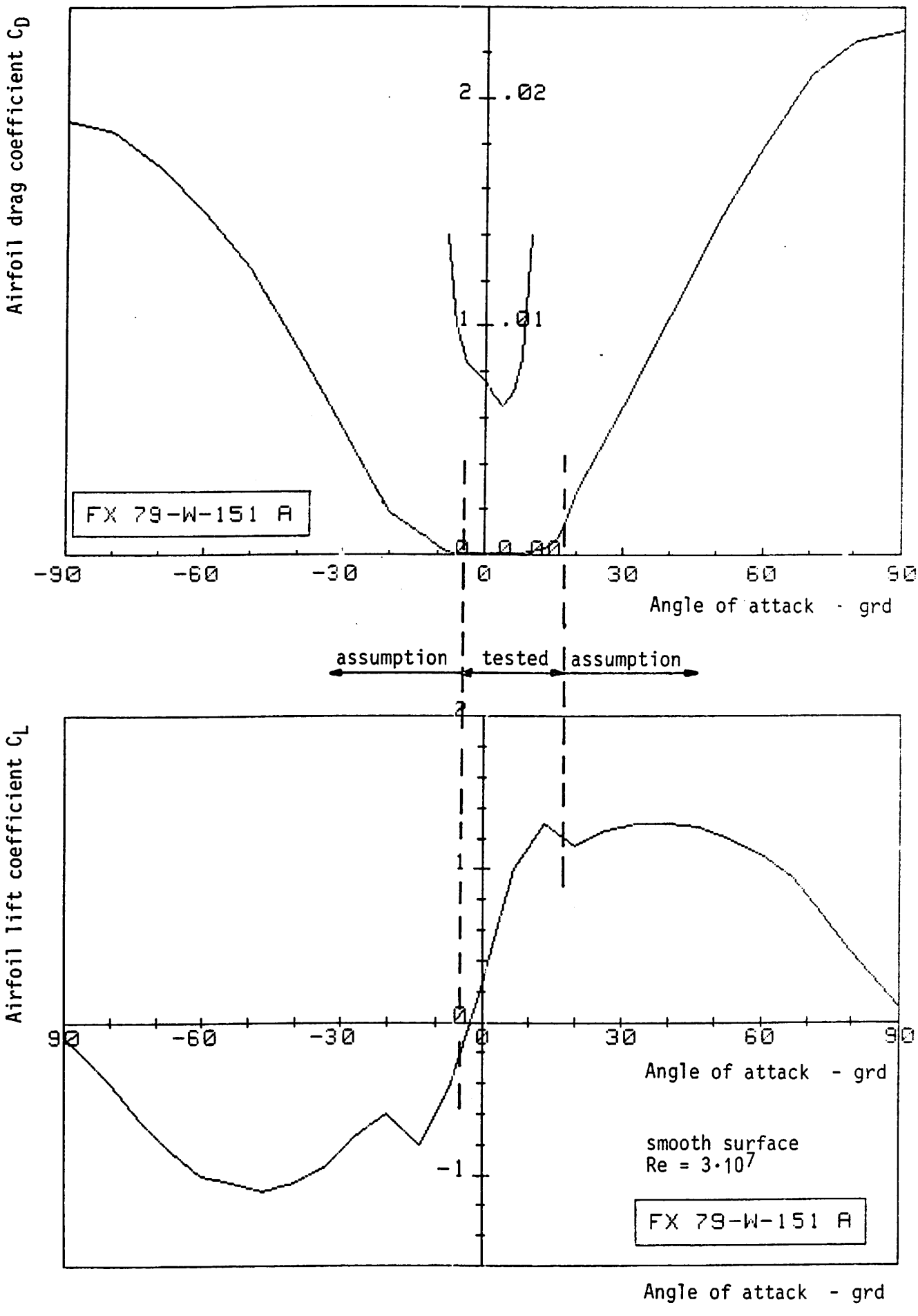

Fig. 10: Aerodynamic airfoil data of FX 79-W-151 A (15 % rel. thickness) used with GROWIAN

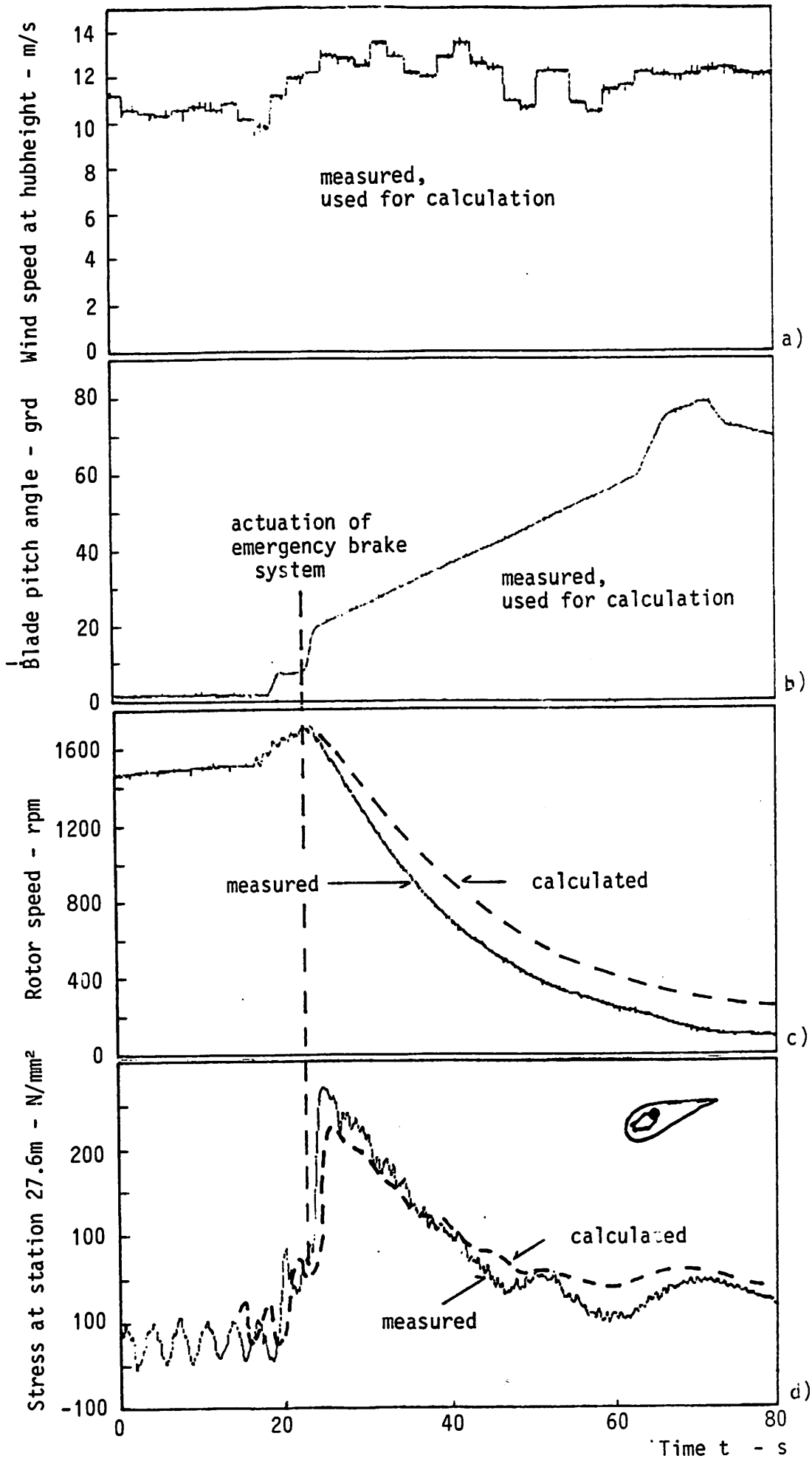

Fig. 11: Time history of an emergency shut down of GROWIAN

The dashed line is for the recalculation of this procedure, based on measured time history of wind speed and blade pitch angle. The curves show that the rotor brakes down faster in reality than in computation. The measured stresslevel is also higher than calculated. The reason for this deviation may be primarily the higher aerodynamic forces acting on the blades due to the effects mentioned above. Investigations are still going on in order to analyse these effects in detail.

4. Conclusion

The comparison of the measured and calculated power curve shows that the blade element theory works in stationary operation in a sufficient way. Also when comparing the aerodynamic loads on the rotor blades for different load cases, the blade element theory turns out as an excellent and quick tool for calculations. Only for some cases, where fast instationary operation conditions are implicated, there are differences between theoretical modelling and measurement which cannot be neglected. Obviously, it seems that the limits of the validity of the stationary theory are reached under these conditions.

References

(1) Lissaman P.B.S., Wilson R.
Applied Aerodynamics of Wind Power Machines
Oregon State University, Oregon, 1974

(2) Huss G., Pernpeintner R.
Aerodynamische Rotorauslegung der großen Windkraftanlage GROWIAN
3. Internationales Sonnenforum, Hamburg, 24. - 27.06.1980

(3) Huss G., Zeckau J.
Effect of Blade Geometry on the Performance Characteristics of a Wind Turbine Presented for the Large Wind Energy Converter GROWIAN
Euromech 153 Conference, Poitiers, Apr. 1982

(4) Gilhaus A., Pearson G.
Windmessungen an einem Modell M 1:25 des GROWIAN-Rotors
Internal paper, MAN-München, 1981

(5) Körber F.
Statusbericht GROWIAN Juni 1984
Internal paper, MAN-München, 1984

(6) Dürmeier S.
Theoretisches Modell zur Berechnung des Anfahrverhaltens von propellerartigen Windturbinen im Bereich niedriger Schnellaufzahlen
Internal paper, MAN-München, 1981

(7) Multhopp H.
Die Berechnung der Auftriebsverteilung von Tragflügeln
Luftfahrt-Forschung 15 (1938) 153-169

Aerodynamic Performance of a New LM 17.2 m Rotor

Flemming Rasmussen

Summary

The paper describes measurements of the aerodynamic properties of a 17.2 m diameter LM rotor mounted on a VESTAS 55 kW windmill. Power curves were measured for a range of blade tip angles to find the best angle both in relation to energy production and stalling characteristics. With this optimum blade setting the flapwise blade root bending moment was measured as a function of wind speed. Also the drag coefficient at 90° angle of attack is calculated from measurements of the integrated value, i.e. the flapwise blade root bending moment as a function of wind speed during stand still.
With some simplified considerations the profile properties (C_L, C_D curves) are estimated from aerodynamic calculations and the results compared to existing profile data from 3-dimensional wind tunnel measurements.

The flapwise blade root bending moment versus blade angular position during one revolution was measured in skew wind and is compared with calculations.

The influence of surface roughness introduced at a certain percentage of the section chord and the dependency on the Reynolds Number is investigated and discussed from observed discrepancies in the measured power curves.

1. INTRODUCTION.

The investigation presented in this paper concerns the first prototype of the 17.2 m rotor from LM Glasfiber. The rotor was installed on a VESTAS 55 kW machine at The Test Station for Windmills and tested in operation for about one year from January 1983. The tests covered both aerodynamics and structural response, but only investigations concerning aerodynamics are presented in this paper.

The focus is on more fundamental aerodynamic properties that could make a basis for a change of different parameters if necessary.

The design was after these investigations slightly modified and the performance of the final commercially available rotor is described in Ref. (1). The main data for the prototype rotor and the Vestas machine are described in Table 1 and the measurement parameters in Table 2.

2. FUNDAMENTAL MEASUREMENTS

Of direct importance, of course is the power curve of the actual rotor. It has to be measured in order to define its performance because the prediction of the power curve may be very inaccurate. But afterwards, what is important is the possibility of gaining information that makes it possible to predict the behaviour of modified rotors.

To describe the aerodynamic behaviour of a rotor the fundamental parameters are the rotor shaft torque and the axial thrust. The axial thrust is equivalent to the forces producing the flapwise blade root bending moment, and this parameter is more convenient to measure. The rotor shaft torque and the flapwise blade root moment represent the inplane forces and forces perpendicular to the rotorplane, respectively. These forces result from the section lift and drag, and thus make it possible to gain information on the actual lift and drag coefficients as they form during the operation of the rotor.

2.1 Power curves

The electrical power curve was measured for three different blade tip angle settings to find the optimum in relation to efficiency and stalling characteristics. The result is shown in Fig. 1. The power curve at high wind speeds at 2.5° tip angle is measured at reduced rotor rotational speed (25 rpm) and converted to 50 rpm. The power curve is sensitive mainly to blade tip angle in the stalling region. To avoid too much drop off of the power after the stalling point a blade tip angle of 2.5° is the most convenient and is used for all further investigations in this paper.

The mechanical power curve at 2.5° tip angle was not measured directly. It is derived based on earlier measurements of drive train and generator efficiency of the VESTAS machine, and is also shown in Fig. 1.

2.2 Flapwise Blade Root Moment Curve

The flapwise blade root bending moment was measured at a distance r = 0.87 m from the centre of the rotor and as a function of wind speed. The curve is shown in Fig. 2. At wind speeds above 17 m/s the curve is converted from measurements at reduced rotational speed (25 rpm). It is seen that the relation is nearly linear, and the shape of the curve rather typical for a stall controlled rotor (see Ref. (2)).

2.3 Drag Coefficient

The drag coefficient at 90° angle of attack is important when calculating the extreme loads to which a windmill is exposed during stand still at high wind speeds and generally when making aerodynamic calculations. This drag coefficient could be found from measurements of the blade root bending moment as a function of wind speed with the blade stopped in an upright position and with the nacelle direction following the wind direction.

This measurement was performed and the result is shown in Fig. 3. The drawn curve is a fitted second order curve where the bending moment is expressed by

$$MBX(N) = 14.5 \cdot V^2 \ (m/s)$$

The drag coefficient is now found by integrating the moment performed by the drag force along the blade. Assuming that the drag coefficient is constant we get:

$$C_D = 1.24$$

This value around 1.3 is found from earlier measurements on another blade with other profile section, and is in agreement with wind tunnel measurements on a flat plate with aspect ratio about 7, but far from two dimensional measurements where approximately 2 is obtained.

3. ESTIMATION OF PROFILE PROPERTIES

The basis for aerodynamic calculations and thereby the design of new rotors with qualifications desired is the profile data for an angle of attack of from 0 to 90°. These data are normally nonexistent but with some simplified considerations they could be estimated from aerodynamic calculations.

The basis for the estimation is to obtain as good agreement as possible between the measured and the calculated power curve and flapwise blade root moment curve, respectively. This means that the measured and calculated moments derived from the sum of the total aerodynamic forces on the blade are identical both in magnitude and direction.

The estimation is made by assuming constant profile properties along the blade and just correcting the C_L and C_D values to give the right results.

Figure 4 shows the C_L and C_D curves estimated under these assumptions; the corresponding calculated mechanical power curve and flapwise blade root moment curve are shown in Figs. 1 and 2, respectively. The power curve is very close to the measured one but the flapwise moment curve is somewhat different at about 10 m/s. Some of the difference could be explained by the release of a few percent of the load on the blade when bending due to the centrifugal force. This means that the flapwise moment from the aerodynamic force is slightly higher than measured.

When making these kinds of estimations the measurement accuracy should be very high as the estimated values are very sensitive to changes in the power and flapwise blade root moment curves. Probably we are operating near the limit of what could be obtained from these kinds of measurements.

One application of these estimated profile properties is to predict the properties of rotors using the same blades but with changes in rotational speed, rotor diameter or tip angle (see also Ref. (3)). Another application is when designing new blades using the same profiles. In these cases one would expect that even if the profile properties are perhaps not definitely correct, they are adjusted to give results in accordance with reality.

Investigating the lift and drag coefficient curves in Fig. 4 more closely one recognizes that up to angles of attack of about 16° they are in very good agreement with two-dimensional wind tunnel measurements on the same profile.

Also shown in Fig. 4 is a reproduction from Ref. (4) of C_L and C_D values for a wing with an aspect ratio of 8 and two free tips. The airfoil is Clark Y. One realises that reasonably good agreement is obtained above the stall point, at least much better than corresponding to two dimensional data. Even better agreement is obtained, especially for the drag, if the estimated values are compared to the measurements of Ref. (4) at different aspect ratios and in such a way that the aspect ratio is decreased with increasing angle of attack.

These calculations lead to the conclusion that two dimensional data for the specific profile are adequate up to about 16° angle af attack. In the stall region the lift and drag coefficients depend as well upon the specific profile used, and could probably not be estimated exactly without previous measurements.

4. DYNAMIC LOADS IN SKEW WIND

One important aspect of a stall-controlled rotor is the occurrence of dynamic loads in skew wind. The phenomenon is fully described in Refs. (2) and (5). To investigate the loads for this specific blade the flapwise blade root bending moment was measured as a function of wind speed, yaw angle and blade angular position using a "three-dimensional method of bins" described in Ref. (2).

One result is presented in Fig. 5 as the flapwise blade root bending moment during one revolution at a wind speed of 13.2 m/s and -32° yaw (definition, see Ref. (2)). Also shown is the calculated curve under the same conditions. The calculation in skew wind is performed by The Department of Fluid Mechanics, The Technical University of Denmark, using a code based on ordinary momentum theory. The blade is assumed to be infinitely stiff. There seems to be a systematic difference in the mean value but according to dynamics the two curves are in quite good agreement. There is a small phase lag of the measured curve which could be explained by the delayed response of the rather soft blade when activated by the 0.85 Hz oscillating load.

One interesting thing is seen at a blade angular position of 300° where the load suddenly drops off. A similar phenomenon is seen on another rotor under nearly the same conditions (Ref. (2), Fig. 15). It could be explained by the fact that at this blade position a great deal of the outer part of the blade goes from the stall region back to a condition of unseparated flow (determined from the calculations). Under these dynamic circumstances probably the re-creation of the unseparated flow is delayed, and this causes the drop in the bending moment.

5. INFLUENCE OF SURFACE ROUGHNESS

It could generally be of interest to investigate the possibility of changing the profile properties and thereby the power curve by introducing roughness at a certain part of the blade. If it is generally possible to decrease the stalling power without decreasing the efficiency at lower wind speeds, it would be seen as an advantage.

An investigation on this problem was performed with the LM-rotor where a 20 mm broad strip of rough tape was placed all along the blade at different percentage of the blade section chord.

The first tape investigated had an average grain size of about 0.3 mm and the power curve at 50 rpm was measured with the tape placed first at the leading edge, then at 5% chord and at last at 20% chord at the upper side of the profile. No significant changes in the power curve was obtained by using this tape. The second tape had a mean roughness height of about 1 mm and measurements were carried out only with the front tape edge at 5% chord all along the blade.

The power curves were measured both at normal (50 rpm) and reduced (25 rpm) rotational speeds and are shown in Figs. 6 and 7, respectively, together with the ones without roughness tape. It is obvious that at 50 rpm the maximum power is decreased about 7 kW, but there is also a reduction at lower wind speeds down to about 8 m/s where the two curves coincide. This means that the reduction of the peak power in this case also infers a reduction of energy production at lower wind speeds.

Quite opposite and perhaps somewhat surprising results are obtained at the reduced rotational speed (reduced Reynolds Number), where the power output has been generally increased by using the roughness tape.

This increase in efficiency with roughness at low Reynolds Numbers led to the assumption that it would be possible to increase the maximum power coefficient slightly at normal rotational speed by placing tape only on the inner half of the blades, where the Reynolds Number is low. The test was initiated but no sure verification was obtained before the test had to be interrupted.

6. CONCLUSION

A description has been given of important measurements to define the behaviour of a stall controlled rotor. It seems that the method used to estimate the profile properties gives data that are quite reasonable. The procedure therefore seems rather adequate for design purposes.

The calculations in skew wind gives the right fundamental relationship, but the method probably could be developed to result in better absolute accordance with measurements. But measurements could also be performed at greater accuracy and this is probably essential in order to develop the calculational method.

References

1. Risø M-2457. "Performance of the LM 17 m rotor".
   Flemming Rasmussen
2. Risø-M-2402. "Blade and rotor loads for VESTAS 15".
   Flemming Rasmussen
3. Risø-M-2432. "Simplified Laws of Similarity for Wind Turbine Rotors".
   Helge Petersen.
4. RFP-3387 UC-60. "A Catalog of Law Reynolds Number Airfoil Data for Wind Turbine Applications".
   S.J.Miley.
5. Risø-M-2346. "Measurements and Calculations of Forces on the Blades of a Stall Regulated HAWT".
   Flemming Rasmussen, T.F.Pedersen.

Table I. Main data for LM 17.2 m/VESTAS 55 kW

Rotor

Three-bladed, stall-regulated, horizontal-axis rotor positioned in front of tower.

Direction of rotation:	Counter clockwise
Rotor diameter:	17.20 m
Rotational speed:	50.3 rpm
Reduced rotational speed:	25.1 rpm
Cone angle:	0°
Tilt angle:	5°

Blades

Blade manufacture:	LM 8.6 m
Natural frequency flapwise:	2.4 Hz
Profile series:	NACA 63-212/24

Blade data:

Radius (m)	Chord (m)	Twist (Deg)	Thickness %
1.375	1.07	14.9	24.7
1.80	1.033	11.6	22.7
2.65	0.955	7.4	19.5
3.50	0.876	4.8	18.0
4.35	0.796	3.1	17.0
5.20	0.717	2.0	16.0
6.05	0.638	1.2	15.0
6.90	0.558	0.7	14.0
7.75	0.478	0.3	13.0
8.60	0.400	0.0	12.0

Generator

Rated power:	55/11 kW
Slip at full load	2%

Table II. Measurement parameters

Meteorological readings

- o Air pressure.
- o Air temperature.
- o Wind speed, two rotor diameter upstream.
- o Wind direction, two rotor diameters upstream

Turbine structure readings

- o Flapwise blade root bending moment at a distance of 0.87 m from the rotor centre.
- o Rotor rotational speed
- o Electrical power
- o Nacelle direction
- o Blade angular position
- o Rotor shaft torque

Table III. Normenclature

V	Wind speed
PE	Electrical power
PM	Mechanical rotor power
MBX	Flapwise blade root moment, r=0,87 m
r	Radius
C_L	Lift coefficient
C_D	Drag coefficient
Alpha	Angle of attack
POS	Angular position of blade (Blade upwards: POS=0)
Yaw	Angle of skew wind

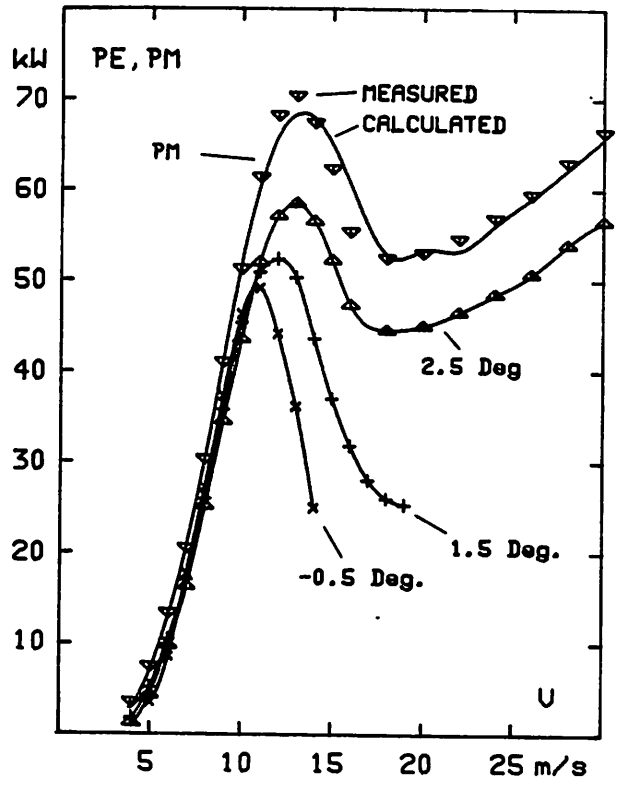

Fig. 1. Measured electrical power curves at different blade tip angles and measured mechanical power curve at 2.5° tip angle compared to a calculated curve.

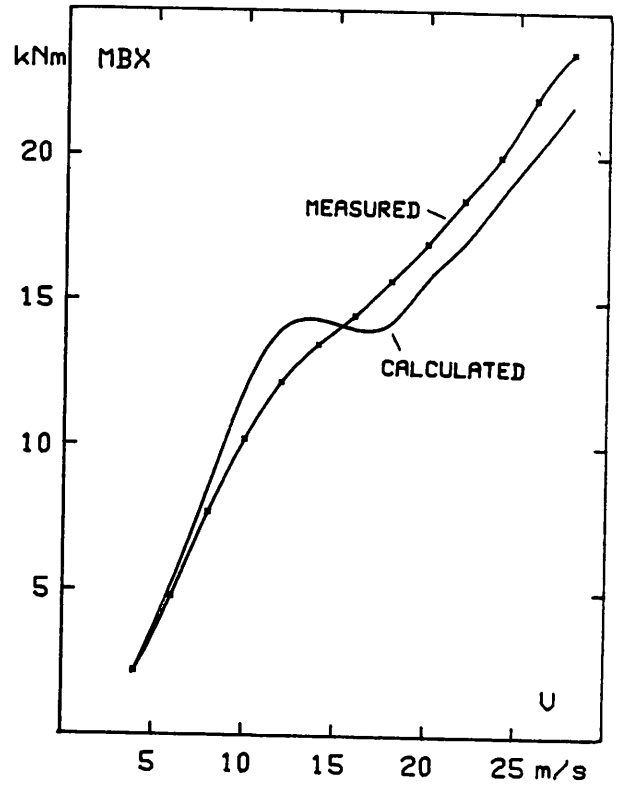

Fig. 2. Measured and calculated flapwise blade root bending moment curves at 2.5° blade tip angel.

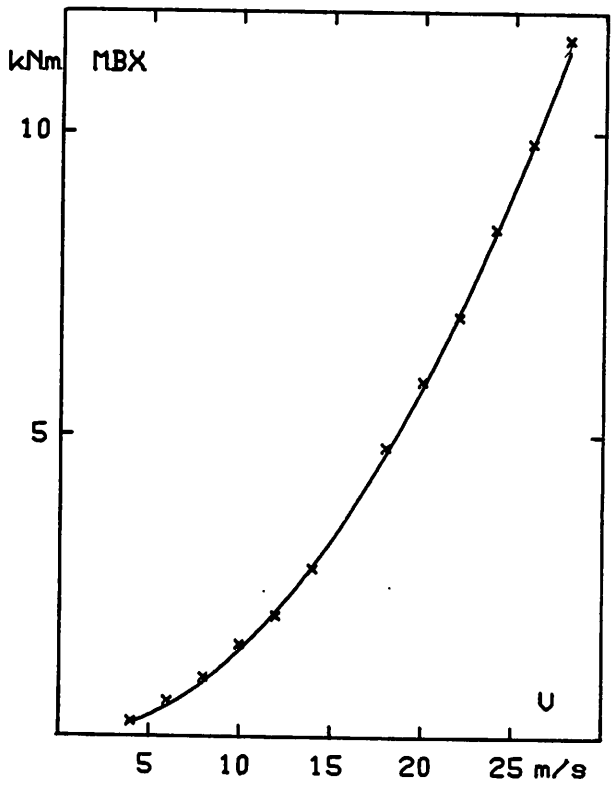

Fig. 3. Measured flapwise blade root moment as a function of wind speed during stand still.

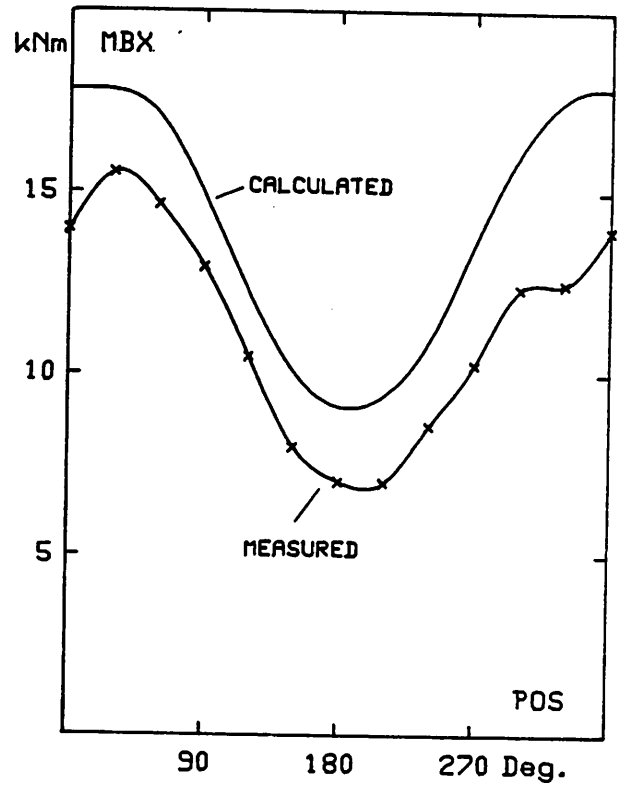

Fig. 5. Measured and calculated flapwise blade root moment as a function of blade angular position at V = 13.2 m/s and Yaw = -32°.

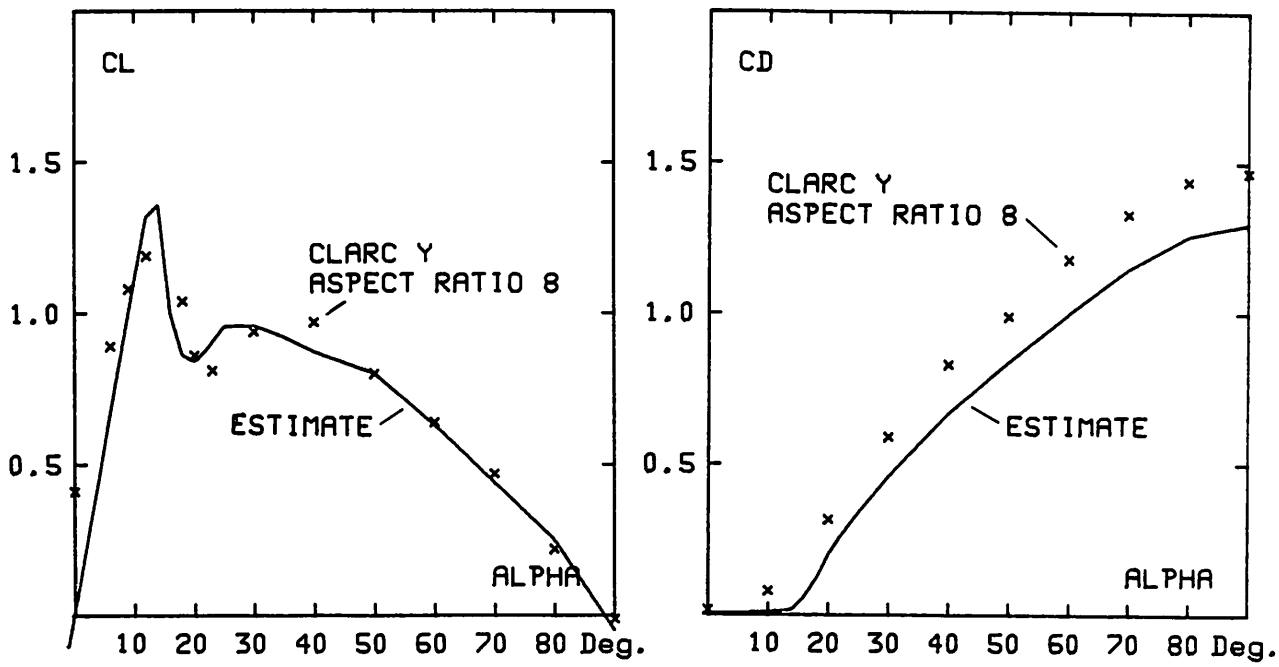

Fig. 4. Estimated lift and drag coefficient curves for the blade profiles.

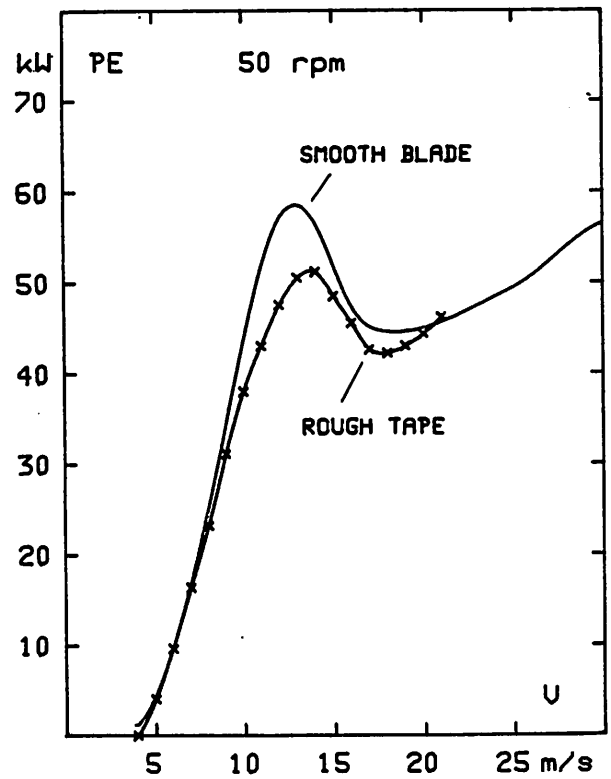

Fig. 6. Measured power curves with and without roughness tape at 50rpm.

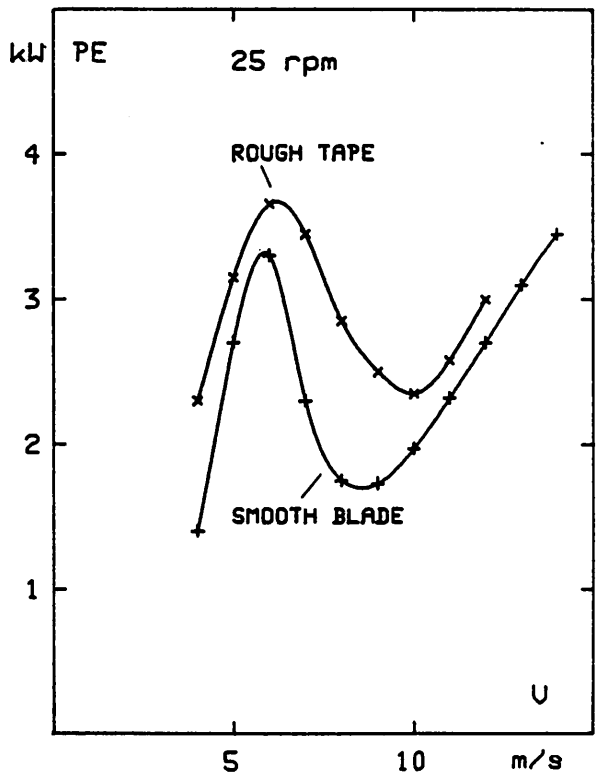

Fig. 7. Measured power curves with and without roughness tape at 25 rpm.

AERODYNAMIC RESEARCH ON WIND TURBINES AT NLR

by
Otto de Vries

1. INTRODUCTION

The presentation is limited to the aerodynamic calculation of a horizontal-axis wind turbine in a steady and homogeneous flow, and focusses on three different aspects.

The first aspect is an empirical extension of an existing blade-element calculation method into the turbulent wake state. This empirical relation was discussed in Appendix C of NLR Report NLR TR 81069 L, and is reproduced in this presentation.

The second aspect is the development of a vortex calculation method, based on a lifting-line approximation, with a relaxed vortex wake. This work was done in the framework of research on the tipvane concept, which concept originated at the Technical University of Delft in The Netherlands.
The calculations with this vortex method are compared with results obtained from the existing blade-element theory and also with two sets of experimental results. The first set of results is obtained by ECN from the 25 m HAWT at Petten, and the second set is obtained by NLR from a model rotor in a wind tunnel (see report NLR TR 81069 L).

The third aspect is a short comment on the yaw stability at small angles of yaw. This comment consists of an article, offered for publication in "Wind Engineering", which is reproduced in this presentation.

These three aspects may give an indication of the work, NLR has been done and is doing in the field of aerodynamic research on wind turbines.

2 EXTENSION OF A BLADE-ELEMENT CALCULATION METHOD INTO THE TURBULENT WAKE STATE BY MEANS OF AN EMPIRICAL RELATION

LIST OF SYMBOLS

a = axial induction factor (-)

a' = tangential induction factor (-)

A = empirical factor (-)

B = number of rotor blades (-)

C = empirical factor (-)

c = local chord of blade element (m)

$C_D = D/(\frac{1}{2}\rho U^2 \pi R^2)$ = rotor drag coefficient (-)

C_d = profile drag coefficient of blade element (-)

C_ℓ = lift coefficient of blade element (-)

$C_N = N/(\frac{1}{2}\rho U^2 \pi R^2)$ = normal force coefficient of one blade (-)

$C_P = P/(\frac{1}{2}\rho U^3 \pi R^2)$ = power coefficient (-)

$C_T = T/(\frac{1}{2}\rho U^2 \pi R^2)$ = tangential force coefficient of one rotor blade (-)

D = rotor drag (N)

F = tip loss factor (-)

i = local setting angle of blade element (degrees)

N = normal force on one blade (N)

P = power (W)

R = maximum radius of rotor (m)

r = local radius of blade element (m)

T = tangential force on one blade (N)

U = wind velocity (m/s)

U_{rel} = velocity relative to blade element (m/s)

$X = \Omega r/U = \lambda r/R$ = local tip-speed ratio (-)

α = angle of attack of the blade element (degrees)

Θ = angle between rotor area and U_{rel} (degrees)

Θ_p = blade-pitch angle (degrees)

$\lambda = \Omega R/U$ = tip-speed ratio (-)

ρ = density of the air (kg/m^3)

$\sigma' = Bc/(2\pi r)$ = local solidity ratio of the rotor (-)

Ω = angular velocity of the rotor (rad/s)

C.1 INTRODUCTION

The crucial point in the calculation method for a wind turbine (or some other rotor system) is the determination of the induced velocities in the plane of the rotor. These velocities are induced by the trailing vortex system of the rotor. To avoid the cumbersome task of calculating these velocities from the vortex system itself, average values are estimated from momentum considerations (see e.g. Ref. C.1).
In the case of a wind turbine, the axially induced velocities are opposite to the wind velocity, in that way decreasing the velocity through the rotor. When the induced velocities in the plane of the rotor become larger than one half of the wind velocity, the momentum theory leads to contradictory results (zero velocity and return flow far downstream).
What physically happens, can be roughly described as follows. The increase of the induced velocities (thus decrease of the velocity through the rotor) is coupled with an increase of the wake width behind the rotor (continuity equation). The trailing vortex system is axially compressed and radially stretched by this wake expansion. At a certain moment, this deformed vortex structure becomes unstable and the originally ordered wake structure breaks down into turbulence, thus creating the so-called "turbulent wake state". The assumptions of the momentum theory no longer apply, but also a more cumbersome vortex method does not give a possibility to solve the problem.
It appeared from helicopter-oriented experiments, that velocities through the rotor smaller than one half of the velocity far in front of the rotor, are physically realizable.
At the moment, there is no mathematical model available to describe and calculate the turbulent wake state. Therefore, some empirical relations between the axial force and the velocity through the rotor disk have been found (Ref. C.2 and C.3).
In order to implement these relations into the existing calculation method, a differential form of the relation between total (integral) axial force and average velocity through the rotor disk has to be assumed.

A discussion of this empirical relation, the assumed differential form, the implementation into the existing calculation method and a discussion of the results obtained with this modified calculation method, are given in the next Sections.

C.2 EMPIRICAL RELATION FOR THE TURBULENT WAKE STATE

From the momentum equation and the assumption, that the velocity through the rotor disk is the arithmetic mean of the velocity far upstream and far downstream of the rotor, a one-dimensional flow consideration leads to a well-known relation between the induced axial velocity at the rotor disk (aU) and the axial force of the rotor (D), written in a non-dimensionalized form:

$$C_D = 4a(1-a) \quad . \tag{C.1}$$

The relation between the rotor drag (C_D) and the velocity through the rotor disk (1-a), according to Eq. (C.1), has been plotted in figure C.1. Eq. (C.1) can be evaluated for values of a > 0.5, notwithstanding the fact, that the induced velocities far downstream lead to contradictory results.
Experimental data, shown in reference C.3 and plotted in figure C.1, clearly indicate that the momentum theory is unable to predict the flow behaviour when a > 0.5.

Reference C.2 proposes the following empirical relation between C_D and 1-a:

$$4/C_D = 5/2 + 4/3 \left\{4(1-a)^2/C_D\right\}^{5/9},$$

which can also be written in the following form:

$$1-a = \frac{1}{2}(C_D)^{1/2} \left\{\frac{3}{4}\left(\frac{4}{C_D} - \frac{5}{2}\right)\right\}^{9/10} \quad . \tag{C.2}$$

This relation is also plotted in figure C.1.

In view of the large scatter of the experimental data, the relation of Eq. (C.2) seems too complicated to justify its application. A linear interpolation formula could be used as well.
There is a strong indication from the experiments, that the deviation from the momentum theory starts already at (1-a) ≈ 0.6 instead of at (1-a) = 0.5. Therefore, the following linear relation is suggested:

$$C_D = A - C\,(1-a), \tag{C.3}$$

with A = 1.6 and C = 1.0666.

C.3 IMPLEMENTATION INTO THE EXISTING CALCULATION METHOD

In order to implement the relation of Eq. (C.3) into the existing calculation method of reference C.1, it has to be assumed that the relation is also valid for each blade element (annular area). Further, the relation has to be expressed in C_ℓ and θ (lift coefficient on blade element and angle between the relative velocity and the plane of the rotor).

When the axial force on an element of one blade is denoted by dN, the average force divided by the annular area $2\pi r\,dr$ (i.e. the pressure) of a B-bladed rotor is:

$$\frac{B\,dN}{2\pi r\,dr} = \frac{B\,dN}{\pi R^2}\,\frac{\pi R^2}{2\pi r\,dr},$$

or non-dimensionalizing with $\frac{1}{2}\rho U^2$,

$$\frac{B}{2(r/R)}\,\frac{dC_N}{d(r/R)}. \qquad (C.4)$$

The differential form of Eq. (C.3), therefore, becomes:

$$\frac{B}{2(r/R)}\,\frac{dC_N}{d(r/R)} = A - C\,(1-a). \qquad (C.5)$$

When a blade element is considered with a lift coefficient C_ℓ and a relative velocity U_{rel}, which makes an angle θ with the plane of rotation, the normal force coefficient on one blade element becomes (not using the momentum equation):

$$dC_N = \frac{2}{B}\,\frac{r}{R}\,\sigma'\,C_\ell\,\cos\theta\left(\frac{U_{rel}}{U}\right)^2 d\left(\frac{r}{R}\right),$$

with $\sigma' = Bc/(2\pi r)$ and c = chord of the rotor blade element. When this is substituted into Eq. (C.5), the empirical relation can be written as:

$$\sigma'\,C_\ell\,\cos\theta\,(U_{rel}/U)^2 = A - C\,(1-a). \qquad (C.6)$$

For the determination of U_{rel}/U, some additional assumptions have to be made. There are two points on this linear relation, that can be calculated with more or less certainty, viz.:

- The point at (1-a) = 0.6, which must coincide with the existing calculation method.
- The point at (1-a) = 0.

The value of θ for the first point can be obtained from the equation (Ref. C.1)

$$1-a = 0.6 = \sin\theta(\sin\theta + X\cos\theta),$$

with $X = \Omega r/U = \lambda r/R$.
This value can be rather quickly obtained by iteration from the formula

$$\tan 2\theta = 1/X + 0.2/(X\cos\theta), \qquad (C.7)$$

starting with the value

$$2\theta = \arctan(1/X).$$

The corresponding value of C_ℓ can then be obtained from:

$$\sigma' C_\ell \cos\theta (U_{rel}/U)^2 = 4F\sin\theta\cos\theta(\sin\theta + X\cos\theta)(\cos\theta - X\sin\theta), \qquad (C.8)$$

with

$$F = \frac{2}{\pi}\arccos\left(\exp -\frac{B}{2}\frac{1-r/R}{(r/R)\sin\theta}\right),$$

the so-called "tip correction factor".

For the calculation of the second point, the velocity triangle at the blade element of figure C.2 has to be considered. When (1-a) = 0, it follows that $\theta = 0$. In that case, the lift (C_ℓ) has no tangential component and it seems more or less logical to assume, that there is no induced tangential velocity (a' = 0). It then follows from the velocity triangle of figure C.2, that $U_{rel} = \Omega r$, or

$$U_{rel}/U = \Omega r/U = X.$$

When this is substituted into Eq. (C.6), reminding that (1-a) = 0 and $\theta = 0$, the lift coefficient can be calculated from:

$$\sigma'(C_\ell)_{\theta=0} = A/X^2. \qquad (C.9)$$

For the points in between, a relation for U_{rel}/U has to be found. It happens, that the formula from the momentum theory of reference C.1, viz.

$$U_{rel}/U = (1-a)/\sin\theta = \sin\theta + X\cos\theta \qquad (C.10)$$

is a good interpolation formula, because it gives a correct answer at the point a = 0.4, and is also correct when $\theta = 0$. Substitution of Eq. (C.10) into Eq. (C.6) and reminding from Eq. (C.10) that $(1-a) = \sin\theta(\sin\theta + X\cos\theta)$, leads to

$$\sigma' C_\ell \cos\theta (\sin\theta + X\cos\theta)^2 = A - C \sin\theta(\sin\theta + X\cos\theta) \qquad (C.11)$$

When the value of A = 1.6 is retained, which fixes the value of $\sigma' C_\ell$ at $\theta = 0$, the value for C follows from a comparison of the Eqs. (C.8) and (C.11) at a value of θ obtained from Eq. (C.7).
Results of such a calculation are shown in figure C.3, which clearly shows, that the relation between $\sigma' C_\ell$ and θ is also almost linear.
In order to reduce the computation time and in view of the large scatter in the experimental points in figure C.1 (on which the original empirical relation was based), a linear relation between C_ℓ and θ has been adopted for the modified calculation method, viz.:

$$C_\ell = (C_\ell)_2 - \left\{(C_\ell)_2 - (C_\ell)_1\right\} \theta/\theta_1 \qquad (C.12)$$

with

$(C_\ell)_1$ calculated from Eq. (C.8) with $\theta = \theta_1$,

θ_1 calculated from Eq. (C.7),

$(C_\ell)_2$ calculated from Eq. (C.9), with A = 1.6.

Figure C.4 shows, why the modification gives a solution in cases, where, with the original programm, no solution was possible. When the operating point of the blade element has been determined from the point of intersection between Eq. (C.12) and the profile data of the blade element (see Fig. C.4), the normal force coefficient, the tangential force coefficient and the power coefficient of that blade element can be calculated from the equations below (C_P for B blades):

$$dC_N/d(r/R) = \frac{1}{\pi} C_\ell \, (c/R)\cos\Theta(\sin\theta + X\cos\theta)^2(1 + (C_d/C_\ell)\mathrm{tg}\,\Theta),$$

$$dC_T/d(r/R) = \frac{1}{\pi} C_\ell \, (c/R)\sin\theta(\sin\theta + X\cos\theta)^2(1 - (C_d/C_\ell)\mathrm{cotg}\,\theta),$$

$$dC_P/d(r/R) = \lambda B(r/R)\, dC_T/d(r/R). \qquad (C.13)$$

The normal force and tangential force for the complete rotor blade can then be calculated from

$$C_N = \int_{(r/R)_{hub}}^{1} dC_N/d(r/R)\, d(r/R)$$

$$C_T = \int_{(r/R)_{hub}}^{1} dC_T/d(r/R)\, d(r/R). \qquad (C.14)$$

The rotor drag and the power coefficient of the complete rotor can be calculated from

$$C_D = B\, C_N,$$

$$C_P = \int_{(r/R)_{hub}}^{1} dC_P/d(r/R)\, d(r/R). \qquad (C.15)$$

C.4 APPLICATION OF THE MODIFIED CALCULATION METHOD

The modified calculation method has been applied to the geometry of the existing model turbine, and the results of the calculation are compared in the figures C.5 through C.7 with the test results, corrected for tunnel wall constraint according to Appendix B. The original and modified calculations coincide in figure C.5.

The prediction of the rotor drag in the turbulent wake state seems acceptable, but there is no real improvement in the predicted power coefficient.

There is a tendency, that the predicted rotor drag it too high. A reduction could be obtained by reducing the value of A = 1.6 to A = 1.4 or even lower. The influence on the predicted power coefficient will be too small to explain the large discrepancy with the experimental results.

In the calculation method, the blade elements have been assumed to be independent of each other. Therefore, the turbulent wake state starts at a certain value of λ at the tip and the number of blade elements along the span with a turbulent wake state increases towards the hub with increasing tip-speed ratio. This behaviour is shown in figure C.8 for different values of the blade-pitch angle θ_p.
It is remarkable, however, that the root sections of the rotor blade do not enter the turbulent wake state. This is due to the assumed independence of the blade elements, but will certainly not be in accordance with physical reality.

It can be concluded, that the empirical relation makes it possible to extend the calculations to high values of λ at negative values of θ_p, but only the rotor drag can be predicted with some confidence. The power prediction is still very uncertain.
An improvement of the power prediction is only possible by investigating the actual flow behaviour behind the rotor in the turbulent wake state.

C.5 LIST OF REFERENCES

C.1 De Vries, O. — The aerodynamic performance of a horizontal-axis wind turbine in a stationary parallel flow. Discussion of existing theories, of a parameter study and of consequences for a wind-tunnel model design. NLR TR 78084 L (July 1978).

C.2 Miller, R.H., et al. — Wind energy conversion (final report, February 1975 - October 1976). NSF/RA-760569 (October 1976), pp. II-54 through II-56.

C.3 Stoddard, F.S. — Momentum theory and flow states for windmills. Wind Technology Journal, 1, 1 (Spring 1977), pp. 3-9.

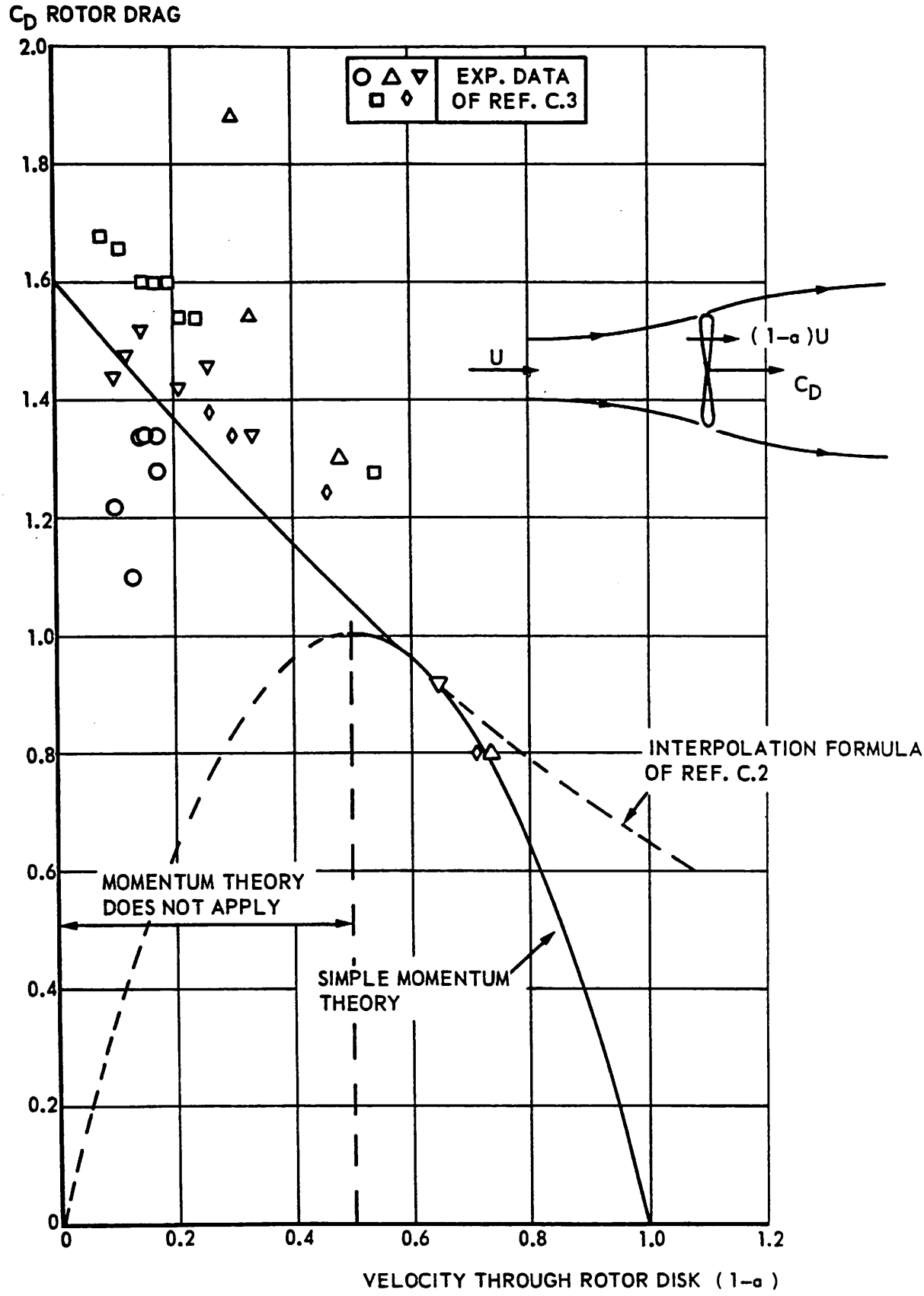

Fig. C.1 Relation between the rotor drag and the average velocity through the rotor disk, according to the simple momentum theory and according to helicopter experiments (Ref. C.2 and C.3).

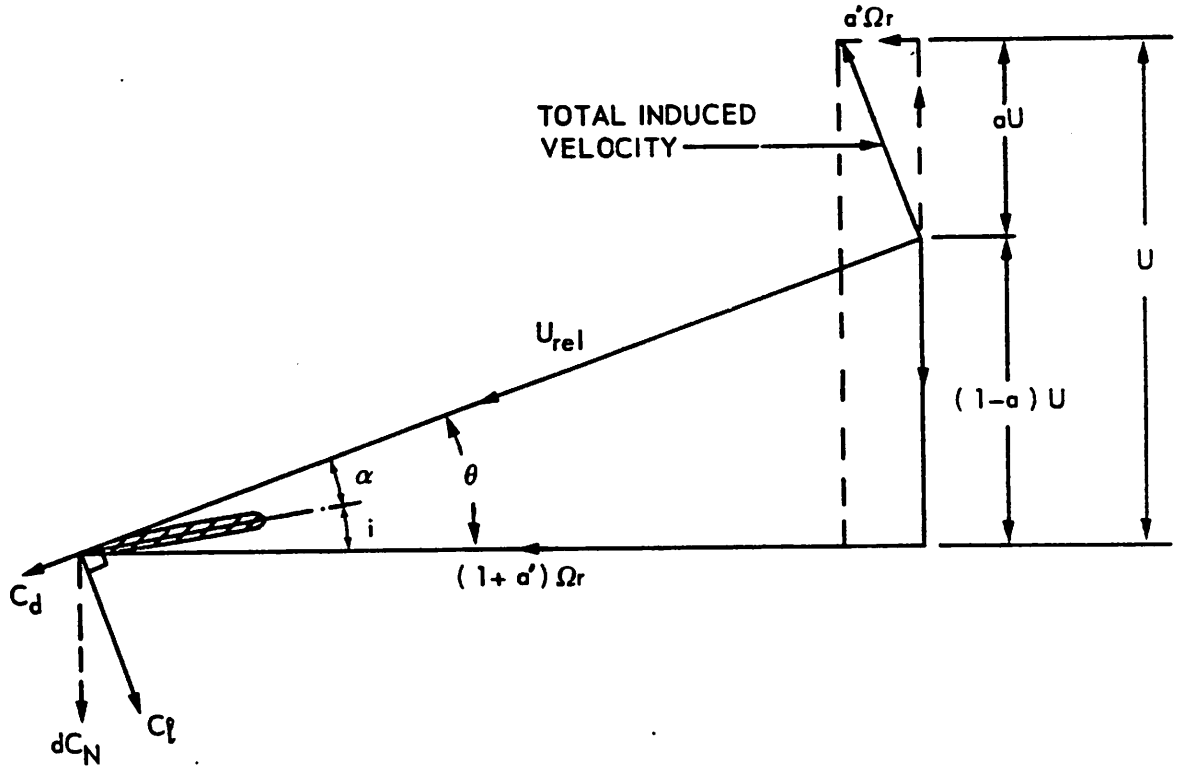

Fig. C.2 Velocity triangle at a blade element. U is the undisturbed wind velocity and Ωr is the velocity due to the rotation of the blade element.

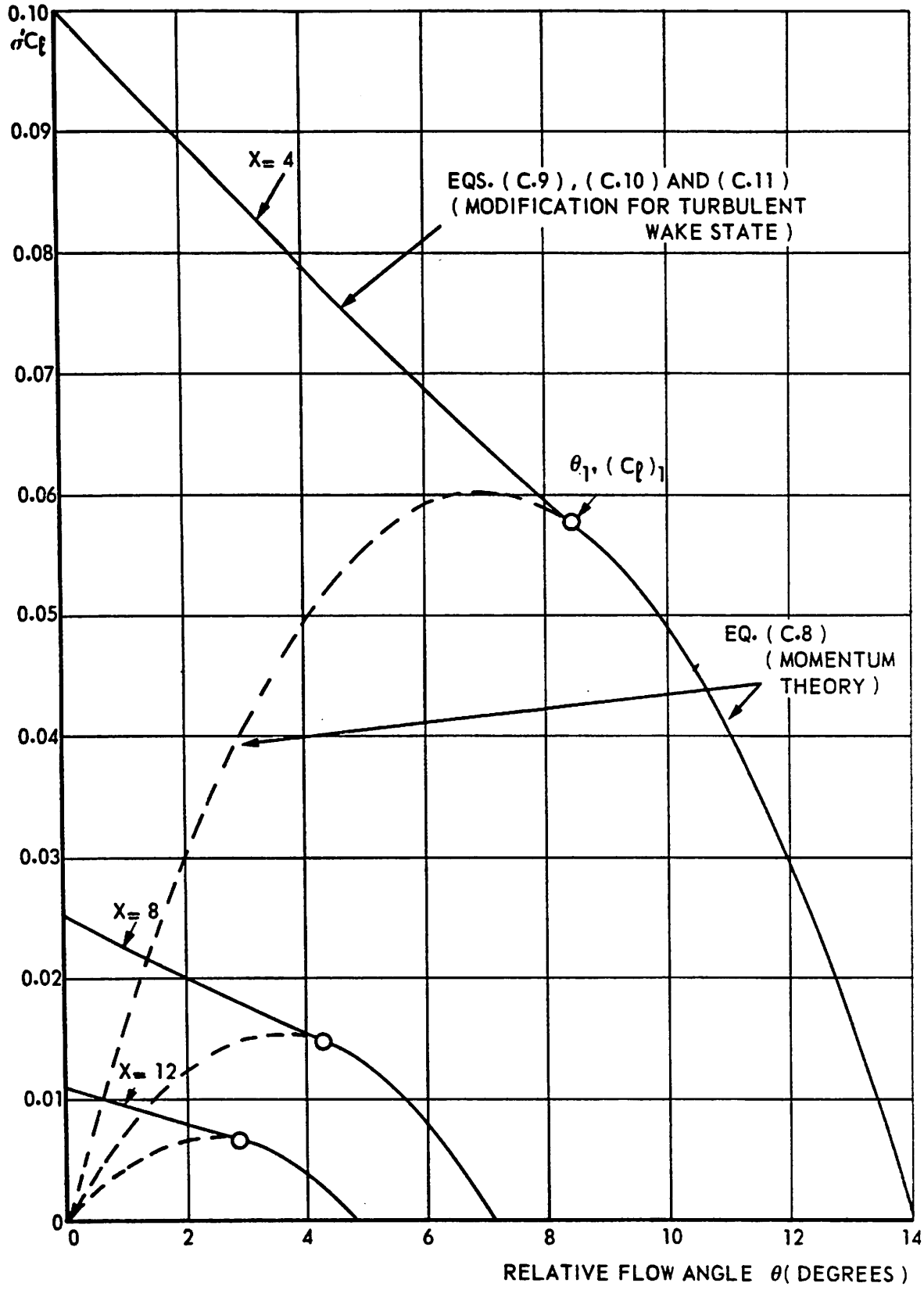

Fig. C.3 The relation between lift coefficient and flow angle for a blade element, according to the momentum theory and the modification in the turbulent wake state.

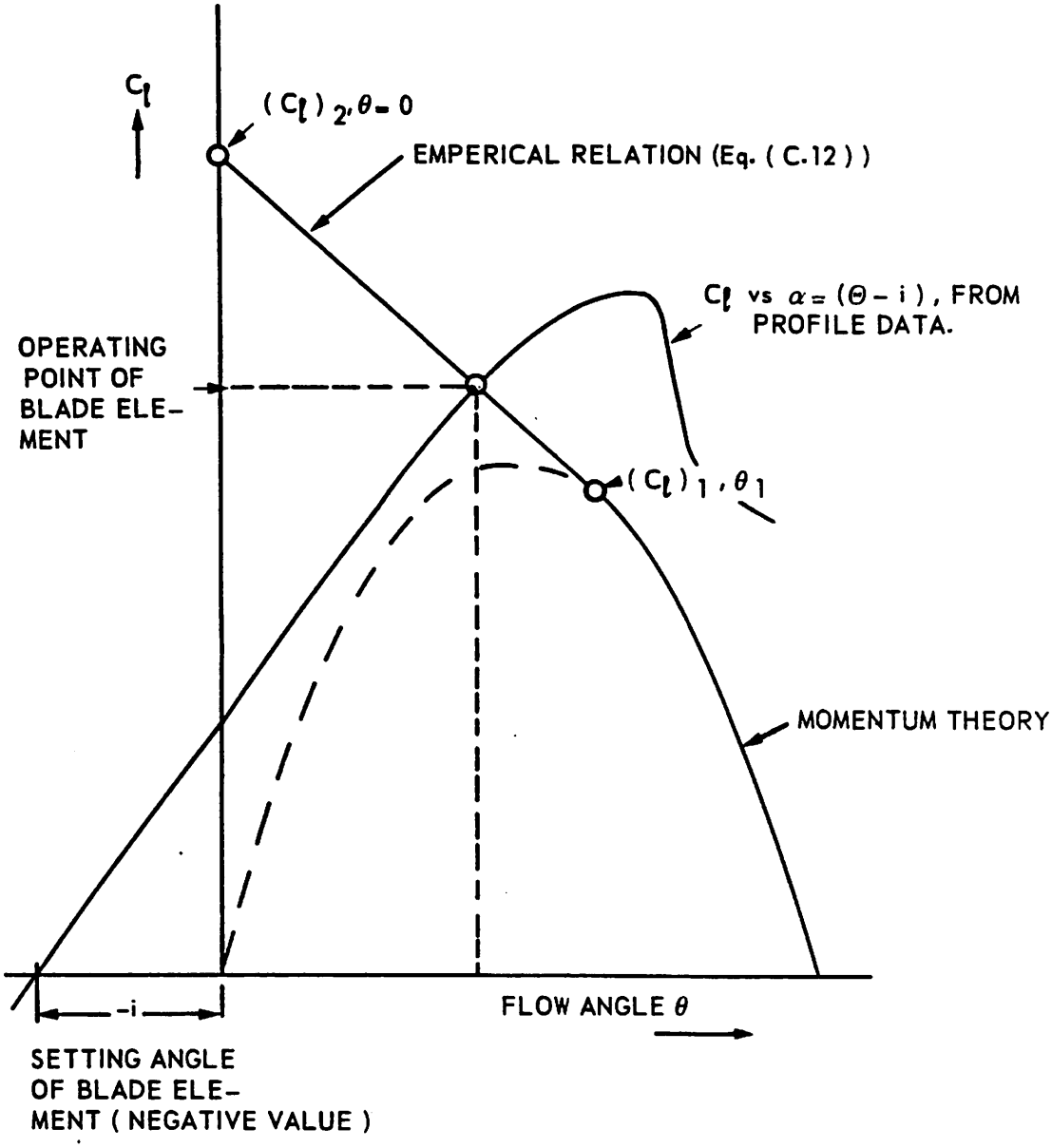

Fig. C.4 Determination of operating point of a blade element in the turbulent wake state.

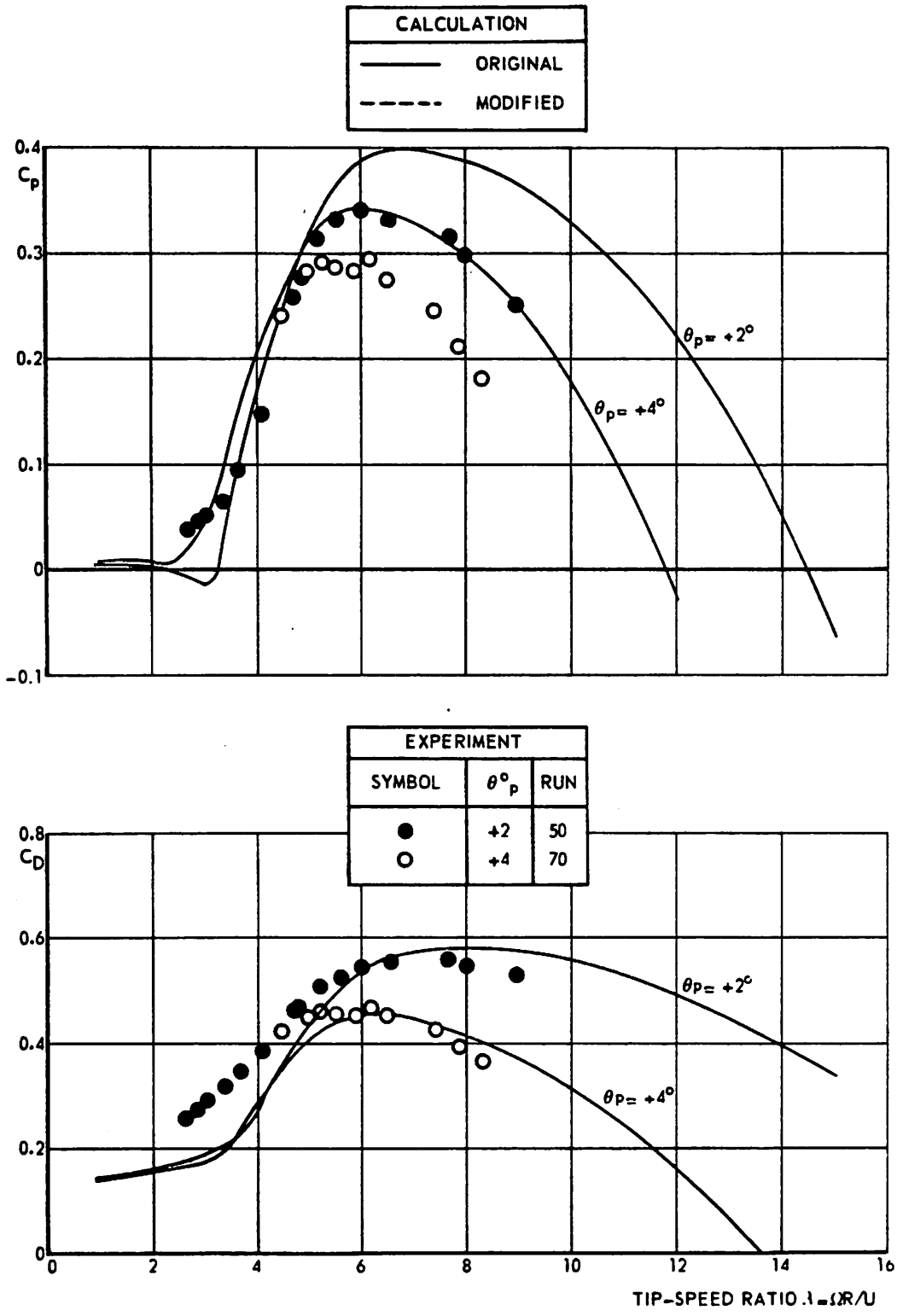

Fig. C.5 Influence of modification of calculation method and comparison with experiments.
Note: original and modified calculations coincide.

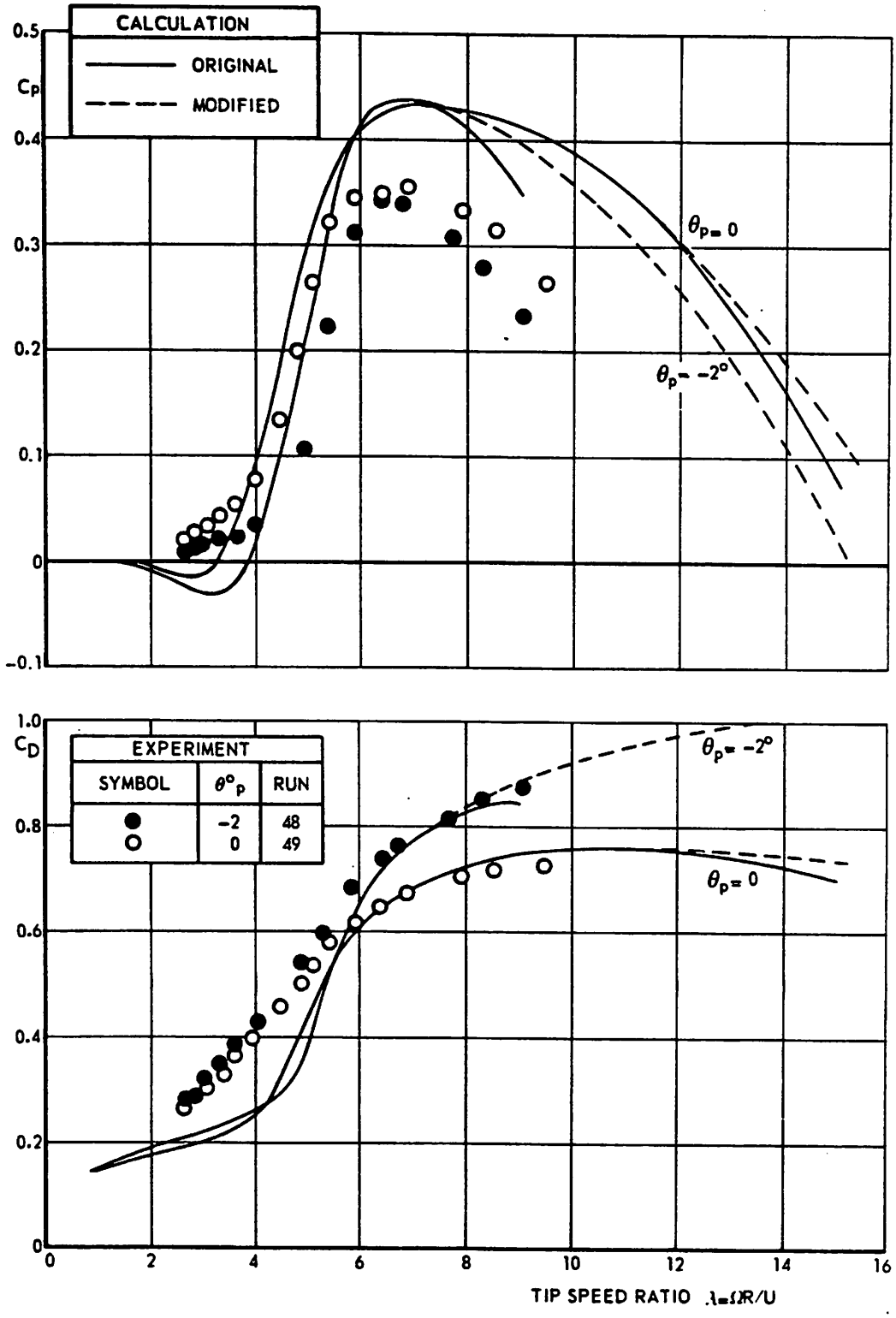

Fig. C.6 Influence of modification of calculation method and comparison with experiments.

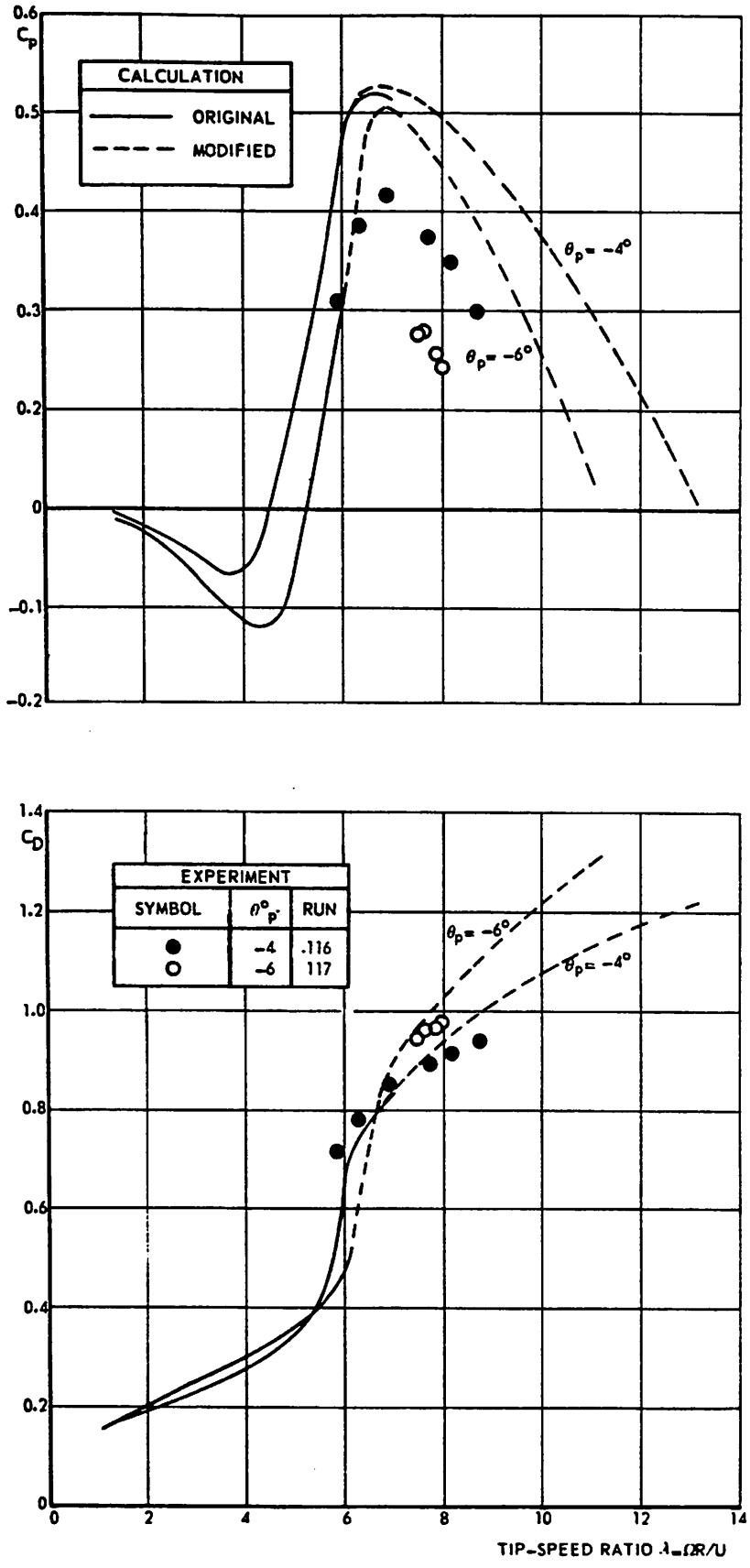

Fig. C.7 Influence of modification of calculation method and comparison with experiments.

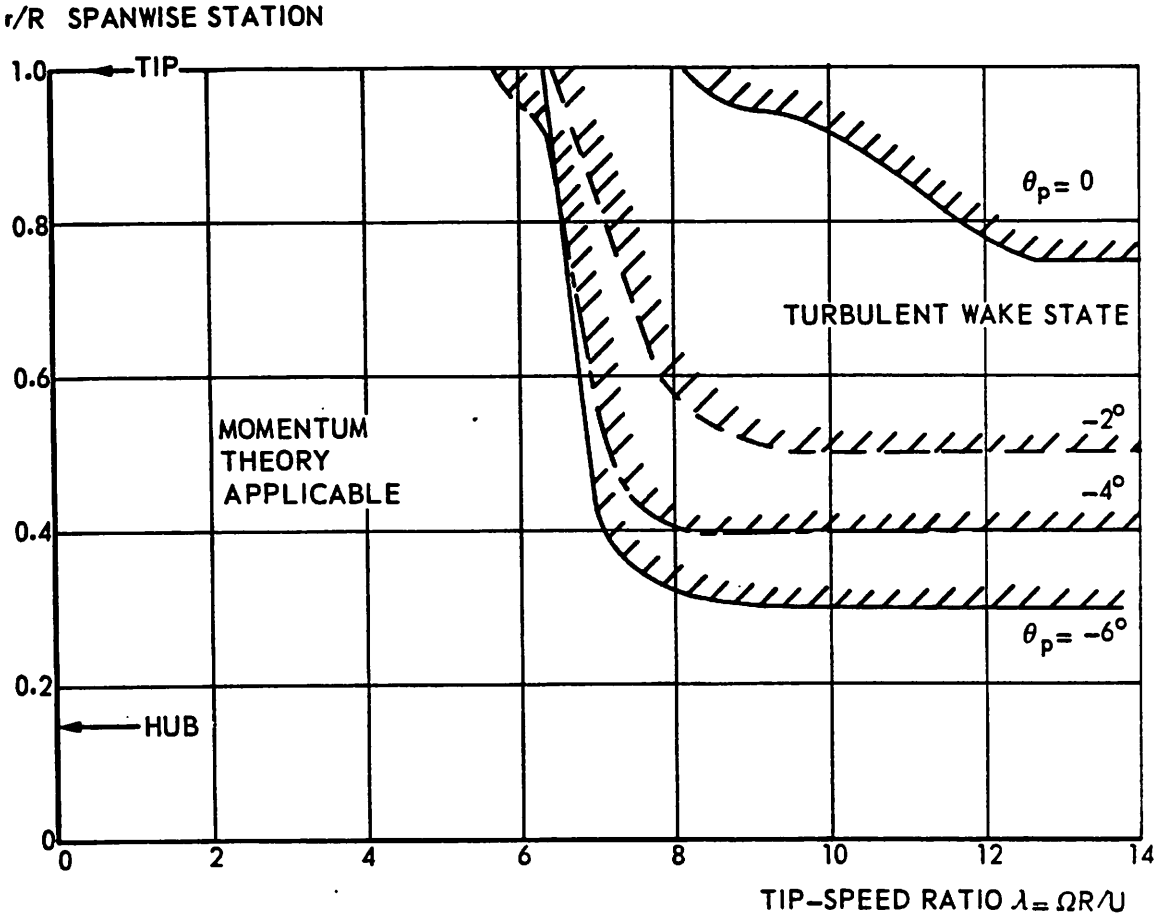

Fig. C.8 Spanwise station at which the turbulent wake state starts, as a function of the tip-speed ratio and the blade-pitch angle θ_p. (Calculated).

3 VORTEX METHOD WITH A RELAXED WAKE

3.1 Short description of the method

The program HELIX represents the aerodynamic active surfaces by lifting lines. The main problem, however, is the modelling of the vortex wake downstream of the rotor. This wake deformation was necessary to include because of the tipvane representation (for which this program was actually developed), but it turned out to be also necessary to obtain reliable results for a conventional horizontal-axis wind turbine.

The shape of the vortex sheets is determined by the wind velocity, the anguler speed of the rotor and the induced velocities at the vortex sheets. Because the induced velocities are discontinuous at the vortex sheets, the continuous part of the induced velocities have to be taken for the calculation of the deformation of the vortex sheets.
In order to keep the calculational proces within bounds, the local pitch angle of the vortex sheet has been determined inside the wake by the axial induced velocities, averaged along a radius in the vortex sheet. Because the continuous part of the induced velocities vary strongly at the wake boundary, it was necessary to handle the outermost part of the vortex sheet (tip vortices) separately.
Moreover, for the determination of the local pitch angle of the vortex sheets, the tangential induced velocities have been neglected. It is emphasized here, that the tangential velocities are only neglected in the calculation of the shape of the vortex sheets, not in the calculation of the forces on the lifting lines.

Due to the axial variation of the induced velocities, the local pitch angle of the vortex sheets varies downstream, and, by continuity, the wake width will also increase downstream. These wake deformations have been described with a limited number of parameters, which parameters are determined by an iteration procedure for a prescribed circulation distribution.

For a given circulation distribution, the vortex strengths of the trailing vortices remain constant during the iteration procedure, which makes the proces relatively simple.
The proces does not converge, however, when the product of the number of rotor blades, the circulation of the rotor blade and the chosen tip-speed ratio becomes too large. This numerical instability originates from the strong axial compression and lateral expansion of the wake at high rotor loading, which is probably connected with the physical instability of the vortex wake at the so-called "turbulent wake state".

From the above described iteration procedure, the direction and the magnitude of the total relative velocity at the lifting line can be determined. With given profile characteristics, one can determine the shape of the rotor blade, which could generate the given circulation distribution. It is then also possible to determine the viscous losses and, thus, the performance of the rotor.

The calculation of the performance of a given rotor shape with HELIX is more complicated. One has to start with a chosen circulation distribution and to calculate, with the above described iteration procedure, the velocity components at the lifting line. With the given blade shape and profile data, the circulation on the rotor blade can be calculated.
The calculation is repeated with the new circulation distribution. The proces is repeated, until convergence is obtained.

3.2 Comparison with blade-element theory and experiments

In order to get some confidence in this program HELIX, the program has been used to calculate the performance of two rotor shapes, for which experimental results were available. The same was done with an existing blade-element theory (described in Report NLR TR 78084 L).

The experimental results consisted of field experiments on the 25 m HAWT at Petten, The Netherlands and of model rotor tests in a wind tunnel, carried out at NLR (see Report NLR TR 81069 L).
The first set of experiments is hampered by the unavoidable

velocity variations and the fact, that only the power has been measured (not the axial force), whereas the second set of experiments is hampered by the large wake-blockage correction, which means an uncertainty in the final results.

The comparison of HELIX with the blade-element theory is interesting, because the blade-element theory makes use of two assumptions, which are a bit suspicious, viz.:

1: It is assumed, that the axial induced velocity in the plane of the rotor is ½ times the axial induced velocity far downstream. This is only valid for a vortex wake with a constant local pitch angle of the vortex sheets downstream. It can be easily shown, that this is not valid for a deformed vortex wake.

2: The effect of a finite number of rotor blades is calculated with the so-called "tip-correction factor", based on work of Prandtl and Goldstein for a propeller. In these cases, the local pitch angle of the vortex sheets was also kept constant downstream.

Figure 1 shows the geometry of both rotors (R = 12.5 m for the 25 m HAWT and R = 0.375 m for the model rotor).
The results for the 25 m HAWT are given in the figures 2 through 4 and for the model rotor in the figures 5 through 9. In the calculations, pure two-dimensional profile data have been used.

There are only slight discrepancies between HELIX and the blade-element theory (program RHO). The only difference is, that program RHO can calculate into the turbulent wake state, whereas program HELIX cannot be pushed that far, because of the numerical instabilities.Possible errors due to the assumption concerning the axial induced velocities and the possible error due to the tip-correction factor, probably compensate each other in the blade-element theory.

Comparison with the 25 m HAWT experiments shows, that close to the optimum blade-pitch angle (zero), C_P is rather well predicted, but is underestimated at higher blade-pitch angles (Figs. 3 and 4).

Comparison with the model rotor experiment is hampered by an uncertainty in the wake-blockage correction (uncorrected data are open symbols). Contrary to the 25 m HAWT, C_P is here overestimated at larger blade-pitch angles (Figs. 7 through 9). Though the wake-blockage correction seems to fit at high tip-speed ratio for the axial force C_D, this is not the case for C_P.

The large discrepancies between calculated and experimental C_P and C_D at very low tip-speed ratios, is probably connected with the pure two-dimensional profile data used in the calculations. It is a strong indication, that the "stall" in a rotating system does not show such a high lift loss as in a pure two-dimensional situation in parallel flow.

Program HELIX is, apart from usual numerical approximations, still not exact. This originates from the neglect of the tangential induced velocity components in calculating the wake deformation (which effect is strongest close to the hub and at low tip-speed ratios). Moreover the application of a radially averaged induced velocity inside the wake for the calculation of the local pitch angle of the vortex sheet, might differ from the actual situation, especially at blade pitch angles different from the optimum situation (zero blade pitch), where the velocity distribution through the rotor disk is less constant.

3.3 Remarks on the optimum blade shape

The blade-element theory gives, for a given tip-speed ratio, an optimum value for the local solidity times local lift coefficient and for the local flow angle (i.e. angle of the total relative velocity with respect to the plane of rotation), at each spanwise station. To minimize the viscous losses, the optimum C_ℓ/C_d has to be applied along the entire blade span.

This means, that C_ℓ, and thus α, has to be constant along the blade span.
Figure 10 shows the (calculated) circulation and angle of attack distribution along the blade of the 25 m HAWT, operating in its optimum. The angle of attack distribution is far from constant, especially near the hub.

When the circulation distribution of figure 10 is compared with the optimum distribution according to the blade-element theory (program RHO, see figure 11), it is seen, that also the circulation distribution deviates strongly from the optimum one. This is due to the simplification of the blade geometry necessary to obtain a practicable blade shape.
Figure 12 shows which optimum values of C_p could have been obtained by these optimum shapes, as a function of the chosen λ and the C_ℓ/C_d.

This gives rise to two questions, which are unanswered up till now, namely:

1: Is it possible to approximate the "ideal" circulation distribution of figure 11 a bit better, without introducing too much structural complexity (e.g. a varying taper near the tip instead of a constant taper along the entire blade span).
2: Gives program HELIX an optimum circulation distribution that differs from the optimum according to program RHO.

Figure 1

GEOMETRY OF ROTOR BLADE OF 25 m HAWT AND OF MODEL ROTOR
both are two-bladed rotors.

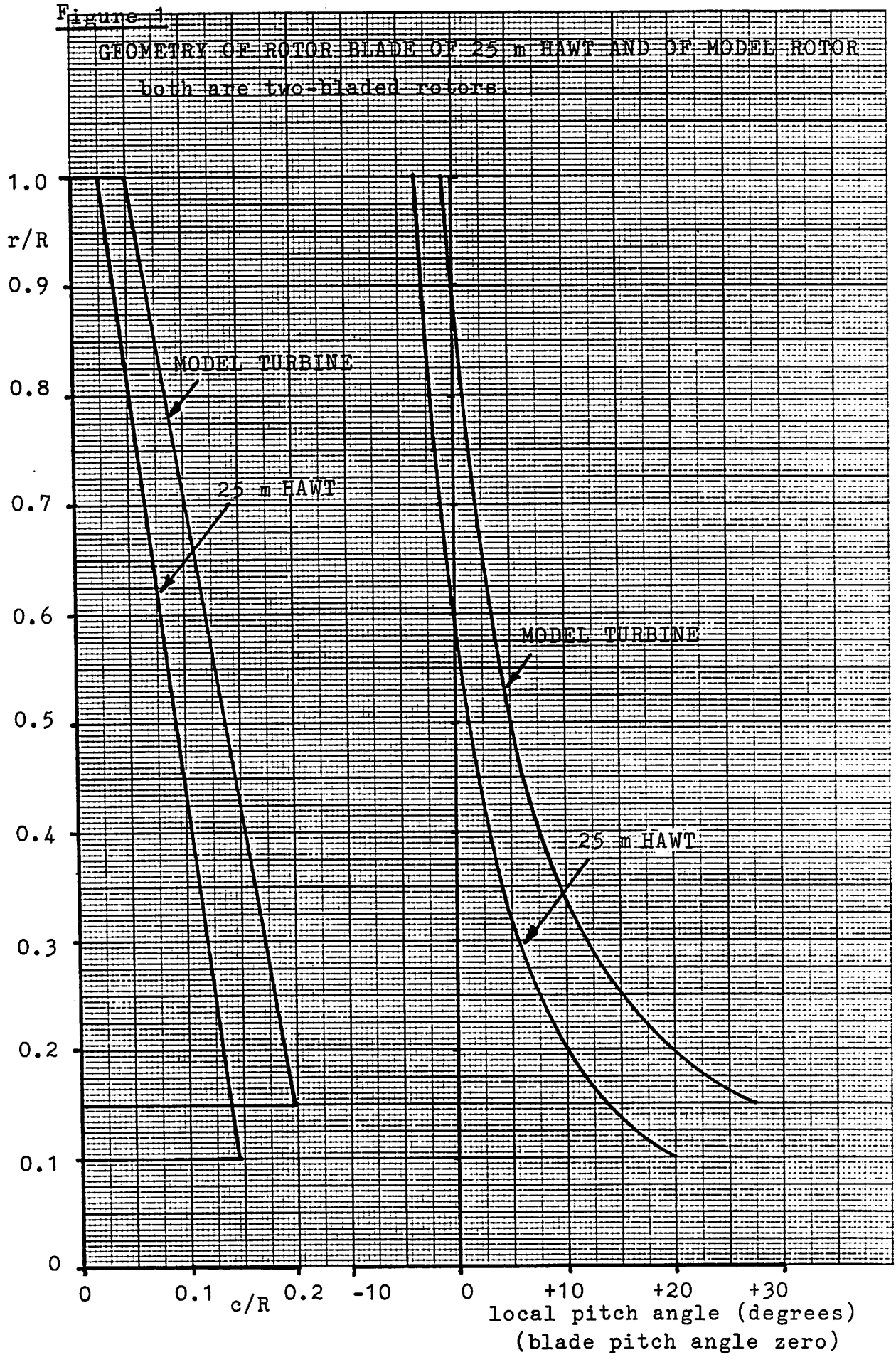

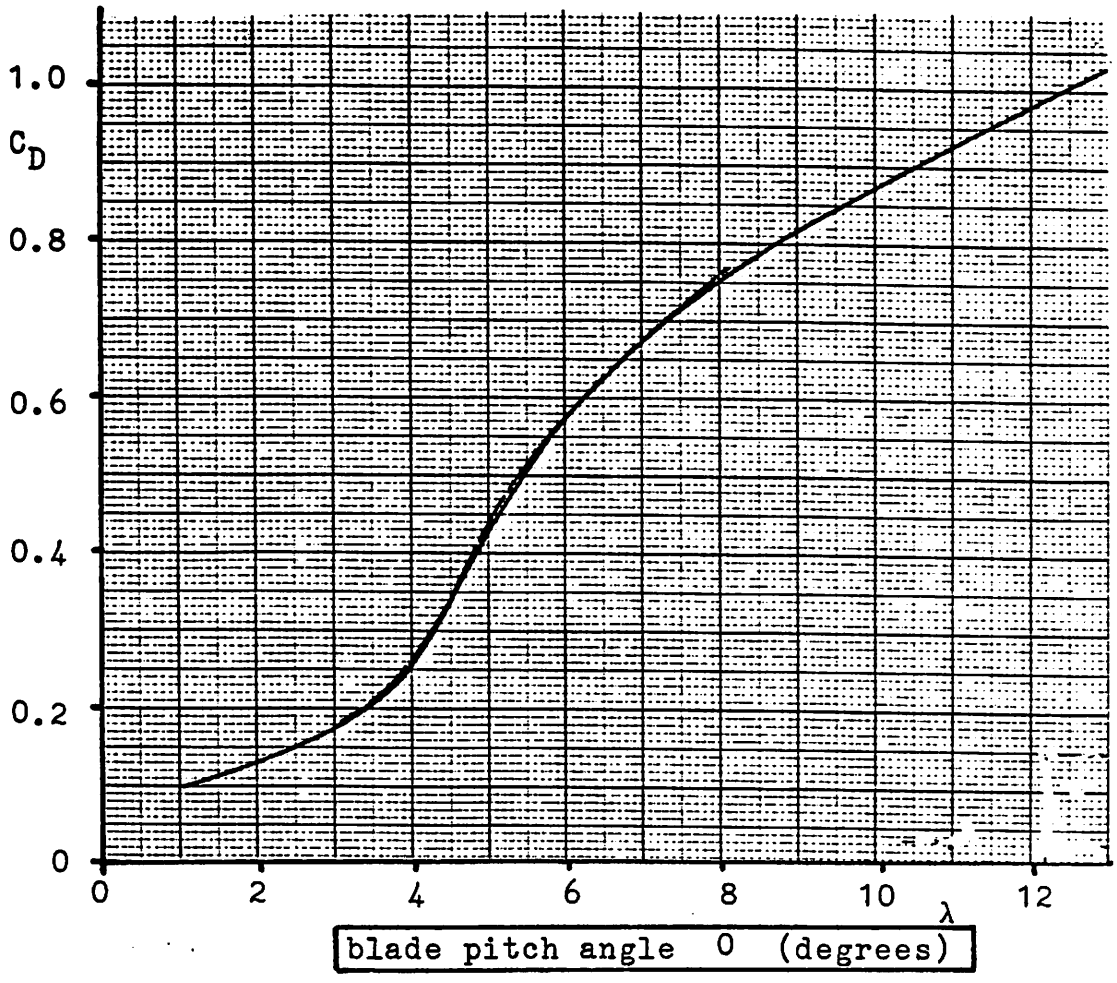

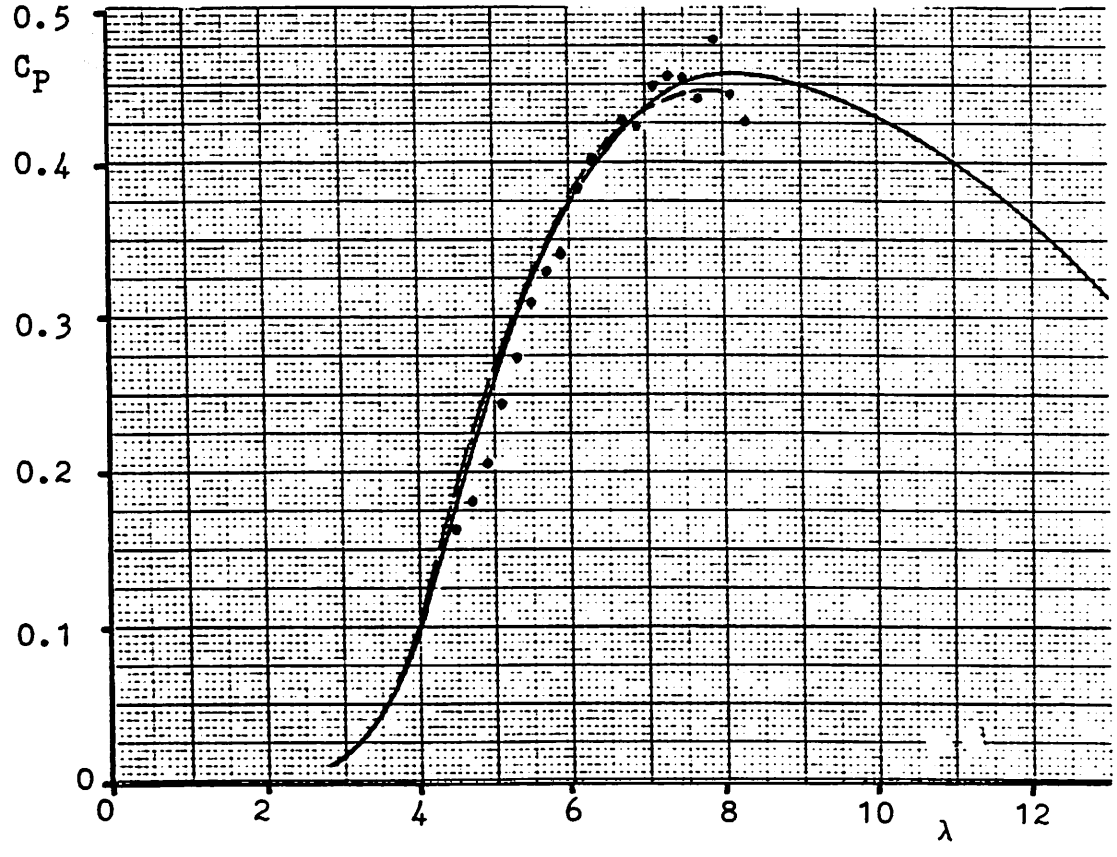

25 m HAWT, PETTEN. ● measured ;
calculated: ——— program RHO; - - - - - program HELIX

Figure 2

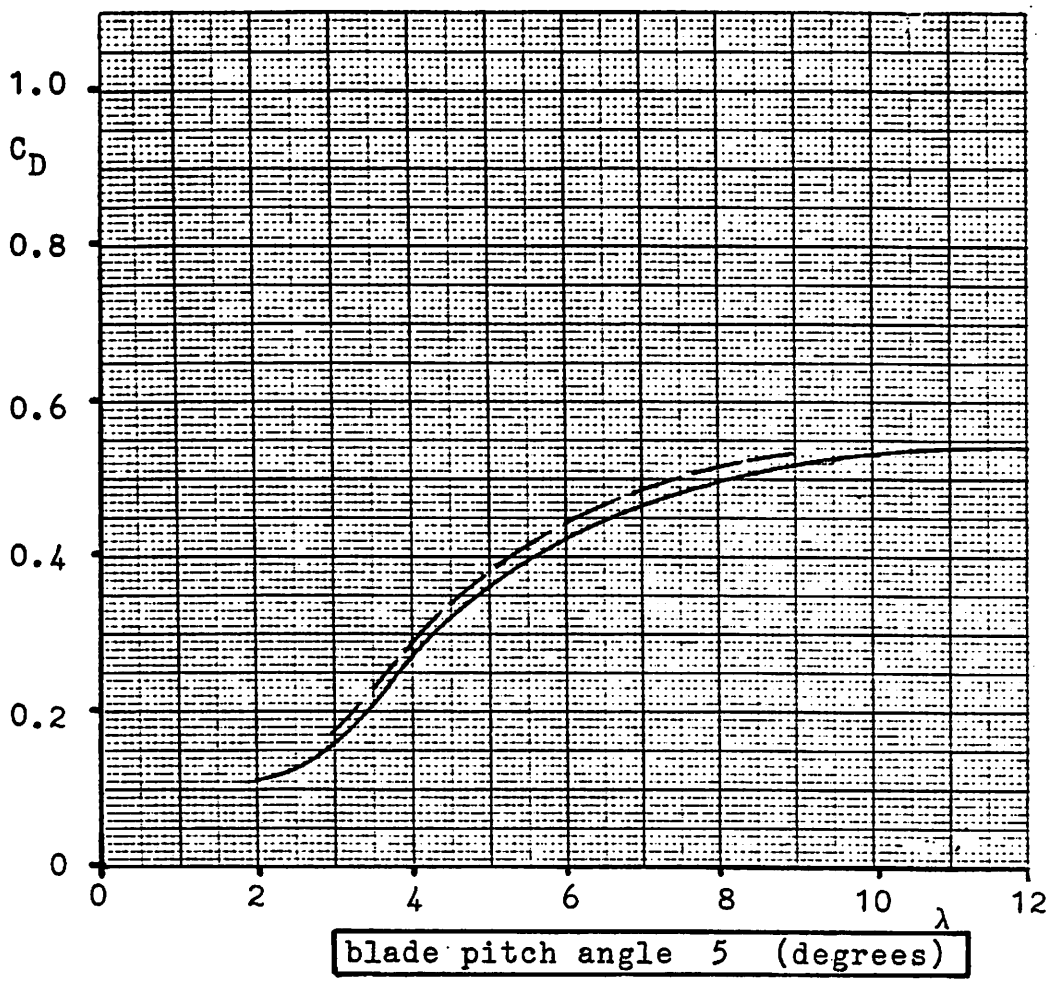

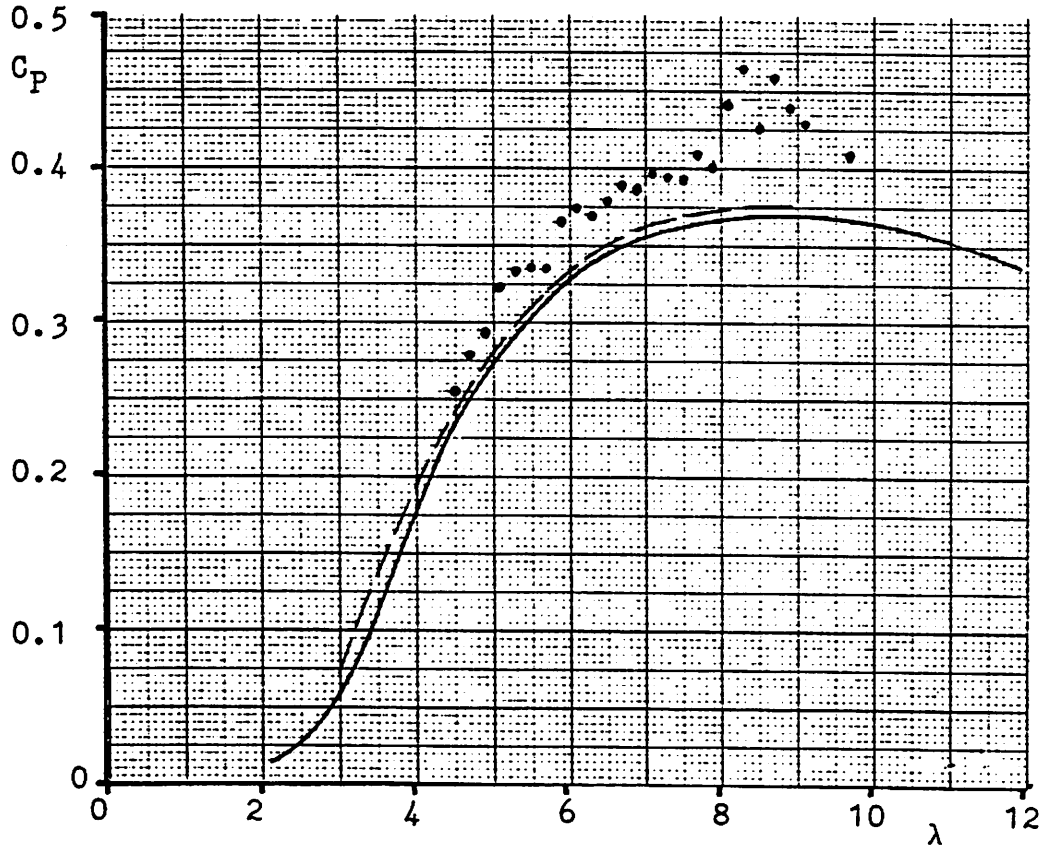

25 m HAWT, PETTEN. ● measured ;
calculated: ——— program RHO; - - - - - program HELIX

Figure 3

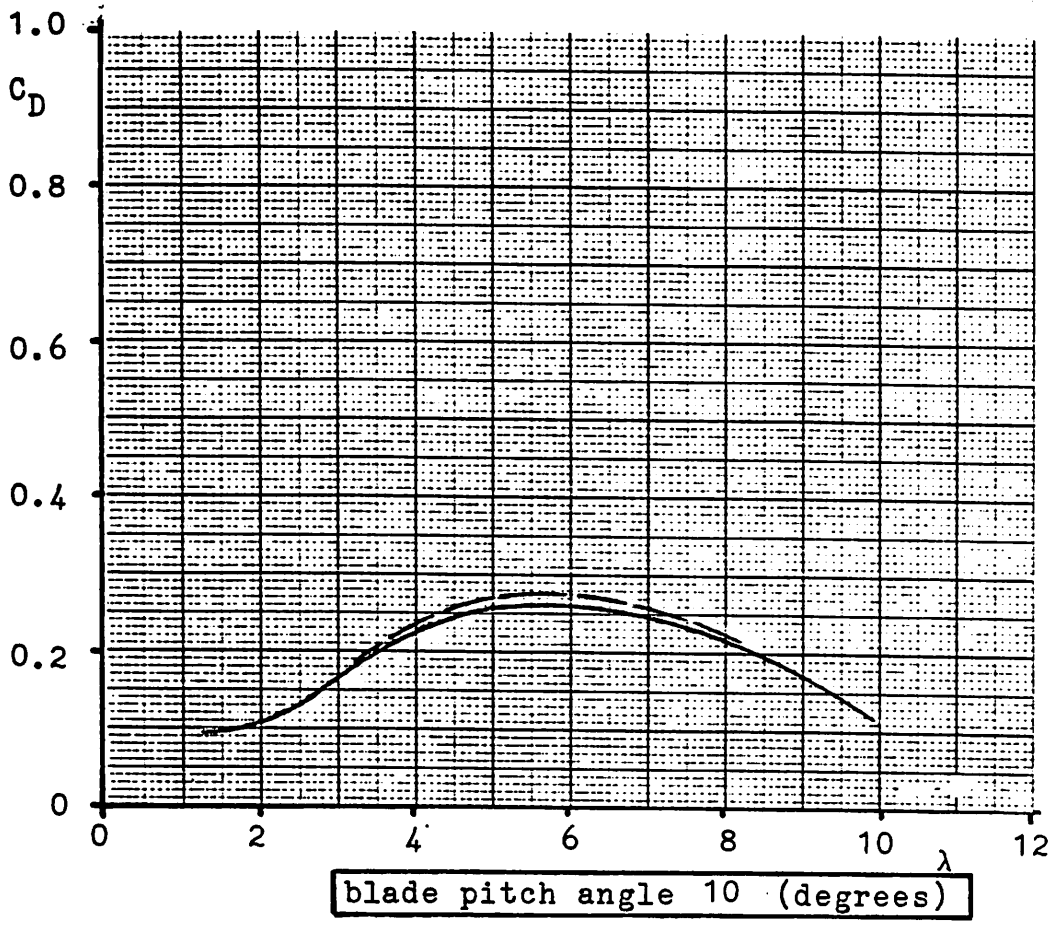

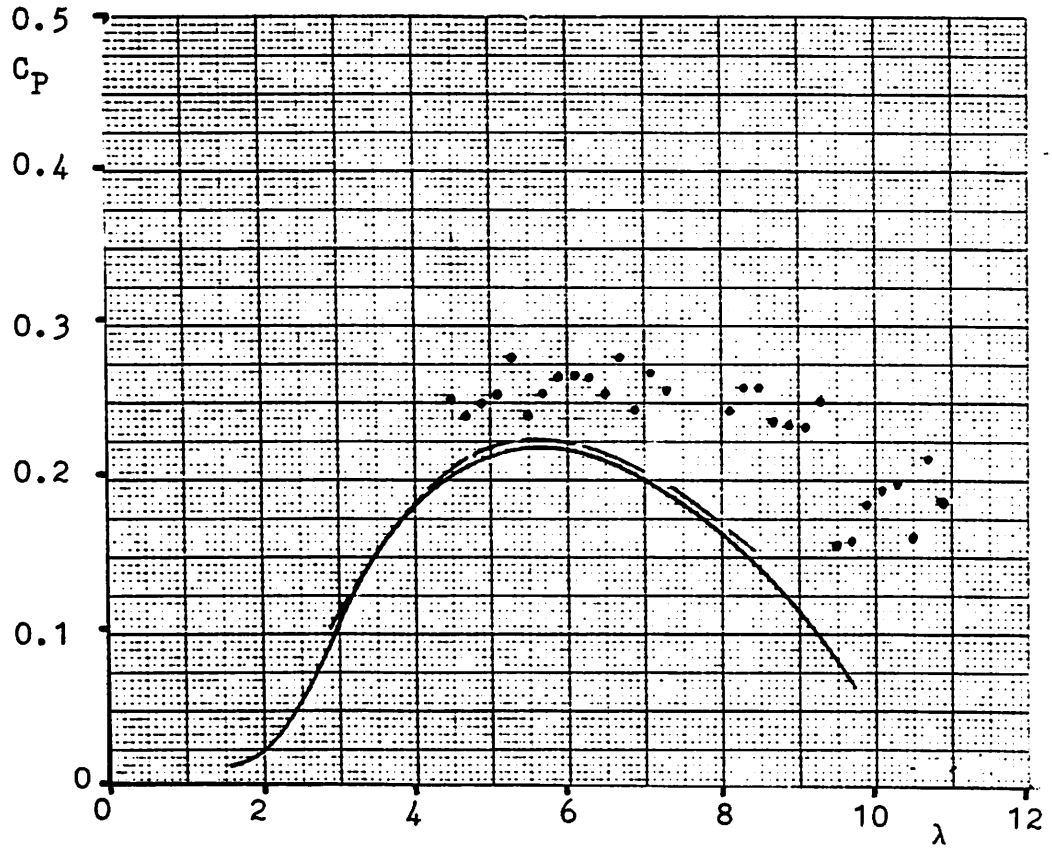

25 m HAWT, PETTEN. ● measured ;
calculated: ——— program RHO; - - - - - program HELIX

Figure 4

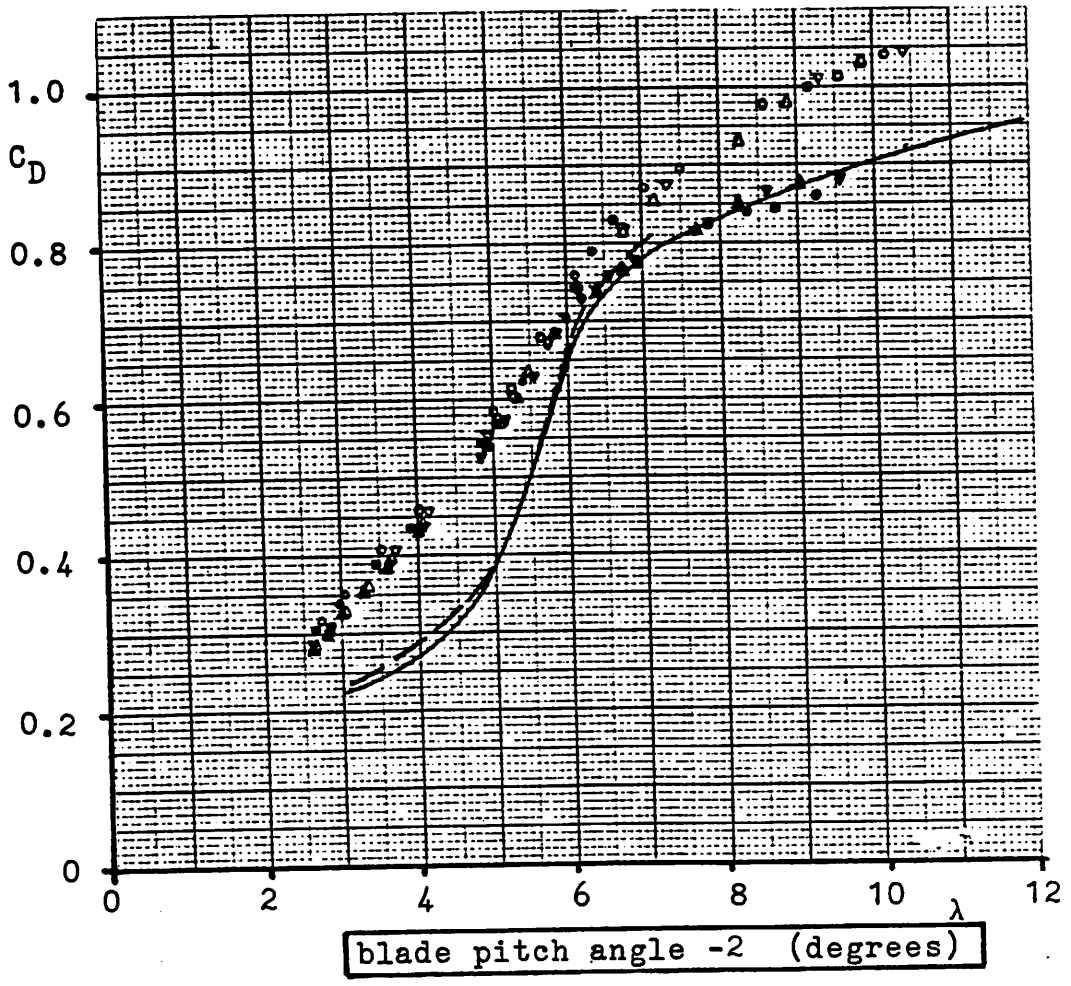

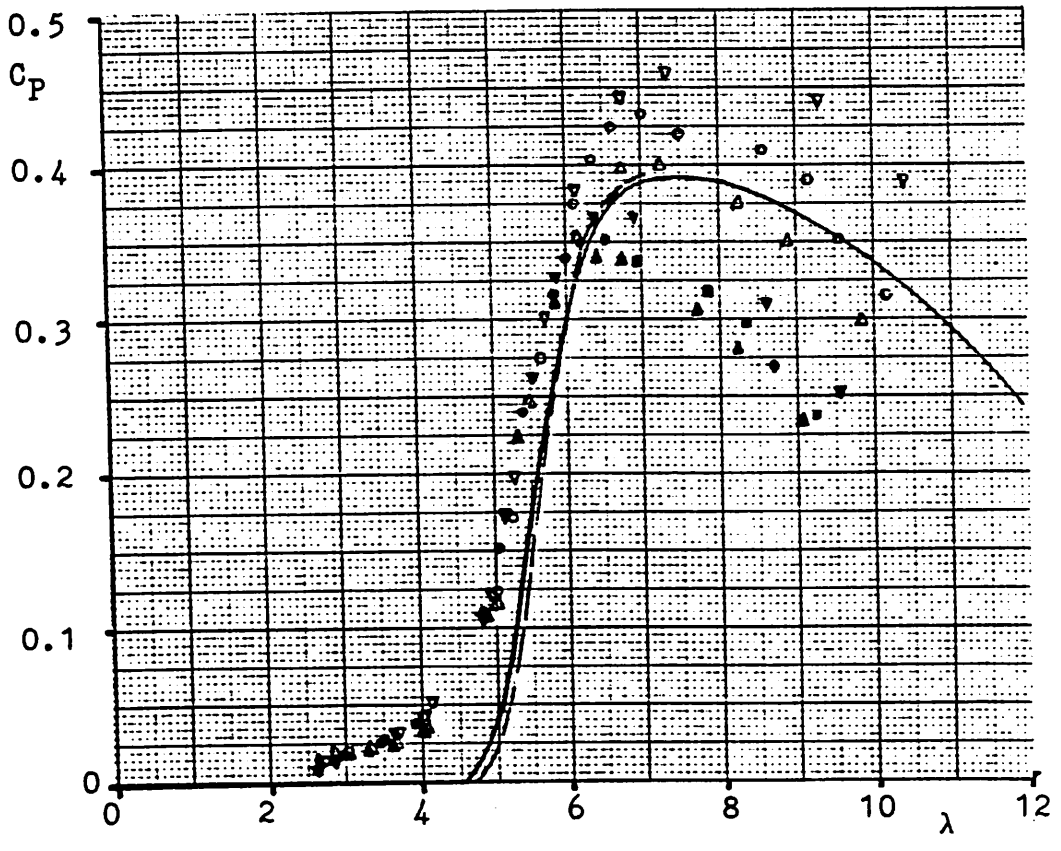

MODEL TURBINE NLR, measured in low-speed wind tunnel
calculated: ——— program RHO; - - - - - program HELIX
measured : △ ○ ▽ not corrected for wake blockage
▲ ● ▼ corrected for wake blockage

Figure 5

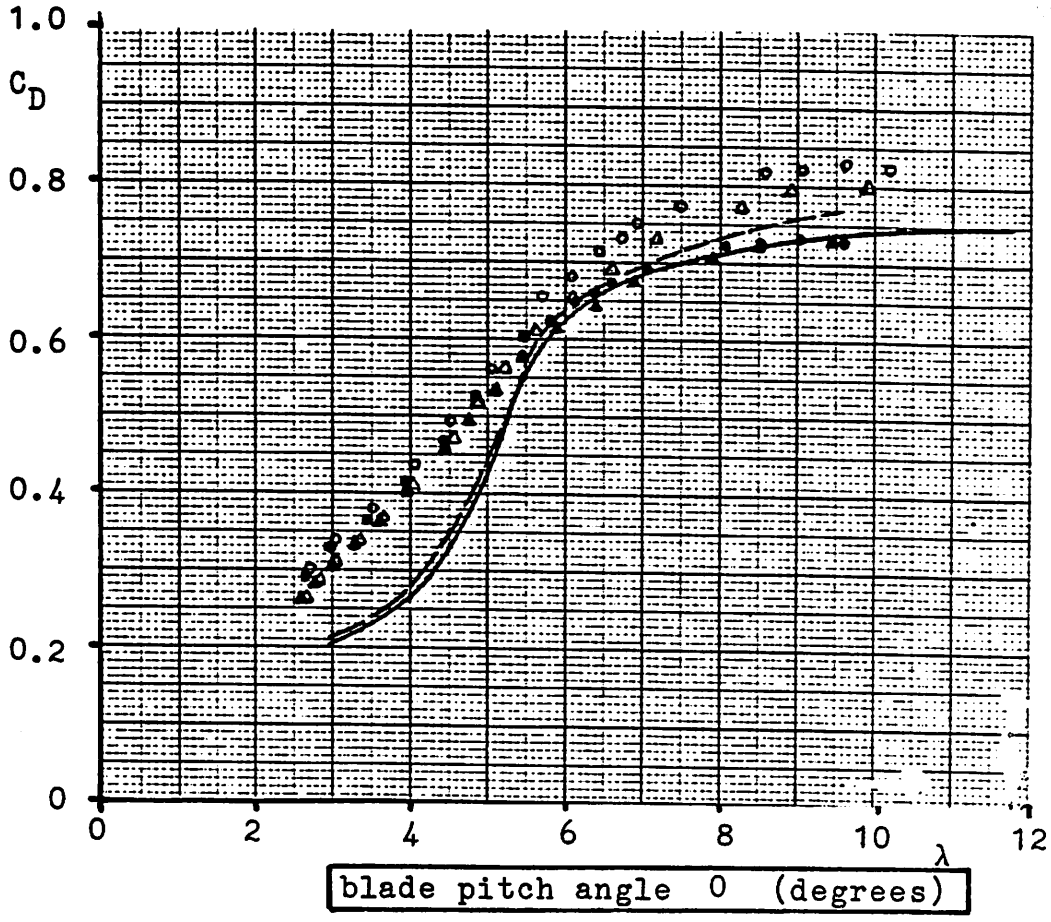

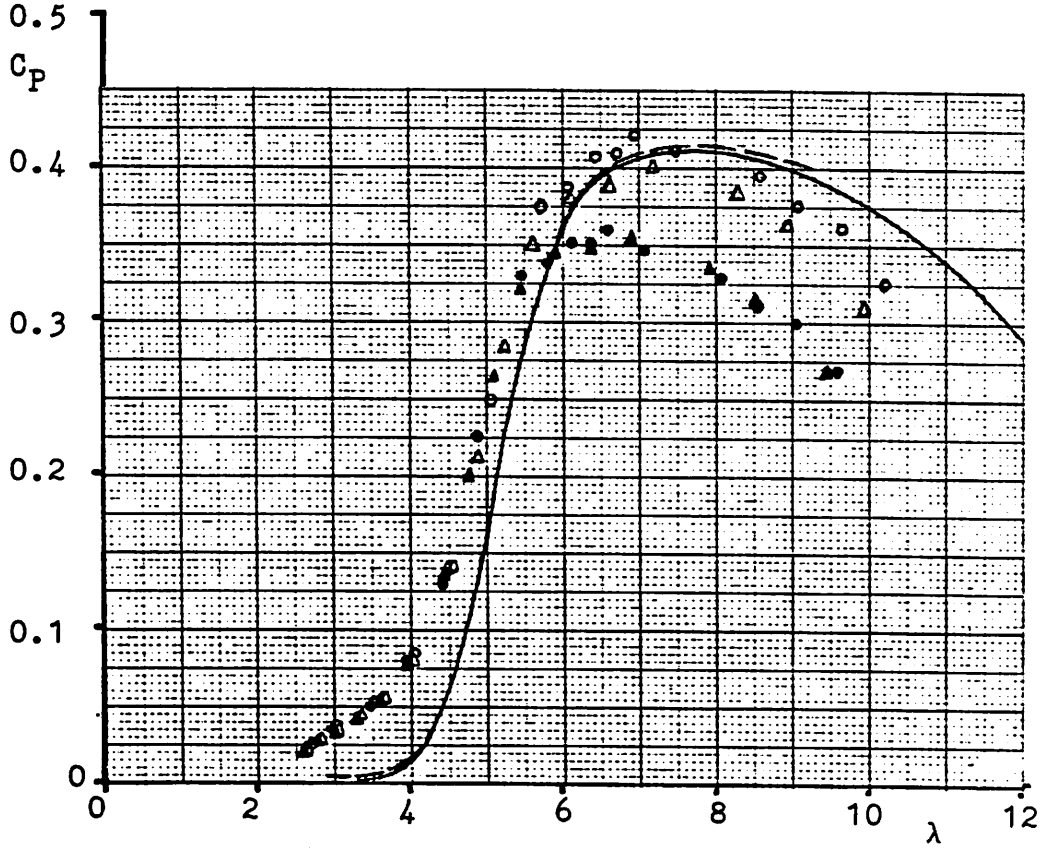

MODEL TURBINE NLR, measured in low-speed wind tunnel
calculated: ——— program RHO; - - - - - program HELIX
measured : △ ○ not corrected for wake blockage
▲ ● corrected for wake blockage

Figure 6

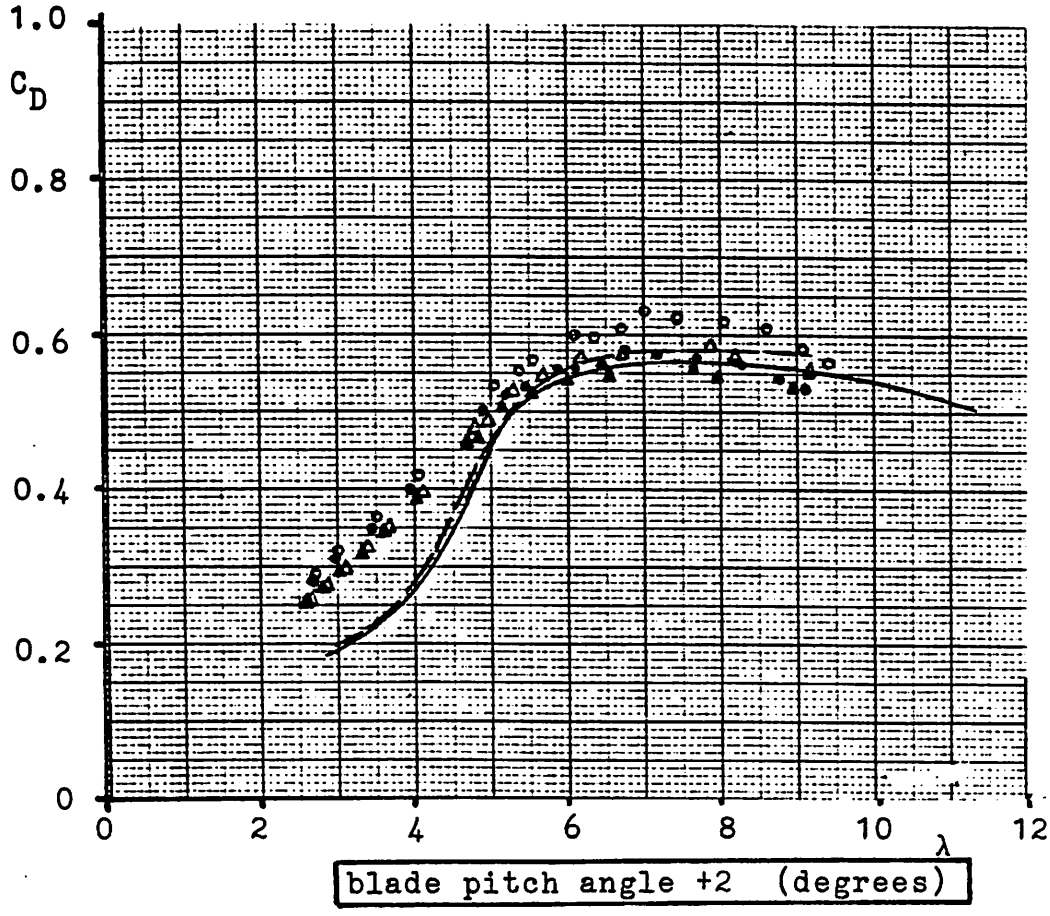

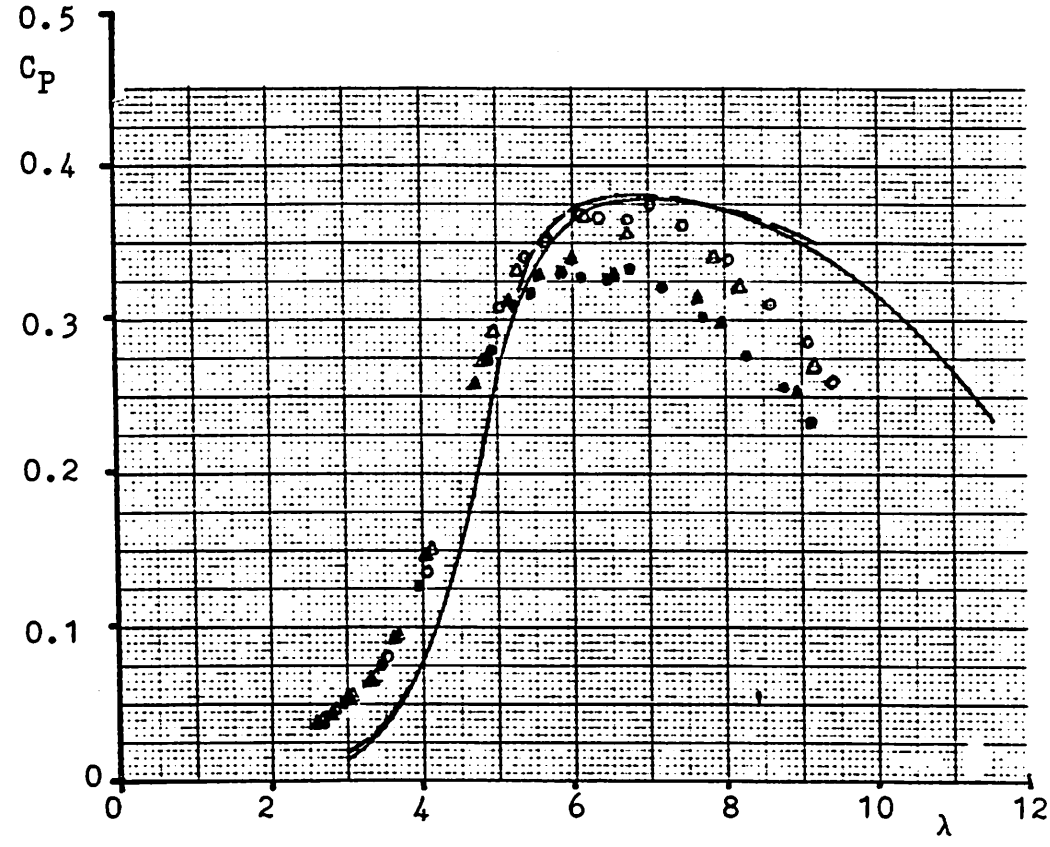

MODEL TURBINE NLR, measured in low-speed wind tunnel
calculated: ——— program RHO; - - - - - program HELIX
measured : {△ ○ not corrected for wake blockage
▲ ● corrected for wake blockage

Figure 7

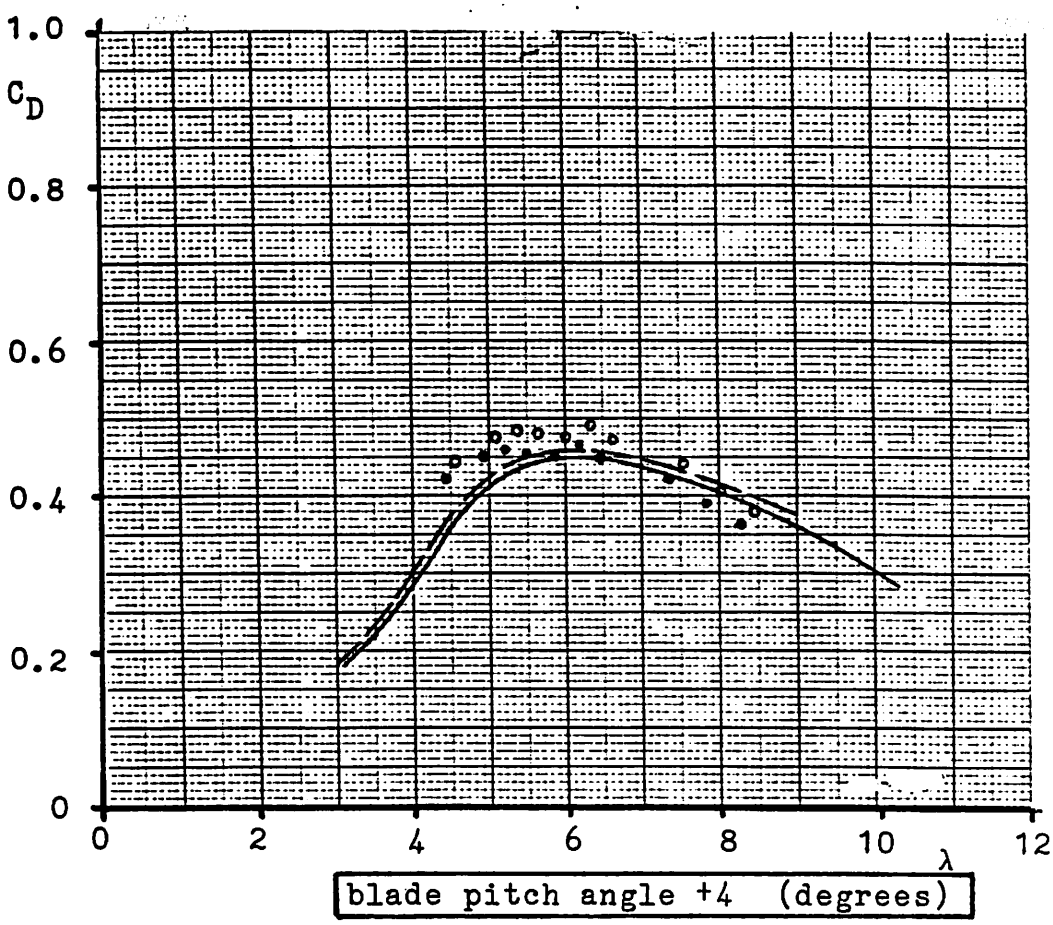

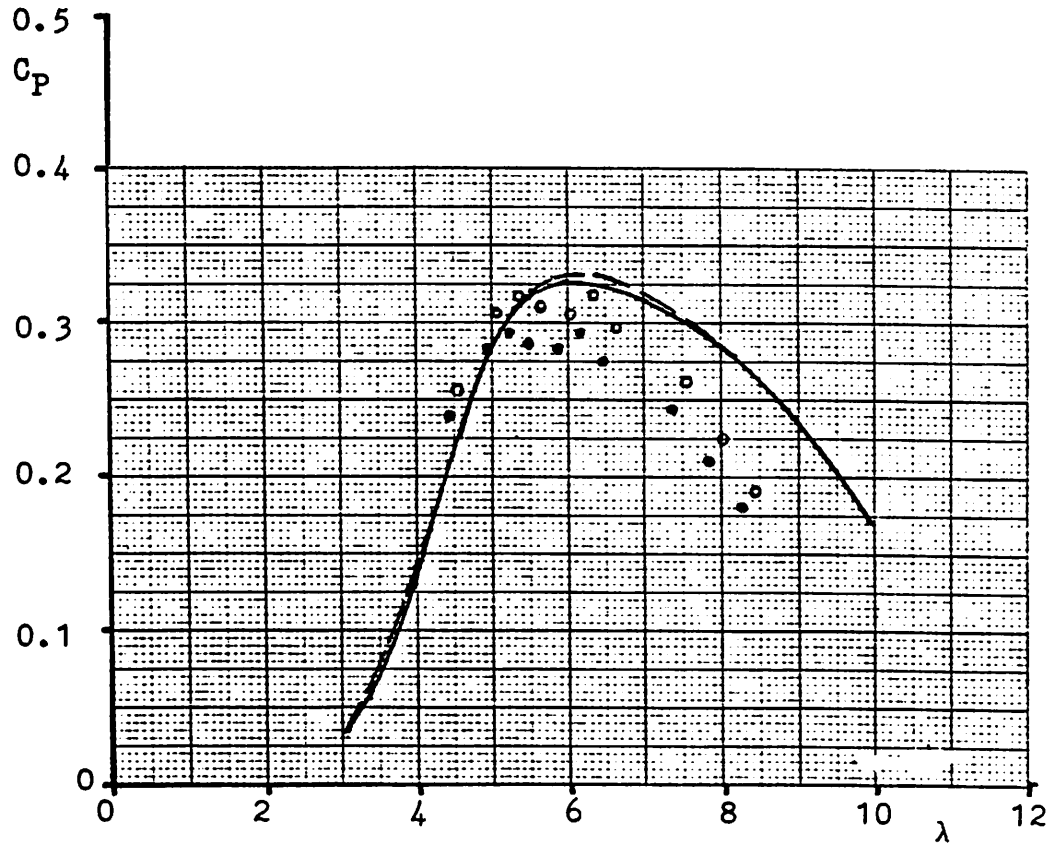

MODEL TURBINE NLR, measured in low-speed wind tunnel
calculated: ——— program RHO; - - - - - program HELIX
measured : { o not corrected for wake blockage
● corrected for wake blockage

Figure 8

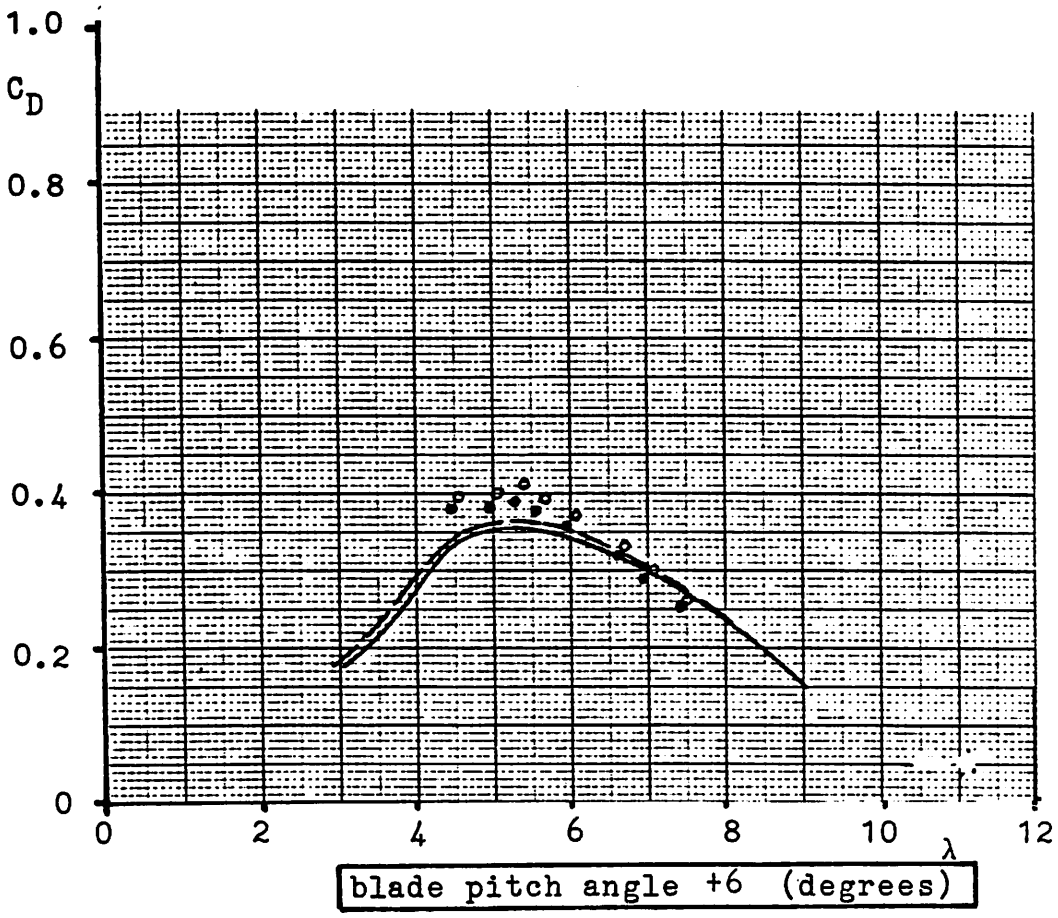

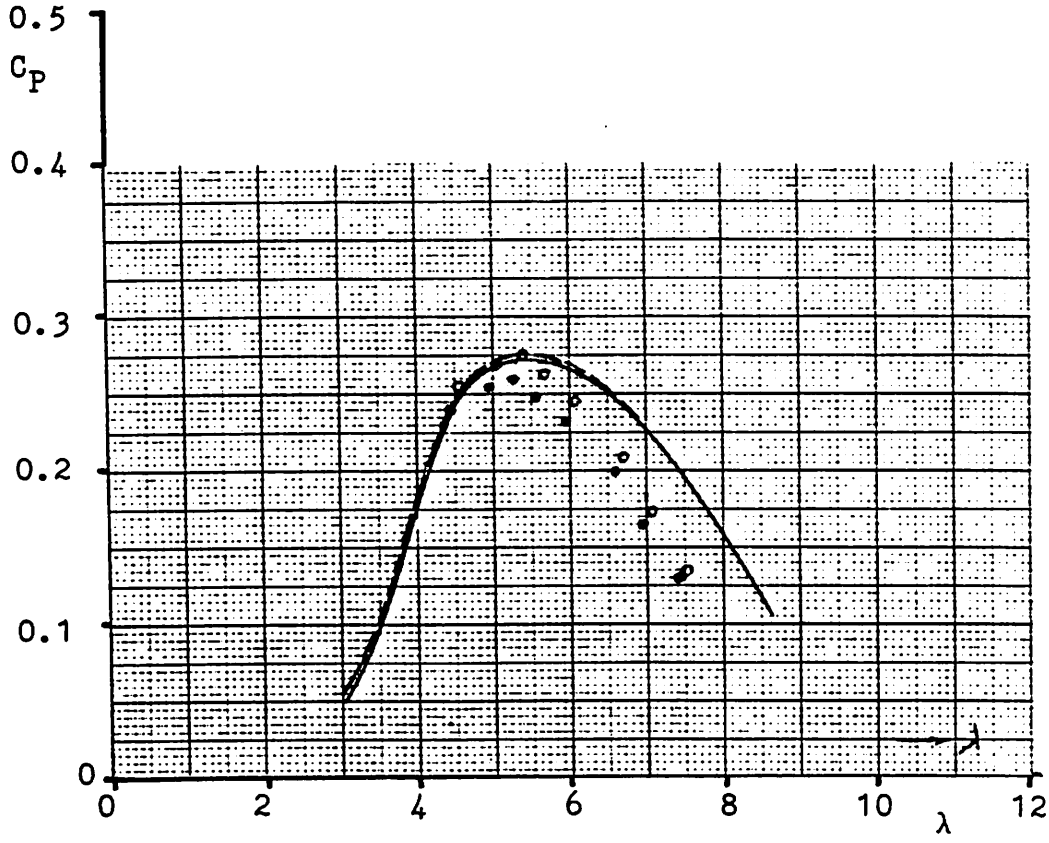

MODEL TURBINE NLR, measured in low-speed wind tunnel
calculated: ——— program RHO; - - - - - program HELIX
measured : { o not corrected for wake blockage
● corrected for wake blockage

Figure 9

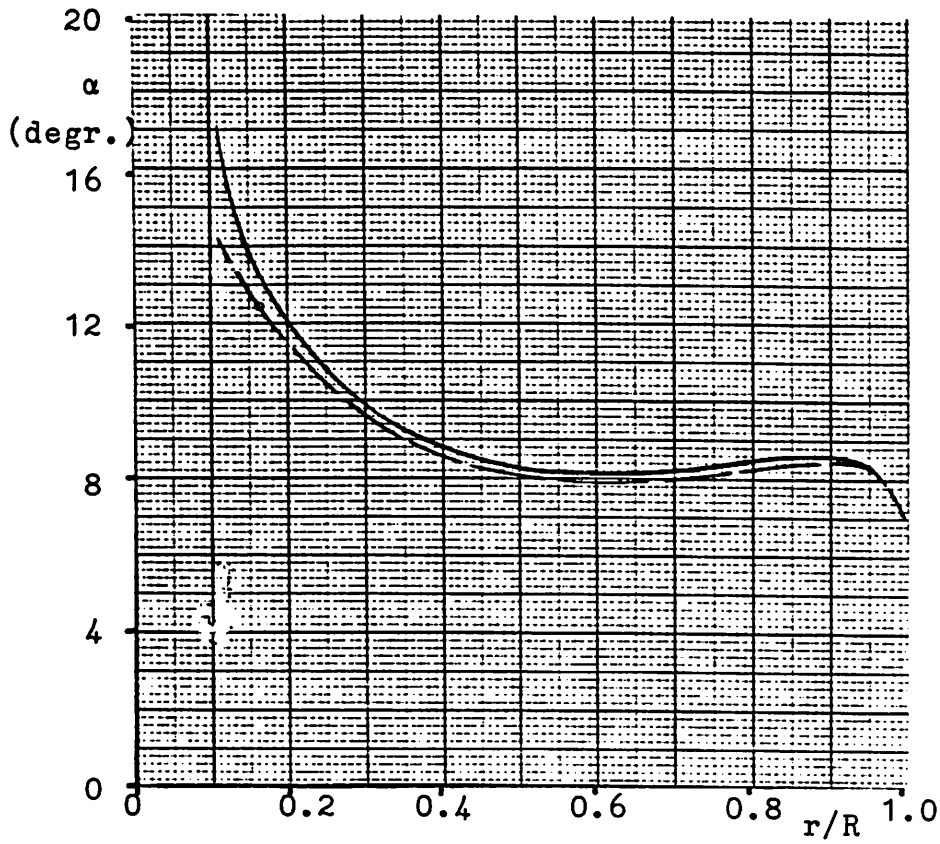

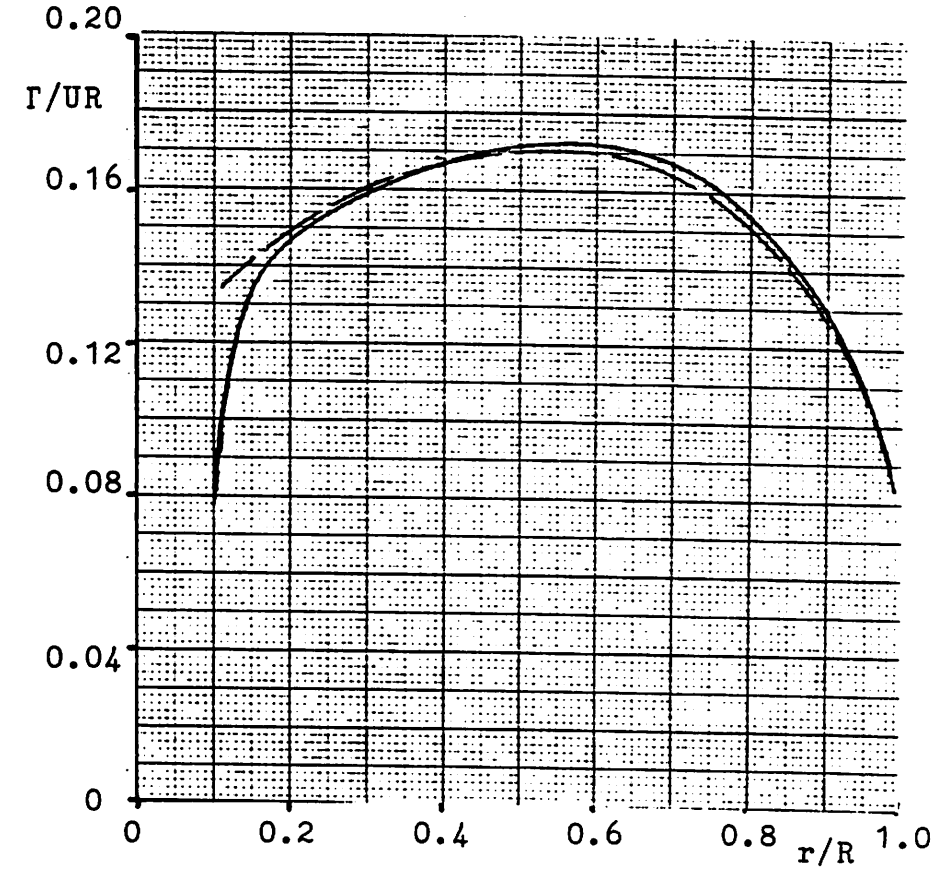

25 m HAWT, PETTEN blade pitch zero; $\lambda = 8$

——— program RHO; ---- program HELIX

Figure 10

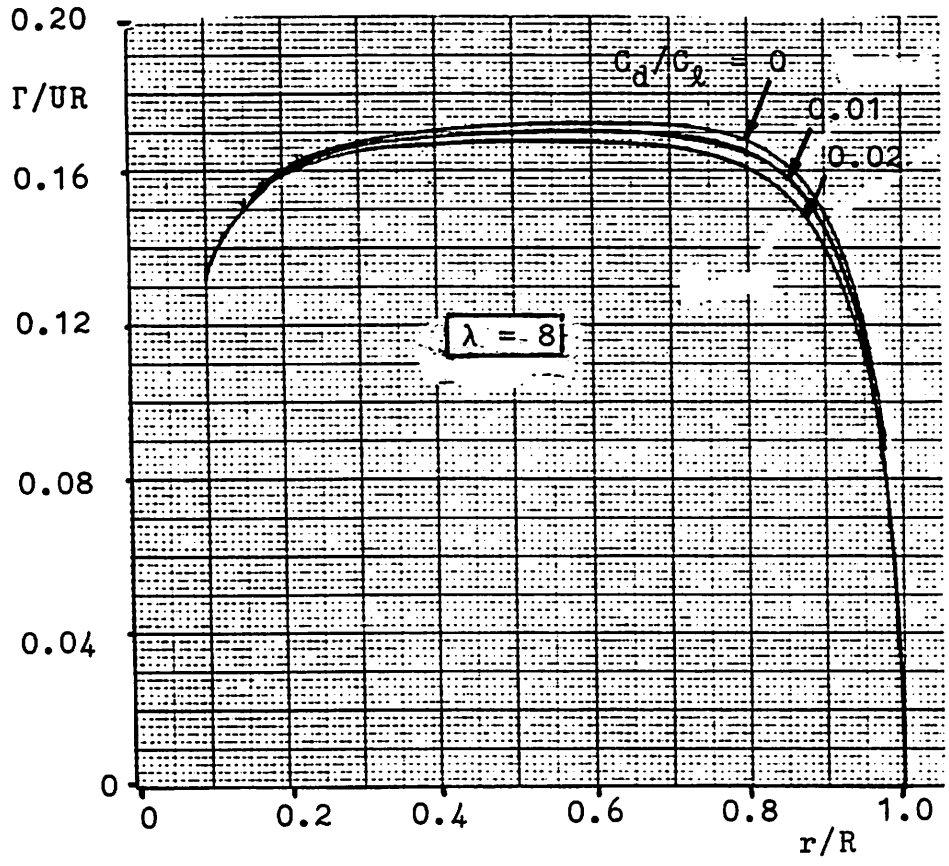

Optimum circulation distribution according to program RHO

Figure 11

calculations with program RHO

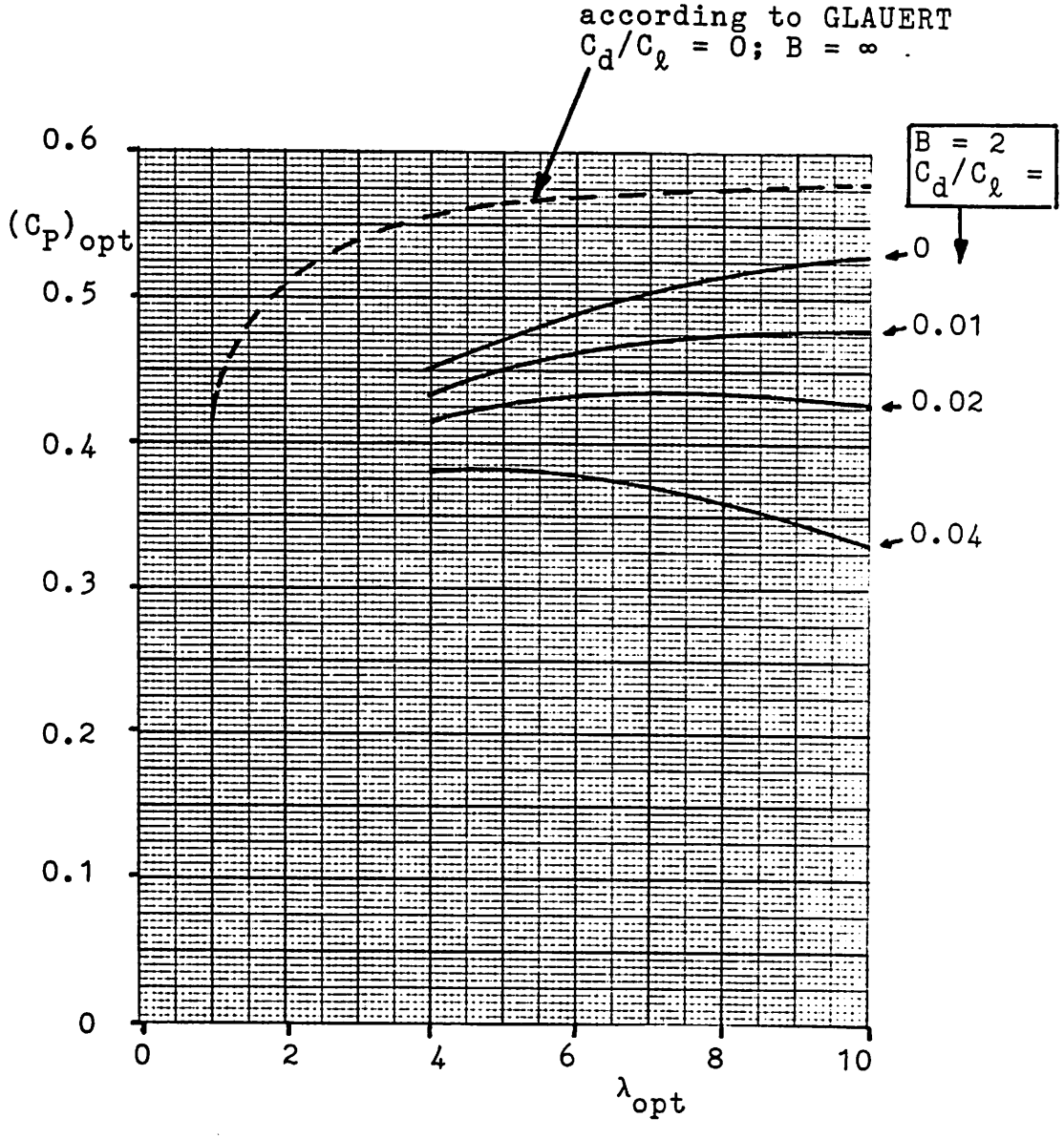

optimum power coefficient as a function of λ and C_d/C_ℓ, in which C_ℓ is assumed to be constant along the blade span.

Figure 12

4 COMMENT ON THE YAW STABILITY OF A HORIZONTAL-AXIS WIND TURBINE AT SMALL ANGLES OF YAW

NOMENCLATURE

A constant

B number of rotor blades

C constant

c = c/R, dimensionless blade chord

C_D = $D/(\frac{1}{2}\rho U^2 \pi R^2)$, axial force coefficient of the rotor

C_ℓ lift coefficient of the rotor blade section

C_{mz} = $M_z/(\frac{1}{2}\rho U^2 \pi R^3)$, yawing moment coefficient

$\bar{C}_{mz}$ time-average of C_{mz}

D total axial force on the rotor

f = $\frac{1}{B}(\partial C_D/\partial r)$, dimensionless blade loading

M_z yawing moment

R tip radius of the rotor

r = r/R, dimensionless local radius

U undisturbed wind velocity

u =u/U, dimensionless axial component of the induced velocity

x =x/R, dimensionless coordinate in wind direction

α angle of attack of the rotor blade section

θ angle of relative velocity at blade element (Fig. 4)

λ = $\Omega R/U$, tip-speed ratio

Ω angular velocity of the rotor

ρ density of the air

ϕ orbital position of a rotor blade in the rotor disk

ψ angle of yaw

INTRODUCTION

The aerodynamic yawing moment of a rotor, due to a non-zero angle of yaw, is of interest for the calculation of the yaw stability of a free-yawing rotor, but also for the design of the powered yaw nechanism of a horizontal-axis wind turbine (HAWT).

The commonly used blade-element theory, applied by Glauert (Reference 1) to a yawed propeller and extended by Wilson, et al. (Reference 2) to wind turbines, predicts an almost neutral stability in yaw. When the axial force is taken into account, this leads to the conclusion, that a downwind rotor position with respect to the tower (yaw axis) is necessary for a free-yawing rotor and favourable for a rotor with a powered yaw mechanism, because of the reduction in drive power.

However, small-scale wind-tunnel experiments at the Eindhoven University of Technology (Smulders, et al. Reference 3) revealed a stable yawing moment at almost all operating conditions. Even a solid flat plate perpendicular to the windstream showed this yaw stability in an upwind position with respect to its hinge axis. This indicates a shortcoming in the blade-element theory, when applied to the yawing moment.

It is clear, that the discrepancy has to be found in the neglect of the variation of the velocities, induced by the (trailing vortex) wake, downstream of the rotor disk. It is, however, difficult to comprehend, why the small deformation of the wake at small yaw angles should have such a large effect on the induced velocities.

Studies on the tipvane wind-turbine concept, sponsored by the Dutch

Ministry of Economic Affairs, have led to the consideration of simplified vortex models for wind turbines. As a spin-off of these considerations, some light was shed on the above-mentioned yawing moment discrepancy.

It was realized that, at small angles of yaw, the vortex wake, and the velocities induced by it, remain almost "frozen" to the wind direction, whereas the rotor disk is yawd with respect to this "frozen" axis-of-reference. Due to the large downstream gradient of the axial induced velocities, the induced velocities at the rotor disk vary significantly, which leads to a variation of the angle-of-attack distribution across the rotor disk. It is easily visualized, that this gives rise to a positive yaw stability.

At larger angles of yaw, the deformation of the vortex wake cannot be neglected and the calculation of the induced velocities across the rotor disk becomes awkward.

The intent here is to show, in a way as simple as possible, the basic differences between both theories. It is not intended to expose a complete calculation method.

It is hoped, that this comment stimulates further studies, theoretically as well as experimentally, on the yaw stability of an upwind HAWT, which rotor position is preferable from a point of view of blade fatigue and noise.

BLADE-ELEMENT THEORY

It will be shown in this Section how the blade-element theory and the additional assumptions of Glaubert (Reference 1) lead to a neutral yaw stability for a HAWT.

Starting point of the calculation is the (dimensionless) blade load distribution f as a function of the spanwise station $r = r/R$ and the tip-speed ratio $\lambda = \Omega R/U$, in which r is the local radius, R the tip radius, Ω the angular velocity of the rotor and U the undisturbed wind velocity.

This blade load distribution function f has to be known for a yaw angle $\psi = 0$ and is defined for a B-bladed rotor by the total axial force coefficient C_D:

$$C_D = D/(\tfrac{1}{2}\rho U^2 \pi R^2) = B \int_0^1 f \, dr, \qquad (1)$$

in which D is the total axial force on the rotor, ρ is the density of the air and B is the number of rotor blades.

For the present demonstration, a triangular load distribution is assumed, i.e.:

$$f = \left(\frac{A+C\lambda}{B}\right) r. \qquad (2)$$

In Eq. (2), A and C are constants, which choice has to be such that realistic values of C_D are obtained for a desired (limited) range of λ-values ($C_D = \frac{1}{2}(A+C\lambda)$).

When the wind velocity U comes in at a yaw angle ψ (Fig.1), the axial component U cos ψ is constant across the disk area and does not contribute to the yawing moment. The lateral component U sin ψ gives rise to a component normal to the blade span, which depends on the orbital position ϕ of the blade, thus:

$$U \sin\psi \sin\phi. \qquad (3)$$

This component affects the tip-speed ratio at each orbital position by the amount:

$$\lambda + \Delta\lambda = \frac{\Omega R + U \sin\psi \sin\phi}{U \cos\psi},$$

or, for small values of ψ ($\cos \psi = 1$, $\sin \psi = \psi$):

$$\Delta\lambda = \psi \sin \phi. \tag{4}$$

Glauert now assumes, that the influence of yaw on the load f of the blade element can be taken into account by the variation of the tip-speed ratio (Eq.(4)) and the load distribution for $\psi = 0$ (Eq.(2)). The implicit assumption is, that the influence on the load of a blade element is the same, as if the variation of λ acted on the entire rotor disk instead of on one element of a blade at one orbital position.

The variation of f due to the variation of λ can be obtained from the Eqs.(2) and (4), namely:

$$\Delta f = \frac{\partial f}{\partial \lambda} \Delta\lambda = \psi \sin \phi \frac{\partial f}{\partial \lambda} = \frac{C}{B} r \psi \sin \phi. \tag{5}$$

The yawing moment for a B-bladed rotor can be calculated from the equation (when it is assumed that $C_{mz} = 0$ at $\psi = 0$):

$$C_{mz} = \sum_{i=1}^{B} \int_0^1 \Delta f_i \, r \cos \phi_i \, dr. \tag{6}$$

Because

$$\frac{1}{B} \sum_{i=1}^{B} \sin \phi_i \cos \phi_i = \begin{cases} 0 & , \text{ if } B \geq 3, \\ \sin \phi \cos \phi & , \text{ if } B \leq 2, \end{cases}$$

the Eqs.(5) and (6) yield

$$C_{mz} = \begin{cases} 0 & , \text{ if } B \geq 3, \quad (7) \\ \frac{1}{2} C \psi \sin \phi \cos \phi & , \text{ if } B \leq 2. \quad (8) \end{cases}$$

Eq.(8) gives a variation of the yawing moment during a revolution from positive to negative, with a zero time-average.

In an actual case, a more complicated expression for $f(r, \lambda)$ has to be used, but the general conclusion with respect to the yaw stability will not be affected.

"FROZEN" VORTEX-WAKE CONCEPT

Apart from the angular velocity of the rotor and the wind velocity, the forces on the rotor blades are determined by the so-called "induced" velocities, which are "induced" by the trailing vortices downstream of the rotor (vortex wake).
It is very complex to calculate these velocities from the vortex-wake structure by the so-called "law of Biot-Savart". In the case of a yawed rotor, Glauert tried to circumvent this problem by starting from the $\psi = 0$ load distribution. In this distribution, the influence of the induced velocities are already taken into account, but only for the $\psi = 0$ condition (axi-symmetric flow).

As figure 2 indicates, in the case of a yawed rotor, the vortex wake changes in two ways, namely (i) the cross section (viewed in wind direction) becomes elliptic, and (ii) the cylindrical vortex wake is cut-off aslant $x = 0$. In that case, the semi-infinite vortex wake, and the velocities induced by it, are no longer axi-symmetric in the rotor disk. Therefore, the "independence" of the various blade elements (implicitly assumed by Glauert) is unlikely to hold for a yawed rotor.

On the other hand, it is also difficult to comprehend why, at small angles of yaw, the induced velocities should vary that much. However, when the wake structure and its induced velocities in the $\psi = 0$ case are considered as "frozen" to the wind-axis system of reference, and the rotor disk turns over an angle ψ with respect to this system of reference, it is clear, that the gradient of the induced velocities in wind direction becomes important (Fig. 3). This gradient is such, that the resulting total axial velocity decreases downstream. This means,

that the axial velocity in the yawed condition increases for the upwind part of the rotor disk and decreases for the downwind part. An increase of the axial velocity means an increase of the angle of attack of the rotor blade and thus an increase of the blade load (pointing downstream) and vice versa. This results in a restoring (stable) yawing moment.

In the study of symplified vortex models for wind turbines, it was found that the following expression for the downstream distribution of the axial induced velocity $u = u/U$ represents a useful approximation, viz.:

$$u(x) = u(0)\left(1+\frac{x}{\sqrt{(1+x^2)}}\right). \qquad (9)$$

In Eq.(9). $x = x/R$ is the axial coordinate ($x = 0$ is at the rotor disk at $\psi = 0$; positive downstream). This equation is only a first-order estimation. The correct calculation of the gradient of the induced velocities is more complex, but for the present demonstration, Eq.(9) will suffice.

When the rotor disk is rotated about an angle ψ with respect to the wind direction, a blade element at position (r, ϕ) is displaced in x-direction:

$$\Delta x = r \cos\phi \sin\psi. \qquad (10)$$

For small ψ, thus for small Δx, Eq.(9) yields

$$u = u(0)(1+ r\,\psi \cos\phi).$$

The total axial velocity becomes, with $U = 1$:

$$1 - u(0)(1+ r\,\psi \cos\phi). \qquad (11)$$

When the induced tangential velocities and the componeht of the wind

velocity (Eq.(3)) are neglected with respect to the tangential velocity due to rotation λr, the angle of the relative wind velocity with respect to the plane of rotation θ (see Fig. 4) is:

$$\theta + \Delta\theta = \arctan \{\frac{1-u(0)}{\lambda r} - \frac{u(0)}{\lambda} \psi \cos \phi\}. \qquad (12)$$

Subtracting the value of θ for the situation $\psi = 0$, yields for the variation of the flow angle $\Delta\theta$ approximately:

$$\Delta\theta \approx - \frac{u(0)}{\lambda} \psi \cos \phi, \qquad (13)$$

which can also be interpreted as the variation of the angle of attack $\Delta\alpha$ of the blade element due to yaw.

When the lift curve slope $\partial C_\ell / \partial\alpha \approx 2\pi$ is introduced and the (dimensionless) relative velocity at the blade element is approximated by λr ($\lambda >> 1$), the variation of the blade loading can be obtained from:

$$\Delta f = 2\pi \Delta\theta \; c \; \lambda r = - 2\pi \; u(0) \; \psi \; c \; r \cos \phi, \qquad (14)$$

in which $c = c/R$ is the dimensionless chord length of the rotor blade.

The yawing moment can now be calculated from Eq.(6). Because

$$\sum_{i=1}^{B} \cos^2\phi_i = \begin{cases} B \cos^2\phi & , \text{ if } B \leq 2, \\ \frac{1}{2}B & , \text{ if } B \geq 3, \end{cases}$$

and assuming that u(0) is constant across the rotor disk, the instantaneous yawing moment is

$$C_{mz} = - 2\pi \; u(0)\psi \; \{\begin{matrix} \cos^2\phi \\ \frac{1}{2} \end{matrix}\} \int_0^1 Bc \; r^2 dr. \qquad \{\begin{matrix} B \leq 2 \\ B \geq 3 \end{matrix}\} \qquad (15)$$

The time-average value can be calculated from

$$\bar{C}_{mz} = \frac{1}{2\pi} \int_0^{2\pi} C_{mz} \, d\phi,$$

and is the same for all values of B, namely:

$$\bar{C}_{mz} = - \pi \; u(0)\psi \int_0^1 Bc \; r^2 dr. \qquad (16)$$

The integral in the Eqs.(15) and (16) is a geometric moment of inertia of the rotor. The negative sign indicates, that it is a stable yawing moment (see Fig.1).

NUMERICAL EXAMPLE

As an example, both methods, the blade element and the "frozen" vortex wake, will be applied to the two-bladed 25 m diameter HAWT, located at Petten, the Netherlands.

For the blade-element method, only the constant C (Eq.(2)) has to be chosen, which constant is equal to $C = 2(\partial C_D/\partial\lambda)$. From test results, the value of C at $\lambda = 8$ is $C \approx 0.16$. Figure 5 shows the value of C_{mz} as a function of ϕ for a yaw angle $\psi = 10^o$ ($\approx$0.17 radians). The time-average value is zero.

For the frozen-wake method, the value of u(0) at $\lambda = 8$ is taken as $u(0) \approx 0.33$ (close to optimum condition). The geometric moment of inertia can be calculated from the chord distribution

$$c = 0.160 - 0.136\ r,$$

which runs from $r = 0.1$ to $r = 1$. This yields for the moment of inertia a value equal to 0.0387. The results, obtained from the equations (15) and (16) with $\psi = 10^o$, are also shown in figure 5.

The estimates (shown in figure 5) are very crude, but the differences between the results of the two methods are so characteristic, that it should be possible to verify it experimentally.

CONCLUDING REMARKS

The theory presented in this comment supports the experimental evidence about the yaw stability of a HAWT, found in small-scale wind-tunnel experiments at the Eindhoven University of Technology.

The exposition of the theory is strongly simplified to attract the attention to the main item. Moreover, the theory is valid for small angles of yaw only.

When the stability of a rotor at large angles of yaw is important, more effort has to be put in research on simplified models for the wake structure at large angles of yaw.

Meanwhile, it should be very interesting to verify the present theory at small angles of yaw by some carefully planned experiments.

REFERENCES

1 Glauert, H. "Miscellaneous Airscrew Problems", Aerodynamic Theory (ed. W.F. Durand), Div. L, Chapter XII, Dover Publ. Inc., N.Y., 1934.

2 Wilson, R.E., Lissaman, P.B.S., Walker, S.N. "Aerodynamic Performance of Wind Turbines", Department of Mechanical Engineering, Oregon State University, Corvallis, Oregon, ERDA/NSF/04014-76-1, June 1976.

3 Smulders, P.T., Lenssen, G., Leeuwen, H. van. "Experiments with Wind Rotors in Yaw", Wind Energy Group, Lab. of Fluid Dyn. and Heat Transfer, Dept. of Physics, Eindhoven Univ. of Techn., The Netherlands. Presented at: Intern. Symp. on "Appl. of Fluid Mech. and Heat Transfer to Energy and Environmental Problems", Patras, Greece, June 29 - July 3, 1981.

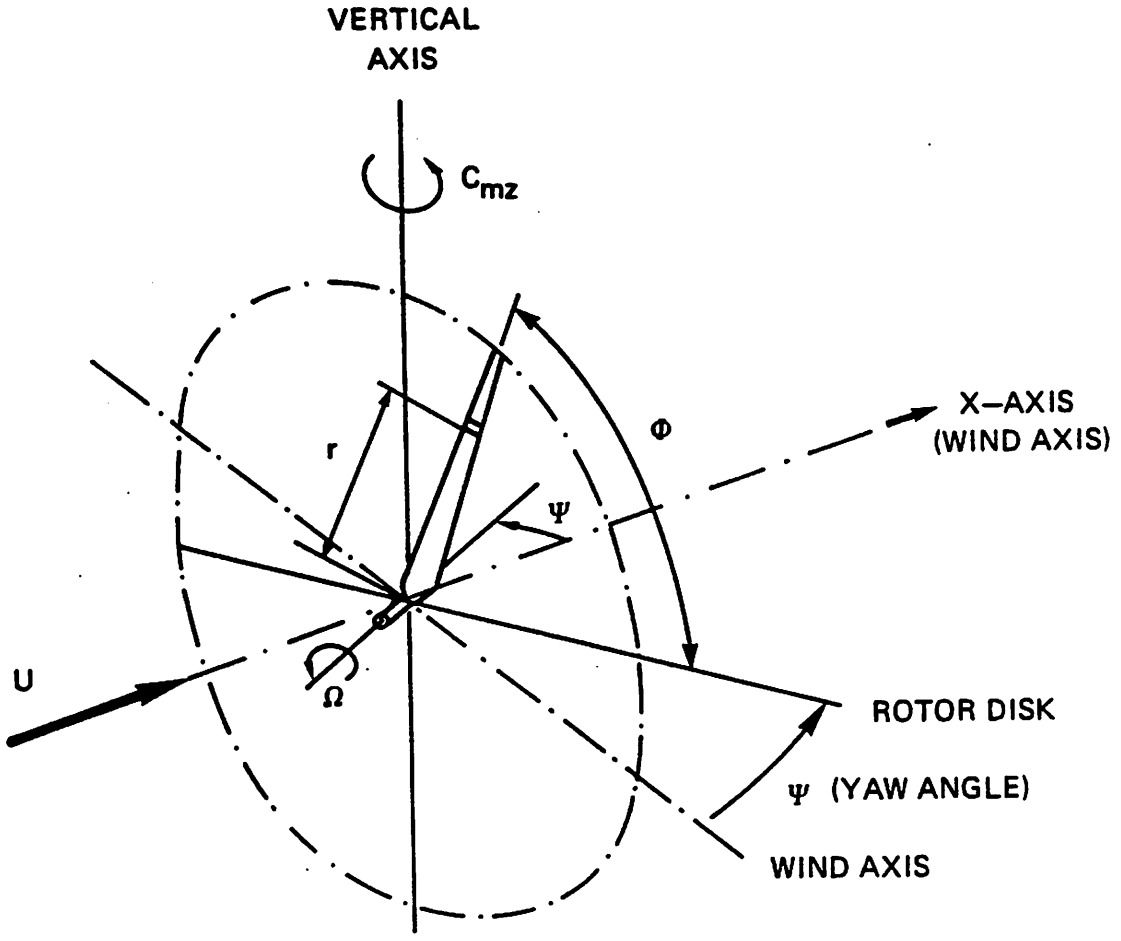

Fig. 1 Coordinate system for a yawed rotor.

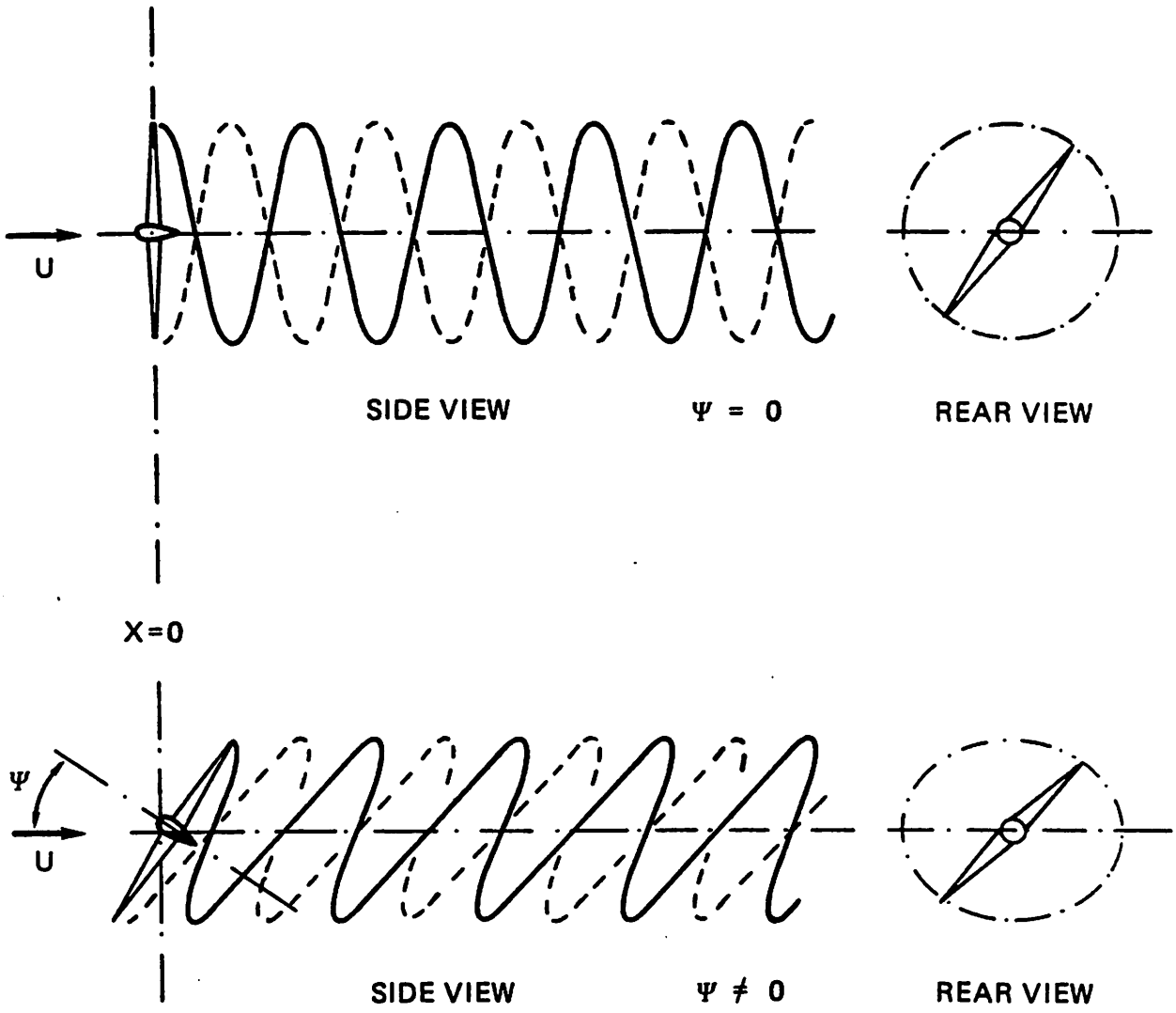

Fig. 2 Schematic representation of the vortex wake deformation due to yaw

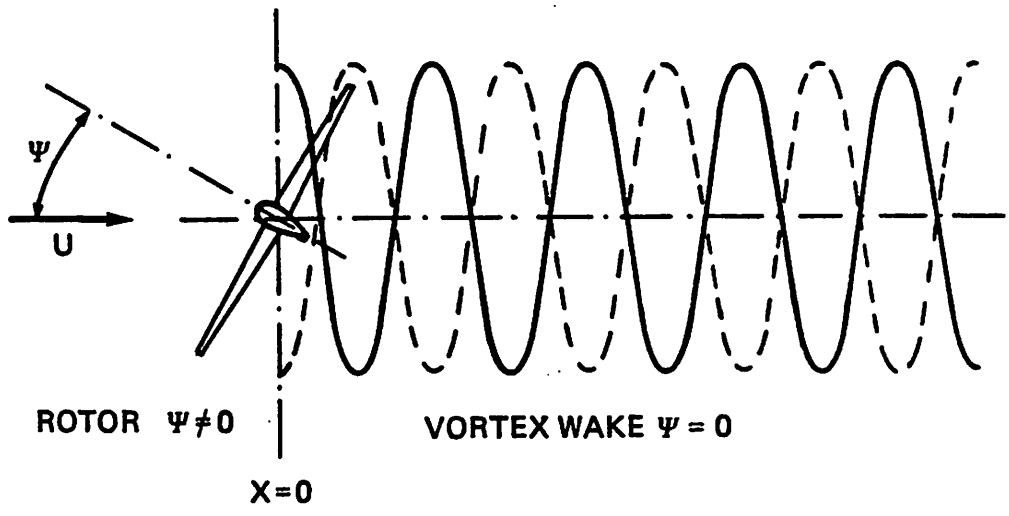

Fig. 3 Schematic representation of the "frozen" vortex wake concept.

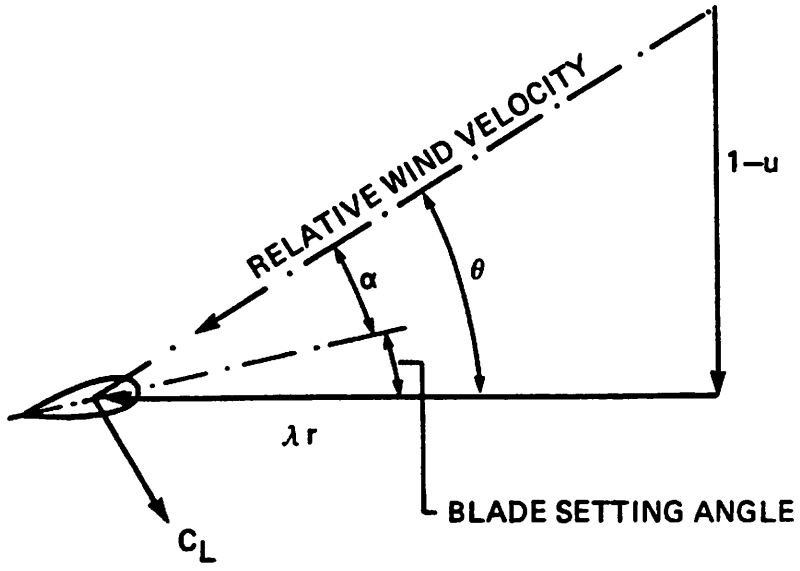

Fig. 4 Velocity triangle at a blade element at a spanwise station r = r/R. The undisturbed wind velocity is U = 1 and λ = ΩR/U.

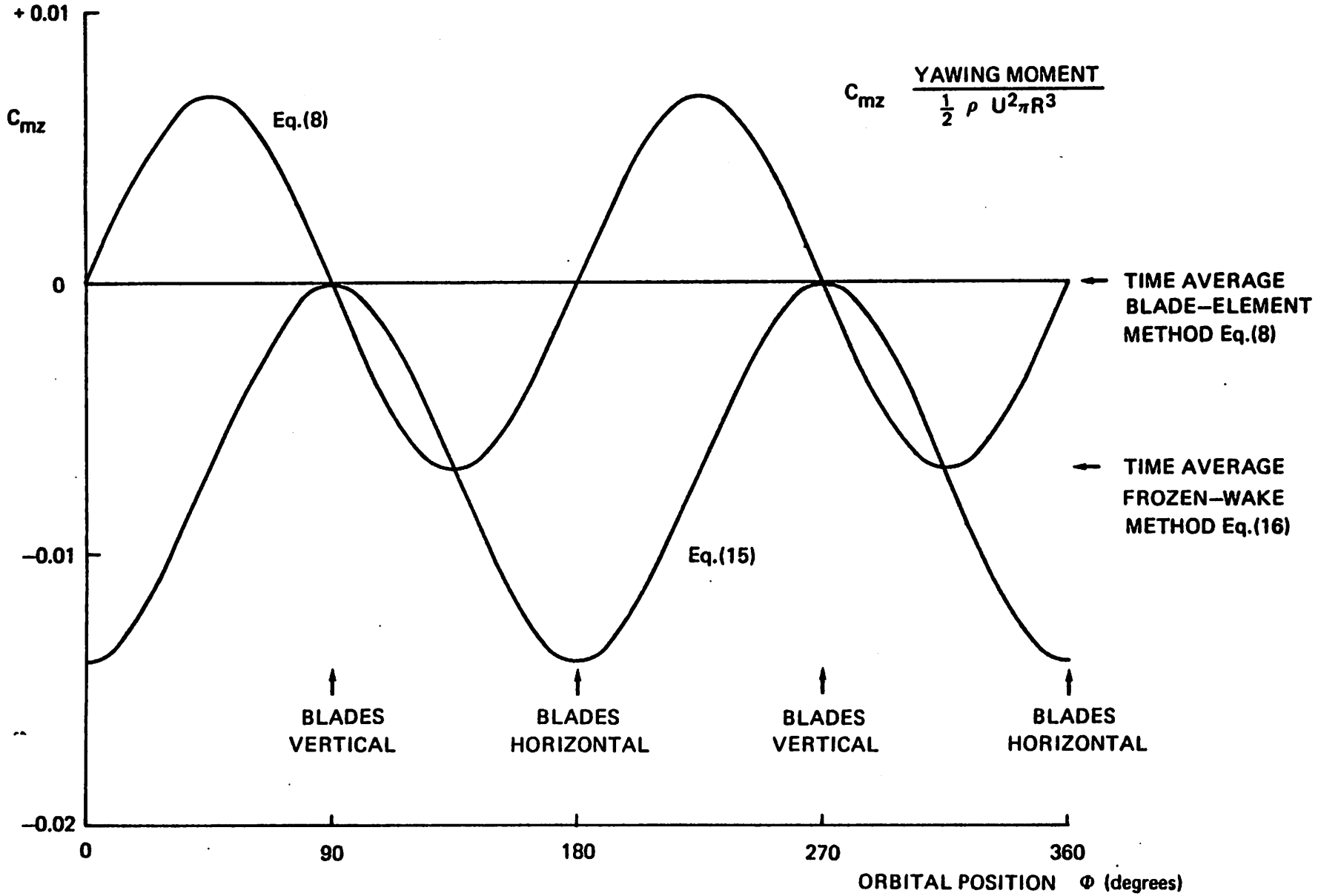

Fig. 5 Rough estimate of the yawing moment variation during a revolution for a two-bladed rotor at a yaw angle of 10 degrees. Comparison between the blade-element and the frozen-wake method.

AERODYNAMIC RESEARCH EFFORTS AT SERI WIND ENERGY RESEARCH CENTER AT ROCKY FLATS

James L. Tangler

The Solar Energy Research Institute (SERI) under contract to the U.S. Department of Energy (DOE) conducts in-house and subcontracted aerodynamic research studies. These efforts deal mainly with performance prediction and enhancement of horizontal axis wind turbines (HAWT's). Two levels of performance prediction theory are currently being used and refined while performance enhancement is being pursued through the development of new special purpose airfoils. A general purpose blade-element/momentum code (PROPSH) has been developed for rapid parametric studies and for use in annual energy calculations. A desirable feature of this code is a post-stall airfoil data synthesization routine that accounts for blade aspect ratio effects. A version of the performance code is also being developed to provide a better determination of dynamic stall effects on blade loads and performance as influenced by machine yaw angle, unsteady winds, tower shadow, and wind shear. For detailed wind turbine blade optimization, a more sophisticated lifting-surface/prescribed-wake analysis has recently been developed. This computer code is a transfer of current state-of-the-art helicopter theory into a wind turbine design analysis. The special purpose airfoil design effort is directed toward satisfying the need to tailor airfoil characteristics specifically for HAWT's. The design criteria and the current status of this effort are presented.

1. INTRODUCTION

In the late 1970s wind turbine aerodynamic design concerns centered on the issues of 1.) the accuracy and usefulness of the various performance prediction codes, 2.) the impact dynamic stall has on wind turbine performance and blade loads, 3.) the appropriate method of measuring rotor performance for establishing an accurate performance curve, and 4.) the need to consolidate low Reynolds number airfoil data into a catalog for wind turbine design. These issues were addressed through contracted and in-house research efforts at the Wind Energy Research Center (WERC) at Rocky Flats, which has recently been consolidated with the Solar Energy Research Institute (SERI).

To address the question of how well the various performance prediction codes predict net rotor performance, four contractors used their performance models to calculate the performance of two wind turbines and compared their results to test data. Three codes evaluated were based on blade-element/momentum theory and the fourth was a lifting-line/prescribed-wake model. Three objectives were addressed in this comparison: 1.) to evaluate the limitations and accuracies of the various analytical models; 2.) to identify areas where existing performance models were inadequate; and 3.) to identify where existing test methods are inadequate for correlation purposes. Documentation of this effort can be found in (1). Some of the more pertinent conclusions drawn from this study are:

- Blade-element/momentum theory substantially underpredicts peak and post-peak power when two-dimensional (2-D) airfoil data tables are utilized after stall. Reasonable agreement can be achieved in this region using synthesized 3-D airfoil data (2).
- In the windmill brake state, the Glauert empirical approximation has little influence on predicted performance for optimum blade pitch. At pitch angles toward stall the Glauert approximation predicts higher power coefficients than momentum theory.
- In order to determine wind turbine power from measured generator power at high tip speed ratios (low windspeed), the elimination of hysteresis effects in measured power and accurate determination of the generator efficiency essential.
- Based on this limited study, no definitive statement can be made on the relative accuracy of blade-element/momentum analysis versus analysis using discrete vortex-type wakes. Further study is needed to systematically compare differences in their respective blade element data.

Dynamic stall, as influenced by wind gusts and tower shadow, was investigated under contract (3) to determine its effect on predicted performance and blade loads for horizontal and vertical axis wind turbines. For fixed pitch horizontal axis wind turbines, the results showed that dynamic stall effects may increase a blade's normal loads and torsional moments by about 10 percent; for vertical axis machines, dynamic stall effects may increase normal blade loads marginally, but would likely result in a substantial increase in the blade's peak torsional moment. The consequence of these loads was indicated to be a reduction in fatigue life. An extensive literature review of dynamic stall is also included in this study. This work—one of the first investigations of dynamic stall effects on wind turbines—is by no means comprehensive. However, it does provide a good starting point, with recommendations for initiating new studies on the subject.

Evaluating the merit of aerodynamic performance prediction codes involves comparing predictions to measurements. However, measured performance data can include as much uncertainty as th predictions if certain precautions aren't observed in the data acquisition process. An

awareness of the proper use of the "Method of Bins" in collecting data is essential to eliminate potential sources of error. Discussions of this subject can be found in (4) and (5). In addition, test data need to be accurately characterized by complete information on machine operating characteristics (i.e., blade pitch, yaw tracking, etc.) along with wind characteristics such as directionality, steadiness, and turbulence.

Performance prediction for wind turbines requires airfoil data at relatively low Reynolds numbers. Available airfoil data for this purpose are in a variety of publications not readily known to most designers. To facilitate the location and use of these data, a contracted effort was undertaken with Texas A&M University to consolidate them in a single source (6). The resulting catalog includes data up to a Reynolds number of 3,000,000. Airfoil series in the catalog include those by Eppler, the Wortmann FX-series, the Gottingen-Go series, and NACA four-digit, five-digit, and six-digit airfoils. A cautionary note on the use of the catalog concerns those airfoils having a sharp drag rise at stall such as for the Eppler and FX-series airfoils. These data possess excessive smoothing of the drag data in this region due to the cubic spline curve fitting routine used in generating the curves from discrete data. An addendum containing corrected curves for these data is available (7).

As with any research, it tends to uncover as many new issues as it resolves. Past aerodynamic studies concentrated on accurately calculating net rotor performance for determining annual energy output and the cost of energy. Recent work has recognized the importance of determining the cyclic aerodynamic blade loads for dynamic and fatigue analyses, which strongly affect machine reliability. A meeting of aerodynamic specialists, sponsored by the Wind Energy Research Center at Rocky Flats and the NASA Wind Energy Project Office, focused on current needs and provided recommendations for future aerodynamic research work (8). The present aerodynamic research activities at WERC are based on these observations and recommendations. High priority items from this list that are currently being pursued are:

- Post-stall airfoil characteristics need to be better understood to explain why fixed pitch rotors perform better in high winds than can be predicted using 2-D post-stall airfoil data.
- A more comprehensive study of dynamic stall to include the effects of yawed flow, tower shadow, wind shear, unsteady winds, or any combinations of these factors is needed to quantify its effect on blade loads and performance.
- Blade pressure measurements under controlled conditions with an anemometer array windspeed measurements are needed before performance prediction codes can be further developed to account for unsteady effects.
- Development of special purpose airfoils to improve the aerodynamic and structural performance of horizontal axis wind turbines.

The first three activities support an ongoing in-house task to verify and improve our general purpose blade-element/momentum performance prediction code (PROPSH) and our special purpose lifting-surface/prescribed-wake code used for detailed aerodynamic optimization. The fourth activity supports our in-house task devoted to performance enhancement. The remainder of this paper discusses the two performance prediction codes and related activities along with our special purpose airfoil design activities.

2. BLADE-ELEMENT/MOMENTUM CODE (PROPSH)

At WERC, the standard blade-element/momentum code used for routine performance predictions is called PROPSH. This code was developed in-house from the nondimensional AeroVironment blade-element/momentum PROP code (1). A desirable feature of the AeroVironment PROP code is that it is an efficiently written short code that can sweep tip speed ratio and blade pitch in one computer run. The code includes the Glauert empirical approximation (9) for low windspeed analyses and can accommodate different airfoil data tables for each blade element. Because of these features, the AeroVironment PROP code was considered an ideal building block from which a more useful code, PROPSH, could be developed for general engineering purposes.

The key features that distinguish the WERC PROPSH code from the AeroVironment PROP code are:

- The suffix "SH" in the PROPSH name stands for shaft because yawed flow effects were added to analyze machines operating off the wind axis or with shaft tilt.
- A 3-D post-stall airfoil data synthesization routine was added for better performance prediction at high windspeeds.
- The code was reprogrammed in a dimensional format for practical engineering use.
- Variable blade segment number and airfoil data input (up to 20) was added.

The development of PROPSH was motivated by the need for an easy to operate performance prediction code. The routine use of such a code is not only desirable for rotor blade design but also for performance verification and blade pitch determination for maximum energy extraction at a given wind site. Due to the recent proliferation of microcomputer systems, the PROPSH code has been made available to the wind industry for a nominal fee. The code is available in either Fortran or an IBM operational compatable Microsoft Basic language. Computational time for the Fortran version on an IBM PC is approximately 7 seconds per performance point (i.e., one blade pitch angle at a given tip speed ratio). This version of the code is available directly from SERI WERC. Similar computational times are associated with the Microsoft Basic version, which is offered by JETSTREAM wind systems designers (10).

3. LIFTING-SURFACE/PRESCRIBED-WAKE CODE

The lifting-surface/prescribed-wake performance prediction code being developed by Computational Methodologies is based on state-of-the-art theory (11,12) used in the helicopter industry. A sophisticated design code as this is suitable both for blade geometry optimization and to support research efforts requiring a more accurate estimation of the blade loading in both the spanwise and chordwise directions. A noteworthy feature of this approach is that lifting-surface theory provides the flexibility to account for performance differences due to tip shape geometry, due to aerodynamic surfaces mounted perpendicular to the blade such as dynamic inducers, and resulting from gaps or different pitch in the case of two piece blades. In addition, real wake induced effects on the blade are represented that account for radial and axial wake expansion as influenced by the blade loading.

A lifting-surface blade representation accounts for induced effects associated with aspect ratio or blade geometry. No tip loss correction is applied to the blade loading. Unlike lifting-line theory, both the chordwise distribution of induced velocity and the chordwise variation of freestream velocity are accounted for at each blade station. An accurate estimate of induced drag is dependent on these chordwise properties. Being a thin surface theory, airfoil thickness effects are reflected through the airfoil data tables used in the analysis. The lifting surface blade grid can consist of up to 20 spanwise panels and 5 chordwise panels.

A prescribed-wake geometry provides a rational approach for calculating wake induced effects at the rotor blade. A free wake representation is impractical because of the associated numerical problems and the extensive computer time. Past helicopter research studies (11) have shown that a rotor's wake geometry, in terms of contraction rate and pitch, is related to key rotor parameters such as blade number, twist, and thrust coefficient. In a similar manner, a wind turbine's wake is also governed by these parameters. However, unlike a helicopter wake, flow visualization studies suggest the geometry is dominated by freestream displacement and that distortion due to induced effects are secondary. Based on these considerations, the blade wake interface and near wake region can be defined. The far wake, which begins after the fourth tip vortex passage beneath the blade, is best represented using a generalized vortex cylinder model.

The computer implementation of this code is written in Fortran 77 and was developed on a fixed-disk based microcomputer system with floating point hardware. The source code is 4600 lines, of which 40 percent are comments, and requires 300kb of RAM. Depending on the size of the problem selected (i.e., number of spanwise and chordwise stations), execution time varies from 2 to 7 minutes per performance point.

4. CURRENT PERFORMANCE PREDICTION RESEARCH

A weakness of performance prediction codes is their inability to consistently predict peak power and blade loads on which the machine structural design and cost are strongly dependent. In many cases these quantities are much higher than can be predicted using current performance analyses. In any performance code, peak power and associated blade loads are dependent on an accurate assessment of the airfoil's static and dynamic stall characteristics. The relative importance of each of these has yet to be fully quantified. In an attempt to resolve the influence of each, two studies were undertaken. One of these efforts was to further validate the post-stall (static) synthesization routine of (2) against a comprehensive airfoil data base acquired in the Texas A&M University wind tunnel. The second effort was to develop a version of the PROPSH code with a time variant dynamic stall routine.

The post-stall synthesization routine of (2) is based largely on empirical relationships shown to provide good correlation for the larger NASA machines. This routine was chosen for use in PROPSH because it accounts for post-stall aspect ratio effects and because of its user friendly nature. Without any required user interaction, the routine automatically provides a smooth curve fit from where the airfoil 2-D data leave off up through the highest angle of attack experienced by the blade. A comparison of this synthesization routine to wind tunnel test results is presented in (13). For this comparison, nonrotating wing sections were tested in the Texas A&M wind tunnel. Post-stall performance characteristics were established as a function of aspect ratio, airfoil thickness, and Reynolds number. The test models had a 0.30-m chord and were of the NACA 44XX family of airfoils. Blade aspect ratios of 6, 9, 12, and ∞ were tested for airfoil thicknesses of 9, 12, 15, and 18 percent at Reynolds numbers of 250,000, 500,000, 750,000 and 1,000,000.

Results of the wind tunnel tests (14) showed that in the light stall region, from 15 to 30 degrees, the thinner airfoils acted more as flat plates and produced higher drag, while aspect ratio effects could not be discerned. In this region, the higher induced drag associated with lower aspect ratio is neutralized by the lower pressure drag associated with lower aspect ratio. Aspect ratio effects are not seen to have a net effect on C_D until the angle of attack exceeds 27 degrees. Above this angle, the post-stall airfoil characteristics of C_L and C_D are a strong function of aspect ratio (as expected) and a weak function of airfoil thickness. In the post-stall region, the influence of Reynolds number was negligible for the range tested. Comparison of the equations of (2) showed that they provided substantially higher L/D ratios after stall than could be substantiated by the C_L and C_D test data of Figures 1 and 2. Because of the more optimistic post-stall L/D ratio, when used in blade-element/momentum type analyses, these equations provide a better peak power prediction than is achieved by using equations based on the wind tunnel test. Potential causes of the differences are the inability of nonrotating wind tunnel tests to represent the influence of radial flow effects, which are thought to delay stall, and possible elastic twist effects resulting from the divergence of the post-stall moment coefficent.

The purpose of developing a dynamic stall version of the PROPSH code was to provide a useful tool that would allow dynamic stall to be studied in greater depth than in previous investigations. The new code, being developed under contract by Aerovironment Inc., includes the four causes of dynamic stall: wind shear, tower shadow, yawed flow, and unsteady winds. This code is being exercised for both two- and three-bladed wind turbines to determine the magnitude of dynamic stall effects in terms of rotor blade loads, torsional loads, and power output. Results of the dynamic stall effort to date show a very small loss in peak power. Dynamic stall for HAWT's appears to pertain more to fatigue through its contribution of cyclic loads.

The analysis of the static and dynamic stall effects on blade loads and performance raises many new questions that can only be answered through intensive experimental studies to better quantify the characteristics of the wind as seen by the rotor (15,16) and the causual relationship to both steady and unsteady blade loads. Anemometer arrays are needed to establish the spatial and temporal distribution of the wind inflow while aerodynamic blade loads need to be acquired through the use of pressure transducers encircling the airfoil at one or more blade stations. The response to these loads can then be acquired with strain gages located to measure bending, inplane, and torsional loads. The resulting steady and cyclic loads provide the critical inputs for determining rotor fatigue life and reliability (17); they also provide the basis for the next level of analytical refinements to the theory.

5. PERFORMANCE ENHANCEMENT

In the continuing effort to reduce the cost of energy, various means of enhancing the aerodynamic performance of horizontal axis wind turbines have been proposed and tested. Performance augmentation devices attached to the blades such as dynamic inducers (18) and stationary ones such as concentrators and diffusers (19) have shown substantial power ouput gains. However, when compared to conventional rotors of increased size for comparable power output, their relative cost and reliability is questionable. At WERC, performance enhancement is being pursued through the development of special purpose airfoils, in which performance gains and increased machine reliability are believed possible without impacting machine cost.

Airfoils currently used on horizontal axis wind turbines vary from cambered plates, to well-known airfoils of the NACA 44XX and 23XXX series, to recently designed, special purpose general aviation airfoils such as the LS(1)-0417 Mod. Early airfoil design, during the 1930s, used an empirical design approach to develop the NACA 44XX and 23XXX series airfoils. Over the years, airfoil design theory has progressed to where new airfoils can be designed analytically as was done for the LS(1)-0417 Mod. airfoil currently used on such wind machines as the Carter 250 and EST 80/200. Validated analytical design codes such as the low Reynolds number Eppler code (20) allow airfoils to be tailored for specific applications.

For horizontal axis wind turbines, better performance can be achieved with airfoils designed to be more machine specific in terms of Reynolds number, rotor solidity, mean annual windspeed, and machine operational mode. For low solidity rotors, better performance is achieved when L/D_{max} occurs at medium-to-high values of C_L, while for high solidity rotors lower values of C_L are desired for L/D_{max}. In a similar manner, the higher the mean annual windspeed for which the rotor is being designed, the more desirable it is to shift L/D_{max} to higher values of C_L. Machine operational modes such as fixed blade pitch versus variable blade pitch and constant rpm versus variable rpm also govern the airfoil design. For fixed pitch machine operation, designers have expressed the need for airfoils having a predictable $C_{L_{max}}$ insensitive to airfoil roughness effects. This quality provides for more consistent power output and helps eliminate unexpected operating characteristics that may be detrimental to rotor life. For variable pitch machines, this requirement can be relaxed since the blades can be feathered to avoid stall during high winds. However, for variable rpm machines, the airfoil must be designed to operate effectively over a wider Reynolds number range.

Acknowledging the general airfoil design dependency on rotor solidity, mean annual windspeed, and machine operational mode, the first family of special purpose airfoils was directed toward a class of wind turbines having the following properties:

- Fixed pitch 10-m diameter rotor
- Low solidity rotor with twist and taper
- Mean annual windspeed of 5 to 7 m/sec.

The airfoil family was to consist of three airfoils. The primary airfoil was to be designed for a radial station of (r/R = 0.75), while secondary airfoils would be designed for r/R = 0.40 and 0.90. The thickness of the airfoil for r/R = 0.40 and 0.90 would be expected to be thicker and thinner than the primary airfoil, respectively. To achieve the designed rotor operating characteristics, substantially different design criteria might be required for the inboard airfoil versus the outboard airfoil.

Specific design criteria established for the primary airfoil (r/R = 0.75) were that it have:

- High L/D through laminar flow
- $C_{L_{max}}$ insensitive to surface roughness
- Airfoil thickness of 12 to 15 percent.

With respect to the high L/D, the question arises as to whether it should occur at low, medium, or high lift coefficient. To answer this question, a C_L versus C_D airfoil polar was modified to imulate these hypothetical cases as shown in Figure 3. In cases 1, 2, and 3, a laminar flow

bucket was assumed to exist between the C_L values of 0.0 to 0.4, 0.4 to 0.8, and to 0.8 to 1.2, respectively. Rotor performance was calculated using these three cases. The influence on the power coefficient versus tip speed ratio curve is shown in Figure 4. For case 1, the laminar flow bucket at low C_L resulted in some performance improvement at high tip speed ratios (low windspeeds) but contributes little to annual energy output. For case 2, a substantial increase in performance is achieved at medium to high tip speed ratios. Whereas case 3 results in substantial performance improvement at low tip speed ratios (high windspeed). Based on this comparison, a laminar bucket covering the C_L range of 0.4 to 0.8 showed the greatest potential for enhancing annual energy output. The midpoint of the bucket (C_L = 0.6) was chosen as the point for which L/D was to be maximized. Associated with this bucket placement, it was also discovered that $C_{L_{max}}$ over the outboard portion of the blade had to be restrained so that power output at high windspeeds would not be excessive. This restrain also helps hold down the airfoil moment coefficient, which can contribute to high control loads or elastic twist during stall.

Using this design philosophy, Dan Somers of Airfoils Incorporated is in the final design phase of the first family of special purpose airfoils. Upon completion of this task the primary airfoil of the family is scheduled to be wind tunnel tested to verify its performance characteristics—particularly its $C_{L_{max}}$ roughness sensitivity. A diagram of the primary airfoil (r/R = 0.75) is shown in Figure 5. The airfoil geometry is characterized by a rather sharp leading edge with very little forward camber. A moderate amount of laminar flow is present on the upper surface and extensive laminar flow is present on the lower surface. Trailing edge camber is held to a minimum in an effort to restrain $C_{L_{max}}$ and minimize the airfoil's pitching moment coefficient. Also illustrated in Figure 6 is an approximation of one of the secondary airfoils designed for the blade root. This thicker airfoil is designed to have its L/D_{max} at a slightly higher value of C_L. The airfoil is designed for a $C_{L_{max}}$ as high as possible without any restrain put on the pitching moment coefficient. The combination of these two airfoils designed to the same camber family is expected to improve the performance at low windspeeds and limit peak power at high windspeeds, independent of roughness effects.

6. CONCLUDING REMARKS

Performance prediction methods at WERC have evolved from the relatively simple blade-element/momentum approach (PROPSH), which is ideal for rapid parametric type analyses, to the more rigorous lifting-surface/prescribed-wake approach used for detailed blade optimization. Current and future embellishments of these codes include refinements to the post-stall 3-D airfoil data synthesization routine, the incorporation of dynamic stall unsteady effects, and inclusion of sophisticated turbulent wind input models. Completion of these efforts will establish the need for a more rigorous level of validation characterized by detailed time dependent measurements of wind input, blade airfoil pressure distributions, and strain gauge measurements of cyclic loads. From these data current theory can then be evaluated and refined to provide design codes that better characterize the aerodynamic loads upon which dynamic and fatigue analyses are based. In turn, machine reliability should improve and help provide the needed energy cost reduction that will insure the survival of this viable energy source.

Performance enhancements of HAWT's is being pursued through the development of special purpose airfoil families. It is recognized that rotor airfoil requirements are unique in terms of Reynolds number, rotor solidity, mean annual windspeed, and operational mode. Accounting for these factors, new airfoil families are being developed for fixed and variable pitch wind turbines with consideration of both the constant and variable rpm operational modes. The first of these airfoil families is for the 10-m, constant rpm, fixed pitch class of machines. Desired performance characteristics being sought are enhanced performance at low-to-medium windspeeds through laminar flow and predictable $C_{L_{max}}$ independent of roughness effects at high windspeeds. Properly incorporating these characteristics into new machines should also reduce energy cost through improved annual energy output and machine reliability.

REFERENCES

1. Horizontal-Axis Wind System Rotor Performance Model Comparison, RFP-3508 UC-60, February 1983.
2. Viterna, L. A. and Janetzke, D. C., "Theoretical and Experimental Power from Large Horizontal-Axis Wind Turbines," Fifth Biennial Wind Energy Conference and Workshop, October 1981, Washington D.C.
3. Noll, R. B. and Hamm, N. D., Dynamic Stall of Small Wind Systems, RFP-3523 UC-60, February 1983.
4. Akins, R. E., "Method-of-Bins Update," presented at Wind Energy Expo '82, October 1982, Amarillo, Texas.
5. Hausfeld, T. E., "A Systematic Approach to Using the Method of Bins," Sixth Biennial Wind Workshop, June 1983, Minneapolis, Minnesota.
6. Miley, S. J., A Catalog of Low Reynolds Number Airfoil Data for Wind Turbine Applications, Texas A&M University, February 1982, available from N.T.I.S.
7. Miley, S. J., Addendum to Catalog of Low Reynolds Number Airfoil Data, Texas A&M University, October 1984, available from N.T.I.S.

8. "First Meeting of Specialists on the Aerodynamics of Horizontal-Axis Wind Turbines," sponsored by Rocky Flats Wind Energy Research Center and NASA Wind Energy Project Office, Wichita, Kansas, April 20-21, 1983.

9. Glauert, H., The Analysis of Experimental Results in the Windmill Brake and Vortex Ring States of an Airscrew, Reports and Memoranda, No. 1026, AE 222, February 1926.

10. Fairbank, D. and Rogers, E., PROPFILE (IBM PC Version), P. O. Box 27, Lake Geneva, Wisconsin 53147 USA.

11. Kocurek, J. D. and Tangler, J. L., "A Prescribed Wake Lifting Surface Hover Performance Analysis," American Helicopter Society Journal, January 1977.

12. Kocurek, J. D. and Berkowitz, L. F., "Velocity Coupling - A New Concept for Hover and Axial Flow Wake Analysis and Design," presented at the AGARD Fluid Dynamics Panel Specialists Meeting on Prediction of Aerodynamic Loads on Rotorcraft, London, United Kingdom, May 1982.

13. Tangler, J. L. and Ostowari, C., "Horizontal Axis Wind Turbine Post Stall Airfoil Characteristics Synthesization," DOE/NASA Wind Turbine Technology Workshop, May 1984, Cleveland, Ohio.

14. Ostowari, C. and Naik, D., "Post Stall Wind Tunnel Data for NACA 44XX Series Airfoil Sections," Texas A&M University, June 1984, available from N.T.I.S.

15. Thresher, R. W., et al., "Response of the MOD-0A Wind Turbine Rotor to Turbulent Atmospheric Wind," Sixth Biennial Wind Workshop, June 1983, Minneapolis, Minnesota.

16. Connell, J. R., and George, R. L., "Scaling Wind Characteristics for Designing Small and Large Wind Turbines," Sixth Biennial Wind Workshop, June 1983, Minneapolis, Minnesota.

17. Harper, C. W. et al., "On Uncertainties of the Aerodynamics and Structural Dynamics of Upwind Rotors on Large HAWTs in Relation to Reliable and Long Life Operation," RANN, April 1983.

18. Lissaman, P., et al., Advanced and Innovative Wind Energy Concept Development: Dynamic Inducer System, SERI/TR-8085-1-T2.

19. Augmented Horizontal Axis Wind Energy Systems Assessment, SERI/TR-98003-3, December 1981.

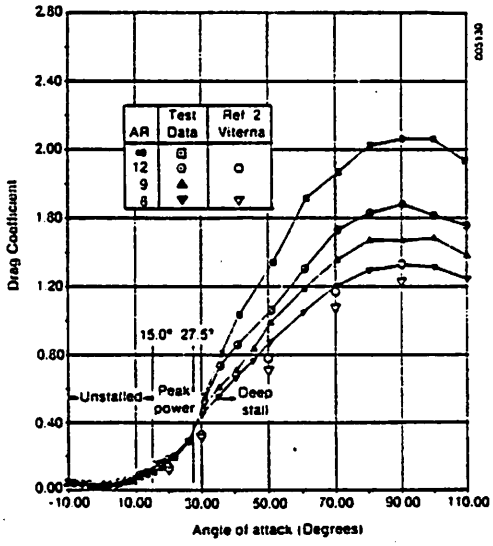

Fig. 1. Effect of Aspect Ratio on Drag Coefficients of the NACA 4418 Airfoil at RN = 0.25 x 10^6.

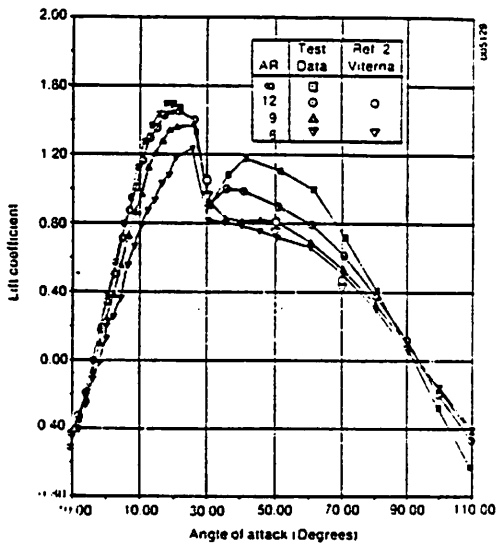

Fig. 2. Effect of Aspect Ratio on Lift Coefficients of the NACA 4418 Airfoil at RN = 0.25 x 10^6.

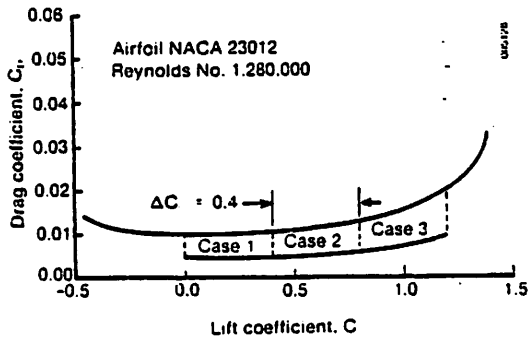

Fig. 3. Evaluation of Laminar Flow Drag Bucket Placement.

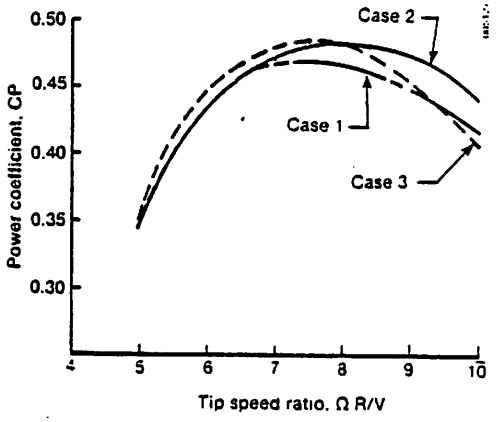

Fig. 4. Effect of Laminar Flow Bucket Placement on Rotor Performance.

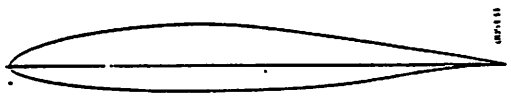

Fig. 5. Special Purpose Airfoil Designed for Blade Outboard Region.

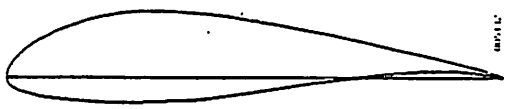

Fig. 6. Special Purpose Airfoil Designed for Blade Root Region.

Aerodynamic Calculational Methods for Curved-Blade Darrieus VAWT WECS

R.J. Templin

National Research Council of Canada

Summary

This informal discussion paper describes recent Canadian experience in the development of methods of calculation of aerodynamic performance and load distributions for the curved-blade Darrieus type wind turbine. Particular attention is paid to the so-called double multiple stream tube (DMST) theory, and to the uncertainties that remain in further developing adequate methods. These include the lack of relevant airfoil data at high Reynolds numbers and high angles of attack, and doubts concerning the accuracy of current models of dynamic stall. A brief summary of wind tunnel tests of several blade aerobrake configurations is also given.

Introduction

For a few years after results of the first wind tunnel tests of the Darrieus turbine had been published, no aerodynamic theory existed that was adequate for engineering design purposes. It seems that Ref. 1, which was published in 1974, was the first of a steadily increasing number of papers on the subject. It is not the purpose of this paper to give a complete survey, but a few references are listed to show some of the main trends. Reference 1 described what has since become known (at least in North America) as the single streamtube (SST) model. It was a simple adaptation of the Betz-Glauert momentum theory, in which the rotor was assumed to be a single actuator disc with uniform distribution of induced velocity parallel to the wind direction. The induced velocity was related to overall rotor drag, and blade element forces were calculated assuming quasi-static two-dimensional airfoil characteristics. The theory was simple, inexpensive of computer time and showed good agreement with overall rotor performance measurements in the unstalled flow regime, and fair agreement in stalled conditions. However, it was probably not accurate for detailed calculation of blade load distribution.

It was followed in 1975 by the development by the Sandia Laboratories of the multiple stream tube theory (MST), (Ref. 2), and still later by NRC and the Institut de Recherche de l'Hydro-Québec (IREQ) of the so-called double-multiple stream tube theory (DMST) (Ref. 3 and 4). Further refinements have recently been made at Queen Mary College, University of London (Ref. 5). All of these theories are based on momentum considerations and effectively assume that there is no interaction between individual streamtubes, although in reference 4 and 5 the expansion and lateral displacement of the streamtubes is allowed for as the flow decelerates through the rotor. The main difference between the MST and the DMST models is that the latter separates the rotor into two actuator discs representing the upstream and downstream surfaces with the assumption that the flow in the streamtubes reaches equilibrium, with static pressure returning to the ambient value, within the rotor. The remainder of this note will be concerned mainly with results obtained with the NRC version of the DMS Theory with dynamic stall effects included, but without some of the other refinements developed in the references.

For completeness, however, it should be pointed out that the last few years have seen developments in rotor vortex theories, which are perhaps to be preferred from the point of view of basic fluid mechanics. Probably the first such theory, for lightly loaded, two-dimensional cross-flow turbines was that described by O. Holme in Reference 6. A general result obtained by Holme was that one-half of the velocity decrement from far upstream to far downstream takes place between the upstream and downstream faces of the rotor, a result which is also automatically satisfied with the DMST theory. The most complete vortex model is that of Reference 7. Although this computer model is not limited to lightly loaded rotors, or to two-dimensional flow with infinitely many blades, it is very expensive to run. A possible compromise which combines some of the best features of vortex and streamtube approaches is the so-called fixed wake theory developed at Oregon State University (Ref. 8).

Comparison of DMST Theory with Experiment

Several comparisons have been made between the predictions of the double multiple streamtube momentum theory, and performance of Darrieus turbines in field tests. Only one such comparison is shown here, in Figure 1, for the 24 m diameter VAWT on the Magdalen Islands in the Gulf of St. Lawrence. Each of the data points shown was a 75-second average of 2000 samples of power and wind speed. The VAWT AERO computer code was the first DMST program in use at NRC and was developed for the Apple II personal computer. The Magdalen Islands turbine normally operates at a constant 36.6 rpm and has a rated power of about 230 kW. However, in order to allow more opportunity to make measurements at wind speeds that would lie in the region of full rotor stall, the turbine was operated at 26.4 rpm for the measurements shown in Figure 1, and the levelling of the power output at high wind speeds is, of course, the result of rotor stall. Note that, when no allowance is made for the effects of dynamic stall, the theory under-estimates maximum power by a substantial margin (25 percent or more).

Dynamic Stall Effects

The failure to predict the maximum power output of stall-controlled Darrieus wind turbines, when quasi-steady aerodynamic assumptions are made, has been realized for a number of years, and the Sandia Laboratories were perhaps the first to incorporate a model of dynamic stall into their computer codes. The model was based on one developed for helicopter rotor computation by R.E. Gormont of the Boeing-Vertol Corp. (Ref. 9). Modified versions of this model are now in use in the DMST computer codes in Canada. The upper theoretical curve in Figure 1 includes one such model, but the agreement with measurements in this case can not be taken as a confirmation of the model. It was in fact this particular set of measurements that was used in revising the NRC version of the stall model, mainly by tapering out the dynamic stall effects so that they become zero for airfoil angles of attack beyond about 45°.

About two years ago a series of experiments was begun in the NRC 2m x 3m low speed wind tunnel to measure dynamic stall effects on a thick (NACA 0018) airfoil of 0.6m chord, cut from a section of the same aluminum extrusion that was used in the manufacture of the Magdalen Islands turbine blades. The airfoil was oscillated sinusoidally, and in some cases non-sinusoidally to more closely simulate the time history of the non-dimensional rate of change of angle of attack at the rotor equator. These experiments differed from most of those that have previously been carried out on airfoils of interest in helicopter design in that the angle-of-attack range used was much higher, and of course the NACA 0018 airfoil is considerably thicker than those used in helicopter rotors. The results of one such run are shown in Figure 2 and 3, where the amplitude of the oscillation in angle of attack extended ± 30°. A comparison with three dynamic stall models is shown: the original Gormont model (Ref. 9), a model based on Gormont, modified by B. Massé (Ref. 3) and the NRC model. The latter two are in fair agreement with the measured lift-curve loops in Fig. 2, but fail to predict accurately the dynamic effects on airfoil drag. Generally, the oscillating airfoil tests have shown little dynamic effect on drag, as suggested by Fig. 3, and hence no dynamic connections are applied to airfoil drag data in the NRC model. It is understood that the same practice is followed by D.J. Sharpe at Queen Mary College (Ref. 5).

It is obvious that the somewhat "doctored" dynamic stall models we are presently using are grossly empirical in nature. Unfortunately experimental measurements for comparison are difficult to make on a Darrieus turbine during field tests. One such investigation was carried out by the Sandia Laboratories, by means of pressure measurements on the airfoil section near the equator of a 17m turbine, (Ref. 10). Figure 4 is reproduced from Ref. 10, and should serve as a warning that the effects of dynamic stall remain difficult to predict. The curves in Fig. 4 suggest that the apparent hysteresis loops, typical of dynamic effects, are occurring only over the upwind face of the turbine, where blade angles of attack are defined as being positive, whereas current models built into DMST computer codes predict dynamic stall on both upwind and downwind faces.

It must be concluded that more research, and more collaboration among groups concerned with VAWT design, is to be encouraged in future. This has been a brief summary of limited Canadian experience, and may not have taken into account adequately recent advances made elsewhere in airfoil dynamic effects.

Airfoil Data

The design of straight and curved blade VAWT's has been hampered by a general lack of suitable airfoil data over the very wide range of angles of attack that occur in constant-speed stall-controlled turbines. Uncertainties also exist concerning the effects of Reynolds number, especially in view of recent trends toward large-scale prototypes, such as Projet ÉOLE, the Canadian 4 MW turbine now under development as a co-operative project between the federal government and the power company, Hydro Québec. Its blade chord is 2.4m, and the nominal Reynolds number at the equator is about 8 million. In order to fill part of this gap in data, a special series of 2-dimensional airfoil tests was carried out in 1983 in the NRC pressurized blowdown 1.5 m tunnel, on an NACA 0018 airfoil over an angle of attack range up to 180° and, at least for part of this range, at Reynolds numbers up to 9 million. (Ref. 11). A summary of some of the lift coefficient measurements is shown in Figure 5. Also shown for comparison are some data taken from Ref. 13, and a curve labelled NRC dataset No. 12. The latter was a set of static measurements made at NRC on the same airfoil used for the oscillatory tests described above, at a Reynolds number of about 3 million. The figure shows the differences that are possible near and beyond stall, among different sets of data, all nominally for the same airfoil. This is, of course, important in the design of stall-controlled VAWT's. Also of interest is the rather large effect of Reynolds number that is apparent over the entire range shown here, up to 9 million. Since the driving component of the airfoil force coefficient for most Darrieus turbines (with no blade toe-in or toe-out) is the chordwise component, and since its maximum value is roughly proportional to the product of $C_{L\ max}$ and the stalling angle, the NRC blowdown tunnel results indicate a large increment as the Reynolds number is varied from 2 to 9 million.

Drag Brake Aerodynamics

Some of the Darrieus wind turbines that have been built commercially in Canada have used drag-type aerobrakes for control of rotor overspeed. For example, the Magdalen Islands turbine was fitted with aerobrakes near the equator that consisted of a flap on each blade, hinged at the airfoil trailing edge and extending both fore and aft of the trailing edge so that when open it presented a flat plate normal to the airfoil chord extending roughly an equal distance on either side of the hinge line. It was known that this type of brake tended to lose much of its effectiveness when stalling occurred on the local portion of the blade airfoil, thus leaving about half of the flap immersed in a separated wake.

For the large ÉOLE rotor it was decided to investigate aerobrakes of other configurations, and wind tunnel results for some of these are shown in Figure 6. Since some of these may offer mechanical simplicity in comparison with blade tip pitch changes, they may be of some interest to designers of fixed-pitch, stall-controlled HAWT's, as well as to those primarily interested in various versions of Darrieus VAWT's. At an early stage in the rotor design for ÉOLE, the aircraft company Canadair Ltd. suggested a split flap, which opened from the airfoil surface, leaving a gap through the airfoil ahead of the hinged flaps. These are referred to as Canadair aerobrakes in the figure. Perhaps the main point of interest in the graph is that the Canadair type of aerobrake maintains a more uniform rearward chordwise component of force up to much higher angles of attack than the "spoiler" type, although the latter are more effective (per unit of exposed area) at angles of attack below airfoil stall. Not shown are the results of tests with the gap closed ahead of the Canadair flaps; these showed, as in the case of the Magdalen Island flap, that effectiveness falls off drastically at angles of attack beyond airfoil stall.

The full results of the tests summarized in Figure 6 are currently being prepared in report form at NRC.

References

1. Templin, R.J. Aerodynamic Performance theory for the NRC vertical-axis wind turbine. NRC Laboratory Technical Report LTR-LA-160. June 1974.

2. Strickland, J.H. The Darrieus turbine: a performance prediction method using multiple streamtubes. Sandia National Laboratories Report SAND 75-0431. Oct. 1975.

3. Massé, B. Description de deux programmes d'ordinateur pour le clacul des performances et des chares aérodynamiques pour les eoliennes à axe verticale. IREQ Report IREQ-2379, July 1981.

4. Paraschivoiu, I. and Delclaux, F. Double Multiple Streamtube Model with Recent Improvements. J. Energy, Vol. 7, No. 3, May - June 1983.

5. Sharpe, D.J. Refinements and developments of the multiple streamtube theory for the aerodynamic performance of vertical axis wind turbines. Proc. Sixth BWEA Wind Energy Conference, Reading University, 28 - 30 March 1984.

6. Holme, O. A contribution to the aerodynamic theory of the vertical axis wind turbine. Proc. Internat. symposium on Wind Energy systems. Cambridge, England. Sept. 1976.

7. Strickland, J.H., Smith, T. and Sun, K.: A vortex model of the Darrieus turbine: an analytical model and experimental study. Sandia National Laboratories Report SAND 81-7017, June 1981.

8. Wilson, R.E. and Walker, S.N. Fixed wake analysis of the Darrieus rotor. Sandia National Laboratories Report SAND 81-7026, July 1981.

9. Gormont, R.E. A mathematical model of unsteady aerodynamics and radial flow for application to helicopter rotors. U.S. Army Air Mobility R & D Lab report on Boeing-Vertol Contract DAAJ02-71-C-0045. May 1973.

10. Akins, R.E., Klimas, P.C., and Croll, R.H. Pressure distributions on an operating vertical axis wind turbine blade element. American Solar Energy Society Annual Meeting, Sixth Biennial Wind Energy Conference. Minneapolis, June 1 - 3, 1983.

11. Templin, R.J. and Wickens, R.H. Aerodynamic characteristics of the NACA 0018 airfoil at high Reynolds numbers and at angles of attack from 0° to 180°. NRC Wind Energy Technical Memo TM-WE-020, July, 1984.

12. Sheldahl, Robert E., and Klimas, Paul C. Aerodynamic characteristics of seven symmetrical airfoil sections through 180-degree angle of attack for use in aerodynamic analysis of vertical axis wind turbines. Sandia National Laboratories Report SAND 80-2114, March 1981.

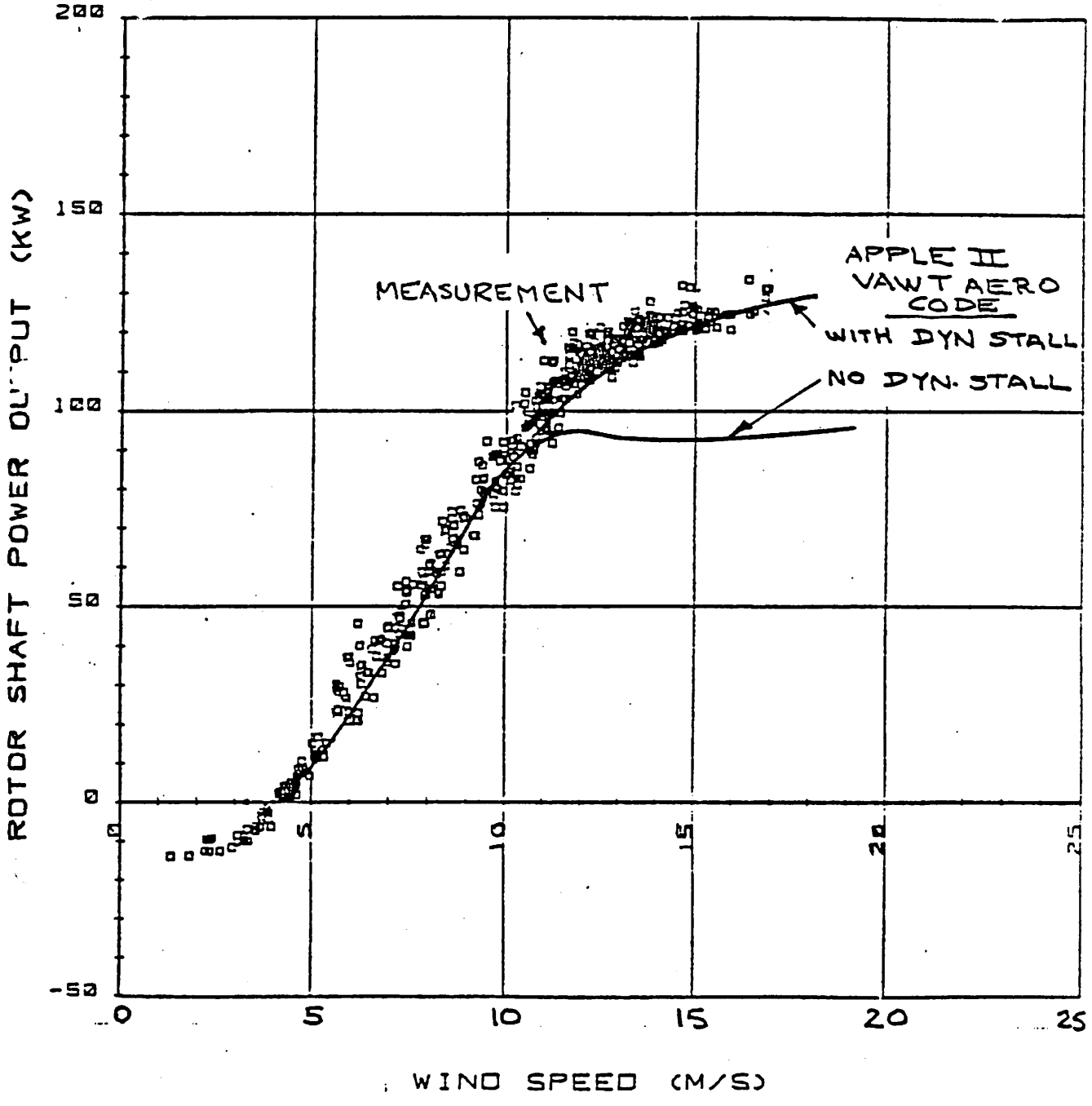

FIG. 1. MAGDALEN ISLANDS VAWT

ROTOR SHAFT POWER vs. WIND SPEED
ROTOR SPEED : 29.4 RPM

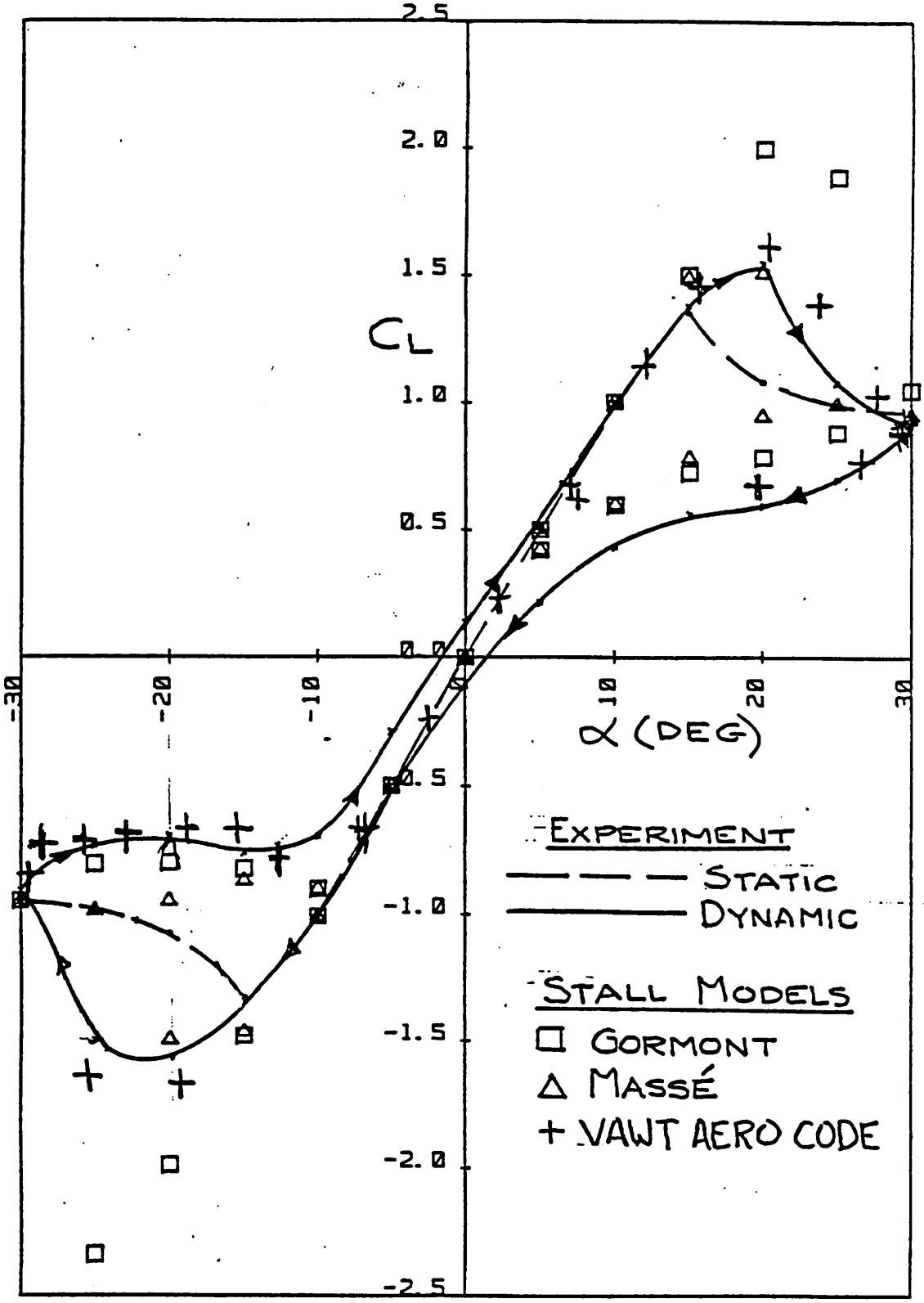

FIG. 2 OSCILLATING NACA 0018 AIRFOIL

CL vs ALPHA

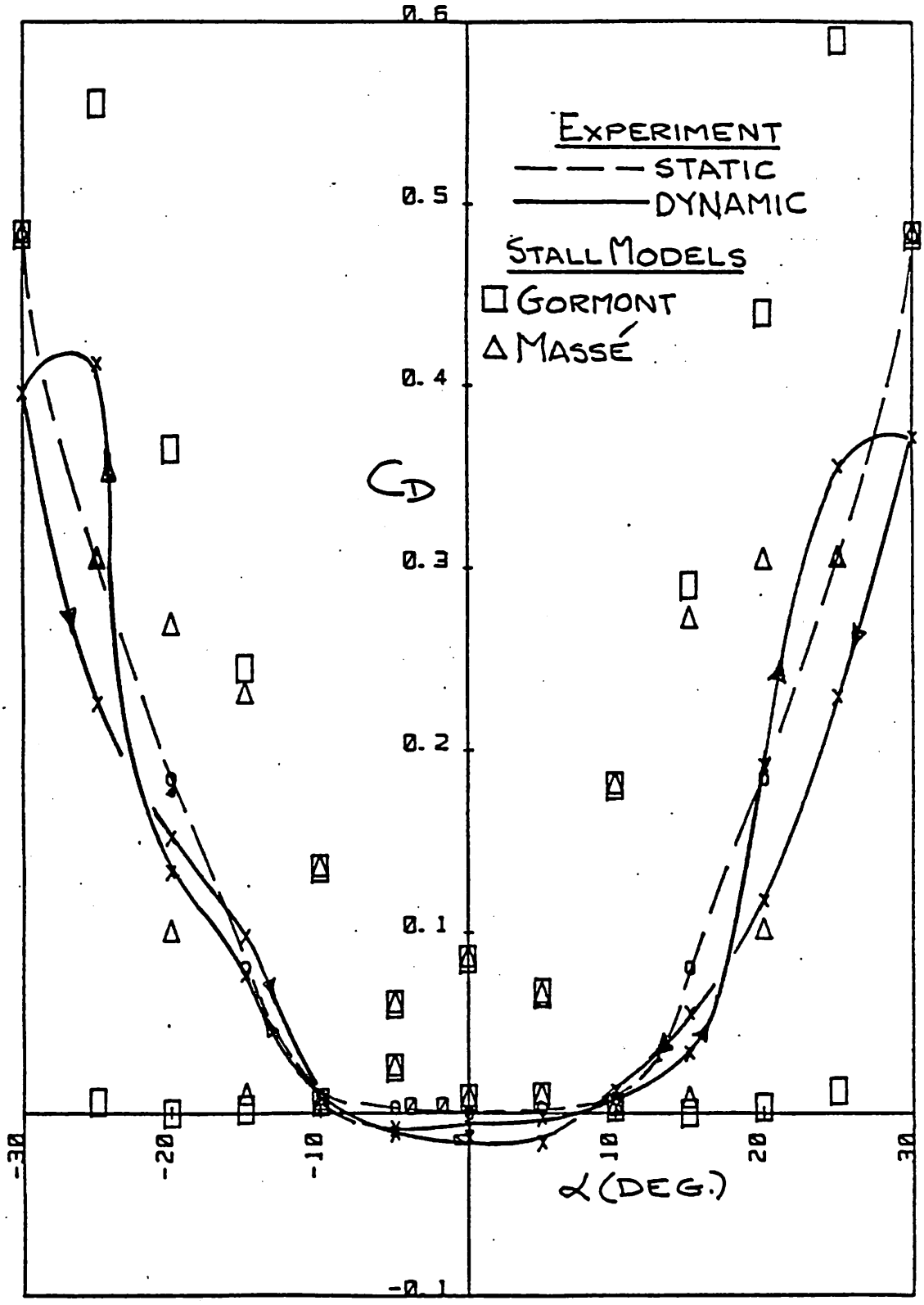

FIG. 3 OSCILLATING NACA 0018 AIRFOIL

CD vs ALPHA

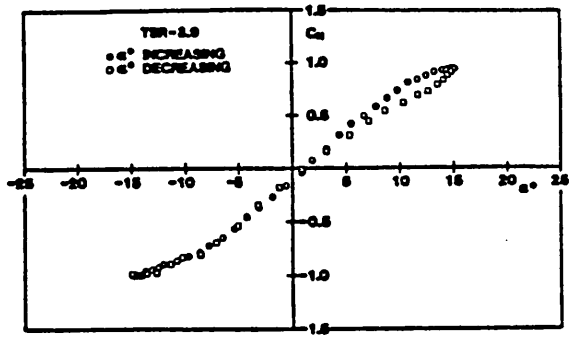

Fig. 6. C_n vs. α^*, TSR 3.9.

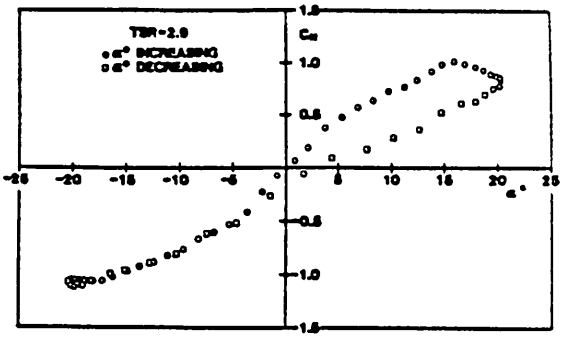

Fig. 9. C_n vs. α^*, TSR 2.9.

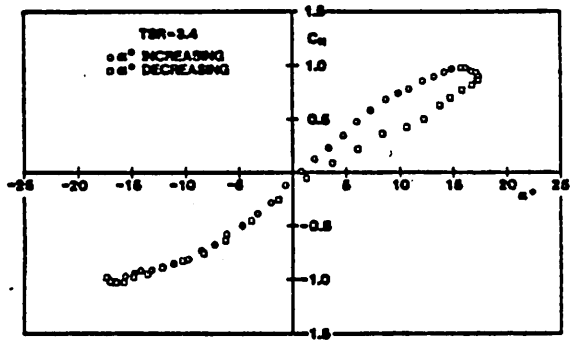

Fig. 7. C_n vs. α^*, TSR 3.4.

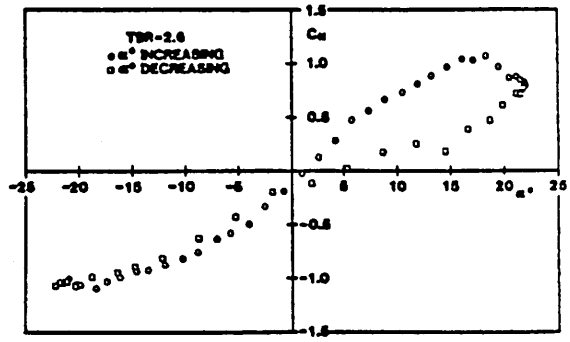

Fig. 10. C_n vs. α^*, TSR 2.6.

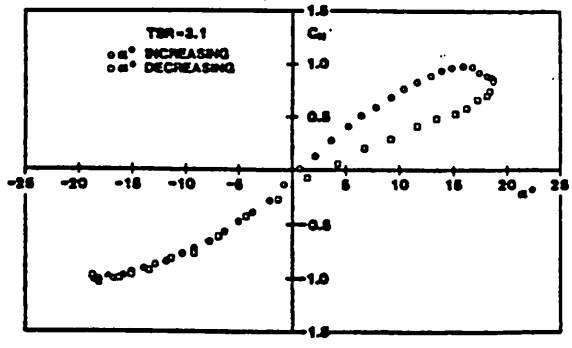

Fig. 8. C_n vs. α^*, TSR 3.1.

FIG. 4 C_N vs α

- MEASURED BY SANDIA LABS. ON 17m TURBINE (REF. 10)

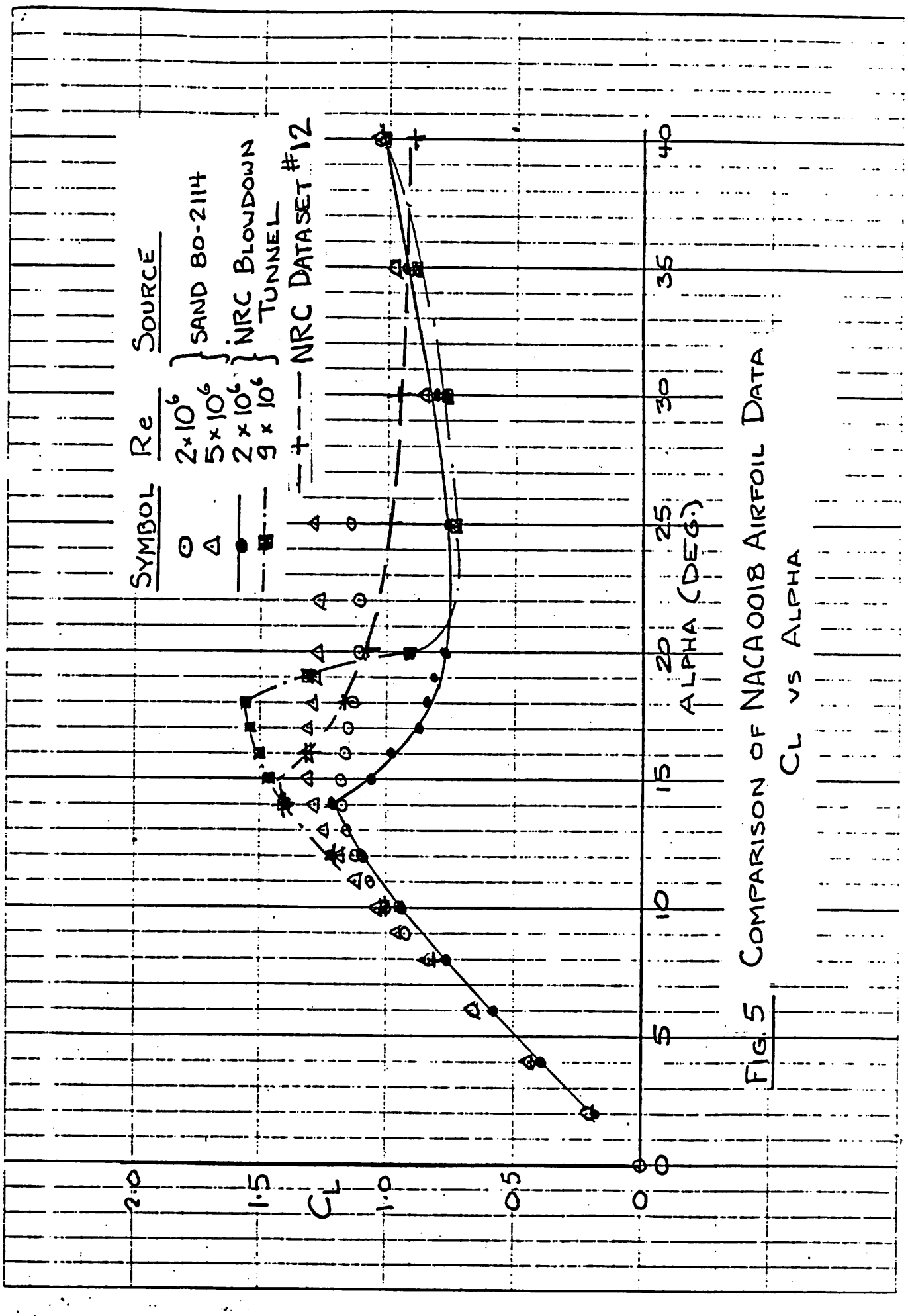

Fig. 5 Comparison of NACA0018 Airfoil Data
CL vs Alpha

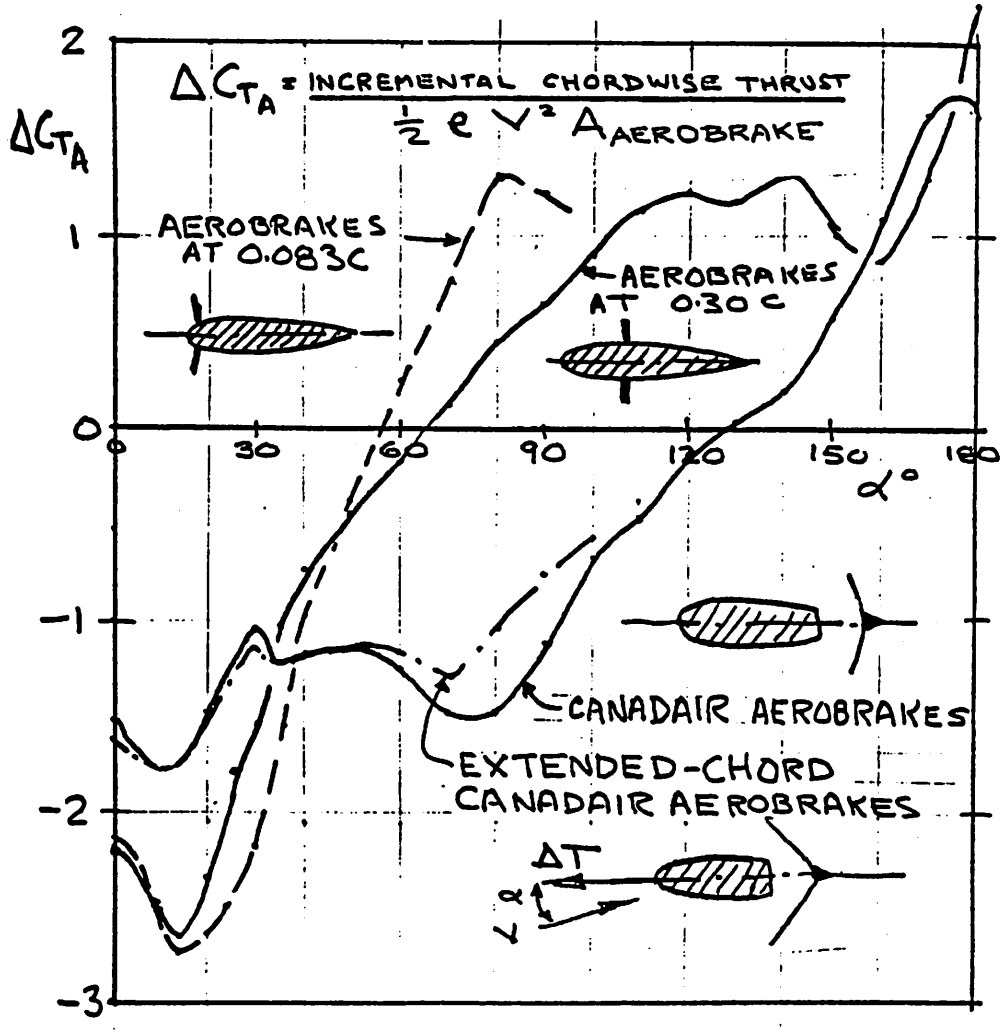

FIG 6 : COMPARISON OF AEROBRAKE CHORDWISE FORCE COEFFICIENT

AERODYNAMIC CALCULATIONAL METHODS FOR WECS

IEA MEETING OF EXPERTS
COPENHAGEN, 29/30 OCTOBER 1984

SUMMARY

prepared by
D.J. Milborrow

The overall impression gained from the meeting was that all the participating countries were looking at broadly similar problems.
12 presentations were made and the concluding discussion identified three major areas of research which were possibly suitable for collaborative effort:

1. Aerofoil characteristics appropriate for wind turbine blades, i.e. as modified by three-dimensional effects.
2. Unsteady aerodynamics.
3. Development of aerofoil sections for specific wind turbine applications, e.g. stall regulation.

The priority for item 3 was uncertain, partly because it could not be tackled in isolation - the cost implications of new profiles also needed to be considered. Germany was mainly involved in this activity, which would continue.

The priority for item 2 was reckoned to be lower than that for item 1, simply because it is necessary to understand 2-D to 3-D modifications before one tackles unsteady effects. There is some uncertainty as to the precise implications for design.

It was therefore agreed that an investigation of the differences between two- and three-dimensional aerofoil characteristics might form the basis of a collaborative investigation under IEA auspices. The topic has implications for blade loads, energy yields, and design of stall-regulated machines.

12th meeting of experts
IEA - LS WECS

AERODYNAMIC CALCULATIONAL METHODS FOR WECS

List of participants

Mike Anderson

Sir Robert M'Acpine & Sons Ltd
40 Bernard St.
London, W1N 1CG
England

Kurt Hansen

Technical University of Denmark
Dept. of Fluid Mechanics
DK-2800 Lyngby, Denmark
02-882222, lok. 4718

Theo van Holten

FDO Technical Consultants
P.O.Box 379
1000 AJ Amsterdam
Netherlands
020.262011

Peter Jamieson

James Howden & Co
195 Scotland St
Glasgow G5 8PJ
Scotland
041-429-2131

Søren Arthur Jensen

Dept. of Windengineering
Danish Maritime Institute
Hjortekærsvej 99
DK-2800 Lyngby
Denmark
02-879325

Reiner John

MBB Messerschmidt-Bölkow-Blohm
Hünefeldstr. 1 - 5
Propulsion Dept. TE 224
28 Bremen
BRD

Peter Hauge Madsen

Meteorology and Wind Energy Dept.
Risø,
DK-4000 Roskilde
Denmark

Staffan Meijer

FFA
Box 11021
161 11 Bromma
Sweden

Siegfried Mickeler

Institut für Aero- u. Gasdynamik
Universität Stuttgart
7 Stuttgart 80
Pfaffenwaldring 21
BRD
0711/685 3433

David Milborrow

Central Electricity Generat. Board
Land House, Newgate Str.
London EC1A 7AV
England
01-634-6468

Björn Montgomerie

FFA
Box 11021
161 11 Bromma 11
Sweden

B. Maribo Pedersen

Technical University of Denmark
Dept. of Fluid Mechanics
Building 404
DK-2800 Lyngby, Denmark
02-882222, lok. 4713

Reinhold Pernpeintner

MAN - Neue Technologie
Dachauer Str. 667
8000 München
BRD

Helge Petersen,
Risø National Laboratory
DK-4000 Roskilde
Denmark

Dave Quarton

Taylor Woodrow Construction
Wind Energy Group
307 Ruislip Rd East
Greenford
Middlesex
UK
01-578-4313, x 226

Flemming Rasmussen

Test Station for Windmills,
Risø
DK-4000 Roskilde
Denmark

Jens Nørkær Sørensen

Technical University of Denmark
Dept. of Fluid Mechanic
DK-2800 Lyngby
Denmark
02-882222, lok. 4710

J.L. Tangler

SERI Wind Energy
Research Center
1617 Cole Blvd.
Golden Colo. 30401
USA
303 497-7134

R.J. Templin

Building M-2
National Research Council
Montreal Road
Ottawa,
Canada, K1A 0R6
(613) 993-2423

O. de Vries

National Aerospace Lab. NLR
Anthony Fokkerweg 2
1059 CM Amsterdam
The Netherlands
020-5113113, ext. 458

Stig Øye

Technical University of Denmark
Dept. of Fluid Mechanics
DK-2800 Lyngby
Denmark
02-882222, lok. 4711

IEA - Implementing Agreement LS-WECS
Previous Expert Meetings

1. Seminar on Structural Dynamics, Munich, October 12, 1978

2. Control of LS-WECS and Adaptation of Wind Electricity to the Network, Copenhagen, April 4, 1979

3. Data Acquisition and Analysis for LS-WECS, Blowing Rock, North Carolina, Sept. 26-27, 1979

4. Rotor Blade Technology with Special Respect to Fatigue Design Problems, Stockholm, April 21-22, 1980

5. Environmental and Safety Aspects of the Present LS WECS, Munich, September 25-26, 1980

6. Reliability and Maintenance Problems of LS WECS, Aalborg, April 29-30, 1981

7. Costings for Wind Turbines, Copenhagen, November 18-19, 1981

8. Safety Assurance and Quality Control of LS WECS during Assembly, Erection and Acceptance Testing, Stockholm, May 26-27, 1982

9. Structural Design Criteria for LS WECS, Greenford, March 7-8, 1983

10. Utility and Operational Experiences and Issues from Mayor Wind Installations, Palo Alto, October 12-14, 1983

11. General Environmental Aspects, Munich, May 7-9, 1984

12. Aerodynamic Calculational Methods for WECS, Copenhagen, October 29-30, 1984

13. Economic Aspects of Wind Turbines, Petten, May 30-31, 1985